UNIVERSITY *of the*
WESTERN CAPE

THE USE OF CHEMOSTRATIGRAPHY AND GEOCHEMICAL VECTORING AS AN EXPLORATION TOOL FOR PLATINUM GROUP METALS IN THE PLATREEF, BUSHVELD IGNEOUS COMPLEX, SOUTH AFRICA:

A CASE STUDY ON THE SANDSLOOT & OVERYSEL FARMS

A thesis
Submitted to the Faculty of Science at the University of the Western Cape

By

Tshipeng Mwenze

In partial fulfilment of the requirements for the degree of Master in geology

Funded by Inkaba ye Africa

Supervisor: Prof. C. Okujeni

Co-supervisors: Dr. R. Bailie and Dr. A-M. Siad

August 2014

Declaration

I certify that *"The use of chemostratigraphy and geochemical vectoring as an exploration tool for platinum group metals in the Platreef, Bushveld Igneous Complex, South Africa: A case study on the Sandsloot and Overysel farms"* has not been accepted in substance for any degree, and is not concurrently been submitted for any degree other than that of Masters in geology being studied at the University of the Western Cape. I also declare that this work is the result of my own investigations except where otherwise identified by references and that I have not plagiarized the work of others.

.....

Tshipeng Mwenze August 2014

Keywords:

Platreef – floor rock interaction

Metasomatic rocks

Geochemical characterization

Mass balance

PGE & BMS mineralisation

Chemostratigraphy

Geochemical vectoring

Sandsloot and Overysel farms

Abstract

The paucity of geochemical criteria for stratigraphic correlations and defining the styles of mineralisation pose serious problems in locating PGE-rich zones in the Platreef. This study is therefore aimed at identifying and appraising process-based mineralogical/ geochemical criteria which may be useful in stratigraphic correlations and characterizing the nature and styles of PGE mineralisation. In addition, the work investigated the possible use of geochemical vectoring as a tool to locate the PGE-rich zones. Boreholes OY 482 and SS 330, drilled at the Overysel and Sandsloot farms respectively, were logged, and a total of 119 quarter cores were sampled for petrographic studies. The elemental contents in the rocks were determined by XRF and ICP-OES analyses and were evaluated using various statistical and mass balance techniques.

In borehole OY 482, where the floor rock is Archaean granite, the Platreef consists of three feldspathic pyroxenite sills referred to as Lower, Middle and Upper Platreef units, from the bottom to the top, respectively. The results show that the Lower and Upper Platreef units have higher median values of Mg# (0.58 and 0.57) and Ni/Cu (0.68 and 0.75) when compared to the Middle Platreef (Mg#: 0.54 and Ni/Cu: 0.67) which may not be totally suggestive of two magmatic intrusive pulses. In borehole SS 330, where the floor rock is dolomite, the rocks consist of clinopyroxenites and olivine clinopyroxenites (variably serpentinised). These two units are intercalated with each other and are products resulting from the injection of Platreef magma sills within the dolomite floor rock.

The hierarchical clustering and mass balance calculations show that when compared to the Platreef feldspathic pyroxenites, which have higher SiO_2, Al_2O_3 and Fe_2O_3 median contents, the clinopyroxenites possess higher CaO median content whereas the olivine clinopyroxenites have higher MgO and LOI median contents. The PGE-rich zones (i.e. Pt+Pd) in clinopyroxenites are marked by low Ca/Mg median values, whereas in both, the olivine clinopyroxenites and the Platreef units, these zones are marked by high Mg/Fe median values.

The suggested base metal index [(Cu/Zn) x (Ni/Co)] used to vector towards PGE-rich zones, which reflects the presence of the base metal sulphides (BMS), correlates with the

Pt+Pd in the BMS-rich zones. This is not always the case in zones of low BMS contents which may reflect changes in the mineralogy of the BMS.

In conclusion, the two boreholes studied show contrasting petrographic and geochemical attributes. This dissimilarity is mainly due to the fact that borehole OY 482 comprises Platreef magmatic rocks whereas borehole SS 330 intersected metamorphic/ metasomatic rocks.

Acknowledgements

The completion of this work has been successfully achieved with the direct or indirect involvement of a number of people to whom my sincere gratitude is dedicated.

Firstly, I would like to thank my supervisors Prof. Charles Okujeni, Dr. Russell Bailie and Dr. Abdi-Mohamoud Siad, who have unconditionally guided me throughout this great achievement.

Special thanks go to Prof. J. V. B. Donker and Prof. L. Holtman who also supported me during the completion of my studies.

A special mention goes out to my dear and lovely wife Bahati Christina Amundala and daughter Chelsea Tshipeng Amundala. Thank you so much for your understanding, love and support.

To my colleagues M. Andrews, Y. Hoosain, J. C. Salmáo, J. Majozi and the departmental staff W. Davids, P. Meyer, H. G. Solomon, J. Becorney and M. Crowley, your contributions are highly regarded and appreciated.

I would also like to express my sincere gratitude to my Late parents Tshipeng Rubuz Nfan† and Kalong a Tshoza Elizabeth†, and to my brothers and sisters for the love and support that they have dedicated throughout my studies.

Very special thanks go to Anglo Platinum for their contribution and Inkaba ye Africa through this achievement.

Lastly to The Almighty God, I surrender.

Table of contents

List of figures

List of plates

List of tables

Chapter 1

1. Introduction

1.1 Rationale and background

The Bushveld Igneous Complex (BIC) of South Africa, with an areal extent of ~65000 km^2 and maximum thickness reaching 7-9 km, is the largest intrusion in the Earth's crust (Eales et al., 1993). Its layered mafic and ultramafic unit, termed the Rustenburg Layered Suite (RLS; Fig. 1) by the South African Commission for Stratigraphy (SACS, 1980), is a major host of platinum group elements (PGE) (Eales et al., 1993). The PGEs comprise of platinum, palladium, rhodium, iridium, ruthenium and osmium and, in addition, some gold, chromitiferous and vanadiferous magnetite deposits (Eales et al., 1993; Wilhelm et al., 1997; Cawthorn, 1999b). These ore deposits outcrop in three main limbs: the Eastern-, Western- and Northern limbs (Fig. 1) and contain the most abundant Pt (75%), Pd (52%) and Rh (82%) resources of the world (Naldrett et al., 2008).

The discovery of the platiniferous ore body (or Merensky reef) in the Bushveld Complex was made in 1924 by Hans Merensky and Andries Lombaard on the farm Maandagshoek, in the Eastern limb (Cawthorn, 1999a). From there, they traced the deposit westwards to the Rustenburg area in the Western limb of the BIC (Cawthorn, 1999b). Because there were similarities in rock types with those outlined by Mellor and Hall (1910) in the Northern limb (Fig. 1) prior to 1924, Merensky prospected this part of the Complex until he discovered the platiniferous horizon (the Platreef; Fig. 1) near Potgietersrus (currently Mokopane) in 1925 (Cawthorn, 1999b; Kinnaird and McDonald, 2005). The Platreef was explored, and mining ceased in 1930 during the Great Depression when the platinum price collapsed (Kinnaird and McDonald, 2005).

In 1952 platinum mining restarted and, up to the 1970s, the Merensky reef was the only source of platinum in South Africa (Cawthorn, 1999b). Although PGE in chromitite layers were reported before the discovery of the Merensky reef, its exploitation was on

hold due to lack of appropriate metallurgical techniques to extract it from its host rock (Cawthorn, 1999b). From the 1970s to the 1990s, with the development of new extraction techniques, the Upper Group 2 (UG2) chromitite has been also mined for PGEs (Cawthorn, 1999b).

About two decades ago (1992) PGE-mining on the Platreef resumed as the result of an important increase in PGE prices (Cawthorn, 1999b; Kinnaird and McDonald, 2005). The success of the high tonnage and low-cost open pit mines at Sandsloot and Zwartfontein, opened in 1992 and 2002, respectively, by Anglo Platinum brought other companies to explore for PGEs on the Platreef in adjacent areas, in the Northern limb (McDonald et al., 2005; Kinnaird and McDonald, 2005; Holwell and McDonald, 2006). As opposed to the Merensky Reef and the UG2, which are thinner and occur at about the same stratigraphic positions in the Eastern and Western limbs, the Platreef is thicker and occurs along 30 km of strike at the base of the igneous sequence in the Northern limb (Lee, 1996). During the last decade, the latter has been the most active exploration centre in the BIC (McDonald et al., 2005; Van der Merwe et al., 2012; Mitchell and Scoon, 2012).

The Platreef is defined as the lithologically variable unit dominated by pyroxenites, which is irregularly mineralised with PGE, Cu and Ni, between the Transvaal meta-sedimentary footwall or Archaean granite/ gneisses and the overlying gabbronorite, gabbro and norite of the Main Zone (MZ) as shown in Fig. 1 (Kinnaird et al., 2005; Manyeruke et al., 2005). This 10 to 400 m thick unit, although predominantly comprised of pyroxenites, has also variable proportions of norites, gabbros, peridotites, serpentinite, rare dunites and xenoliths of meta-sedimentary rocks (Gain and Mostert, 1982; Harris and Chaumba, 2001; Armitage et al., 2002; McDonald et al., 2005; Kinnaird et al., 2005; Yudovskaya and Kinnaird, 2010; Mitchell and Scoon, 2012).

PGE mineralisation is hosted in different lithologies occurring at various stratigraphic heights along the strike of the Platreef and is mostly associated with base metal sulphides (BMS), tellurides, bismuthides, antimonides and arsenides (Gain and Mostert, 1982; Armitage et al., 2002; Hutchinson and Kinnaird, 2005; Holwell and McDonald, 2006).

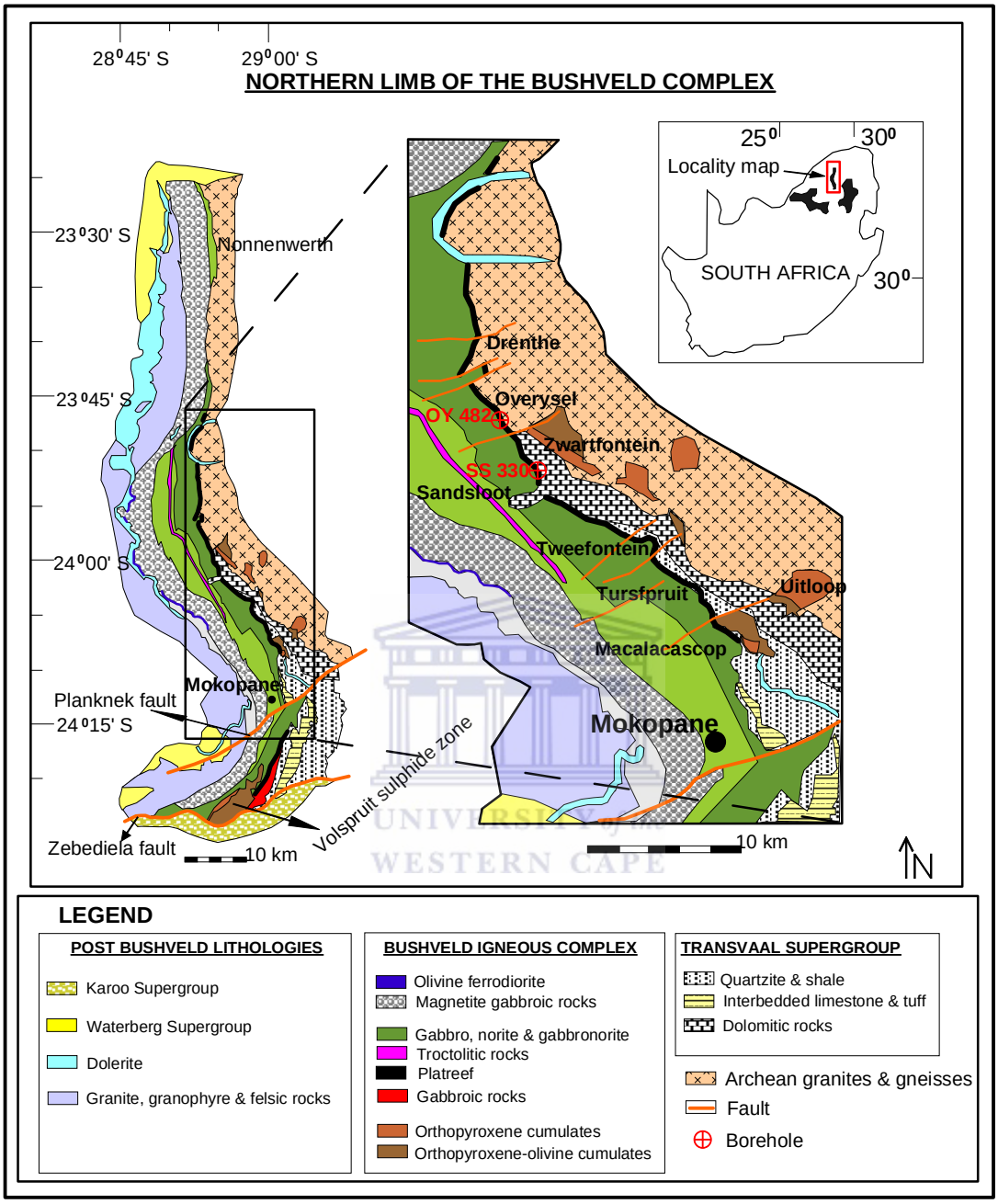

Fig. 1 Geological map of the Northern limb of the Bushveld Igneous Complex after Kinnaird and McDonald (2005), modified from Van der Merwe (1978) and Ashwal et al. (2005). *The inset map shows the outcrop of the Rustenburg Layered Suite in South Africa after Harris and Chaumba (2001) and the expanded map shows the location of the different farms and the two studied boreholes along the strike of the Platreef north of Mokopane.*

Early description of the geology of the Platreef was given by Wagner in 1929 (McDonald et al., 2005). His description highlighted the following: (1) the great thickness of the mineralised layers; (2) the occurrence of the mineralised bronzitite at the base of the

igneous stratigraphy in contact with the various metamorphosed floor rocks; (3) the Pt/Pd ratios ≤ 1; and (4) the occurrence of PGE reef in metamorphosed and metasomatised floor rocks (McDonald et al., 2005).

Later, Wagner (1929) believed that the Platreef and the Merensky Reef represented the same magmatic layer since he observed the presence of the feldspathic bronzitite and pseudoporphyritic poikilitic diallage norite at many sites along the strike of the Platreef, which displayed similar appearance to the rocks of the Merensky Reef that were already known in the Eastern and Western limbs of the BIC (McDonald et al., 2005).

In 1982, Gain and Mostert provided the first detailed description of the stratigraphy and PGE mineralisation of the Platreef. The latter, which consists of a ~250 m thick complex assemblage of different lithologies, occurs between the overlying MZ of the BIC and rests upon Transvaal meta-sedimentary rocks or Archaean granite/ gneisses (Gain and Mostert, 1982). Because of this, the two authors regarded the Platreef to be part of the Critical Zone (CZ) that occurs in the Eastern and Western limbs of the Complex (Lee, 1996). The CZ is up to 1800 m thick, composed of cyclic units of chromitite, harzburgite, pyroxenite through norite to anorthosite that rest upon rocks of the Lower Zone and are overlain by those of the MZ of the BIC (Barnes and Maier, 2002). Gain and Mostert (1982) concluded that the PGE mineralisation resulted mainly from the interaction between the Platreef-forming magma and dolomite, and associated hydrothermal alteration.

The geological complexity of the Platreef, which is marked by the lack of consistent stratigraphy along with PGEs concentrated in different lithologies at various depths and the change in floor rock composition along its strike, has triggered intense studies by researchers to understand the processes involved in its formation useful to provide a genetic explanation of the origin and mechanisms of PGE mineralisation (Hutchinson and Kinnaird, 2005; Holwell and McDonald, 2006; Maier et al., 2008). The different models put forward for the formation of the Platreef are summarized below along the following lines:

In terms of stratigraphy, some researchers have investigated whether the Platreef-forming magma is similar to any of the magma pulses that formed the RLS. McDonald et al. (2005) proposed that the Platreef formed from a very different magma to that of the RLS while other authors (Kruger, 2005; Pronost et al., 2008; Reisberg et al., 2011) suggested that the Platreef represents the same magma that formed the Merensky Reef. However, a different view that supports the similarity between the Platreef-forming magma and the magma that formed the Critical Zone in the northern limb has proposed by other investigators (Kinnaird et al., 2005; Maier et al., 2008; Yudovskaya and Kinnaird, 2010).

Along the same lines, some researchers have investigated the sequence of intrusion and have concluded that the Platreef formed before the MZ magma (Harris and Chaumba, 2001; Manyeruke et al., 2005; Kinnaird et al., 2005; Holwell and Jordaan, 2006; McDonald and Holwell, 2007; Pronost et al., 2008; Yudovskaya and Kinnaird, 2010). Other investigators (Kinnaird, 2005; Manyeruke et al., 2005; Holwell and Jordaan, 2006; Mitchell and Scoon, 2012) have suggested that the Platreef formed from several intrusive magma pulses.

In terms of floor rock assimilation, there has been contamination of the Platreef-forming magma by quartzites and hornfels at Macalacaskop (Kinnaird et al., 2005, Sharman-Harris et al., 2005), by shale and dolomite of the Duitschland Formation at Turfspruit (Sharman-Harris et al., 2005), by banded iron formation at Tweefontein (Ihlenfeld and Keays, 2011), by dolomite at Sandsloot (Harris and Chaumba, 2001; Holwell et al., 2007; Penniston-Dorland et al., 2008; Ihlenfeld and Keays, 2011) and by Archaean granite/ gneisses at Overysel (Barton et al., 1986; Holwell and McDonald, 2006; Ihlenfeld and Keays, 2011). Harris and Chaumba (2001) have also reported fluid-rock interaction after the Platreef intrusion on the Sandsloot farm where the floor rock is carbonate.

In terms of mineralisation, various authors have concluded that the PGE distribution along the strike and depth of the Platreef is primarily controlled by magmatic processes (Armitage et al., 20002; Kinnaird et al., 2005; Holwell and McDonald, 2006; Hutchinson and McDonald, 2008). Nevertheless, processes such as floor rock assimilation, footwall/

hornfels-magma interaction, devolatilisation and partial melting, infiltration of felsic magmas and fluid-rock interaction have affected the style of PGE mineralisation in different regions of the Platreef (Armitage et al., 2002; Kinnaird et al., 2005; Hutchinson and Kinnaird, 2005; Holwell and McDonald, 2006; Hutchinson and McDonald, 2008).

1.2 Problem statement

This work attempts to address two major problems area related to PGE mineralisation in the Platreef as follows:

1) The PGE mineralisation is hosted in different rock types; that is, the Platreef magmatic rocks (Kinnaird et al., 2005; Holwell and McDonald, 2006; Hutchinson and McDonald, 2008; Mitchell and Scoon, 2012) and the metamorphosed/ metasomatised footwall rocks (Wagner, 1929; Armitage et al., 2002; Holwell and McDonald, 2006), which cannot be correlated from core to core, even with cores drilled adjacent to one another (Hutchinson and Kinnaird, 2005).
2) The nature and style of PGE mineralisation varies considerably across strike and with depth. Amongst other factors, possible causes that have influenced PGE mineralisation may be attributed to fluid-rock interaction, floor rock assimilation (Harris and Chaumba, 2001; Sharman-Harris et al., 2005; Holwell and McDonald, 2006; Pronost et al., 2008, Roelofse and Ashwal, 2008; Ihlenfeld and Keays, 2011) and the influence of multiple intrusive Platreef-forming magma pulses (Kinnaird, 2005; Yudovskaya and Kinnaird, 2010; Mitchell and Scoon, 2012).

On these bases, two boreholes were selected for this study. The first borehole, drilled at the Overysel farm (Fig. 1), transects mineralised Platreef pyroxenitic rocks that overlie the Archaean granite as floor rock. The second borehole, drilled at the Sandsloot farm (Fig. 1), crosscuts mineralised metamorphosed/ metasomatised footwall rocks that overlie dolomite of the Malmani Subgroup as floor rock.

These mineralised rocks were chosen to study the mineralogical attributes and elemental patterns and their effects on mineralisation. Secondly, they are suitable to investigate the influence of the floor rocks on the nature and style of PGE mineralisation.

1.3 Project aim and objectives

A major objective of this work therefore is to identify and distinguish processes (such as magmatic, hydrothermal and/ or post-magmatic) based on mineralogical/ geochemical signatures, which may be useful in stratigraphic correlation and characterizing the nature and styles of PGE mineralisation across the strike and with depth of the Platreef and its metamorphosed floor rock. In addition, the work aims at investigating the possible use of geochemical vectoring as a tool to locate the PGE mineralisation within the studied rocks.

In order to achieve these objectives, much emphasis will be placed on understanding the processes that control the formation of, both, Platreef pyroxenitic and metamorphosed/ metasomatised reefs that have resulted from the interplay between magmatic and contact metamorphic/ metasomatic and hydrothermal processes using whole rock geochemical data as an aid to PGE exploration in the mineralised units.

Previous workers concluded that PGE mineralisation in the Platreef pyroxenitic reefs is attributed to orthomagmatic processes where the PGEs are associated with the BMS (Armitage et al., 2002; Kinnaird et al., 2005; Holwell and McDonald, 2006). The general assumption of this process suggests that the mantle derived magma should be fertile in PGE which are hosted by sulphides (Maier, 2005). As the magma ascends and has been later emplaced in the crust, PGE will concentrate in an immiscible sulphide melt only after sulphur saturation has been achieved (Maier, 2005). The dense droplets of sulphide melt will then segregate to the base of the fractionating layered magma chamber to form a PGE-sulphide enriched horizon or reef (Maier, 2005).

In metamorphosed/ metasomatised footwall, the mechanism of PGE mineralisation varies depending on the composition of the floor rocks (Armitage et al., 2002; Hutchinson and Kinnaird, 2005; Holwell and McDonald, 2006).
To the south, on the farms Tweefontein Hill and Turfspruit where the footwall is made of Penge BIF and hornfelsed shales, Hutchinson and Kinnaird (2005) concluded that PGE have not been significantly transported into the footwall. Instead, PGE mineralisation are

associated with sulphide-rich zones settled above refractory and high-grade contact metamorphic footwall that have not developed a partial melt network comparable to that found at Overysel (Hutchinson and Kinnaird, 2005).

In the central sector, at Sandsloot and Zwartfontein, the assimilation and metamorphism of dolomite, which represents the floor rock, has released large amounts of fluids leading to subsequent serpentinisation (Armitage et al., 2002; Holwell and McDonald, 2006). Hence, the PGE mineralisation is strongly influenced by fluid activity giving rise to metamorphic clinopyroxenites, calc-silicates and serpentinites in the footwall resulting in some decoupling of the PGEs from the BMS (Armitage et al., 2002; Holwell et al., 2006).

To the north, at Overysel where the footwall is Archaean granite, Holwell and McDonald (2006) concluded that the PGE were emplaced into the footwall through a gravity driven percolation of sulphide liquid because the gneissic footwall at Overysel produced a felsic partial melt and very few volatiles.

The specific objectives of the work are as follows:

1) The petrographical study on the lithologies was performed on polished slides and thin sections cut from the quarter core rock samples in order to classify them and to aid in identifying the petrographical characteristics useful for stratigraphic correlation.

2) The geochemical classification of the rock samples entailed two steps. At first, the oxide data of the rocks were processed using statistical techniques in order to classify them into groupings that can be correlated with the various rock types/ subtypes identified from the petrography. Then, the major elements that control the mineralogical composition of the rocks were identified using box and whiskers plots.

3) The geochemical characterisation of the different rock types/ subtypes involved the use of spider diagrams to compare their respective trace element fractionation. This was followed by tabulation of the statistical data summaries including minima, maxima and medians of oxides and trace elements, and calculated immobile element

ratios and trace element anomalies from the spider diagrams in order to identify the geochemical signatures of the various rock types/ subtypes.

4) An investigation on elemental exchange between the Platreef magma and the various floor rocks was performed in order to identify the major and trace elements involved in the formation of the various rock types/ subtypes.

5) Developing geochemical indices/ ratios using firstly the major elements to separate the rock types for chemostratigraphic correlations and secondly the trace elements to locate the PGE/ BMS mineralisation within the studied rocks.

6) The geochemical indices and vectors that distinguish the rock types and identify the PGE ore zones, respectively, were spatially evaluated to ascertain their feasibilities.

1.4 Geochemical vectoring/ chemostratigraphy

During the last two decades, the application and potential of geochemical vectoring (Large and McGoldrick, 1998; Brand, 1999; Eilu et al., 2001; Urqueta et al., 2009) and chemostratigraphy (Reátegui et al., 2005; McClenaghan et al., 2006; Ramkumar et al., 2011) have emerged as vital tools for mineral exploration.
Geochemical vectoring implies developing cost-effective indices or trace element ratios that are able to define consistent gradients indicative of an ore zone for mineral exploration to distinguish mineralised from barren complexes (Large and McGoldrick, 1998; Brand, 1999; Eilu et al., 2001).

Chemostratigraphy studies the variations in the chemical compositions of rock layers to characterise them into geochemically distinct units and correlate them by comparing the geochemical signatures in adjacent sections (Pearce et al., 1999; Monterro-Serrano et al., 2010). The latter is also used for establishing geological boundaries and correlating widely separated strata, where other stratigraphic methods (such as lithostratigraphy,

chronostratigraphy, etc.) failed or have limitations (Ramkumar and Sathish, 2006; Wills et al., 2006).

Although many case studies have successfully applied these tools in various parts of the world, very few have used them in the quest for PGE mineralisation. Ames et al. (2007) reported that potential mineralogical and geochemical vectors are being developed for PGE exploration in the Sudbury Complex while the work of Maier et al. (2008) and Keays et al. (2012) used stratigraphic methods for PGE exploration in the Platreef and Stillwater Complex, respectively.

1.5 Study area

The studied areas are situated ~30 and 40 km NW of Mokopane on the farms Overysel 816 LR and Sandsloot 236 KR (Fig. 1), respectively, which are under Anglo Platinum mineral right concession. Both farms are situated within the Mogalakwena municipality, Waterberg district in the Limpopo Province, South Africa.

1.6 Scope of the work

For this study, two boreholes, drilled on the farms Overysel 816 LR and Sandsloot 236 KR, respectively, were logged and sampled (Fig. 1). Borehole OY 482 intersects MZ gabbronorites and various Platreef feldspathic pyroxenite sills overlying the Archaean granite/ gneisses as floor rock, whereas borehole SS 330 intersects metamorphosed/ metasomatised lithologies that rest upon dolomite of the Malmani Subgroup.

Chapter 2

2. Geology

2.1 Regional geology

2.1.1 Bushveld Igneous Complex

The BIC of South Africa was emplaced into the Kaapvaal Craton from about 2.06 to 2.05 Ga (Walraven et al., 1990; Scoates and Friedman, 2008; Scoates et al., 2011). According to Naldrett et al. (2009), the Complex, which is situated in the NE part of South Africa, is 450 km wide along the E-W direction and 350 km along the N-S axis. It overlies rocks of the Transvaal Supergroup, Archaean granitoids and greenstones, and stratigraphically comprises four igneous event suites consisting of: (1) older mafic sills (i.e. the Uitkomst Complex); (2) the Rooiberg felsites; (3) the RLS; and (4) the younger Lebowa Granite Suite (Naldrett et al., 2012).

The RLS's mafic and ultramafic rocks occur in five major lobes: the Western, Far Western, Eastern, South Eastern and Northern limbs (Eales et al., 1993; Cawthorn and Walraven, 1998; Maier et al., 2013). In the Western and Eastern limbs, where the stratigraphic sequence is complete, the RLS is generally subdivided into five zones (Hall, 1932). From the base to the top, the sequence consists of: (1) a Marginal Zone (MaZ), composed of plagioclase-orthopyroxene cumulates at the base, overlain by (2) the Lower Zone (LZ), predominantly composed of harzburgite, dunite and bronzitite, followed by (3) the Critical Zone (CZ); which is dominated by dunites, harzburgites, pyroxenites, chromitites, norites and anorthosites, overlain by (4) the Main Zone (MZ) gabbro-norite and topped by (5) lithologies of the Upper Zone (UZ) dominated by plagioclase, magnetite and iron-rich pyroxenes and olivine (Eales et al., 1993; Eales and Cawthorn, 1996; Barnes and Maier, 2002).

2.1.2 Northern limb of the Bushveld Igneous Complex

The Northern limb, in the Limpopo Province of South Africa, has a sinuous outcrop that strikes N-S over a maximum distance of ~120 km and has a maximum width of 15 km (Fig. 1) (Armitage et al., 2002; Van der Merwe, 2008). Along its N-S strike line; the Northern limb stretches from the Melinda fault, as its northern margin, to the Zebediela fault as its southern margin (Fig. 1) (Van der Merwe, 2008). Some researchers (Kinnaird et al., 2005) suggest the Northern limb to form the eastern edge of a basin, which includes also the mafic rocks in the Villa Nora sector, based on aeromagnetic and gravity data.

Structurally, the Northern Bushveld is separated from the two other major limbs (Western and Eastern) of the Complex by the Thabazimbi-Murchison Lineament (TML; ENE-WSW trend) of which the Zebediela, Planknek and Welgevonden faults are part (Kinnaird et al., 2005; Kinnaird & McDonald, 2005). According to Good and de Wit (1997), the TML resulted from the collision between the Pietersberg and Kaapvaal terranes and has been active from the Middle Archaean to the Late Mesozoic.
In addition, a review of the different faulting events occurred after the emplacement of the Northern limb is presented by Van der Merwe (2008). These faulting events, identified by various authors south of Mokopane, show the following striking trends: (1) E to ENE, N to NNW and NW (Truter, 1947; Van Rooyen, 1954; De Villiers, 1970); and (2) NS, WNW, NE and EW (Hulbert, 1983). In the areas north of Mokopane, the faults are mainly striking NE (White, 1994).

In terms of stratigraphy, the Northern limb's major zones do not occur in a complete succession along strike similar to those in the RLS of the Western and Eastern limbs of the BIC (Von Gruenewaldt et al., 1989; Maier et al., 2008; Yudovskaya and Kinnaird, 2010). However these major zones, wherever developed, are: (1) the Marginal Zone; (2) the Lower Zone; (3) the Platreef; (4) the Main Zone; and (5) the Upper Zone (McDonald et al., 2005; Kinnaird et al., 2005; Van der Merwe, 2008; Mitchell and Scoon, 2012; Holwell et al., 2013).

In the following paragraphs, a brief summary of these major zones are presented.

2.1.2.1 The Marginal Zone (MaZ)

Although some authors (Holwell et al., 2013) have not identified the MaZ norites in the Northern limb stratigraphy, others (Kinnaird et al., 2005) have reported its sporadic occurrence in certain areas (e.g. Macalacaskop and Turfspruit farms). Van der Merwe (2008) provides an account of various investigators (Hulbert, 1983; De Klerk, 2005) who also identified the MaZ lithologies and defined them as product of contact between Bushveld magma and its country rocks to the south of Mokopane.

2.1.2.2 The Lower Zone (LZ)

The lithologies of the LZ, south of Mokopane, occur adjacent to the Transvaal Supergroup sequence in the Grasvally and neighboring farms (e.g. Rooipoort, Moordrift and Jaagbaan) (Hulbert and Von Gruenewaldt, 1986; Maier et al., 2008; Van der Merwe, 2008). In these areas, the LZ consists of more than 1,600 m thick rock succession comprising the Volspruit pyroxenite subzone, followed by harzburgite with chromitites of the Drummonlea subzone and harzburgite-pyroxenite of the Moordrift subzone (Hulbert and Von Gruenewaldt, 1982; McDonald and Holwell, 2007).

There is also a thin succession of rocks called the Grasvally norite-pyroxenite-anorthosite (GNPA) member that caps the LZ only to the south of Mokopane (Hulbert, 1983; Hulbert and Von Gruenewaldt, 1986; Maier et al., 2008). These series contains layered norites, gabbronorites and anorthosites along with a chromitite seam which has been called the ‘‘UG2-like’’ chromitite by Hulbert (1983). Van der Merwe (1998; 2008) has correlated the chromitite layer in the GNPA directly with the Bushveld UG2 chromitite, while others (Von Gruenewaldt et al., 1989) have suggested that the upper unit of the GNPA can be correlated with the Platreef to the north of Mokopane.

From north of Mokopane to Zwartfontein, the LZ occurs as six separated units of layered bronzitites and harzburgites (Kinnaird et al., 2005; Van der Merwe, 2008; McDonald et al., 2009).

Although the LZ in the Northern limb has been equated to that in the rest of the BIC, recent studies (McDonald et al., 2009) have shown that they display different geochemical signatures. The latter was attributed to crustal contamination of the intruding LZ-forming magma to the south and north of the TML (McDonald et al., 2009).

2.1.2.3 The Platreef

The Platreef has been described as a complex succession of nearly horizontal mafic and ultramafic layers, irregularly mineralised in PGE and BMS, that occur between the underlying Transvaal Supergroup and Archaean granites (or just footwall) and the overlying Main Zone in the Northern limb of the Bushveld Complex (Harris and Chaumba, 2001; Armitage et al., 2002; McDonald et al., 2005; Kinnaird et al., 2005; Holwell and Jordaan, 2006; Van der Merwe et al., 2012). It is composed of a 10- to 400 m thick package of pyroxenitic lithologies which comprises mainly pyroxenites with variable amounts of peridotite, gabbros, norites, serpentinite, rare dunites and xenoliths of metamorphosed sedimentary rocks (Armitage et al., 2002; Manyeruke et al., 2005; Hutchinson and Kinnaird, 2005; Holwell and McDonald, 2006; Pronost et al., 2008; Yudovskaya and Kinnaird, 2010; Ihlenfeld and Keays, 2011; Van der Merwe et al., 2012; Mitchell and Scoon, 2012).

The Platreef package, which is only developed to the north of the Ysterberg-Planknek fault, occurs over ~30 km along strike and forms the basal igneous unit of the Northern limb from the farms Townlands in the south to Nonnenwerth further north (Manyeruke et al., 2005; Maier et al., 2008; Van der Merwe, 2008). Its thickness varies from south to north (Kinnaird et al., 2005; Pronost et al., 2008; Ihlenfeld and Keays, 2011). This is mainly due to the uneven nature of its underlying floor rock landscape as a result of folding and faulting (Nex, 2005; Yudovskaya and Kinnaird, 2010) and also partly due to

the reactive nature between the Platreef-forming magma with the various floor rocks (Holwell and McDonald, 2006; Mitchell and Scoon, 2012).

These floor rocks, which are part of the Transvaal Supergroup, comprises of: close to Mokopane, quartzites of the Daspoort Formation (Pretoria Group), followed northwards by the Timeball Hill Formation (i.e. quartzite, shale and dolomite), the Penge banded iron Formation, dolomite of the Malmani Subgroup and quartzites as footwall lithologies (Harris and Chaumba, 2001; Armitage et al., 2002; Kinnaird et al., 2005; Nex, 2005; Holwell and Jordaan, 2006; Pronost et al., 2008; Ihlenfeld and Keays, 2011; Van der Merwe et al., 2012). From Zwartfontein north to Overysel 816 LR and further north, the Platreef transgresses onto Archaean granite as basement rock (Holwell and McDonald, 2006; Maier et al., 2008; Yudovskaya and Kinnaird, 2010).

Various authors have also reported the presence of xenoliths-derived metamorphosed sedimentary rocks within the Platreef package which, in many cases, were found not to correspond with the immediate floor rock (Manyeruke et al., 2005; Kinnaird et al., 2005; Holwell and McDonald, 2006; Hutchinson and McDonald, 2008; Johnson et al., 2010). The occurrence of these footwall-entrained materials (such as hornfels, quartzite, calc-silicate, dolomite) in the Platreef rocks has been interpreted as evidence of floor rock assimilation (Harris and Chaumba, 2001; Manyeruke et al., 2005; Kinnaird et al., 2005; Holwell and McDonald, 2006; Pronost et al., 2008; Ihlenfeld and Keays, 2011; Van der Merwe et al., 2012).
Furthermore, the development of PGE-rich metamorphosed floor rocks along the strike of the Platreef has been reported (Harris and Chaumba, 2001; Armitage et al., 2002; Holwell and McDonald, 2006) and thereby led some authors (Armitage et al., 2002) to recognize it as Pd-Pt-Au skarn deposit, especially when the metamorphosed footwall is carbonate.

With respect to the footwall rock type, Merensky (1925) subdivided the Platreef into three sectors; the northern sector, which comprises of the Archaean granite as footwall, includes the farms Overysel 816 LR, Drenthe 778 LR, Witrivier 777 LR and northwards;

the central sector, which is composed of the Malmani dolomite as footwall, includes the farms Zwartfontein, Sandsloot 236 KR, Vaalkop and Tweefontein; and the southern sector, which has a footwall made of shales, banded ironstones, calc-silicates, mudstones and siltstones, extends from Townlands 44 KS in the south to Tweefontein in the north.
To the south of Mokopane the Platreef package is striking northwest with a dip ranging from 15 to 27º west, while to the north, the strike orientation changes to northwest then north, with dip angles less than 45º towards the west (Kinnaird et al., 2005).

A group of faults; striking NS, ENE and ESE, and dipping west and south, offset the Platreef (Harris and Chaumba, 2001; Armitage et al., 2002; Kinnaird et al., 2005; Nex, 2005; Holwell and Jordaan, 2006; Van der Merwe et al., 2012). According to Bye and Bell (2001), the fault architecture occurred before the Bushveld Complex intrusion. This has led some researchers (Kinnaird et al., 2005) to suggest its control on the thickness of the rock succession, mainly in the southern sector of the Northern limb, while Nex (2005) suggested its control on the PGE mineralisation on Tweefontein Hill.

There are major types of dykes (pegmatoidal mafic, granitic and dolerite) and veins (quartz-feldspathic) cutting across the Platreef which have also been reported (Harris and Chaumba, 2001; Armitage et al., 2002; McDonald et al., 2005; Kinnaird et al., 2005; Van der Merwe et al., 2012). Moreover, Kinnaird et al. (2005) suggested the formation of the major ‘dolomite tongue’ sticking out into the Northern limb at Sandsloot is due to footwall high or a diapiric mobilisation of footwall into a dome as those studied from the Eastern limb by Uken and Watkeys (1997).

In terms of the upper and lower contact of the Platreef, some authors (Kinnaird et al., 2005; McDonald et al., 2005) suggest an irregular contact with its footwall, whereas a sharp and planar contact with the overlying MZ gabbronorite marked, in places, by a ‘mottled-textured’ anorthosite occurring mainly in the southern sector (Kinnaird et al., 2005). White (1994) reports a disturbed contact between the Platreef and its hangingwall indicated by norites and pyroxenites cycle, whereas others have described (1) a tectonised contact at the Sandsloot pit, displaying highly serpentinisation in brittle-ductile shear

zone up to 0.2 m in thickness (Armitage et al., 2002), (2) a chilling and erosional base of the hangingwall (Holwell et al., 2005) and lastly (3) a finger-shaped intrusion of the MZ gabbronorite within the Platreef lithologies (Holwell and Jordaan, 2006).

2.1.2.4 The Main Zone (MZ)

The MZ is up to 2,000 m in thickness and comprises gabbros, gabbronorites and norites with four major pyroxenite layers occurring ~300 m over the Platreef (Van der Merwe, 1978; Roelofse and Ashwal, 2012). There is a troctolite of ~200 m in thickness developed ~1,100 m over the Platreef (Van der Merwe, 1978; Roelofse and Ashwal, 2012), which according to Ashwal et al. (2005) is not present in the rest of the BIC. However, Van der Merwe (1976) identified a pyroxenite showing similarities with the pyroxenite marker in the Western and Eastern BIC, found ~2,000 m over the Platreef. In contrast, this pyroxenite unit was not found south of Mokopane (McDonald et al., 2005) and is missing from the stratigraphy by others authors (Hulbert, 1983; Von Gruenewaldt et al., 1989, Ashwal et al., 2005). Further north from Swerwerskraal 736 LR, the MZ is overlaying the Archaean granite and eventually the UZ caps the Archaean granite in the far north (Van der Merwe, 1978; Roelofse and Ashwal, 2012). Recent studies have suggested the lower part of the MZ intruded by the repetitive intrusion of crystal mushes from a deeper staging chamber (Roelofse et al., 2009; Roelofse and Ashwal, 2012).

2.1.2.5 The Upper Zone (UZ)

The thickness of the UZ is ~1,500 m thick from Ashwal et al. (2005). This zone displays cyclic units comprised of magnetitite layers at the base overlain by magnetite gabbro, gabbro, olivine diorite and anorthosite (Ashwal et al., 2005). McDonald et al. (2005) suggest one of these magnetites to be correlated with the Main Magnetite layer elsewhere in the BIC (Van der Merwe, 1976; Von Gruenewaldt et al., 1989) due to its thickness and vanadium content. To the west of the Northern BIC, the cap rocks comprise a variety of Bushveld granites and meta-sedimentary rocks (Kinnaird et al., 2005).

2.1.2.6 Mineralisation

PGE mineralisation in the Northern limb occurs at various localities and within different lithologies. The more significant are hosted within the Volspruit pyroxenite sub-zone, the GNPA, the Platreef and, further north, in the MZ (Hulbert and Von Gruenewaldt, 1982; Hutchinson and Kinnaird, 2005; McDonald and Harmer, 2010; Kinnaird et al., 2012; Holwell et al., 2013).

In the Volspruit pyroxenite subzone, PGE occurs associated with Cu-Ni sulphides at the base of the mineralised zone (Hulbert and Von Gruenewaldt, 1982). In the GNPA, the top section hosts PGE mineralisation and is xenolith-rich (Von Gruenewaldt et al., 1989). A similar observation was made by Maier et al. (2008) whom, in addition, have also identified a mineralised layer at the base of the GNPA member.

Within the Platreef, the PGE mineralisation is hosted within (1) pyroxenitic lithologies mostly associated with Cu-Ni sulphides (Armitage et al., 2002; Kinnaird et al., 2005; Holwell and McDonald, 2006) and (2) within harzburgite (Mitchell and Scoon, 2012). However in the footwall assemblages, the PGE mineralisation is mainly associated with arsenides, tellurides, antimonides and bismuthides (Armitage et al., 2002; Hutchinson and Kinnaird, 2005; Holwell and McDonald, 2006).

Further north within the Northern limb, on the farms La Pucella 69LR, Nonnenwerth 421LR, Kransplaats 422LR and in the Waterberg project, Cu-Ni-PGE mineralisation is developed in gabbroic rocks of the MZ (Harmer et al., 2004; McDonald and Harmer, 2010; Kinnaird et al., 2012) whereas in the south, on Moordrift farm, the PGE mineralisation, associated with Cu-Ni sulphides, is hosted within a sequence of gabbronorites, anorthosites and pyroxenites (Holwell et al., 2013).

2.2 Local geology

This chapter describes the local geology on the farms Sandsloot 236KR and Overysel 816LR using open pit mapping and/ or borehole information from previously published literatures (Harris and Chaumba, 2001; Armitage et al., 2002; McDonald et al., 2005). In addition to the published information on the geology of the Sandsloot open pit, the

geology of the Zwartfontein south open pit by Holwell and Jordaan (2006) were also considered since the Platreef has the same floor rock and is in the vicinity of the Sandsloot farm. This does not, in any way, suggest a simplified Platreef as it has been proven to be a very complex ore body.

The generalized rock succession on the farms Sandsloot 236KR and Overysel 816LR, from the base to the top, is comprised of (1) the footwall; (2) the Platreef rocks; and (3) the MZ lithologies. The local geology on the two farms is described below.

2.2.1 Local geology of Sandsloot 236 KR farm

The major lithology identified in this part of the Northern limb, from the base to the top, consists of: (1) the metamorphosed and/ or metasomatised dolomite of the Malmani Subgroup, which is the floor rock (or footwall); (2) the Platreef pyroxenite, gabbro and minor peridotite; and (3) the hangingwall norites and gabbronorites usually allocated to the MZ, all of variable thickness (Harris and Chaumba, 2001; Armitage et al., 2002; McDonald et al., 2005; Holwell and Jordaan, 2006). There are also many quartz-rich veins and mafic dykes cutting across the major rock types, and xenoliths of the footwall occur within the Platreef and MZ lithologies which are dipping westwards at a moderate angle (Harris and Chaumba, 2001; Armitage et al., 2002; Holwell and Jordaan, 2006; Ihlenfeld and Keays, 2011).

The footwall is comprised of variably metamorphosed and/ or metasomatised dolomite namely; calc-silicates, clinopyroxenites (with or without olivine) and serpentinites (Harris and Chaumba, 2001; Armitage et al., 2002; McDonald et al., 2005; Holwell and Jordaan, 2006). The calc-silicates are comparatively unaltered floor rock hornfelses. These rocks have retained their sedimentary layering and comprise metamorphic minerals suggestive of various prograde and retrograde reactions.

The clinopyroxenites are clinopyroxene-rich lithologies which may also contain abundant olivine in places (also termed olivine-rich clinopyroxenites). Other minerals that may be present in these rocks are spinel, biotite, calcite, amphibole, chlorite and serpentine. In

these rocks, clinopyroxenes are mainly granoblastic, interlocked with each other and, in places, are recrystallised showing 120˚ grains boundaries.
Footwall serpentinites are altered floor rock hornfels and or olivine-rich clinopyroxenites. They are product of hydrothermal alteration; mainly serpentinisation, of metamorphic olivine present in these rocks. These units are dark (black in color), which makes it difficult to identify whether they had sedimentary or igneous protoliths.

The Platreef comprises mainly feldspathic pyroxenites with varying amounts of gabbros, peridotites and serpentinites (Harris and Chaumba, 2001; Armitage et al., 2002; McDonald et al., 2005; Holwell and Jordaan, 2006).

The feldspathic pyroxenites are predominantly orthopyroxene- rich (~90% by volume) with interstitial plagioclase (~10% vol.). In places, they may contain orthopyroxene (60 - 90% vol.), clinopyroxene (10 - 40% vol.) with interstitial plagioclase (~15% vol.). The pyroxenes are coarse-grained, reaching sometimes a maximum size greater than 10mm. The accessory minerals consist of biotite, base metal sulphides (pyrrhotite, pentlandite, chalcopyrite, bornite, pyrite and etc…) and minor oxides (magnetite, ilmenite, chromite, etc…). In some places, the pyroxene grains are altered to serpentine and talc, whereas plagioclase is altered to fine-grained white mica.
The gabbros are coarse-grained to pegmatoidal with cumulus orthopyroxene (40 - 90% vol.) and clinopyroxene (up to 10% vol.) with post cumulus plagioclase (30 - 50% vol.). Pyroxene grains are sub- to euhedral and are interlocking with each other. The accessory minerals are biotite, base metal sulphides (pyrrhotite, pentlandite, chalcopyrite, etc…), oxides and minor quartz. In this unit, the BMS grains are irregular and coarser than those found in the Platreef feldspathic pyroxenites.
The Platreef serpentinites are highly altered rock resulting from the hydrothermal alteration (or serpentinisation) of the Platreef lithologies (e.g. pyroxenites, gabbros and peridotites). They are dark in hand specimen and most minerals are altered under thin section. Thus, it is very difficult to differentiate them from their footwall counterpart and furthermore to identify their igneous protoliths.

The MZ rock types comprise norites and gabbronorites (Harris and Chaumba, 2001; Armitage et al., 2002; McDonald et al., 2005; Holwell and Jordaan, 2006). The norites are medium-grained and generally comprise cumulus plagioclase laths (60 - 70% vol.) and orthopyroxene (30 - 40 % vol.). Fine-grained clinopyroxenes occur as post cumulus. The accessory minerals, which consist of biotite, oxides and quartz, occur mostly interstitial to plagioclase and orthopyroxene. In places, amphibole is also present as an alteration product of the pyroxenes.

The gabbronorites have mineral grain sizes ranging from medium to coarse. The rock consists of plagioclase laths (~50% vol.), orthopyroxene (~35% vol.) and clinopyroxene (~15% vol.). The pyroxenes are subhedral and, in places, interlocking with each other producing large aggregates, whereas plagioclase laths are randomly orientated. Biotite, oxides and sulphides occur as accessory phases (reaching ~ 5% vol. in places).

The fine-grained ferro gabbro dyke comprises orthopyroxene (50% vol.), plagioclase (40 - 45% vol.) and oxides (5 - 10% vol.). The grain sizes range from 1 - 2 mm. Plagioclase is post cumulus and occurs interstitial to orthopyroxene. The plagioclase is altered to fine-grained white mica in places. In addition, there is also a pegmatoidal mafic dyke of 4 - 5 m thick comprising cumulus feldspar with intercumulus sub- to euhedral pyroxene. Accessory phases are biotite and oxides. The BMS are rare, but when present they are large interstitial blebs of pyrrhotite and pentlandite occurring sporadically.

The quartz-rich vein, which is up to ~1 m in thickness, is mainly composed of albite and quartz interlocking with each other. Biotite, if present, is altered to chlorite in places. In addition, minor calcite grains also occur in the vein.

The PGE mineralisation is mainly hosted within the Platreef and footwall rocks (Harris and Chaumba, 2001; Armitage et al., 2002). Within the Platreef lithologies, the PGE mineralisation was initiated by orthomagmatic sulphide segregation. The PGM were later redistributed in the footwall and other area of the Platreef lithologies by fluid activity, where PGE are associated with antimonides, tellurides, bismuthotellurides and lower-temperature alloys.

2.2.2 Local geology of Overysel 816 LR farm

On this farm, the rock sequence, from the base to the top, consists of: (1) the Archaean Utrecht granite and Hout River gneisses as floor rock; (2) the Platreef feldspathic pyroxenite (fine- to coarse-grained); and (3) the hangingwall MZ gabbronorites and melanorites (Holwell and McDonald, 2006; Ihlenfeld and Keays, 2011). The Platreef feldspathic pyroxenites contain xenolith materials in places and, in some case, occur as sills intercalated by intrusive norites and/ or gabbronorites layers.

The fine- to medium-grained granites are pink in color at hand specimen. The gneisses have variable thickness and are also termed granofels or enderbites on mineralogical and textural attributes (Cawthorn et al., 1985). The granofels are characterized by series of banded gneisses which have quartzo-feldspathic (pale in color) and orthopyroxene-rich layering (Holwell and McDonald, 2006).

The Platreef is comprised of fine- and coarse-grained feldspathic pyroxenites. The coarse-grained feldspathic pyroxenites comprise cumulus orthopyroxene (75 - 90% vol.), interstitial plagioclase (5 - 20% vol.), clinopyroxene (5% vol.) and minor quartz. The accessory minerals are biotite, BMS, chromite and ilmenite. Plagioclase is variably altered to sericite in places. A fine-grained feldspathic pyroxenite, occurring underneath the hangingwall contact, is made up of cumulus orthopyroxenes, clinopyroxene (~10% vol.) and is noted to be not mineralised.

The Platreef feldspathic pyroxenites in contact with the floor rock contain abundant quartz in the interstitial assemblage as well as, disseminated chromite and veinlets of quartzo-feldspathic material. The BMS (mainly pyrrhotite at the core and pentlandite with chalcopyrite at the rims) also occur as blebs. In addition, thin chromitite layers occur within the Platreef feldspathic pyroxenites. These chromitites contain cumulus chromite grains (~50% vol.) within plagioclase and orthopyroxene. The BMS (pentlandite and minor chalcopyrite) are also present.

The intrusive norite contains plagioclase (~55% vol.), orthopyroxene (30% vol.), clinopyroxene (10% vol.) and quartz (5% vol.). The orthopyroxene grains are altered by amphiboles, whereas plagioclase is altered by sericite in places. These norites occur as fine-grained as well as coarse-grained rocks. Both rocks have the same mineralogy. However, the coarse-grained lithology contains abundant quartz as well as BMS blebs, but the fine-grained rock is not mineralised.

Calc-silicate xenoliths are also identified within the Platreef feldspathic pyroxenites marked by a gradational contact between the two rocks. These xenoliths are olivine and clinopyroxene-rich and contain variable proportions of, orthopyroxene, amphibole, wollastonite, calcite, and andradite garnet. They are serpentinised in places (mainly within olivine-bearing xenoliths) and also contain some magnetite and BMS (mostly pyrrhotite). The serpentinised rocks (or simply serpentinites) from olivine-rich meta-sedimentary protolith can be distinguished from those of igneous protolith of the Platreef by their lower Cr content.

The hangingwall MZ gabbronorites comprise cumulus plagioclase laths (40 - 80% vol.) with cumulus orthopyroxene and post cumulus anhedral clinopyroxene. The accessory phases are ilmenite and BMS, which are all occurring in small quantities. The melanorites are fine-grained and are comprised of plagioclase laths (50% vol.), orthopyroxene (35% vol.) and clinopyroxene (15% vol.).

The PGE mineralisation occurs mainly within the feldspathic pyroxenites and footwall gneisses (or granofels) and is mainly associated with the presence of the BMS. In serpentinised calc-silicate xenoliths, hydrothermal activity has played a role in redistributing the PGEs which are associated with low-temperature sulphide assemblages.

Based on the IUGS classification, the feldspathic pyroxenites are norites, but to avoid confusion with the MZ norites and gabbronorites which postdate the Platreef intrusion, the term norite is used for MZ rocks and feldspathic pyroxenite for Platreef to conform to the Bushveld Complex nomenclature (Holwell and McDonald, 2006).

Chapter 3

3. Methodology

3.1 Field methods and sampling

The field work was conducted in April 2010 from the 09th to the 14th. A desk study was carried out prior to the field work relating to the assimilation and/ or contamination of the Platreef-forming magma by different floor rocks and the styles of mineralisation.

A downhole sampling pattern was used in the field whereby quarter cores of about 20 to 30 centimetre in length (Plate 1) were collected from two drill holes provided by Anglo Platinum. Boreholes SS 330 and OY 482 were drilled on the farms Sandsloot 236 KR and Overysel 816 LR, respectively. The sampling was done at irregular intervals and was based on rock type, lithological contacts, alteration and sulphide mineralised areas.

The collection includes a total of 119 samples from which 80 quarter cores were sampled from SS 330 (628 m thickness) and 39 from OY 482 (194 m thickness). The samples were transported to the University of the Western Cape (UWC) in sealed sample bags for petrography and laboratory analysis. The sampling was performed with maximum care to minimize contamination.

3.2 Laboratory studies

3.2.1 Petrography

The detailed petrographical examination was performed at UWC on polished slides and thin sections cut from all rock samples. The mineral and modal compositions, textures, alterations and ore mineralogy (mainly the base metal sulphides) of the various rock types of interest were determined using a binocular microscope.

3.2.2 Geochemical sample preparation

At the laboratory, all rock samples were washed with distilled water and dried. A representative portion from each quarter core, weighing approximately 50g, was cut, crushed with a 5x3 inch Dickie & Stockler® jaw crusher machine and milled into powder for 5 minutes using the Dickie & Stockler® T-S 250 mill.

After each milling, the powder was removed from the milling pot and a handful of medium to coarse quartz grains were milled to remove the remaining powder and avoid contamination of the next rock sample. The milling pot was always washed with distilled water and cleaned to dryness after every single milling. All 119 rock samples were milled, kept in sealed sample bags for X-Ray Fluorescence (XRF) and Inductively Coupled Plasma Optical Emission Spectrometry (ICP-OES) analyses and loss on ignition (LOI) determination. The remaining cores were kept in separate sample bags.

Plate 1: Example of quarter core sampled from the studied boreholes.

For XRF analysis the methods used follow those of Norrish and Hutton (1969), wherein 9g from each milled rock sample were mixed with 2g of EMU wax binder in plastic vial

containers. The mixture was shaken to homogeneity and pressed into pellets at 15 kilo bars ready for major, minor and trace elements measurement.

For LOI, 0.5g from each milled sample was placed in a crucible and dried at 60ºC in an oven for 30 minutes to remove moisture. LOI was performed at 1000 ºC for 45 minutes following the methods described by Potts (1987) using the Labcon® L-1200 furnace.

3.2.3 Laboratory analyses

Analyses for oxides and trace element compositions (i.e. SiO_2, Al_2O_3, Fe_2O_3, MnO, MgO, CaO, Na_2O, K_2O, P_2O_5, TiO_2, SO_3, As, Ba, Ce, Co, Cu, Nb, Ni, Pb, Rb, Sr, V, Y, Zn, Zr, Mo, U and Th) were carried out at the geochemistry laboratories at UWC using a Phillips 1480 XRF spectrometer.

All 119 rock samples were analysed. Oxides are expressed in weight percent (wt %) and trace elements in parts per million (ppm). Platinum, Pd and gold (Au) were analysed by ICP-OES after their pre-concentration from 25g of milled rock sample on lead beads by fire-assay at Scientific Services laboratories in Cape Town using the method described by Hall et al. (1990).

The geochemical dataset containing whole rock analyses of oxides and trace elements determined by the two laboratories using the geochemical methods mentioned above is presented in Appendix II.

3.3 Data quality control/ quality assurance`

Laboratory quality control/quality assurance (QA/QC) measures were included into all analytical work. In addition, internal data quality procedures were used that comprised analysis of reference standards.

A total of ten samples were duplicated and measured by XRF analysis. The oxides and trace element data from the first sample (or simply original) and that of the duplicate were plotted on scatter diagrams to verify the analytical (precision) errors. For example, Figure 2a shows the precision control scatter plot for the original and duplicate data for Al_2O_3. On this plot, all the data points fall on the 1:1 control line and show the analytical

error to be less than 5%. In Figure 2b, the data for Nb shows scattering of the data points on the precision plot whereby four points exceed the 15% error margins.

The precision errors were < 5% for all oxides while all the trace elements have some data points exceeding the 15% error margins.

The accuracy of < 5% was estimated for the following reference standards: NIM-L, NIM-P & SARM-50. For Pt, Pd and Au, the accuracy of < 5% was estimated using the reference standard ST 265 at Scientific Services laboratories by fire-assay / ICP finish.

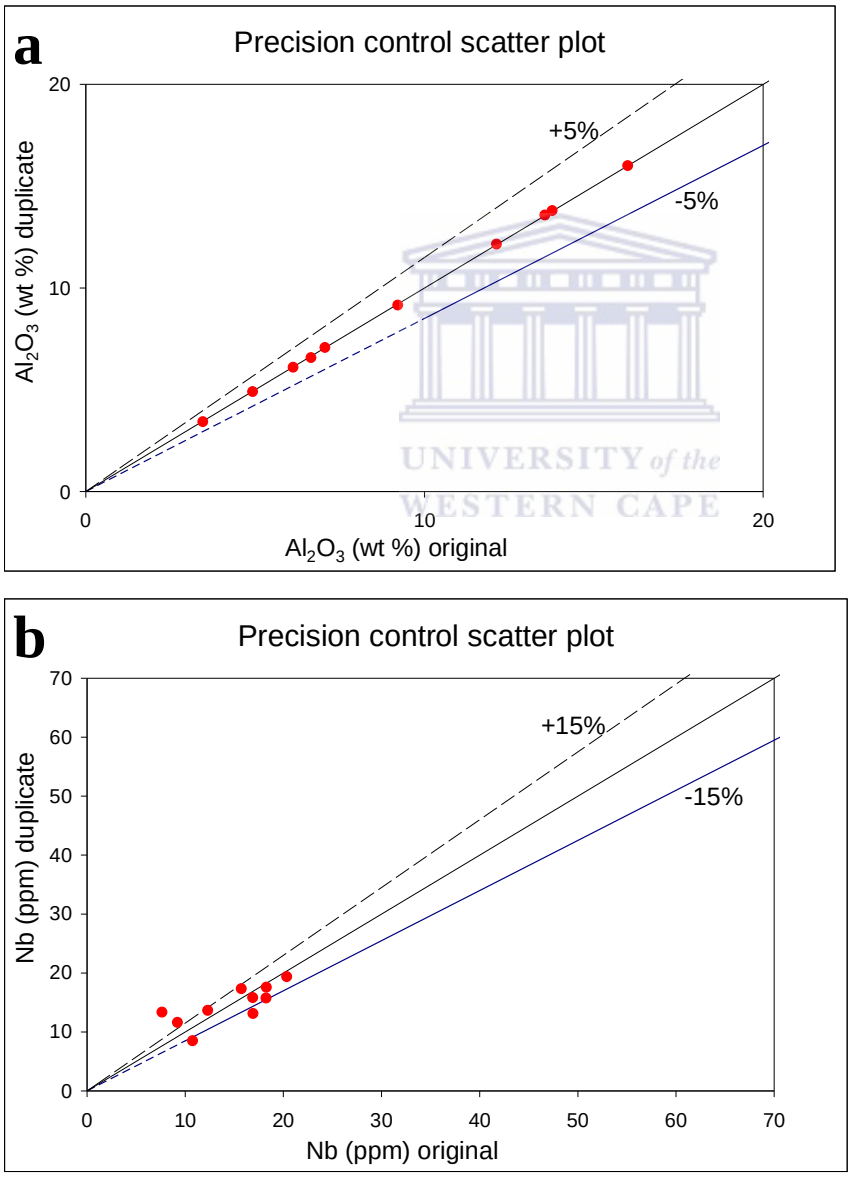

Fig. 2 Precision control scatter plots of selected analytical data

3.4 Data evaluation/ analysis

Prior to data evaluation, the petrographical study was conducted on thin and polished sections cut from quarter core samples taken from the two boreholes to examine their mineral compositions, textures, alterations and ore mineralogy (sulphides). This was firstly done to identify and classify the rock types/ subtypes or metasomatic subzones, and secondly to identify their petrographical attributes that reflect processes useful for stratigraphic correlation. A summary of the petrography is presented in Table 1.

In order to achieve chemostratigraphic correlations and develop geochemical vectors, the analytical data of the two boreholes were processed using computer packages such as; SPSS 20®, Geochemical Data Toolkit® (GCDkit), EASYGRESGRANT® and Downhole Explorer®. Data evaluations were carried out to achieve the following objectives.

First, the geochemical classification was performed using cluster analysis applied on the analytical data of the rocks to identify groupings/ sub-groupings that correlate with the different rock types/ subtypes or metasomatic zones determined from the petrography. This was done in order to determine the geochemical/ chemostratigraphic characteristics of these rock types/ subtypes or metasomatic zones using box and whiskers plots. The results of cluster analysis are presented in the form of dendrograms (Figs. 7, 9, 11 & 13) while, the box and whisker plots are shown in Figures 8, 10, 12 & 14.

Secondly, the characterisation of the aforesaid rock types/ subtypes or metasomatic zones was done using their major and trace element data. In the first step, spider diagrams were used to investigate the behaviour of large ion lithophile elements (LILE; i.e. Sr, Rb and Ba) and high field strength elements (HFSE; Th, U, Ce, Zr, Nb, Ti and Y) in these rock types/ subtypes or metasomatic zones. The second step involved the calculation of various immobile element ratios and trace element anomalies from the dataset of the different rock types/ subtypes. These were tabulated along with statistical summaries of oxides and trace elements to fingerprint the behaviour of the LILE and HFSE in the rock types/ subtypes or metasomatic zones. The result from the spider diagrams are presented

in Figures 15, 16, 17, 18, 19, 20 & 21 while, the statistical summaries are displayed in Tables 2, 3 & 4.

Thirdly, mass balance calculations were executed in order to identify quantitatively the relative elemental exchange, firstly between the metasomatic subtypes and the footwall metadolomite in borehole SS 330 and secondly between the Platreef feldspathic pyroxenites and the Archaean granite/ gneisses floor rock in borehole OY 482, and the metasomatic subtypes in SS 330, which does not intersect pristine Platreef magmatic rocks. The results quantifying the elemental exchange in the aforementioned steps are displayed in Figures 25, 26, 28 and 29.

Fourthly, the geochemical indices/ ratios were developed in two steps. Firstly, the major elements derived from the geochemical classification and characterisation, and the mass balance calculation between the various rock types/ subtypes were used to produce indices that distinguish each rock type from others on bivariate variation plots (Fig. 30). This was followed by establishing the relationship between the major element ratios and the BMS mineralisation using the ternary diagram (Fig. 31). The second step involved the use of the base metal elements (Ni, Cu, Co and Zn) and PGEs (Pt and Pd) to produce base metal indices that are able to delineate PGE-rich zones from barren ones.

Lastly, a spatial assessment of the geochemical indices and vectors was investigated to assess their practicality in delineating lithological units and PGE-mineralised from barren zones, respectively. These were done using down-hole plots form boreholes SS 330 and OY 482, and are presented in Figures 35 and 36.

Chapter 4

4. Petrography

4.1 Stratigraphy and petrography of studied boreholes

The lithostratigraphy of the two boreholes studied was determined from the core logging. However, the rock succession in conjunction with the petrographical observations has provided further details about the lithostratigraphy of these boreholes. The thicknesses of the rocks are not true thicknesses as the boreholes were drilled at certain angles.

Sections 4.2 and 4.3 below summarize the modal mineralogical compositions and textural attributes of the rocks of interest determined from the core logging and petrographical observations in boreholes OY 482 and SS 330, respectively.

4.2 Borehole OY 482

4.2.1 Lithostratigraphy determined from core logging

Borehole OY 482 is 194 m in length (Fig. 3) and was drilled at the Overysel farm (Fig. 1). From bottom to top, the simplified lithostratigraphy in OY 482 consists of ~3 m thick Archaean granite grading into gneisses of ~4 m in thickness (Fig. 3). The latter is overlain by Platreef feldspathic pyroxenites, which occur as 8 interrupted sills of varying thicknesses at various depths, intercalated by fine- to coarse-grained gabbronorite sills (Fig. 3). There is serpentinisation from 390 - 385 m depth and the occurrence of a leuco-gabbronorite sill at ~315 m depth (Fig. 3). The contacts between the various Platreef feldspathic pyroxenites and gabbronorite sills are mainly sharp below 400 m depth and are gradational above this depth (Fig. 3).

In hand specimen, the floor rock Archaean granite and gneisses are similar with those described by Holwell and McDonald (2006). This footwall and gabbronorite sills were not investigated in this study, but an overall description of the gabbronorites will also be given in sections below so as to compare them with the Platreef feldspathic pyroxenites.

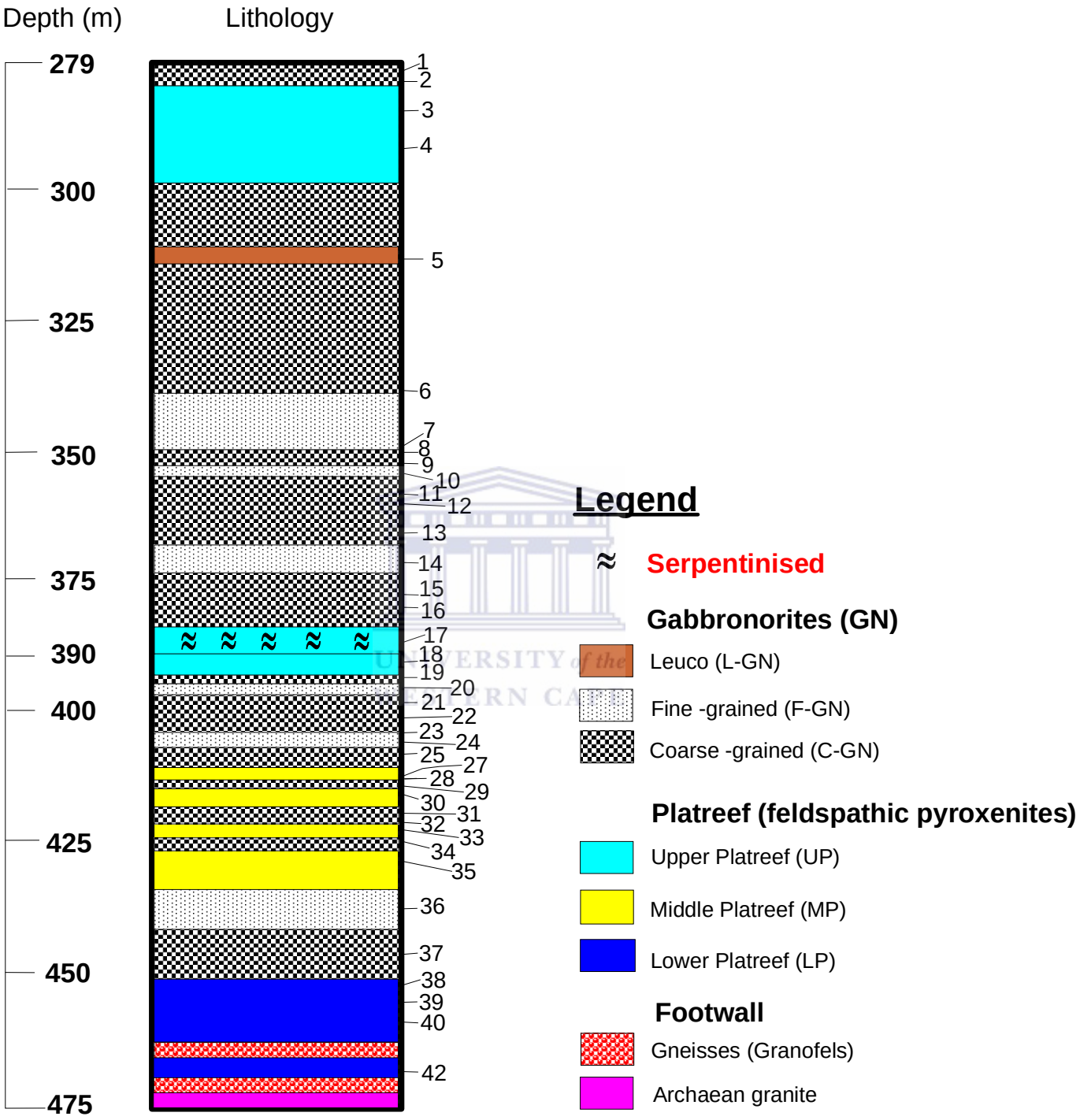

Fig. 3 Stratigraphic log of borehole OY 482 determined from core logging and petrographic observations; i.e. the modal mineralogical compositions and textural attributes. Location of samples investigated in this study is displayed on the right side of the log.

4.2.2 Description of the lithologies investigated

The following petrographic description focuses mainly on the various Platreef feldspathic pyroxenite sills which are irregularly mineralised with BMS and PGE.

On the basis of a synthesis of macroscopic and microscopic observations, and along with their spatial positions relative to the Archaean granite/ gneisses floor rock, the Platreef feldspathic pyroxenite sills in borehole OY 482 can be subdivided into three major lithostratigraphic units (Fig. 3). From the basal contact of the Platreef with the Archaean granite/ gneisses upwards, these units are: 1) the Lower Platreef, consisting of 2 sills, occurs below 450 m depth; 2) the Middle Platreef, made up of 4 sills, is located from 440 - 410 m depth; and 3) the Upper Platreef (has 2 sills above 395 m depth), which has been serpentinised within few meter above 390 m depth (Fig. 3).

Sections below present the microscopic study of the three lithostratigraphic units of the Platreef in borehole OY 482. This study includes the modal mineralogical compositions and textural attributes of the studied rocks, in that order.
Firstly, the modal composition was assessed using the three-phase modal classification scheme (opx-cpx-plag) proposed by Phinney (1972) which defines the modal boundaries for mafic rocks. The modal scheme was not used for the rocks classification in this work to avoid confusion with the Bushveld Complex nomenclature (see chapter 2.2.2), but to confirm the varying pyroxenitic composition of the studied rocks. Their modal data are presented in Appendix I and their modal compositions are shown in Figure 4 below. Secondly, the textural attributes of the studied rocks, which were identified on thin and polished sections from the rock samples, are described in section 4.2.2.1.

Figure 4 below shows the modal mineralogical compositions of the Platreef feldspathic pyroxenites in OY 482. In this figure, it can be seen that all sample points plot within the pyroxenitic modal fields; i.e. pyroxenite and feldspathic pyroxenite, and their mineralogy is predominantly controlled by orthopyroxene.

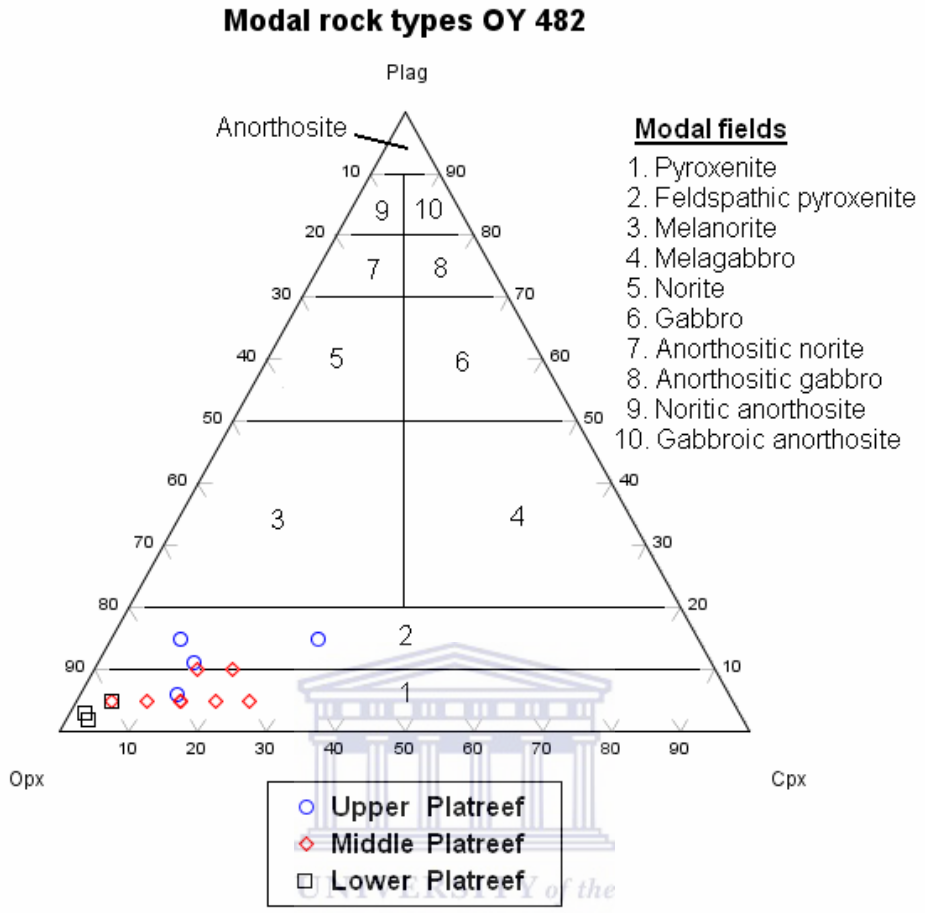

Fig. 4 Modal composition of Platreef feldspathic pyroxenites taken from borehole OY 482 based on relative proportions of orthopyroxene (opx), clinopyroxene (cpx) and plagioclase (plag). The base was taken from Phinney (1972).

The Lower Platreef samples have the highest orthopyroxene and lowest clinopyroxene and plagioclase contents when compared to samples from the other units (Fig. 4). The Middle Platreef samples have fairly consistent plagioclase content (Fig. 4). However, they display varying contents in orthopyroxene and clinopyroxene as opposed to sample of the Upper Platreef (Fig. 4). The latter comprises rock samples which have fairly consistent pyroxenes contents (i.e. orthopyroxene and clinopyroxene) and display a slight gradual increase in plagioclase content as they plot from the pyroxenite up to the feldspathic pyroxenite modal fields (Fig. 4). The serpentinised Upper Platreef sample point shows the lowest orthopyroxene content (Fig. 4). This may be due to the fact that orthopyroxene has been replaced by amphibole.

Section 4.2.2.1 below presents the petrographical attributes of the Platreef feldspathic pyroxenites in OY 482. A brief summary of the gabbronorites is also presented in section 4.2.2.2 for comparison as stated earlier.

4.2.2.1 Platreef feldspathic pyroxenites

As stated earlier, the Platreef feldspathic pyroxenite sills in OY 482 were classified into three major lithostratigraphic units as shown in Figure 3. The following paragraphs present the textural attributes of the Platreef units from the bottom up to the top.

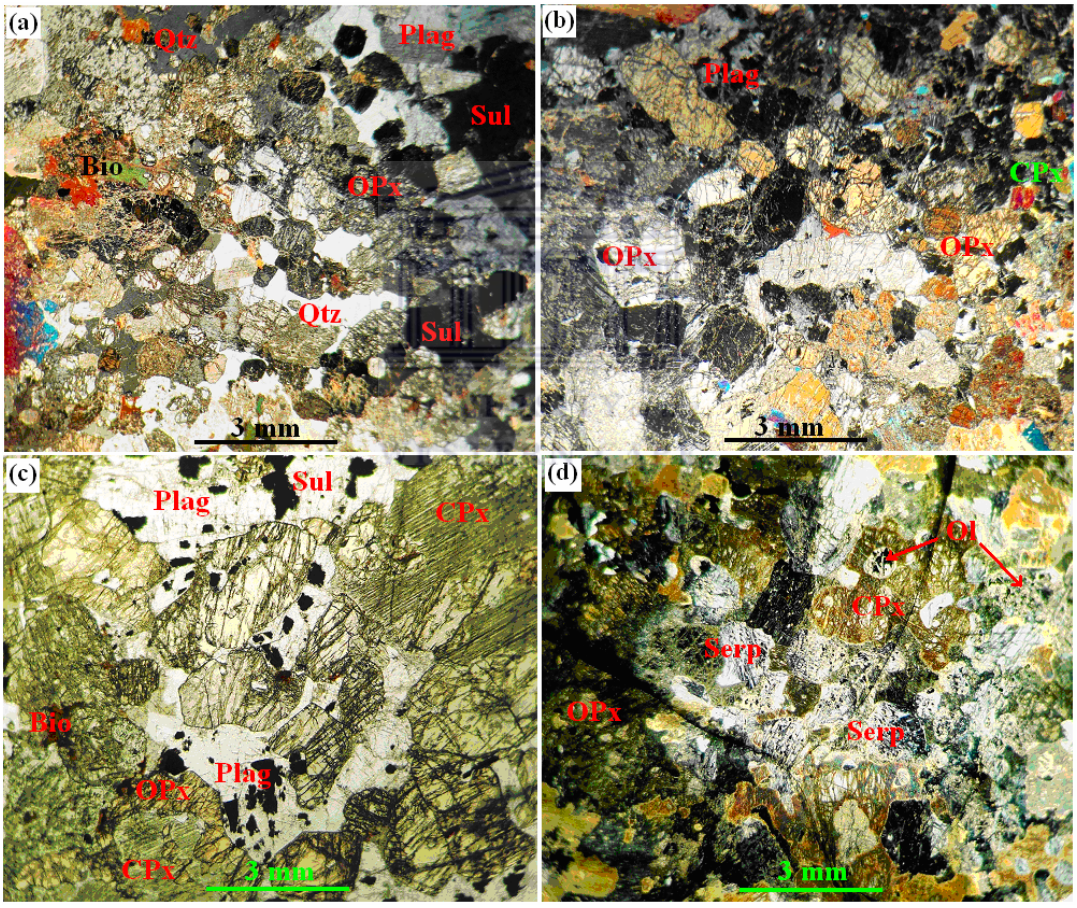

Plate 2: Platreef feldspathic pyroxenites showing: *(a) anhedral quartz enclosing and interstitial to orthopyroxenes within the lower feldspathic unit (XPL); (b) a cumulate texture (Middle feldspathic unit; XPL); (c) an interlocking texture between pyroxenes and plagioclase (Upper feldspathic unit; PPL) and (d) olivine inclusion within pyroxenes (Serpentinised pyroxenite; XPL).* XPL: Crossed polarized light; PPL: Plane polarized light.
Mineral abbreviations: Bio, biotite; Cpx, clinopyroxene; Ol, olivine; Opx, orthopyroxene; Plag, plagioclase; Qtz, quartz; Serp, serpentine; Sul, Sulphide.

4.2.2.1.1 Lower Platreef

The Lower Platreef consists of orthopyroxene (~ 90 vol. %), clinopyroxene (~5 vol. %) and plagioclase (~5 vol. %). Accessories are sulphides, biotite and quartz (~10 vol. %). These rocks are composed mainly of euhedral, fine to medium orthopyroxenes (0.5 to 2 mm in size). The latter occur as aggregates interlocking with each other and in places as single grains which are partially-to-totally enclosed by anhedral quartz grains (Plate 2a). Plagioclase forms single laths (~2 mm in length) mostly in association with quartz. Biotite occurs as single grains (~3 mm in size) interstitial to orthopyroxene grains (Plate 2a). In places minor clinopyroxenes and plagioclase are interstitial to orthopyroxenes. Sulphides occur as irregularly-shaped pyrrhotite, pentlandite and/ or chalcopyrite blebs (3 to 5 mm in size) in between or enveloping the pyroxenes and quartz grains (Plate 2a).

4.2.2.1.2 Middle Platreef

The Middle Platreef consists of orthopyroxene (70 - 90 vol. %), clinopyroxene (<25 vol. %) and plagioclase (<10 vol. %). Accessory minerals are sulphides, biotite and quartz. The rocks are comprised primarily of orthopyroxene grains which are medium-grained ranging from 1 to 3 mm in size (Plate 2b). The grains are euhedral and occur as aggregates interlocked either with each other or with minor interstitial plagioclase associated with small clinopyroxene grains (< 0.5 mm in size) in a cumulate texture (Plate 2b). Orthopyroxenes are variably uralitised in places and biotite occurs as single grains in between the pyroxenes. In places, minor quartz also occurs as anhedral single grains in between the pyroxenes. Interstitial plagioclase laths are variably sericitised and are associated with sulphide grains.

4.2.2.1.3 Upper Platreef

The Upper Platreef has orthopyroxene (70 - 80 vol. %), clinopyroxene (<15 vol. %) and plagioclase (5 - 20 vol. %). Accessory minerals are sulphides and biotite. The rocks in this unit comprise of orthopyroxenes which are medium to coarse ranging in size from 2 to 6 mm (Plate 2c). The grains are subhedral to euhedral and occur as single grains or aggregate with interstitial plagioclase (Plate 2c). The medium to coarse clinopyroxene grains (3 to 8 mm in size) are anhedral, interlocking with plagioclase and in places are

overgrown by orthopyroxenes (Plate 2c). Biotite grains (~1 mm in size) occur as single grains interstitial to pyroxenes (Plate 2c). The plagioclase is partially altered to sericite. Sulphides occur as disseminations of pyrrhotite, pentlandite and/ or chalcopyrite grains associated with the interstitial plagioclase (Plate 2c).

At 388 m depth (Sample 17; Fig. 3), small serpentinised olivine grains (1 to 2 mm in size) are poikilitically enclosed within clinopyroxenes (Plate 2d). The pyroxene grains are variably chloritised and, in places, partially replaced by amphibole. Sulphide grains (0.5 to 1 mm in size) are irregularly-shaped and mostly associated with serpentine.

4.2.2.2 Gabbronorites

The gabbronorite consists of clinopyroxene (40 - 60 vol. %), orthopyroxene (10 - 30 vol. %) and plagioclase laths (30 - 50 vol. %). Accessories are sulphides and biotite (<3 vol. %).

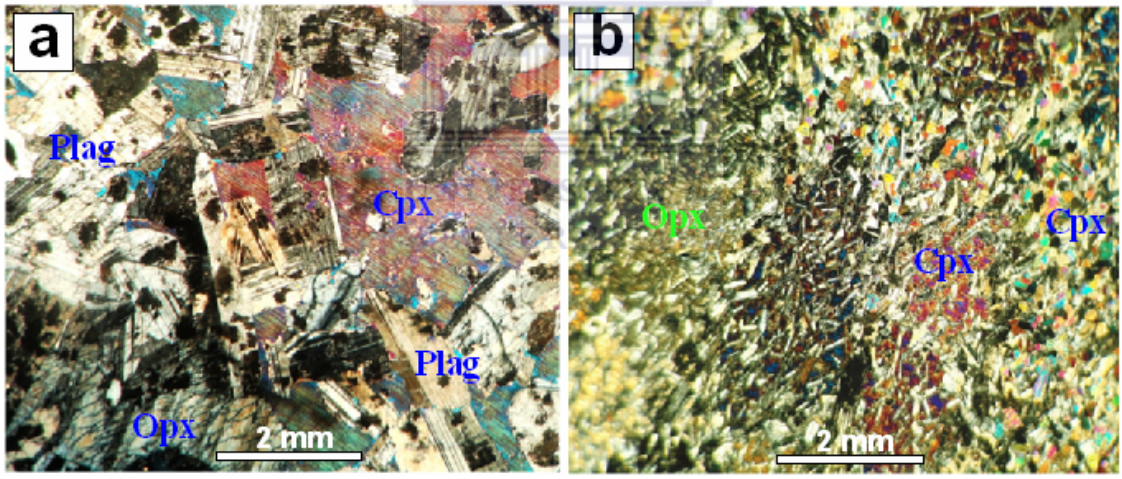

Plate 3: Gabbronorites showing: *(a) an interlocking texture of coarse-grained pyroxenes and plagioclase (XPL) and (b) fine-grained gabbronorite with a porphyritic and an ophitic texture (XPL).*

The coarse-grained gabbronorite is comprised of anhedral pyroxenes (clinopyroxenes and orthopyroxene grains) interlocked with plagioclase laths (Plate 3a). Within the fine-grained gabbronorite, subhedral and lath-shaped clinopyroxenes and orthopyroxenes (~ 4 mm in length) occur as aggregates surrounded by very fine-grained clinopyroxenes (Plate 3b). The pyroxenes also include very small plagioclase laths (Plate 3b). In these rocks, plagioclase laths are variably sericitised.

4.3 Borehole SS 330

The rationale in selecting borehole SS 330 for this study resides in the following facts. Firstly, this section contains economic grade of PGE and BMS mineralisation, and secondly the lithologies, which are not of pure magmatic origin and are products resulting from the injection of Platreef magma sills within the carbonate footwall, are appropriate for investigating the influence of this floor rock on the nature and styles of the PGE mineralisation in comparison to that with the granitic footwall in borehole OY 482.

4.3.1 Lithostratigraphy determined from core logging

Borehole SS 330 is 628 m in length (Fig. 5) and was drilled at the Sandsloot farm as shown in Figure 1. Upward from the base, the simplified rock succession in SS 330 consists of ~104 m thick metadolomite as the floor rock (Fig. 5). The latter grades transitionally into a predominantly Lower clinopyroxenite unit of 70 m thickness, located between 620 and 550 m depth, as seen in Figure 5. This clinopyroxenite unit also grades transitionally into the overlying 125 m thick predominantly olivine-rich clinopyroxenite (up to 425 m depth) which, in turn, is capped by 290 m thick Upper clinopyroxenite unit up to the top of the borehole at 96 m depth (Fig. 5).

A dolomite xenolith (~35 m thick), which is located between 295 and 260 m depth, is present within the Upper clinopyroxenite unit (Fig. 5). Throughout the borehole, various olivine-rich clinopyroxenite sills of varying thicknesses occur within the Lower and Upper clinopyroxenite units, and thin clinopyroxenite sills also occur within the olivine-rich clinopyroxenite unit (Fig. 5). The contacts between the various sills are gradual, but sharp in areas where two felsic veins, of ~1m thickness each, crosscut the borehole at 163 and 500 m depth, respectively (Fig. 5). These olivine-rich clinopyroxenite sills are variably serpentinised throughout the borehole and will be hereafter referred to as simply olivine clinopyroxenites (Fig. 5).

The metadolomite, dolomite xenolith and the two felsic veins were not investigated in this study, but a general account of the metadolomite will also be given in section below since its geochemical data will be used in the following chapter for comparison purposes.

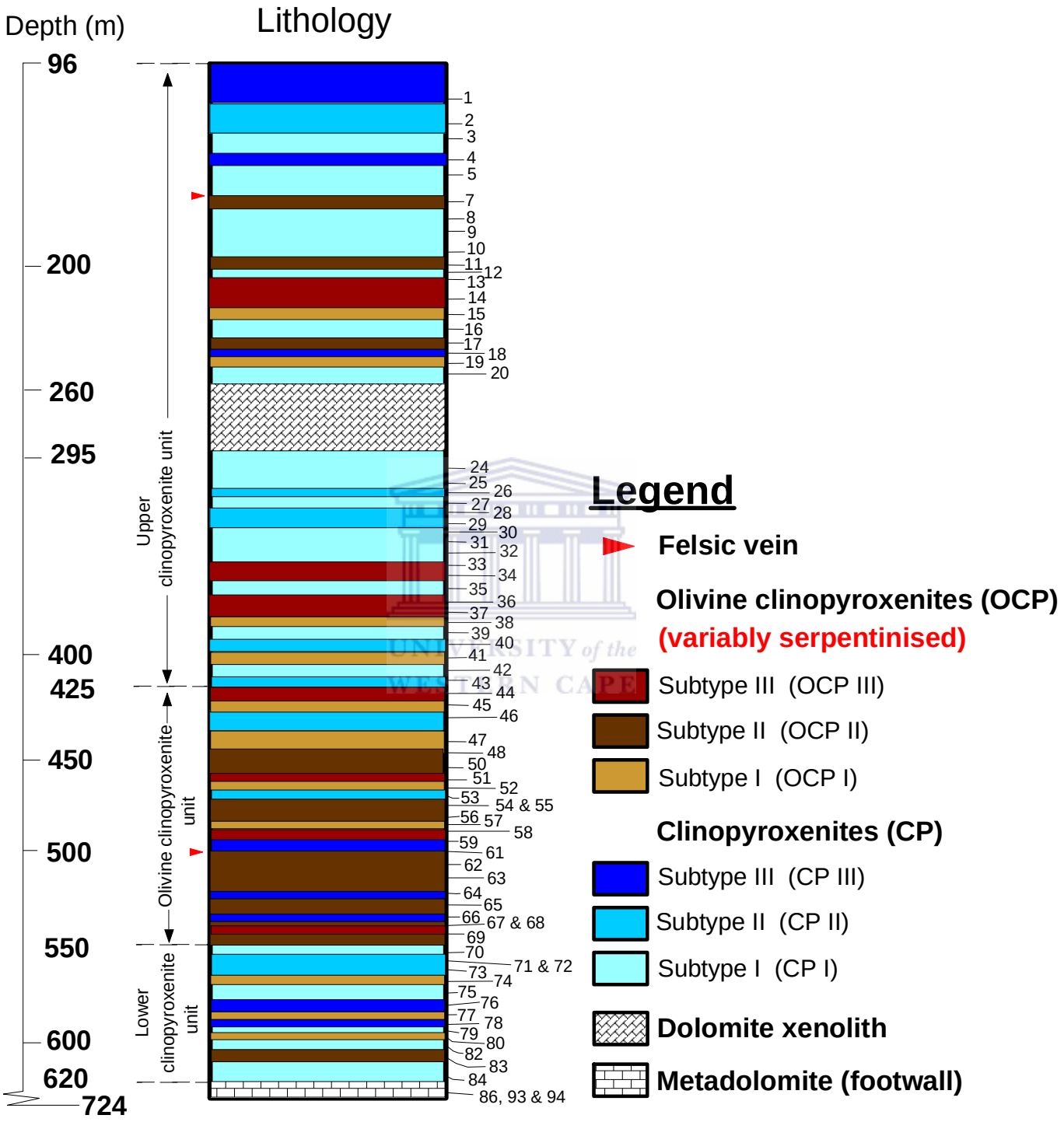

Fig. 5 Stratigraphic log of borehole SS 330 determined from core logging and petrographic observations; i.e. the modal mineralogical compositions and textural attributes. Location of samples investigated in this study is displayed on the right side of the log.

4.3.2 Description of the lithologies investigated

Borehole SS 330 did not intersect the Platreef pyroxenitic rocks (Fig. 5). Hence, the subsequent petrographical study focuses mainly on the two clinopyroxenitic-rich rocks which are irregularly mineralised with BMS and contain PGE.

The term clinopyroxenite, as used in this thesis, refers to calcium-bearing silicates, formed by metamorphism/ metasomatism of impure carbonates, and commonly formed at the contact zone between intrusions and country rocks, in this case the Platreef magma in contact with the Malmani dolomite (Harris and Chaumba, 2001; Armitage et al., 2002). The resulting metamorphic rocks may consist of a wide variety of mineral assemblages depending largely on the geometrical relationship between the intrusive body and the country rocks together with their compositions, the depth of emplacement and the composition of the magmatic fluid as seen from other intrusions (Ferry et al., 2002; Martins et al., 2003; Gaeta et al., 2009; Mollaei et al., 2009) and from the Platreef in particular (McDonald et al., 2005).

In this contact zone (borehole SS 330), two least metasomatised end members are obvious, one with a predominantly carbonate signature, termed clinopyroxenites, and the other with a primarily magmatic signature, in this case termed olivine clinopyroxenites. The rocks nomenclature above, which derived from the petrographic observations in this work and from previous investigation (McDonald et al., 2005), is being adopted for this study. However, on the basis of modal mineralogical compositions and textural attributes, the two clinopyroxenitic rocks are further subdivided each into three subtypes or metasomatic zones (Brady, 1977), as shown in Figure 5 above.

Summarised below is the microscopic study of the rock subtypes (metasomatic zones) in borehole SS 330. The study includes the modal mineralogical compositions and textural attributes of the clinopyroxenites and olivine clinopyroxenites, respectively.
In the first step, the modal mineralogical composition was assessed using the three-phase modal classification scheme (ol-cpx-plag) proposed by Miller et al. (2002) which defines

the modal boundaries for the mafic and ultramafic rocks. The scheme was not used to classify the rock samples of interest which are not magmatic, but to show their varying modal mineralogical compositions useful to determine the rock subtypes or metasomatic zones. The modal data of samples for the various subtypes are presented in Appendix I and their modal compositions are displayed in Figure 6 below. In the second step, the textural attributes of the clinopyroxenites and olivine clinopyroxenites were identified on thin and polished sections cut from the rock samples and are described in sections 4.3.2.2 and 4.3.2.3, respectively.

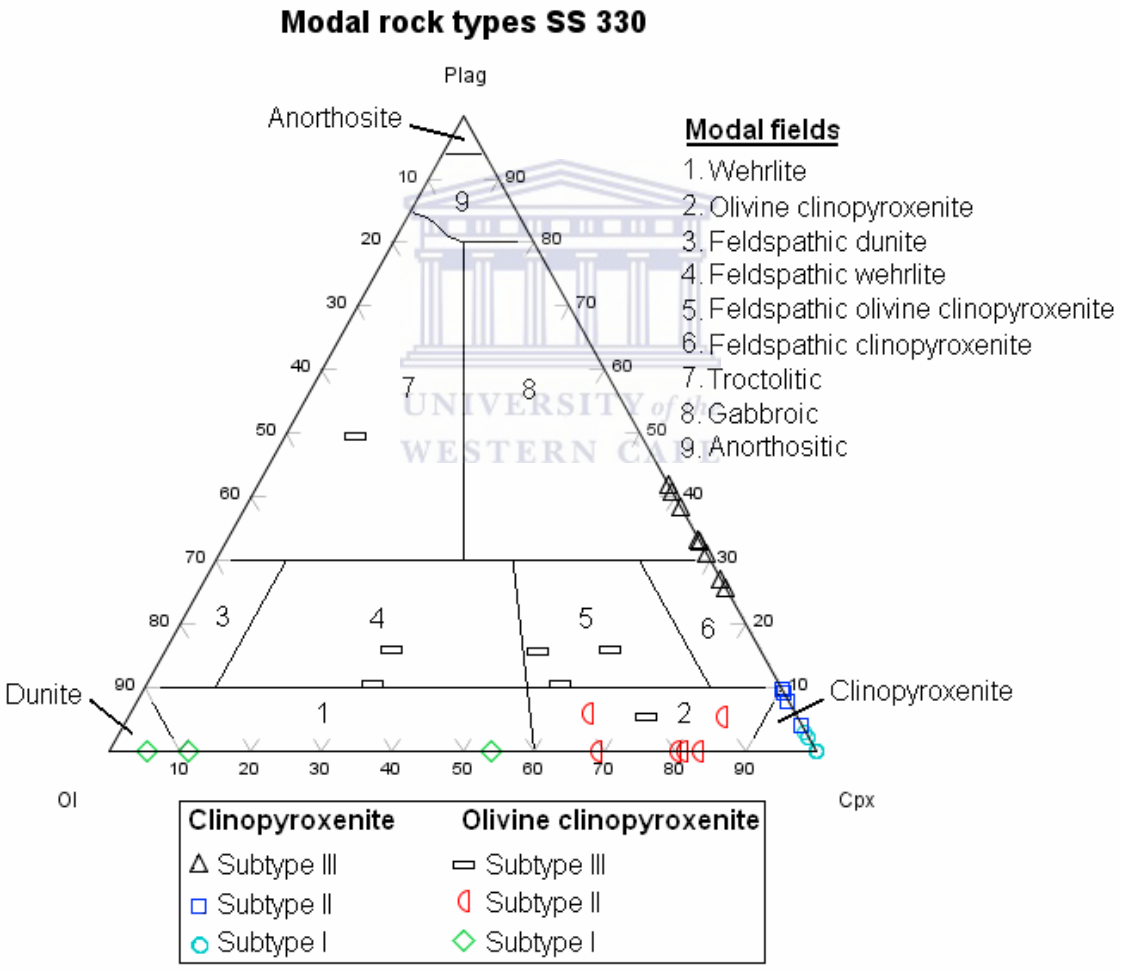

Fig. 6 Modal composition of selected samples taken from borehole SS 330 based on relative proportions of olivine (ol), clinopyroxene (cpx) and plagioclase (plag). The base was modified from Miller et al. (2002).

Figure 6 below shows the modal mineralogical composition of the clinopyroxenite and olivine clinopyroxenite samples which were used to determined the subtypes in SS 330.
In Figure 6, all clinopyroxenite sample points lie on the cpx-plag axis since they do not contain any olivine. However, these sample points range from the clinopyroxenitic to feldspathic clinopyroxenitic up to the gabbroic modal composition fields showing that the mineralogy in clinopyroxenite is mainly controlled by clinopyroxene and plagioclase, in that order (Fig. 6).
The olivine clinopyroxenite sample points are scattered on the plot showing that their mineralogy is mainly controlled by olivine, clinopyroxene and plagioclase (Fig. 6). The sample points range mainly from the wehrlitic-dunitic to the olivine clinopyroxenitic modal fields (Fig. 6). In addition, other sample points fall within the feldspathic field of two abovementioned fields (i.e. wehrlitic to olivine clinopyroxenitic) (Fig. 6). There is also one sample point within the troctolitic field (Fig. 6).

On these bases, the following rock subtypes or metasomatic zones were identified:

- For the clinopyroxenites (Fig. 6):
    - Subtype I: clinopyroxenitic (or weakly metasomatised),
        95 - 100 vol. % clinopyroxene, 0 - 5 vol. % plagioclase.
    - Subtype II: clinopyroxenitic (or moderately metasomatised),
        90 - 95 vol. % clinopyroxene, 5 - 10 vol. % plagioclase.
    - Subtype III: feldspathic to gabbroic (feldspathic moderately metasomatised),
        60 - 80 vol. % clinopyroxene, 20 - 40 vol. % plagioclase.
- For the olivine clinopyroxenites (Fig. 6):
    - Subtype I: dunitic, serpentinitic, wehrlitic (weakly metasomatised/ altered),
        40 - 90 vol. % olivine, 10 - 60 vol. % clinopyroxene.
    - Subtype II: olivine clinopyroxenitic (moderately metasomatised/ altered),
        10 - 40 vol. % olivine, 60 - 90 vol. % clinopyroxene.
    - Subtype III: feldspathic subtypes I & II (highly metasomatised/ altered),
        50 - 90 vol. % olivine + clinopyroxene, 10 - 50 vol. % plagioclase.

The term altered is added where subsequent hydrothermal alteration is observed, which applies particularly to the olivine clinopyroxenites (variably serpentinised; Fig. 5).

Sections 4.3.2.2 and 4.3.2.3 below present the petrographical attributes of the rock subtypes or metasomatic zones in SS 330. A brief summary of the metadolomite is also presented in section 4.3.2.1 as mentioned above.

4.3.2.1 Footwall metadolomites

The mineralogy in the rock consists mainly of fine- to medium-grained calcite/ dolomite and brucite ranging between 0.5 - 1.5 mm size in diameter (Plate 4). The rock displays a xenotopic texture consisting mostly of anhedral calcite/ dolomite crystals with a cloudy core and irregular boundaries (Plate 4). In places, the carbonate crystals have clear cores (Plate 4). In most cases, both carbonate rims have a fine-grained matrix specially when in contact with brucite pseudomorphs (Plate 4). A very fine-grained clay-type material is sporadically present in between the carbonates. Brucite, which occurs as fibrous masses or veins within calcite/ dolomite grains, is evenly distributed in the rock (Plate 4). No accessory phases were identified in the rock.

Given the mineralogy observed, the footwall is considered to have been formed within the chert-poor dolomite horizon of the Frisco Formation, of the Malmani Subgroup.

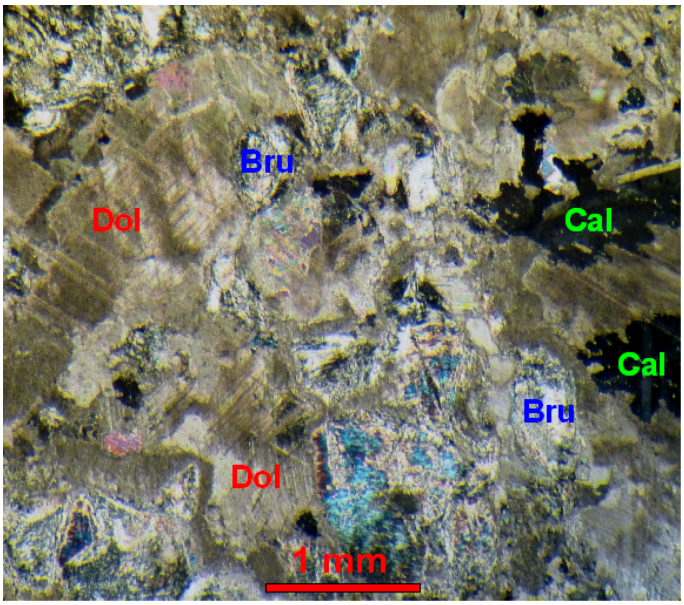

Plate 4: Photograph of the footwall metadolomites in borehole SS 330 (XPL)

Mineral abbreviations: Bru, brucite; Cal, calcite; Dol, dolomite.

4.3.2.2 Clinopyroxenites (CP)

The spatial occurrence of clinopyroxenite subtypes in the SS 330 profile is as follows:

- The weakly metasomatised clinopyroxenites (subtype I) is the most dominant lithology above a depth of 425 m in borehole SS 330 (Fig. 5).
- The moderately metasomatised clinopyroxenites (subtype II) is the most dominant clinopyroxenite between 550 - 400 m depth and encloses the thickest olivine clinopyroxenite sill (Fig. 5).
- The feldspathic moderately metasomatised clinopyroxenites (subtype III) occurs mainly within clinopyroxenites subtype I and olivine clinopyroxenites (Fig. 5).

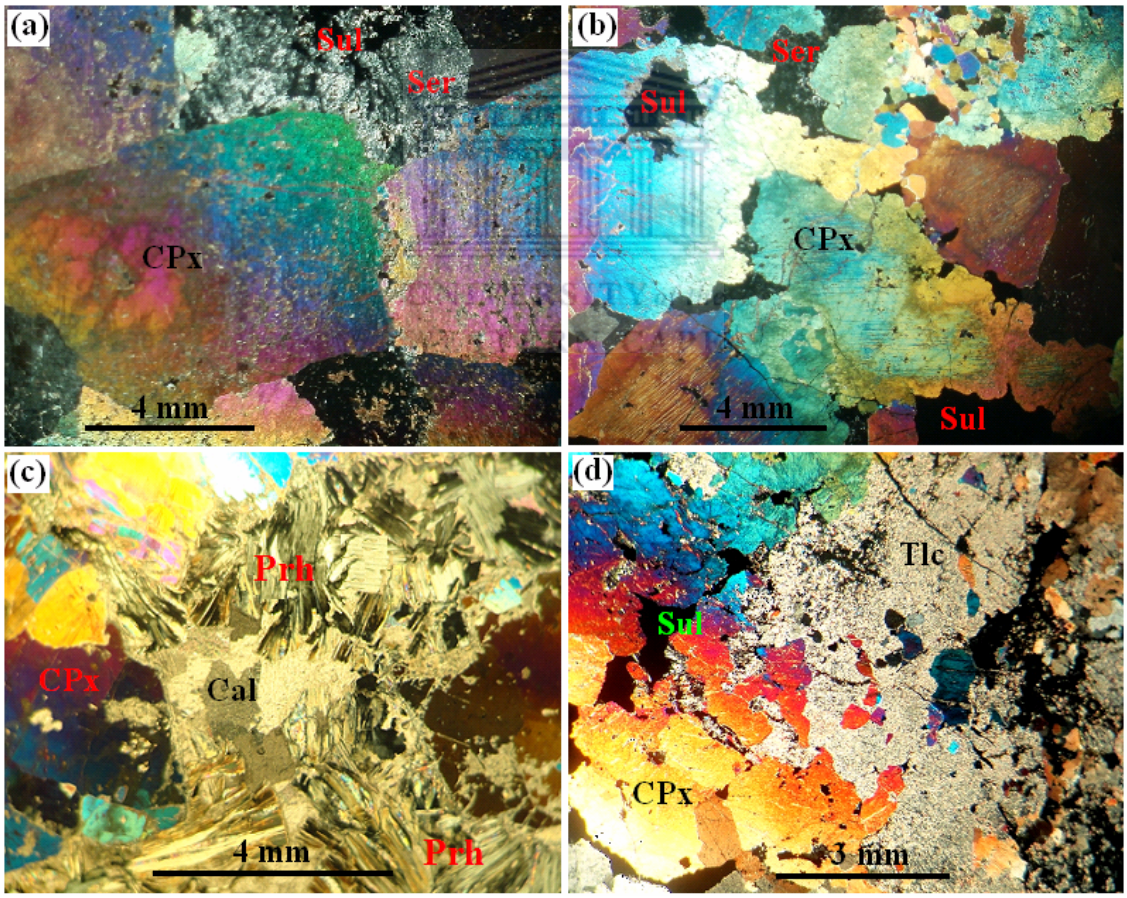

Plate 5: Clinopyroxenite subtype I displaying: *(a) a granoblastic polygonal texture (XPL), (b) a granoblastic interlobate texture (XPL), (c) Prehnite overgrowing clinopyroxene and calcite grains (XPL), and (d) talc grains partially replacing clinopyroxenes (XPL).*
Mineral abbreviations: Cal, calcite; Cpx, clinopyroxene; Prh, Prehnite; Ser, sericite; Sul, Sulphide; Tlc, talc.

4.3.2.2.1 Clinopyroxenites subtype I (CP I)

These rocks are composed predominantly of 8 to 12 mm coarse-grained idioblastic to xenoblastic clinopyroxenes (95 - 100 vol. %) and plagioclase laths (0 - 5 vol. %). Accessory phases are sulphides, talc, biotite, prehnite and calcite (~5 vol. %).

Two granoblastic textures of clinopyroxenes are distinguished:

1) The minerals are equigranular, have well developed crystal faces with straight grain boundaries and triple junctions are present (Plate 5a).
2) The grains are anhedral and have irregular boundaries (Plate 5b).

Coarse-lath shaped plagioclase crystals (4 to 6 mm in length) occur as individual laths and are interlocking with euhedral clinopyroxene grains. In places, they are sericitised and form irregular and small-lath shaped crystals (0.5 to 1 mm in length) which occur as individual grains interlocked with coarse-grained anhedral clinopyroxenes (Plate 5b).

Prehnite forms lath-shaped crystals ranging from 1 to 4 mm in length. They are found as aggregate grains overgrowing and replacing both clinopyroxene and calcite (Plate 5c). In places, biotite occurs as individual crystals associated with sulphide blebs. Locally, fine-grained talc crystals are also replacing coarse-grained clinopyroxenes (Plate 5d).

Sulphides in these zones are composed mainly of pyrrhotite, pentlandite and chalcopyrite. They occur as irregularly-shaped blebs (1 to 3 mm) mainly associated with sericitised plagioclase (Plate 5a), enclosed within clinopyroxenes (Plate 5b) or along grains boundaries between talc and coarse-grained clinopyroxenes (Plate 5d).

Alteration

All plagioclase laths (0.5 to 6 mm in length) are highly altered resulting mainly in the formation of sericite (Plate 5a).

4.3.2.2.2 Clinopyroxenites subtype II (CP II)

The moderately metasomatised clinopyroxenites consist of medium- to coarse-grained (4 to 10 mm in size) subidioblastic to xenoblastic clinopyroxenes (90 - 95 vol. %) and plagioclase laths (5 - 10 vol. %). Accessory minerals are sulphides, talc and calcite (5 - 15 vol. %).

Anhedral clinopyroxenes occur mostly in a granoblastic amoeboid texture as aggregates of interlocking grains (not shown). In places, clinopyroxenes are euhedral and occur as individual grains (4 to 8 mm in size) surrounded by a fine-grained (0.1 to 1 mm in size) clinopyroxene assemblage having straight boundaries and showing triple junctions (porphyroblastic texture) similar to that observed in clinopyroxenite subtype I.

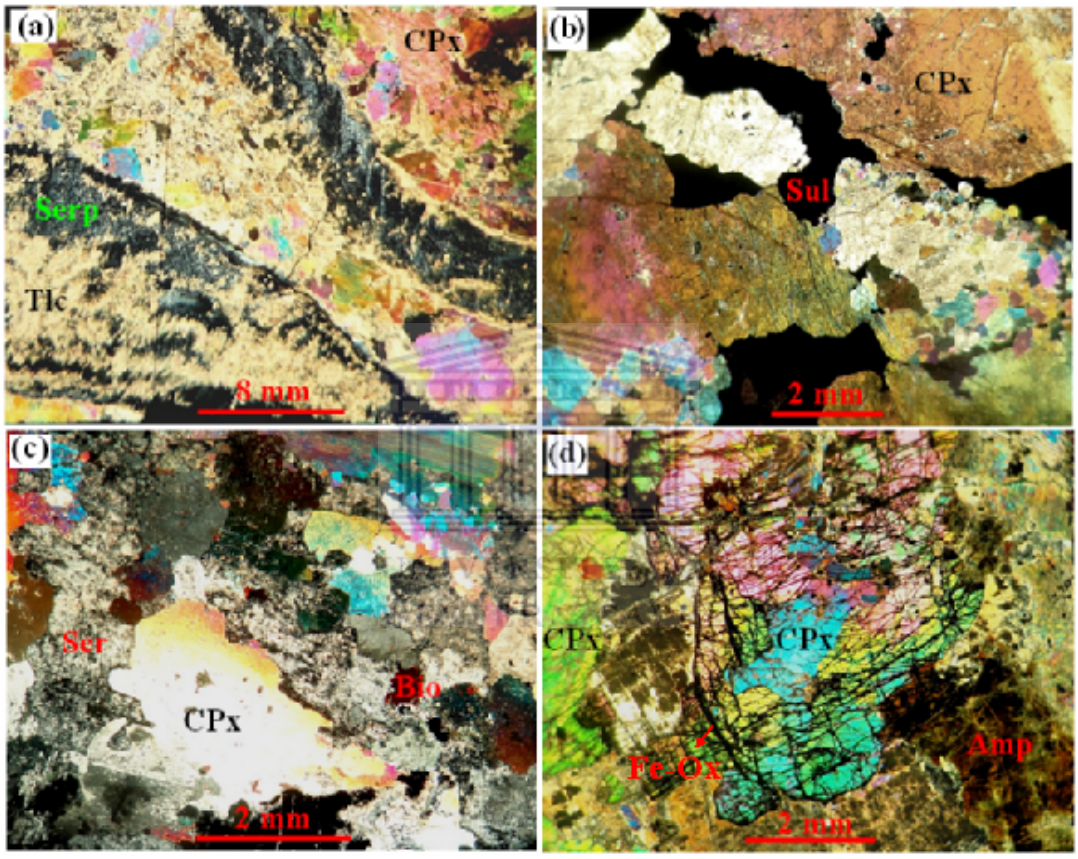

Plate 6: Clinopyroxenites subtypes II and III showing: *(a) talc replacing clinopyroxenes along a serpentine filled fracture (XPL), (b) sulphides are enveloping the pyroxenes (XPL).*
Feldspathic moderately metasomatised clinopyroxenites showing: *(c) clinopyroxene surrounded by sericitised plagioclase (XPL) and (d) iron oxide filled fractures in clinopyroxenes (XPL).*
Mineral abbreviations: Amp, amphibole; Bio, biotite; Cpx, clinopyroxene; Fe-Ox, Iron oxide; Ser, sericite; Serp, serpentine; Sul, Sulphide; Tlc, talc.

Plagioclase forms irregular-shaped crystals ranging in length from 4 to 8 mm. They occur as individual laths and are locally interlocking with clinopyroxene grains, as seen in clinopyroxenite subtype I.

Along serpentine-filled fractures, mineral aggregates of talc, ranging in length from 0.3 to 0.5 mm, replace medium-grained clinopyroxenes (4 to 6 mm in size) along their rims (Plate 6a). In places, calcite veins crosscut coarse-grained clinopyroxenes.

Sulphides vary from disseminations of pyrrhotite, pentlandite and chalcopyrite grains ranging in size from 0.3 to 0.5 mm enclosed within clinopyroxenes, through to blebs mainly composed of pyrrhotite (3 to 8 mm in size) in between the pyroxenes, to semi-massive to net-texture that enveloped clinopyroxenes showing curved grain boundaries (Plate 6b).

Alteration

All plagioclase laths (4 - 8 mm in length) are highly altered to sericite. Clinopyroxenes are altered to talc in places.

4.3.2.2.3 Clinopyroxenites subtype III (CP III)

These rocks are composed mainly of medium- to coarse-grained (4 to 8 mm in size) xenoblastic clinopyroxenes (60 - 80 vol. %) and plagioclase laths (20 - 40 vol. %). Minor phases are sulphides, iron oxides, biotite and calcite (5 - 10 vol. %).

Clinopyroxenes occur as individual grains or aggregates of grains which are mainly surrounded by plagioclase laths (Plate 6c). Large anhedral clinopyroxenes are extensively fractured between 500 and 550 m depth (Fig. 5). The fractures are filled with iron oxides (Plate 6d). Plagioclase forms irregularly-shaped crystals ranging in length from 4 to 10 mm. They occur as aggregates of grains and are interlocking with each other enclosing clinopyroxene grains. In places, the plagioclase laths show twinning.

Irregular, anhedral to subhedral dark brown biotite, ranging from 0.5 to 2 mm in size, occurs interstitially, or along grain boundaries between clinopyroxenes and plagioclase (Plate 6c) and are associated with fine-grained iron oxides concentrated along pyroxene grain boundaries. A single euhedral, medium-grained calcite crystal occurs interlocked with plagioclase and pyroxenes (not shown) in the uppermost lithology (96 m depth; Fig. 5). In the latter, fine-grained calcite occurs as aggregates in between a pyrrhotite bleb and a plagioclase crystal.

Sulphide blebs consist mostly of pyrrhotite and pentlandite (6 to7 mm in size), and are associated with pyroxenes. The disseminated sulphides (0 - 5 vol. %), of < 1mm in size, occur along the edges and/ or within pyroxenes and are associated with biotite laths.

Alteration

All plagioclase laths are extensively altered to sericite (Plate 6c) while, clinopyroxene grains are altered to green amphibole showing the onset of uralitisation (Plate 6d).

4.3.2.3 Olivine clinopyroxenites (OCP)

4.3.2.3.1 Olivine clinopyroxenites subtype I (OCP I)

Weakly metasomatised olivine clinopyroxenites are mainly composed of 1 to 2 mm fine-grained olivine (40 - 90 vol. %), 4 to 12 mm medium to coarse-grained xenoblastic clinopyroxene (10 - 60 vol. %) and plagioclase (<5 vol. %). Accessory minerals are sulphides, spinel, iron oxides and calcite (5 - 7 vol. %).

Olivines are fractured, rounded and subhedral to euhedral (Plate 7a). They occur as aggregates and are interlocked with clinopyroxenes or enclosed within clinopyroxenes (Plate 7a). Locally, olivines are associated with rounded and/ or anhedral, dark green spinel grains ranging in size from 0.5 to 2 mm. The latter, which are also fractured, rimmed by, and cross-cut by iron oxides in places, occur in aggregates forming clusters included in or overgrown by clinopyroxene grains (Plates 7a & 7b).

Poikiloblastic clinopyroxenes occur as coarse-grained having irregular boundaries and contain olivine inclusions in places. Plagioclase, where present, forms irregularly-shaped crystals (2 to 4 mm in length) and occurs interstitial to olivine and clinopyroxene grains. A calcite grain, ~ 4 mm in size, is associated with anhedral, fine-grained clinopyroxenes (1 to 2 mm in size), and both grains are surrounded by serpentine.

The sulphides are composed of irregularly-shaped blebs (1 to 2 mm in size), of mainly pyrrhotite and pentlandite, which occurs partly associated with serpentinised olivines.

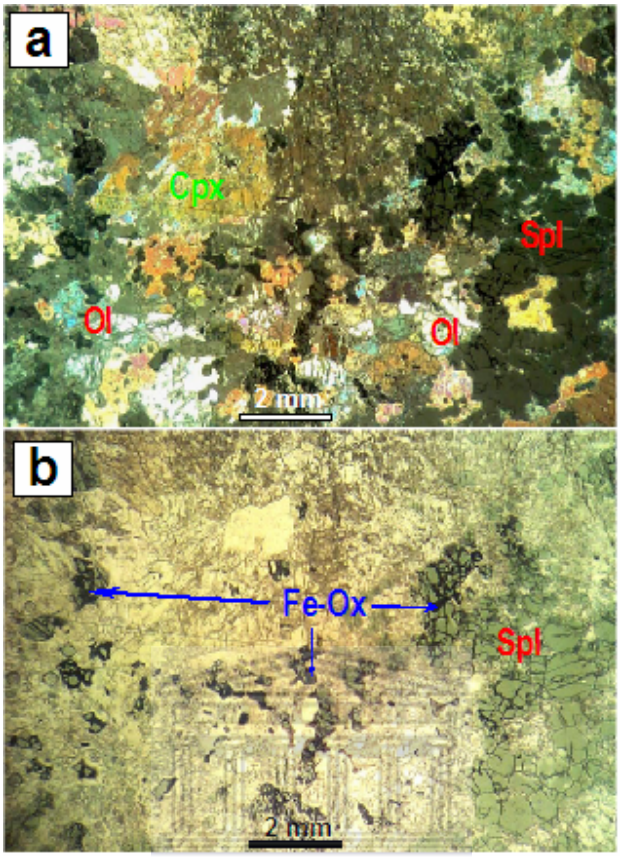

Plate 7: Olivine clinopyroxenite subtype I showing: *(a) clinopyroxene grains in association with olivine and spinel grains (XPL) and (b) Iron oxide filling fractured spinel grains (PPL).*
PPL: Plane polarized light.
Mineral abbreviations: Cpx, clinopyroxene; Fe-Ox, iron oxide; Spl, spinel; Ol, olivine.

Alteration

The olivine grains are altered to serpentine to varying degrees in the rock. Pyroxenes are also altered to serpentine while plagioclase, where present, is altered to sericite.

4.3.2.3.2 Olivine clinopyroxenites subtype II (OCP II)

The primary minerals in these rocks are composed of 1 to 2 mm fine-grained, rounded olivine (10 - 40 vol. %), 6 to 12 mm coarse-grained xenoblastic clinopyroxene (50 - 90 vol. %) and plagioclase (<10 vol. %). The accessory phases are sulphides, spinel and calcite (5 - 10 vol. %). Olivines are fractured and subhedral to euhedral, and occur predominantly as single grains enclosed within clinopyroxenes (Plate 8a) or associated with plagioclase interlocking with clinopyroxenes.

Olivine also occurs as aggregates crosscut by serpentine veinlets. The latter has the same orientation as the general fracturing in olivine which terminates where the grains abut against the large and partially resorbed clinopyroxene grains (Plate 8a). These fractures, in most cases, are filled by iron oxides.

The poikiloblastic clinopyroxenes (6 to 12 mm in size) are skeletal, have irregular grain boundaries and contain mainly olivine inclusions, minor spinel and sulphide blebs (Plate 8a). Between 450 and 550 m depth, clinopyroxenes are extensively fractured (Plate 8b), and the spinel grains decrease in content with increasing depth.

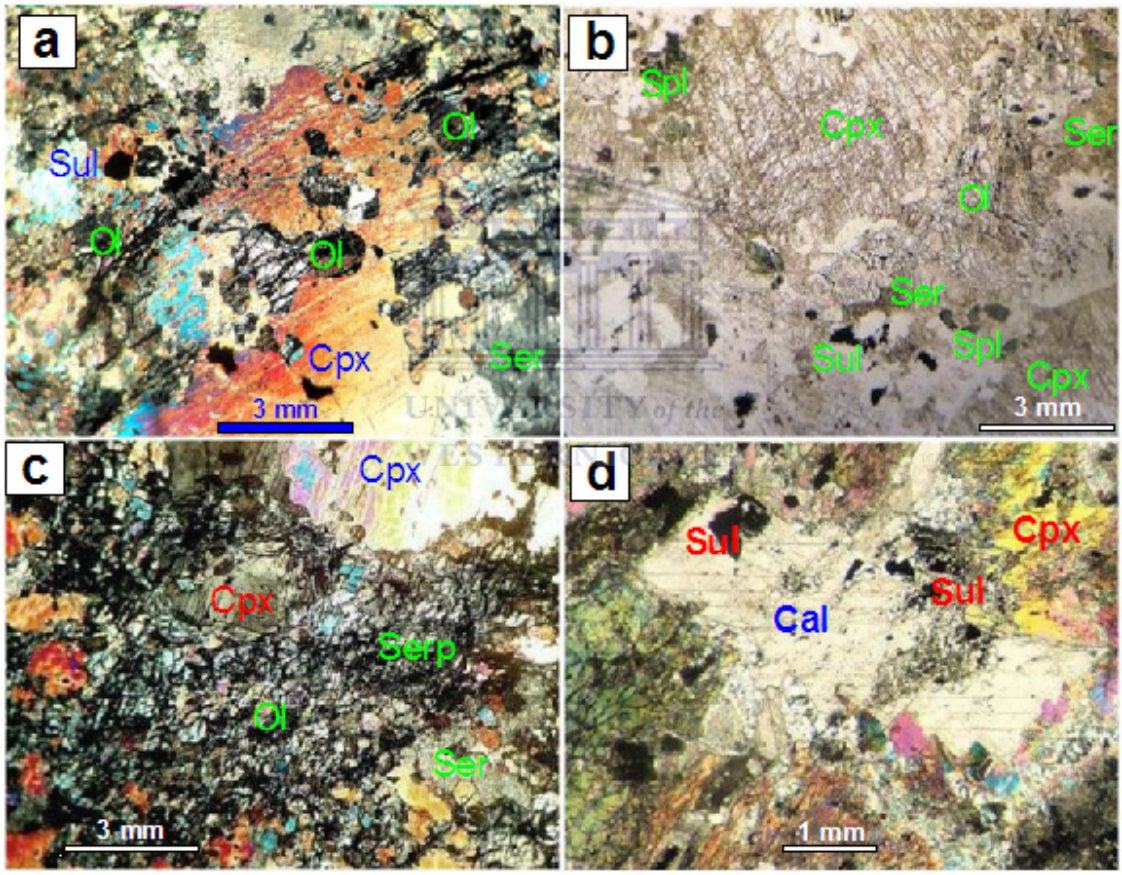

Plate 8: Olivine clinopyroxenite subtype II showing: *(a) a poikiloblastic texture; note the orientation of the general fracturing in the various olivine grains (XPL), (b) sulphide and spinel grains associated with sericite in contact with olivine (PPL), (c) serpentinisation of olivine and clinopyroxene grains (XPL) and (d) a calcite grain in between clinopyroxenes (XPL).*
Mineral abbreviations: Cal, calcite; Cpx, clinopyroxene; Spl, spinel; Ol, olivine; Ser, sericite; Serp, serpentine; Sul, sulphide.

Plagioclase laths, 1 to 2 mm in length, occur in association with olivine, but not within the skeletal clinopyroxene grains. Spinel grains are fine-grained (0.1 to 0.5 mm size). They occur as single grains associated with fractured olivine and sericitised plagioclase. Anhedral calcite grain (~ 4 mm in length), associated with very fine sulphide grains (<0.5 mm in size), occurs within clinopyroxene (Plate 8d).

Sulphides occur mainly as disseminated grains (0.1 to 0.3 mm in size) of pyrrhotite, pentlandite and chalcopyrite in serpentinised areas. Locally, they are associated with fractured olivine grains and sericitised plagioclase laths (Plate 8b). Minor blebs (1 to 5 mm in size) occur in between clinopyroxenes, or as irregularly-shaped grains partly aligned to the preferred fracture orientation in olivine.

Alteration

The olivine grains are altered to serpentine to varying degrees in the rock. Pyroxenes are also altered to serpentine and plagioclase laths are altered to sericite (Plates 8b & 8c).

4.3.2.3.3 Olivine clinopyroxenites subtype III (OCP III)

Olivine clinopyroxenites III are primarily composed of olivine + clinopyroxene (50 - 90 vol. %) and plagioclase (10 - 50 vol. %). The accessory phases are sulphides, spinel, iron oxides and biotite (5 - 15 vol. %).

Olivines are fine- to medium-grained (1 to 4 mm in size). The crystals are euhedral, fractured and occur mainly as aggregates interlocked with plagioclase. Minor olivine also occurs as inclusions in clinopyroxenes. Most fractures in olivine are filled by iron oxides which occur as veinlets. These have a similar orientation as the fracturing which ends where olivine grains abut against plagioclase laths and/ or clinopyroxene grains (Plates 9a, 9b & 9c). Clinopyroxene xenoblasts are medium- to coarse-grained (4 - 12 mm in size). They have irregular grain boundaries and are skeletal in places (Plate 9c). They are interlocked with each other, fractured (Plates 9a & 9b) and enclose small grains of spinel ranging in size from 0.5 to 1 mm as well as sulphide grains.

Plagioclase forms laths (0.5 to 6 mm in length). They occur predominantly interlocked with olivine and also as partial inclusions within the skeletal clinopyroxenes in places.

Dark brown biotite is irregularly-shaped. They occur as single grains (~ 2 mm in size) associated with sulphide grains (~0.5 mm in size) along grain boundaries between coarse-grained clinopyroxenes and serpentinised olivines interlocked with sericitised plagioclase (Plate 9b).

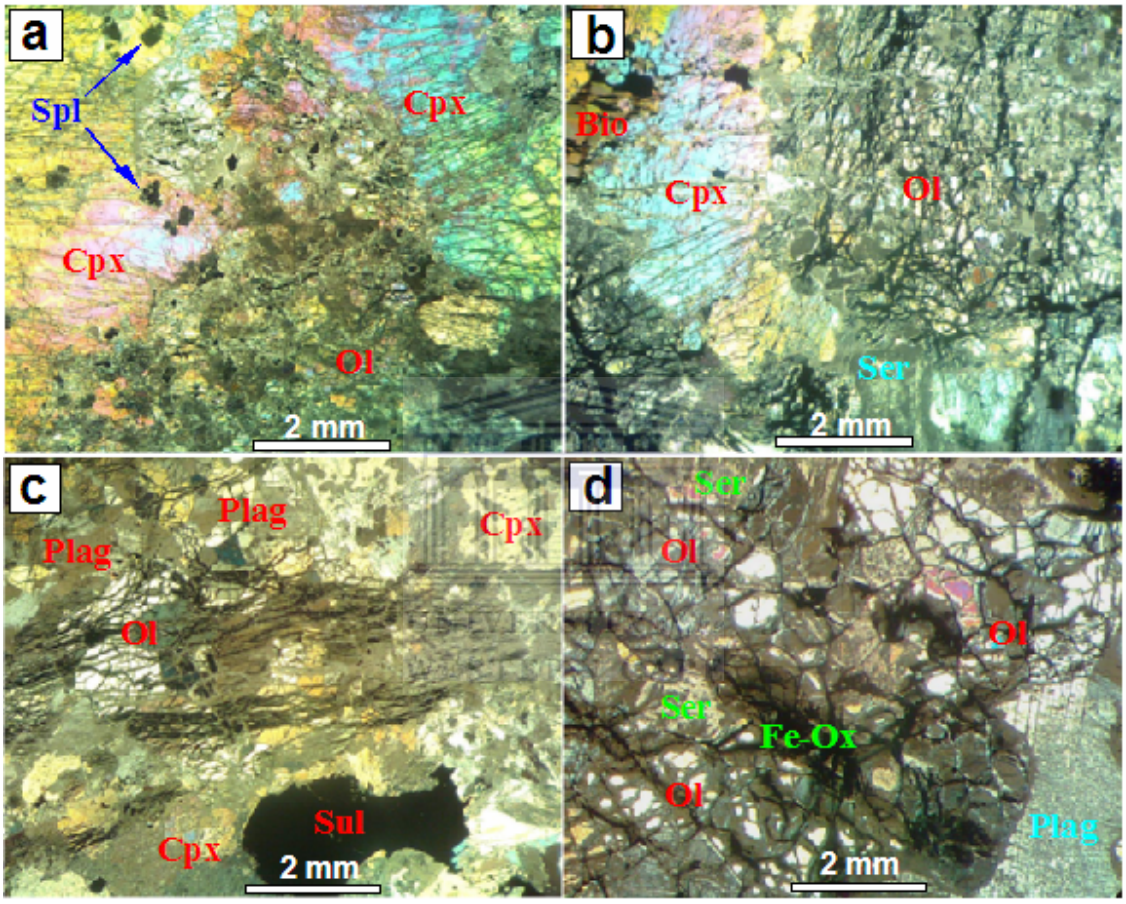

Plate 9: Olivine clinopyroxenite subtype III showing: *(a) & (b) fine grained olivine associated with sericitised plagioclase interlocking coarse clinopyroxenes (XPL), (b) a biotite grain along the contact boundary between clinopyroxene and serpentinised olivine (XPL), (c) the orientation of the general fracturing in olivine terminating against the pyroxenes (XPL) and (d) extensively fractured olivine interlocking with plagioclase (XPL).*
Mineral abbreviations: Bio, biotite; Cpx, clinopyroxene; Fe-Ox, iron oxide; Spl, spinel; Ol, olivine; Plag, plagioclase; Ser, sericite; Sul, sulphide.

Locally, rocks of this group display two main textures:

1) Fine- to medium-grained, fractured and serpentinised olivines are interlocked with small sericitised plagioclase laths and clinopyroxene (Plates 9a & 9b), which are poikiloblasts in places (Plate 9c).

2) Coarse-grained, fractured and serpentinised olivine grains are interlocked with large and partly-sericitised plagioclase laths (Plate 9d).

Sulphides occur mainly as disseminated (< 0.5 mm in size) pyrrhotite, pentlandite and chalcopyrite grains mainly associated with serpentinised olivine grains and sericitised plagioclase laths or as inclusions in clinopyroxenes. Minor and irregularly-shaped blebs, reaching a maximum size of 5 mm in places, occur in between pyroxenes.

Alteration

Olivine grains are altered to serpentine and plagioclase laths generally are altered to sericite.

4.4 Summary

Table 1 summarises the relevant textural and mineralogical attributes related to the rock of interest; mainly the Platreef feldspathic pyroxenites from borehole OY 482 and the olivine-rich clinopyroxenites and clinopyroxenites from borehole SS 330.

Borehole OY 482, drilled at Overysel, intersected Bushveld lithologies, which comprises of Platreef feldspathic pyroxenites sills interrupted by gabbronorite sills, that overlies the Archaean granite (Fig. 3). Microscopic study on the Platreef rock allowed the distinction of three lithostratigraphic units (Table 1). These units are: Lower- (overlying the granites floor rock), Middle- and Upper Platreef (Table 1).

At Sandsloot, drilled core SS 330 intersected metamorphosed/ metasomatised footwall unit which consists of alternating clinopyroxenite and olivine-rich clinopyroxenite layers overlaying metadolomite of the Frisco Fm, of the Malmani Subgroup, as floor rock (Fig. 5). Microscopic study distinguished the occurrence of three rock subtypes or metasomatic zones within each rock unit (Table 1).

Table 1: A summary of the petrographic attributes of the rocks from the studied boreholes.

Boreholes	Rock types	Lithostratigraphic units / Metasomatic zones	Textures & *alterations*	Mineral assemblages (in vol. %)
OY 482	Gabbronorites	Fine- grained & coarse-grained	- Porphyritic - Ophitic - Interlocking	Primary: Clinopyroxene + Orthopyroxene + Plagioclase Accessories: Biotite+ oxide
	Feldspathic pyroxenites (Platreef)	Upper Platreef	- Interlocking - *Sericitisation & serpentinisation*	Primary: Orthopyroxene (70-80 vol. %) + Clinopyroxene (<15 vol. %) + Plagioclase (5-20 vol. %) Accessories: Biotite Sulphides: Pyrrhotite + pentlandite + chalcopyrite blebs & disseminations
		Middle Platreef	- Cumulate	Primary: Orthopyroxene (70-90 vol. %) + Clinopyroxene (<25 vol. %) + Plagioclase (<10 vol. %) Accessories: Biotite + quartz Sulphides: Pyrrhotite + pentlandite + chalcopyrite blebs & disseminations
		Lower Platreef	- Interlocking - Cumulate	Primary: Orthopyroxene (>90 vol. %) + Clinopyroxene (<5 vol. %) + Plagioclase (<5 vol. %) Accessories: Biotite + quartz Sulphides: Pyrrhotite + pentlandite + chalcopyrite blebs & disseminations
SS 330	Olivine clinopyroxenites (OCP)	Highly metasomatised / altered (OCP III)	- Poikiloblastic - Interlocking - *Sericitisation* - *Serpentinisation*	Primary: Clinopyroxene & Olivine (50-90 vol. %) + Plagioclase (10-50 vol. %) Accessories: Spinel + biotite + iron oxides + calcite. Sulphides: Pyrrhotite + pentlandite + chalcopyrite blebs & disseminations
		Moderately metasomatised / altered (OCP II)	- Poikiloblastic - *Sericitisation* - *Serpentinisation*	Primary: Clinopyroxene (60-90 vol. %) + Olivine (10-40 vol. %) + Plagioclase (10-15 vol. %). Accessories: Spinel + biotite + iron oxides + calcite. Sulphides: Pyrrhotite + pentlandite + chalcopyrite blebs & disseminations
		Weakly metasomatised / altered (OCP I)	- Poikiloblastic - *Sericitisation* - *Serpentinisation*	Primary: Clinopyroxene (10-60 vol. %) + Olivine (40-90 vol. %) + Plagioclase (<5 vol. %) Accessories: Spinel + biotite+ iron oxides + calcite. Sulphides: Pyrrhotite + pentlandite + chalcopyrite blebs & disseminations
	Clinopyroxenites (CP)	Feldspathic Moderately metasomatised (CP III)	- Granoblastic amoeboid - *Sericitisation*	Primary: Clinopyroxene (60-80 vol. %) + plagioclase (20-40 vol. %) Accessories: Biotite + iron oxides + calcite. Sulphides: Pyrrhotite + pentlandite + chalcopyrite blebs & disseminations
		Moderately metasomatised (CP II)	- Granoblastic amoeboid - Porphyroblastic - Recrystallisation - *sericitisation*	Primary: Clinopyroxene (90-95 vol. %) + plagioclase (5-10 vol. %) Accessories: Talc + calcite. Sulphides: Pyrrhotite + pentlandite + chalcopyrite in semi-massive, net- textured, blebs & disseminations
		Weakly metasomatised (CP I)	- Granoblastic polygonal - Granoblastic interlobate - *sericitisation*	Primary: Clinopyroxene (95-100 vol. %) + plagioclase (<5 vol. %) Accessories: Prehnite + talc + calcite + biotite. Sulphides: Pyrrhotite + pentlandite + chalcopyrite blebs
	Metadolomite	Frisco Fm (Malmani Subgroup)	- Xenotopic texture	Primary: Calcite/ dolomite (90 - 95 vol. %) + brucite (5 - 10 vol. %). Minor clay.

The summarised stratigraphy in Table 1 illustrates the general lithostratigraphic setting in the Northern limb; i.e., from the base upwards, the footwall unit (metadolomites, clinopyroxenites and olivine clinopyroxenites), the Platreef (feldspathic pyroxenites) and the Main Zone made up of gabbronorites.

Considering the above, the studied rocks describe a contact relationship between the Platreef magma and the floor rock. This will be investigated in the following chapter in order to identify the geochemical parameters, which reflect the petrographical attributes of each unit, useful to develop chemostratigraphic indices and geochemical vectors that may indicate areas of PGE mineralisation using XRF and ICP-OES data.

The platinum group metals were not identified during the petrographical observations.

Chapter 5

5. Whole rock geochemistry

This work is aimed at defining petrographic and geochemical criteria, such as chemostratigraphic indices and geochemical vectors that can act as indicators to the proximity of PGE mineralisation within the Platreef lithologies. The chemostratigraphic indices and geochemical vectors to PGE mineralisation will be derived from whole rock geochemical data obtained from the XRF and ICP-OES analyses. The data, comprising of the major oxides, trace elements and PGE (Pt, Pd and Au), mainly from two boreholes, SS 330 and OY 482 located at Sandsloot and Overysel, respectively, are presented in Appendix II. These have been evaluated along the following steps:

1) **Geochemical classification of the rock types and subtypes.**

   The main rocks identified are Platreef feldspathic pyroxenites and gabbronorites in borehole OY 482, and olivine clinopyroxenites and clinopyroxenites in borehole SS 330. These rocks, especially the olivine clinopyroxenites and the clinopyroxenites commonly display transitional boundaries that are difficult to demarcate and are therefore difficult to classify due to their hybrid nature. A chemostratigraphic classification based on major elements was therefore undertaken using hierarchical clustering as follows:

   In step one of the hierarchical clustering analyses of the geochemical data would enable identifying groupings with geochemical attributes that define clinopyroxenites and olivine clinopyroxenites in borehole SS 330, and Platreef feldspathic pyroxenites and gabbronorites in borehole OY 482, as identified in the petrography.

   In step two, hierarchical clustering analysis was used to further classify the clinopyroxenites and olivine clinopyroxenites into groupings that reflect their varying degree of metasomatism and alteration as observed in the petrographic studies. This

step defined the chemostratigraphic attributes of the metasomatic/ alteration zones or the rock subtypes.

Once the aforementioned were achieved, the geochemical data of clinopyroxenites, olivine clinopyroxenites and Platreef feldspathic pyroxenites obtained from the hierarchical clustering analysis were processed using box and whisker plots to identify the variation of elements that controls the clustering distribution of samples in the various rock types/ subtypes. The ensuing results were also used to refine the demarcations of lithological boundaries in the log sections (Figs. 3 & 5).

2) **Geochemical characterisation of the rock types and subtypes.**

Geochemical data, comprising of major and trace elements, were used to characterise the rock types and associated metasomatic zones or rock subtypes as follows:

First, spider diagrams were used to study the patterns of enrichment and depletion or the behaviour of selected elements, especially the LILE (Sr, Rb and Ba) and HFSE (Th, U, Ce, Zr, Nb, Ti and Y) in each of the clinopyroxenites, olivine-rich clinopyroxenites and Platreef feldspathic pyroxenites subgroups or subtypes, and in the gabbronorites.

Second, various immobile element ratios and anomalies were calculated from the spider diagrams and tabulated along with statistical summaries of oxides and trace elements for each rock subtype or metasomatic zone. These data were used to fingerprint the behaviour of the LILE and HFSE in the metasomatic zones or rock subtypes.

3) **Mass balance, metasomatism and elemental exchange between Platreef magma and floor rocks.**

The occurrence of various metasomatic zones within clinopyroxenite and olivine-rich clinopyroxenite rocks is widely accepted to emanate from the interaction of magma and floor rocks. The objective of the mass balance study is therefore to determine the

relative intensity of elemental exchange between the magma and the floor rocks for each metasomatic zone or rock subtype as follows:

Firstly, mass balance calculations were applied to the median element contents in clinopyroxenites and olivine clinopyroxenites relative to the metadolomites in order to identify the relative elemental exchange between these metasomatic rocks and the Malmani dolomite floor rock and the Platreef magma in borehole SS 330.

In step two, a mass balance study was undertaken in which, the median element contents of the olivine-rich clinopyroxenites, Lower Platreef and Upper Platreef were compared with the Middle Platreef in borehole OY 482. This was performed in order to ascertain the different intensity of element exchange, firstly between Platreef feldspathic pyroxenites and the Archaean granite/ gneisses floor rock in borehole OY 482 and secondly between olivine clinopyroxenites and Platreef from OY 482 since borehole SS 330 did not intersect pristine Platreef magmatic rocks.

4) Geochemical indices and the PGE/ BMS mineralisation.

Element patterns identified from the geochemical classification and characterisation of the lithological zones and associated element mass balance were integrated and used to define chemostratigraphic indices and geochemical vectors that can locate PGE mineralisation within the rocks studied:

Step one involved the identification of major element ratios/ indices that clearly discriminate clinopyroxenites, olivine-rich clinopyroxenites and Platreef feldspathic pyroxenites from one another. This was followed by the use of ternary diagrams to establish the relationship between the major elements indices and the BMS mineralisation.

Step two involved the use of the base metal elements (Ni, Cu, Co and Zn) and PGEs (Pt and Pd) in order to produce base metal indices that are able to locate the PGE-rich zones from barren ones.

5) **Geochemical vectoring towards PGE/ BMS mineralisation.**

In this last section of the study, a spatial study was undertaken to ascertain the viability of the chemostratigraphic indices and geochemical vectors that define or predict the location of the metasomatic and mineralised zones. The down-hole lithogeochemical variation plots in boreholes SS 330 and OY 482 were produced to assess the effectiveness of the various ratios developed.

The results obtained from the preceding data evaluation outline are presented in the following sequence of chapters: Geochemical classification of the rock types and subtypes is given in section 5.1. Section 5.2 presents the geochemical characterisation of the rock types and subtypes. The mass balance, metasomatism and elemental exchange between the Platreef magma and the floor rocks is given in section 5.3, while section 5.4 presents the geochemical indices and the PGE/ BMS mineralisation. Lastly, section 5.5 presents the geochemical vectoring towards PGE/ BMS mineralisation

5.1 Geochemical classification of the rock types and subtypes

5.1.1 Introduction

Classification of the rock of interest, based on petrographical studies in chapter 4, shows that borehole OY 482 comprises Platreef feldspathic pyroxenites, whereas the lithologies in borehole SS 330 consist of metamorphosed/ metasomatised clinopyroxenites and olivine-rich clinopyroxenites. Clinopyroxenites are granoblastic and are composed of clinopyroxene (60 - 100 vol. %), plagioclase (<5 - 40 vol. %) with accessory sulphides, prehnite, biotite and calcite. Olivine clinopyroxenites, which are poikiloblastic, contain variably serpentinised olivine (10 - 90 vol. %), clinopyroxene (10 - 90 vol. %) and plagioclase (<5 - 50 vol. %) with accessory sulphides, spinel, oxide, biotite and calcite. The rocks also show evidence of fluid flow and hydrothermal alterations. The Platreef in borehole OY 482 are composed of orthopyroxene (70 - 95 vol. %), clinopyroxene (<5 - 25 vol. %), plagioclase (<5 - 20 vol. %) with accessory sulphides, biotite and quartz.

This section is aimed at a chemostratigraphic classification of the studied rock types using their major oxide contents. Nowadays, diverse statistical techniques are routinely used for classification purposes in various fields. One of the main advantages of these techniques, such as factor analysis, discriminant analysis, cluster analysis and principal component analysis, is the ability to analyze large datasets, which have many variables (Ragno et al., 2007).

In this work, cluster analysis was selected as the suitable statistical technique to classify rock samples since it produces a graph that allows visual sample ID groupings, which can be correlated with thin section studies for rock type identification.
Box and whisker plots were also used for comparison in order to identify the variation of elements that controls the clustering distribution of samples of the studied rocks useful to firstly establish the relationship between the rock-forming minerals and the oxides, and secondly to identify element associations useful for chemostratigraphic correlations.

The results obtained from the chemostratigraphic classification were validated using the results of the thin section studies and core logging. Element associations for each rock type and metasomatic zones/ subtypes were also defined.
Detailed principles of the cluster analysis techniques and box and whiskers plots as applied in the rock classification are given below.

5.1.2 Cluster Analysis

Cluster analysis (CA) is an analytical technique used to classify cases into a finite, and ideally, small number of groups based upon two or more variables (Finch, 2005).
The goal is to group the variables of a matrix in a way that the characteristics of the variables within the groups are as homogeneous as possible, but the characteristics of the variables between groups are as contrasting as possible, according to some distance measure (Stahl and Demuth, 1999).

In hierarchical clustering analysis (HCA), each case is taken as a separate group initially, and groups are formed by merging cases into bigger and bigger clusters, eventually ending up with a unique group (Abdel-Halim and Abdel-Aal, 1999). Cases or clusters are assembled according to their 'nearness' based upon a given distance or similarity measure (e.g. Euclidean, squared Euclidean, cosine, etc.) and their merges into bigger clusters depends on the clustering method used (e.g. average linkage, single linkage, nearest neighbour, etc.) (Abdel-Halim and Abdel-Aal, 1999). The outcome of the last clustering depends on the combination of the clustering method used and distance measure adopted (Abdel-Halim and Abdel-Aal, 1999).

Two clusters to be joined are chosen in the midst of all potential candidate cluster pairs such that this distance measure adopted is minimized in the resulting cluster (Abdel-Halim and Abdel-Aal, 1999). The final result is a graph (called dendrogram) that allows easy visual assessment of the similarities and differences between the investigated cases (Ragno et al., 2007).

In this work, HCA applies the Ward's method (Ward, 1963), described as the best performing hierarchical clustering as opposed to other clustering methods when dealing with geochemical data by Templ et al. (2008), whereas the distance elaboration between two cases was performed by adopting the squared Euclidean distance. The latter adds up the squared differences between the values of all variables for the two cases and the Ward's clustering computes the sum of the squared Euclidean distance between each case and the cluster centre, and takes it as a dispersion 'error' which should be reduced (Abdel-Halim and Abdel-Aal, 1999). The rationale is to classify rock samples into groups so as to correlate it with the thin section studies in order to identify the rock types and subtypes.

5.1.3 Box and whiskers plots

Box and whisker plots (Tukey, 1977), which were first proposed by statistician John Tukey in 1970, is a technique that graphically focuses on statistical variability (Banacos, 2011). The box and whisker plot is a graphical 7-number summary of a given dataset,

which includes: the median, the interquartile range (shown by the box), the outer range (shown by the whiskers) and the outliers (or maximum and minimum values) as described by Banacos (2011).

The median is the central observation in an ordered dataset (or mean of the two centred observations for an even numbered dataset) and is a measure of the central trend of the data (Banacos, 2011). The interquartile range is the box representing the middle 50% of the ranked data and is drawn from the lower quartile value to the upper quartile value (Banacos, 2011). The outer ranges are the whiskers which are drawn as vertical lines expanding outward from the ends of the box (Banacos, 2011). The outliers are maximum and minimum values of the dataset to the box and whisker plot. The computation of each of these values can be found in Banacos (2011).

Box and whisker plots describe data in a way that is (1) compact and makes easy comparison with similar datasets, and (2) retains the ability to interpret asymmetric aspects of the data and outliers (Banacos, 2011). The two main advantages of the box and whisker plot are the facility to (1) see dataset skewness and (2) compare multiple datasets alongside (Banacos, 2011). In data skewness, the median is moved toward the lower portion of the box with a wider range of observations in the upper quartile as compared to the lower quartile and the opposite is an example of negative skewness (Banacos, 2011). In comparing datasets, the important characteristics of each dataset (median, skewness, dispersion, and outliers) are easy to interpret and visualize, as described by Banacos (2011).

In this work, the box and whisker plots methodology was applied to the datasets of clinopyroxenites, olivine clinopyroxenites, Platreef pyroxenites and gabbronorites for comparison in order to identify the variation of oxides that controls the clustering distribution of samples of the studied rock types and the metasomatic zones or subtypes. This allowed, in the first step, to establish the relationship between the mineralogy of the rocks and the oxides, and secondly to identify oxides classifying the rock types and the metasomatic zones or rock subtypes.

Section 5.1.4 below shows the geochemical classification results for the studied rock types using HCA. Although gabbronorites are not a Platreef lithology, their respective data were also processed to assess the rock classification in borehole OY 482.

5.1.4 Results of cluster analysis

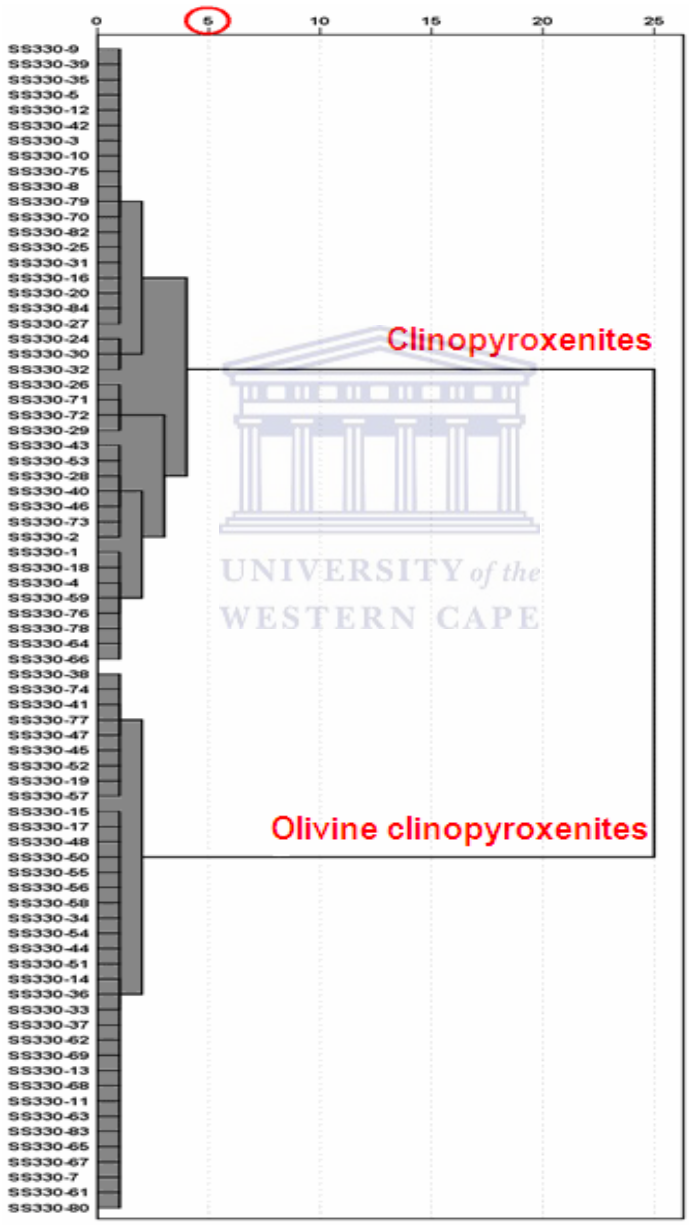

Fig. 7 Dendrogram for sample points cluster identification from data of borehole SS 330: A cut-off distance value of 5 defines clinopyroxenite and olivine clinopyroxenite samples. Their respective samples are annotated by core-sample ID.

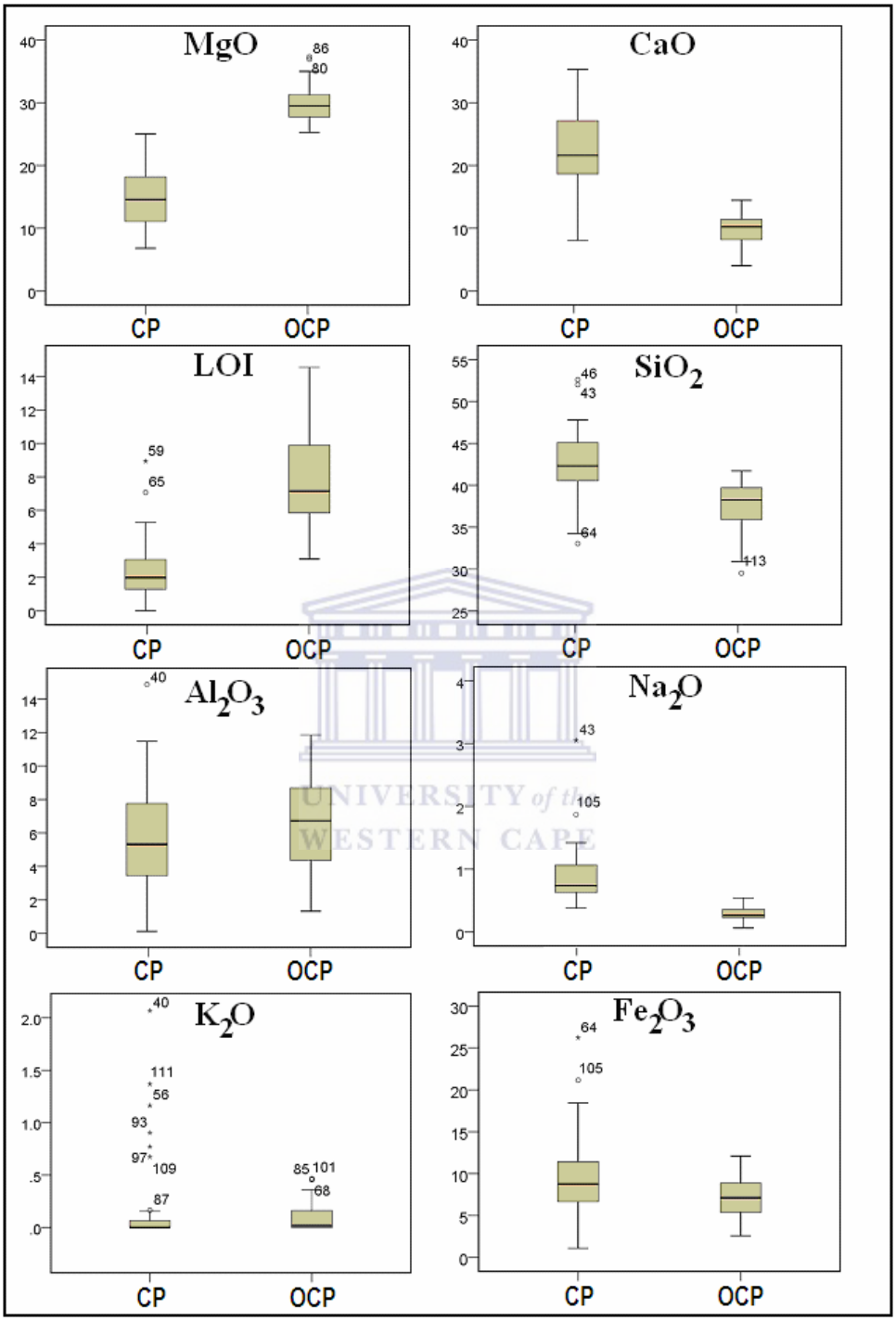

Fig. 8 Selected major element box and whisker plots for clinopyroxenites (CP) and olivine clinopyroxenites (OCP) in borehole SS 330.

As stated earlier in chapter 5, the initial step was the use of HCA to the rock sample data in boreholes SS 330 and OY 482 independently. Firstly, HCA classified clinopyroxenites

and olivine clinopyroxenites in borehole SS 330, and secondly Platreef feldspathic pyroxenites and gabbronorites in borehole OY 482.

This step was followed by the use of HCA to the data of clinopyroxenites and olivine clinopyroxenites separately to classify their respective samples into the three metasomatic subzones or rock subtypes as recorded from the petrographic examination in both lithological units. Although thin section studies identified three Platreef units (Lower, Middle and Upper) in borehole OY 482, HCA was not separately applied to the data due to insufficient samples for statistical analysis.

Data for 77 and 39 rock samples from boreholes SS 330 and OY 482, respectively, were processed separately. Only the oxide contents were used since lithological classification based on the rock-forming minerals was desired.
The standardization method was not included prior to clustering since the oxides have unique scales. The approach used to classify rock samples in this study is similar to that used by Ragno et al. (2007).

The results are presented in the following order:

- The dendrogram of sample point clusters classifying clinopyroxenites and olivine clinopyroxenites in borehole SS 330 is shown in Fig. 7 and the variations of oxides controlling the clustering distribution of samples between the two rock types are shown in Fig. 8.

- The dendrogram of sample point clusters classifying the 3 clinopyroxenite subtypes in borehole SS 330 is shown in Fig. 9 and the variations of oxides controlling the clustering distribution of samples between these subtypes are shown in Fig. 10.

- The dendrogram of sample point clusters classifying the 3 olivine clinopyroxenite subtypes in borehole SS 330 is shown in Fig. 11 and the variations of oxides controlling the clustering distribution of samples between these subtypes are shown in Fig. 12.

- The dendrogram of sample point clusters classifying Platreef feldspathic pyroxenites and gabbronorites in borehole OY 482 is shown in Fig. 13 and the variations of oxides controlling the clustering distribution of samples between the two rocks are shown in Fig. 14.

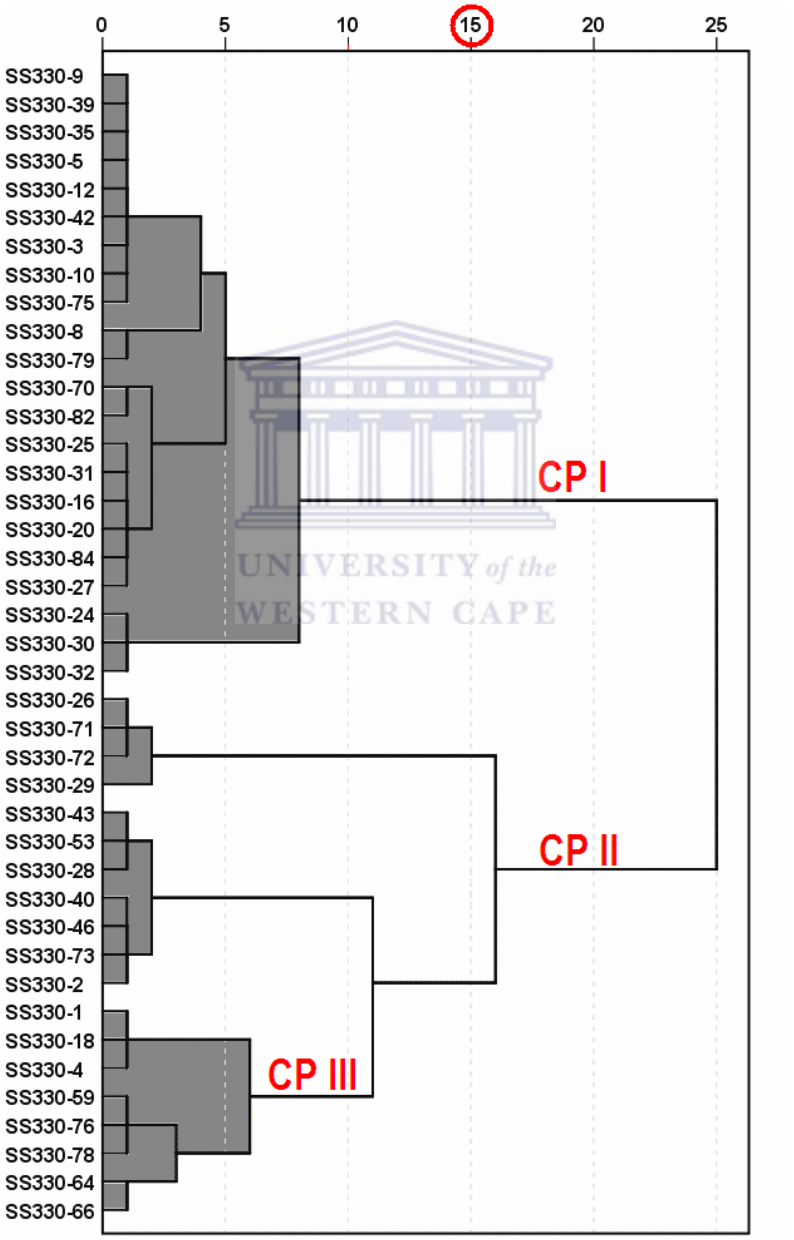

Fig. 9 Dendrogram for sample points cluster identification from data of the clinopyroxenites: A cut-off distance value of 15 defines the clinopyroxenite subtypes (CP I, CP II and CP III). Their relevant samples are annotated by core-sample ID.

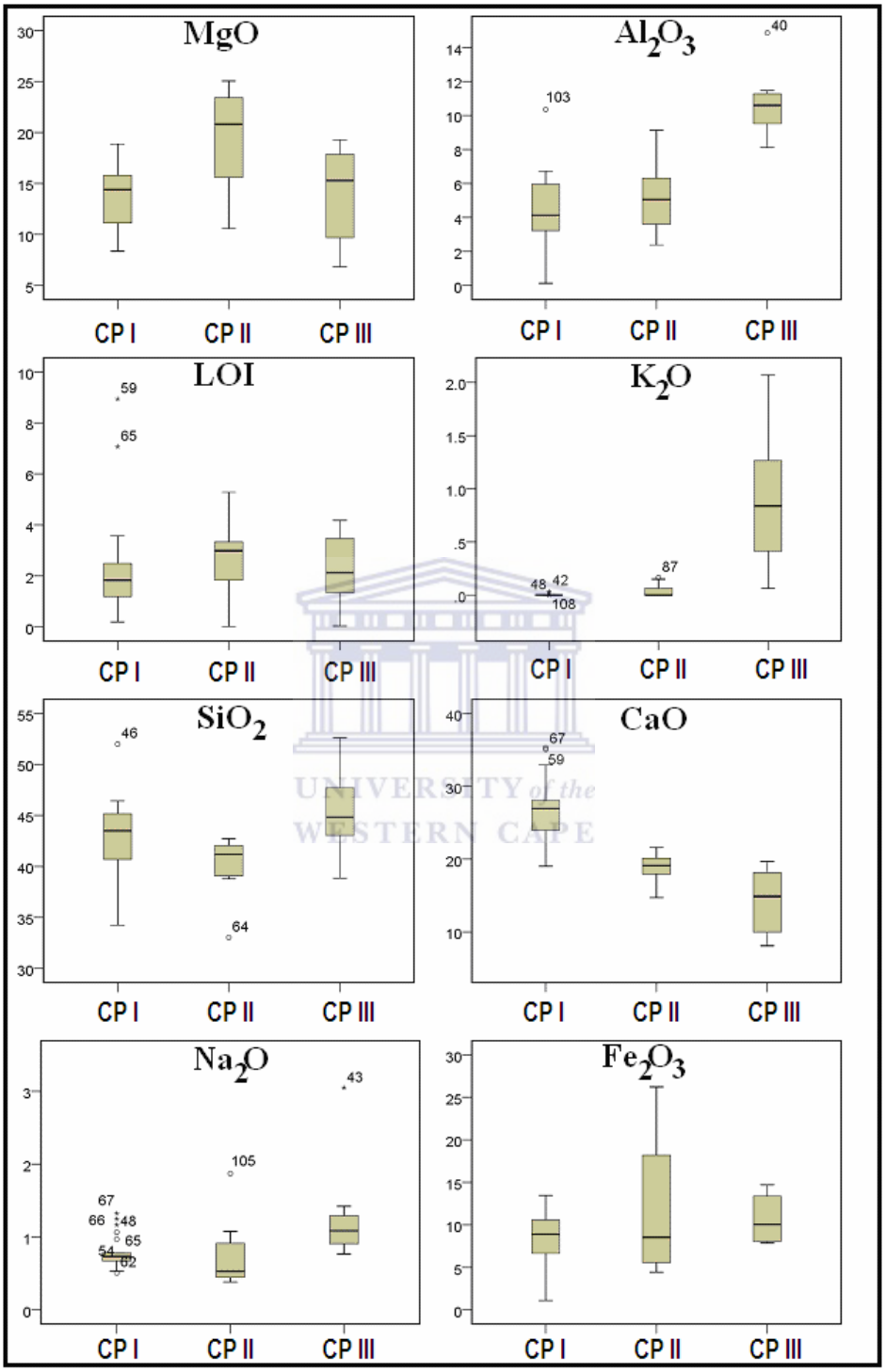

Fig. 10 Box and whiskers plots showing the variation of various oxides between the three clinopyroxenite subtypes. *The subtypes are abbreviated as CP I, CP II and CP III.*

5.1.4.1 Clinopyroxenites and olivine clinopyroxenites (SS 330)

The application of HCA to the sample data for borehole SS 330 classified clinopyroxenites and olivine clinopyroxenites (Fig. 4) using a cut-off distance of 5 as seen in Fig. 7, and the box and whisker plots displaying the pattern of oxides content variation for the two rock types is presented in Fig. 8.

The dendrogram in Fig. 7 shows two major clusters marked by a break between the samples SS 330-66 and SS 330-38 that separates the clinopyroxenites from the olivine clinopyroxenites. The olivine clinopyroxenites consist of two subgroups while the clinopyroxenites display a more complex dendrogram structure with multiple sub-groupings beneath the cut-off distance of 5 (Fig. 7). The clinopyroxenites and the olivine clinopyroxenites sample groups, as seen in Fig. 7, therefore deserve further detailed HCA, the results of which will be presented in section 5.1.4.2 onwards.

In the box and whiskers plot in Fig. 8, the olivine clinopyroxenites show a higher average content of MgO, LOI and Al_2O_3 when compared to the clinopyroxenites. The latter displays a higher average content of CaO, SiO_2, Na_2O and Fe_2O_3 than the olivine clinopyroxenites (Fig. 8).

5.1.4.2 Clinopyroxenite subtypes or metasomatic subzones

Application of HCA in classifying the clinopyroxenites, using a cut-off distance of 10, resulted in 3 subgroups, which represent the clinopyroxenites subtypes or metasomatic subzones (Fig. 9). The box and whisker plots have again been used to show the pattern of oxides content variation for the three clinopyroxenite subtypes (Fig. 10). These subtypes have been designated as subtype I (or CP I) which are weakly metasomatised clinopyroxenites, subtype 2 (CP II) as moderately metasomatised clinopyroxenites, and subtype 3 (CP III) as feldspathic moderately metasomatised clinopyroxenites (Fig. 9).

The box and whiskers plot of the major oxides in the three clinopyroxenite subtypes show four trends:

- CaO decreases in average content from the weakly metasomatised (or CP I) to the feldspathic clinopyroxenite (CP III), as seen in Fig. 10.
- Al_2O_3 and K_2O increase in average content from the weakly metasomatised (CP I) to the feldspathic clinopyroxenite (CP III), as seen in Fig. 10.
- MgO and LOI show their peak average contents in the moderately metasomatised clinopyroxenite (CP II), which decrease towards the feldspathic clinopyroxenite (CP III) and the weakly metasomatised clinopyroxenite or CP I (Fig. 10).

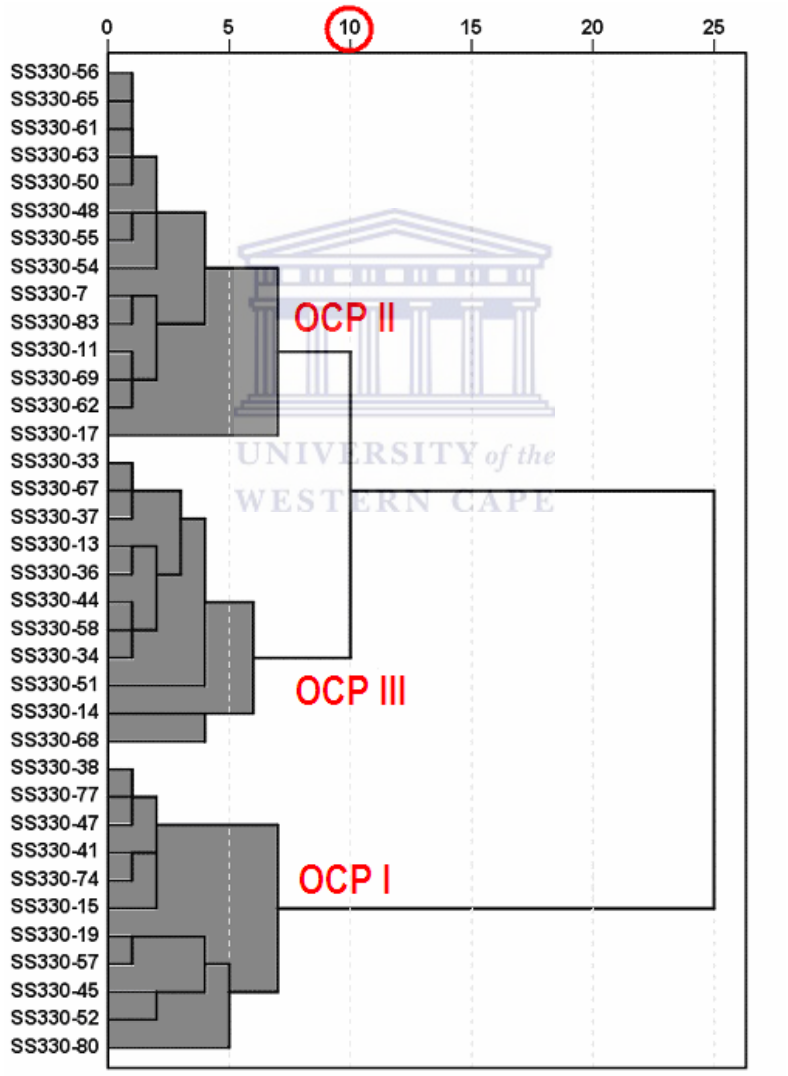

Fig. 11 Dendrogram for sample points cluster identification from data of the olivine clinopyroxenites: A cut-off distance value of 10 defines the olivine clinopyroxenite subtypes (OCP I, OCP II and OCP III). Their respective samples are annotated by core-sample ID.

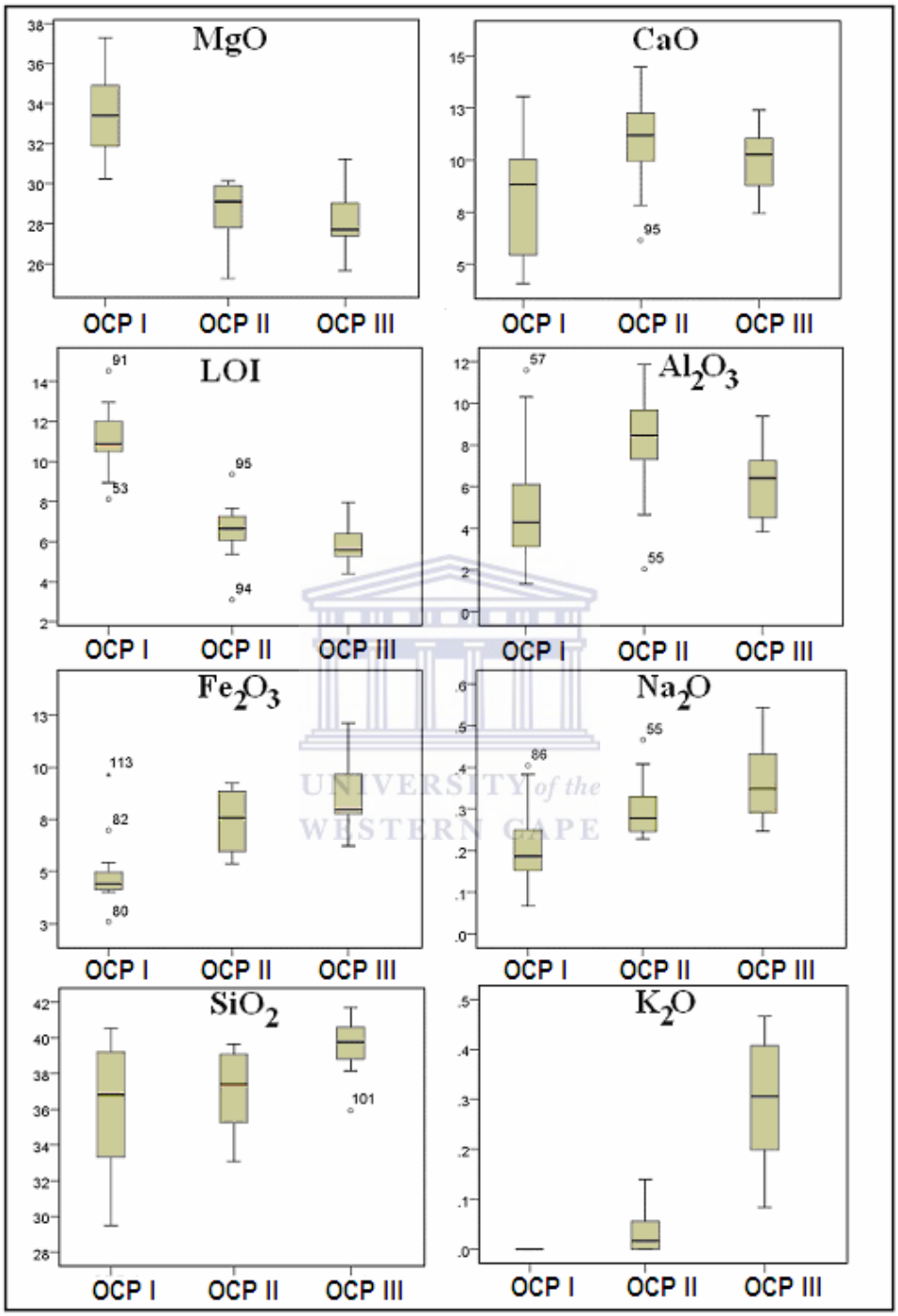

Fig. 12 Box and whiskers plots showing the variation of various oxides between the three olivine clinopyroxenite subtypes. *The subtypes are abbreviated as OCP I, OCP II and OCP III.*

- SiO_2, Fe_2O_3 and Na_2O show their lowest average contents in the moderately metasomatised clinopyroxenite (CP II), which increases towards the weakly

metasomatised clinopyroxenite (CP I) and the feldspathic clinopyroxenite (CP III), as seen in Fig. 10.

5.1.4.3 Olivine clinopyroxenite subtypes or metasomatic/ alteration subzones

Application of HCA in classifying the olivine clinopyroxenites, using a cut-off distance of 10, also resulted in three subtypes, which represent the olivine clinopyroxenite subtypes or metasomatic/ alteration subzones (Fig. 11). The box and whisker plots were used to show the pattern of oxides content variation for the three olivine clinopyroxenite subtypes (Fig. 12). These subtypes are designated as subtype 1, which are weakly metasomatised/ altered (or OCP I), subtype 2 as moderately metasomatised/ altered (OCP II) and subtype 3 as highly metasomatised/ altered or OCP III (Fig. 11).

Metasomatism, as understood here, is a chemical alteration of a rock by hydrothermal and other fluids, which can occur through the action of hydrothermal fluids from an igneous or metamorphic source (http://en.wikipedia.org/wiki/Metasomatism). The nomenclature adopted for the classification of the olivine clinopyroxenites therefore considers the contact metamorphic aureole and related mass transfer and their varying degree of hydrothermal alteration by metamorphic/ magmatic fluids.

The box and whiskers plots of the major oxides in the three olivine clinopyroxenite subtypes show three trends:

- MgO and LOI decrease in average content from the weakly metasomatised/ altered (OCP I) to the highly metasomatised/ altered olivine clinopyroxenites (OCP III), as seen in Fig. 12.
- Fe_2O_3, Na_2O, K_2O and SiO_2 increase in average content from the weakly metasomatised/ altered (OCP I) to the highly metasomatised/ altered olivine clinopyroxenites or (OCP III), as seen in Fig. 12.
- CaO and Al_2O_3, which show their peak average contents in the moderately metasomatised/ altered (OCP II) olivine clinopyroxenites decrease towards the highly

metasomatised/ altered (OCP III) and weakly metasomatised/ altered olivine clinopyroxenites (OCP I), as seen in Fig. 12.

5.1.4.4 Platreef feldspathic pyroxenites and gabbronorites (OY 482)

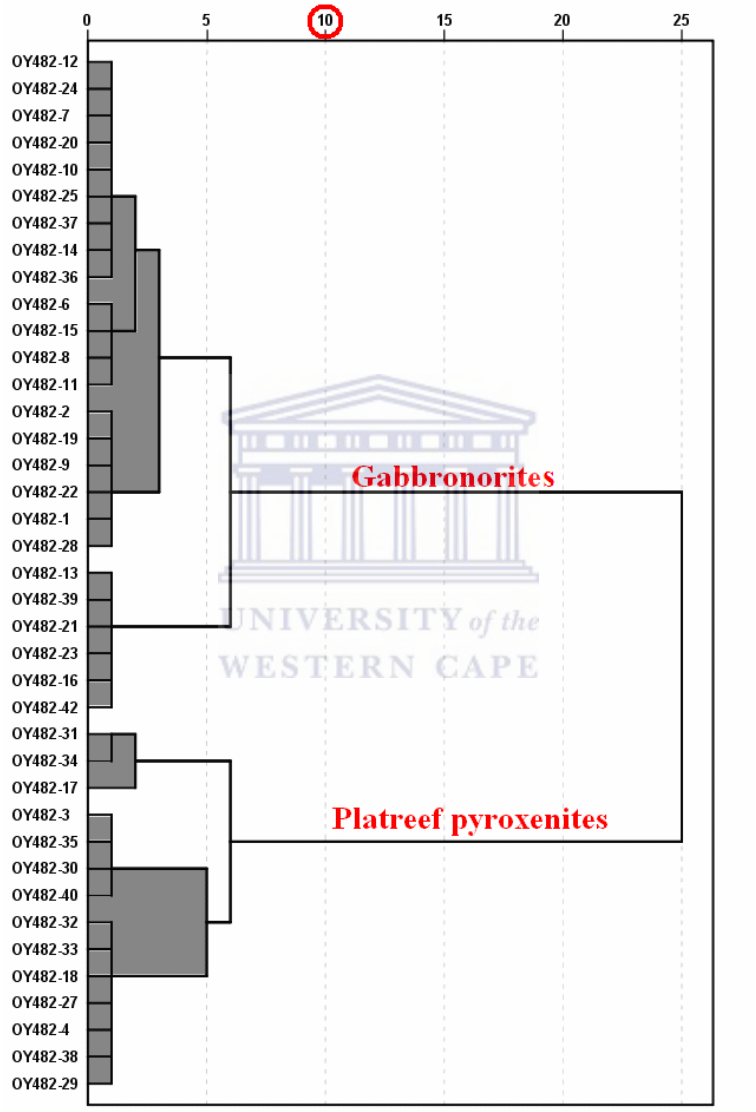

Fig. 13 Dendrogram for sample points cluster identification from data of borehole OY 482: A cut-off distance value of 10 defines the Platreef feldspathic pyroxenites and gabbronorites. Their respective samples are annotated by core-sample ID.

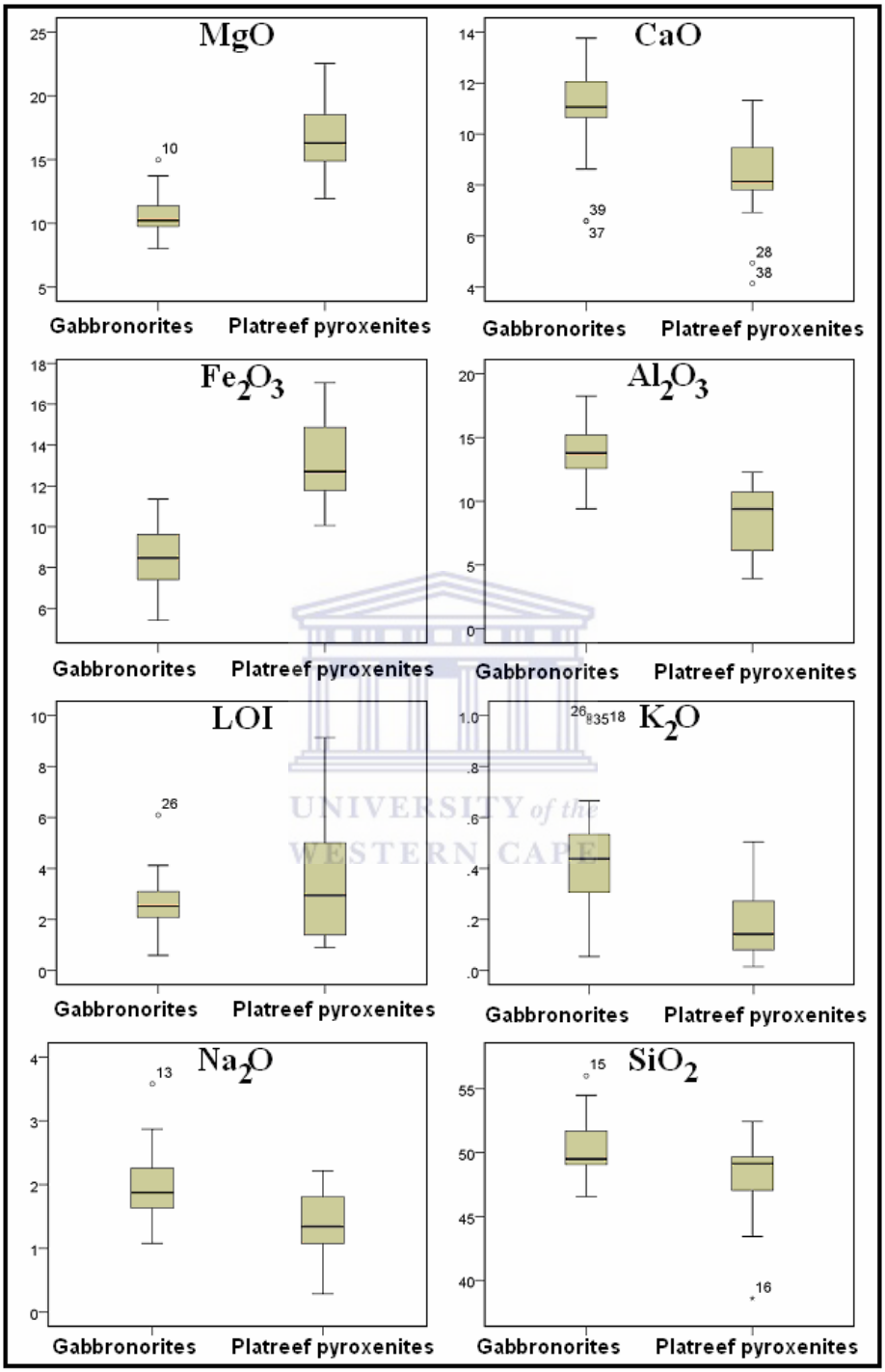

Fig. 14 Box and whiskers plots showing the variation of various oxides between the Platreef feldspathic pyroxenites and gabbronorites in borehole OY 482

HCA was applied to classify samples from borehole OY 482 using major oxide contents in Platreef feldspathic pyroxenites and gabbronorites, using a cut-off distance of 10 (Fig. 13). The box and whisker plots were used to show the pattern of oxides content variation for the Platreef feldspathic pyroxenites and the gabbronorites (Fig. 14). It should be noted that there are two to three gabbronorite and Platreef feldspathic pyroxenite units or subgroups each in the drill section, which may be referred to at a later stage.

The box and whiskers plots of the major oxides in the Platreef feldspathic pyroxenites and gabbronorites show two major distinguishing features:

- A higher average content of MgO, Fe_2O_3 and LOI in the Platreef feldspathic pyroxenites compared to the gabbronorites (Fig. 14).
- Conversely, the average content of CaO, Al_2O_3, Na_2O, K_2O and SiO_2 are higher in the gabbronorites than the Platreef feldspathic pyroxenites (Fig. 14).

5.1.5 Summary

In summary, the most important features to note from the rock classification are:

- Clinopyroxenites have the highest average content of CaO relative to olivine clinopyroxenites and Platreef feldspathic pyroxenites in that order. In terms of comparing the three clinopyroxenite metasomatic subzones, there is a progressive increase in the average contents of Al_2O_3 and K_2O, coupled with a decrease in the average CaO content from the weakly metasomatised to the feldspathic moderately metasomatised subzones.
- Olivine clinopyroxenites have the highest average contents of MgO and LOI when compared to Platreef feldspathic pyroxenites and clinopyroxenites respectively. In terms of comparing the 3 olivine clinopyroxenite metasomatic subzones, there is a progressive increase in the average contents of SiO_2, Fe_2O_3, Na_2O and K_2O coupled with a decrease in the average contents of MgO and LOI from the weakly metasomatised/ altered to the highly metasomatised/ altered subzones.

- Platreef feldspathic pyroxenites have the highest average SiO_2, Al_2O_3, Fe_2O_3, Na_2O and K_2O contents relative to clinopyroxenites and olivine clinopyroxenites respectively. In addition, they also have the highest average MgO, Fe_2O_3 and LOI contents relative to the gabbronorites.
- Gabbronorites have the highest average CaO, Al_2O_3, Na_2O, K_2O and SiO_2 contents when compared to the Platreef feldspathic pyroxenites.

5.2 Geochemical characterisation of the rock types and subtypes

5.2.1 Introduction

Hierarchical clustering analysis was successfully used in classifying the major lithologies in boreholes SS 330 and OY 482 using their major element contents. The box and whiskers plots for the clinopyroxenites and the olivine clinopyroxenites also point to interconnected patterns in the elements/ oxides variation between their subtypes or subzones. The aim of this section is to verify if the clinopyroxenites and olivine clinopyroxenites can be linked to a unitary or single process of contact metasomatism. If so, can the trace elements be used to characterise and fingerprint this process?

Rocks have been classified and characterised using various techniques. For example, King et al. (1997) used discriminant diagram to classify different types of granites and characterise them based on their feldspar content. Ridley (2012) suggests the use of trace elements in spider diagrams as a useful way of graphically representing the abundance of trace elements in rocks. For example, Xu (2002) used the spider diagrams to characterise metasomatised pyroxenites.

Ordóñez-Calderón et al. (2008) exemplified the use of HFSE and rare earth elements (REE) in characterizing and interrelating metasomatic processes associated with clinopyroxenites in the Ivisaartoq greenstone belt using spider diagrams. For this reason, a similar approach will be applied in this study.

5.2.2 Spider diagrams

Ridley (2012) describes spider diagram as an extension of the familiar REE-normalized abundance diagram. Each single pattern, called spidergram, is constructed by plotting an array of trace elements on the X-axis in order of decreasing incompatibility against elemental abundances on the Y-axis (Ridley, 2012). The spidergram can be adjusted to an array of normalizing values, depending upon the difficulty at hand, for e.g., primordial or primitive mantle, chondrite and mid ocean ridge basalt (MORB) (Ridley, 2012).
The reasoning behind normalizing trace element concentrations to a common reference standard (e.g. primordial or primitive mantle, chondrite and MORB) is because these reservoirs, which normalization is done, are thought to be relatively unfractionated samples (Rollinson, 1993).

The primordial mantle is the composition of the mantle before the continental crust formed (Rollinson, 1993). Some of the most popular estimates of its composition are that of Wood et al. (1979) and McDonough et al. (1992); a slight revision of Sun and McDonough (1989). There are number of variations in the list of elements plotted whose concentrations are relatively high in mafic rocks and readily analysed by XRF, and elements are arranged in order of increasing compatibility with respect to a small percentage melt of the mantle (Rollinson, 1993). The normalizing values can be found in various published literature such as Rollinson (1993).

Thompson (1982) suggested normalizing elemental abundances using chondritic values rather than Primitive mantle because chondritic values are measured and not estimated. The order of element is different from that of Wood et al. (1979) and arbitrary to some extent, but was chosen to give the smoothest overall fit to data for Icelandic lavas and North Atlantic ocean-floor basalts. This form of spider diagram approximates to one of increasing compatibility from left to right and since concentrations below about ten times chondrite approach the detection limit for most techniques, caution should be applied in such cases (Thompson et al., 1983).

Pearce (1983) proposed MORB-normalized spider diagrams which are most appropriate for evolved basalts, andesites and crustal rocks. This spider diagram is based on two parameters. Firstly ionic potential (element ionic charge vs. oxidation state/ ionic radius) measures the mobility of the element in aqueous fluid (mobile elements have ionic potential values <3 and >12; immobile have intermediate ionic potential values) (Pearce, 1983). Secondly, the bulk distribution coefficient for the element between garnet lherzolite and melt is used as a measure of incompatibility of an element in small-degree partial melts (Pearce, 1983).

Elements are arranged so that the most mobile are placed on the left of the diagram in order of increasing incompatibility Pearce (1983). The immobile are placed from right to left in order of increasing incompatibility. A slightly different version is used by Saunders and Tarney (1984). These authors suggest that data should be normalized to Zr =10 in order to eliminate concentration differences arising from low-pressure crystal fractionation.

The plotted composition of a trace element lying off the general trend defined by the other elements on a spidergram may define a positive anomaly if it lies above the general trend or a negative anomaly if it lies below the trend (Rollinson, 1993).

Quantifying an anomaly of a specific trace element can be obtained by interpolating the normalized values of the two trace elements adjacent to that specific trace element using the formula suggested by Taylor and McLennan (1985) with respect to $Eu^* = ½(Sm_N + Gd_N)$.

As stated earlier in chapter 5, spider diagrams were used in this study to identify the behaviour of various groups of trace elements; mostly the LILE (Sr, Rb and Ba) and HFSE (Th, U, Ce, Zr, Nb, Ti and Y) in the clinopyroxenites, olivine clinopyroxenites and feldspathic pyroxenites. Transition metals (e.g., Ni, Cu, Co, V and Zn) were excluded since these elements are related to mineralisation.

The above mentioned step enabled a link to be established between element fractionation within the various clinopyroxenite and olivine clinopyroxenite subtypes, and to compare trace element fractionation between the metasomatic rocks (i.e. clinopyroxenites and

olivine clinopyroxenites) in SS 330, magmatic rocks in OY 482 (Platreef feldspathic pyroxenites) and metadolomite floor rock of the Malmani Subgroup (SS 330).

For this study, trace element concentrations were normalized using the primitive mantle values from Sun and McDonough (1989) and the results are presented in Appendix III. The primitive mantle values were chosen since it offers variations in the list of elements plotted whose concentrations are readily analysed by XRF.
The Rb^* (½[Ba_N]), K^*(½[Nb_N + Ce_N]), Sr^*(½[Pb_N + P_N]), Zr^*(½[P_N + Ti_N]) and Ti^*(½[Zr_N + Y_N]) anomalies were calculated with respect to the neighbouring immobile elements following the method of Taylor and McLennan (1985) and the results are presented in Appendix IV.

The following paragraphs present the geochemical characterisation of clinopyroxenites, olivine clinopyroxenites, Platreef feldspathic pyroxenites and gabbronorites.

5.2.3 Geochemical characterisation of the rock types/ subtypes

A composite summary table was compiled to geochemically characterise each rock type (i.e. clinopyroxenites, olivine-rich clinopyroxenites, Platreef feldspathic pyroxenites and gabbronorites). The data used in the Tables (2, 3 & 4) derived from the chemical analyses of the various rock types.

These tables include minima, maxima and medians, and five element groups were also considered. These groups include the oxides, trace elements, calculated elemental ratios (i.e. Al_2O_3/TiO_2, Ti/Zr, and Zr/Y) and mantle normalized trace element anomalies (Rb^*, K^*, Sr^*, Zr^* and Ti^*), and PGE (Pt, Pd and Au).

Immobile element ratios and trace element anomalies were included to compare their variation patterns between the rock types and subtypes. The median data for the metadolomites in borehole SS 330 and those of the Lower Platreef in borehole OY 482 are also included in these tables for comparison.

The least altered samples comprise three metadolomite samples from the Malmani Subgroup. These were taken below the depth of 620 meters in borehole SS 330 and are as follows: Samples SS 330-86, 93 and 94 (Fig. 5). Those of the Lower Platreef comprise four samples (OY 482-38, 39, 40 and 42; Fig. 3). These are plotted as a grey field in each spider diagram.

The results are presented in the following order:

- The spider diagrams for the clinopyroxenites I, II and III are shown in Figs. 14, 15 and 16 respectively, and the statistical summary of associated data are presented in Table 2.
- The spider diagrams for the olivine clinopyroxenites I, II and III are shown in Figs. 17, 18 and 19 respectively, and the statistical summary of associated data are presented in Table 3.
- The spider diagrams for the Upper and Middle Platreef are shown in Fig. 21a and the statistical summary of associated data is presented in Table 4.
- The spider diagram for the gabbronorites is shown in Fig. 21b and the statistical summary of associated data is presented in Table 4.

5.2.3.1 Clinopyroxenites

The statistical summary of oxides, trace elements, element ratios and mantle normalized anomalies from the spider diagram for the metadolomites of the Malmani Subgroup, the Lower Platreef from borehole OY 482 and the clinopyroxenites from borehole SS 330 are presented in Table 2.

When compared to the clinopyroxenites, metadolomites of the Malmani Subgroup typically show higher CaO, MgO and LOI contents whereas the Lower Platreef are higher in SiO_2 and lower in CaO contents, as seen in Table 2.

Table 2: Statistical summary of oxides (wt. %), trace elements (ppm), element ratios, mantle normalized ($_{MN}$) trace anomalies and PGE (g/t) for clinopyroxenites. Median for metadolomites (M-Dol., SS 330) and Lower Platreef (LP, OY 482) are used for comparison.

Rock type	Clinopyroxenite I (N=22)			Clinopyroxenite II (N=11)			Clinopyroxenite III (N=8)			M-Dol. (N=3)	LP (N=4)
Variable	Min	Max	Median	Min	Max	Median	Min	Max	Median	Median	Median
SiO_2 (wt %)	34.25	51.98	43.49	33.04	42.71	41.17	38.85	52.59	44.82	0.01	51.10
Al_2O_3	0.13	10.35	4.14	2.39	9.13	5.06	8.12	14.85	10.60	<0.01	10.84
Fe_2O_3	1.11	13.46	8.90	4.44	26.22	8.53	7.86	14.70	10.06	<0.01	10.70
MnO	0.19	0.49	0.24	0.22	0.79	0.34	0.14	0.35	0.23	0.26	0.16
MgO	8.35	18.87	14.39	10.59	25.04	20.80	6.84	19.27	15.29	28.71	14.03
CaO	19.02	35.27	26.91	14.72	21.60	19.13	8.10	19.68	14.88	35.15	6.59
Na_2O	0.51	1.33	0.73	0.38	1.87	0.53	0.77	3.05	1.09	0.62	2.05
K_2O	<0.01	0.03	<0.01	<0.01	0.17	<0.01	0.06	2.07	0.84	<0.01	0.34
P_2O_5	0.01	0.17	0.03	0.01	0.04	0.02	0.02	0.07	0.02	0.01	0.05
TiO_2	0.04	0.65	0.31	0.04	0.52	0.31	0.14	0.32	0.23	0.01	0.23
SO_3	0.01	0.36	0.11	0.00	3.17	0.14	0.02	0.29	0.11	<0.01	0.29
LOI	0.20	8.94	1.84	0.02	5.28	2.99	0.04	4.18	2.13	37.95	2.92
As (ppm)	4.58	353.42	19.75	0.75	116.21	10.11	4.57	25.31	18.41	101.15	4.53
Ba	36.96	112.68	54.98	37.77	106.54	50.95	57.48	717.96	368.89	54.69	144.67
Ce	0.06	209.58	102.12	13.86	299.65	88.03	7.74	139.93	96.15	85.61	78.85
Co	0.03	110.02	40.94	0.03	202.69	33.80	32.66	130.97	76.34	0.86	95.29
Cu	35.65	1531.61	320.34	13.39	3123.06	183.86	57.92	889.87	395.78	28.85	1034.30
Nb	3.22	16.38	8.26	7.40	21.45	12.74	8.89	20.34	14.05	9.47	18.54
Ni	75.02	4623.34	438.17	80.62	4286.82	1075.22	188.53	2647.32	769.73	7.70	1653.05
Pb	0.07	152.61	7.26	0.07	11.52	8.12	2.85	18.83	7.61	1.07	8.21
Rb	0.66	5.45	2.52	0.25	29.07	2.19	7.96	130.09	34.00	2.19	19.77
Sr	4.06	36.69	12.52	3.39	27.13	12.41	33.88	496.33	233.87	28.69	208.31
V	11.35	245.85	138.58	4.74	295.10	76.86	50.24	206.66	91.91	0.57	88.31
Y	0.08	82.00	8.55	1.06	15.78	6.99	0.08	9.36	4.89	1.08	7.10
Zn	36.77	262.76	60.35	44.40	478.98	60.36	46.83	97.30	74.12	21.60	94.22
Zr	5.84	107.45	28.92	0.85	78.91	34.00	10.06	44.46	17.65	3.22	27.84
Mo	1.32	13.14	5.05	0.02	8.07	2.91	1.98	7.58	3.32	0.02	4.05
U	<0.01	2.51	<0.01	<0.01	<0.01	<0.01	<0.01	<0.01	<0.01	<0.01	0.39
Th	0.20	0.20	0.20	0.20	0.20	0.20	0.20	188.41	46.90	0.20	46.35
Al_2O_3/TiO_2	3.64	33.20	13.07	6.15	80.11	16.82	32.09	79.46	49.62	0.07	46.80
Ti/Zr	20.00	231.09	65.34	29.28	295.52	55.98	42.58	100.89	70.64	15.70	51.15
Zr/Y	0.32	134.50	3.49	0.80	16.38	5.37	1.07	382.50	5.73	5.00	5.65
$Rb^*_{(MN)}$	0.13	1.62	0.49	0.04	3.00	0.54	0.71	2.35	1.19	0.44	1.89
$K^*_{(MN)}$	<0.01	0.07	<0.01	<0.01	0.36	<0.01	0.08	5.87	0.63	<0.01	0.37
$Sr^*_{(MN)}$	<0.01	0.74	<0.01	<0.01	0.63	0.01	0.05	0.31	0.23	0.18	0.15
$Zr^*_{(MN)}$	0.43	4.14	1.92	0.23	4.98	2.78	0.97	2.77	1.57	1.75	1.81
$Ti^*_{(MN)}$	0.05	0.89	0.66	0.36	1.25	0.61	0.45	1.25	0.78	0.20	0.50
		(N=11)			(N=5)			(N=5)			(N=2)
Au (g/t)	0.05	0.30	0.09	0.05	1.02	0.33	0.12	2.05	0.20	n.d	0.12
Pd	0.05	2.53	0.75	0.16	12.24	2.94	0.07	30.00	0.57	n.d	1.08
Pt	0.05	4.00	0.72	0.14	30.00	2.65	0.16	30.00	0.22	n.d	0.94

In other words, relative to the metadolomites of the Malmani Subgroup, the clinopyroxenites show higher median values for SiO_2, Al_2O_3, Fe_2O_3, TiO_2, Ce, Pb, Y, Zr and lower median values of CaO, MgO, LOI and As (Table 2). Similarly, the clinopyroxenites display higher median values of CaO, MgO and MnO, and lower median values of SiO_2, Al_2O_3, Fe_2O_3, Na_2O, Nb, Th and U when compared to the Lower Platreef, as seen in Table 2.

The three clinopyroxenite subtypes or subzones have highly variable geochemical characteristics (Table 2; Figs. 15, 16 and 17). Clinopyroxenite I has variable CaO (19.02 - 35.27 wt. %), Al_2O_3 (0.13 - 10.35 wt. %), K_2O (<0.01 - 0.03 wt. %), Nb (3.22 - 16.38 ppm) and Y (0.08 - 82.00 ppm) contents, as seen in Table 2. These rocks also exhibit Al_2O_3/TiO_2 and Zr/Y ratios mostly between 3.64 - 33.20 and 0.32 - 134.50 respectively (Table 2). The median values of these ratios are lower than those obtained for the lower feldspathic pyroxenites with the exception of the median value of the Zr/Y ratio, which is lower than that in the metadolomites (Table 2).

On the primitive mantle normalized trace element diagrams (Figs. 15a & 15b), clinopyroxenites I displays near flat HFSE pattern with trace element ratios in Table 2 which are relatively higher than those in the dolomites coupled with a comparatively lower LILE pattern with ratio values which are lower than to those in the Lower Platreef. The clinopyroxenites I display marked negative K ($K^*_{(MN)}$ = <0.01 - 0.07), Sr ($Sr^*_{(MN)}$ = <0.01 - 0.74) and Rb ($Rb^*_{(MN)}$ = 0.13 - 1.62) anomalies when compared to the Lower Platreef, while the Zr ($Zr^*_{(MN)}$ = 0.43 - 4.14) and Ti ($Ti^*_{(MN)}$ = 0.05 - 0.89) anomalies are positive compared to the metadolomites (Table 2; Figs. 15a & 15b).

Clinopyroxenite II, when compared to the clinopyroxenite subtype I, shows lower contents of CaO (14.72 - 21.60 wt. %) and Y (1.06 - 15.78 ppm), and higher Al_2O_3 (2.39 - 9.13 wt. %), K_2O (<0.01 - 0.17 wt. %) and Nb (7.40 - 21.45 ppm) contents (Table 2). This clinopyroxenite subtype is characterised by Al_2O_3/TiO_2 and Zr/Y ratios ranging between 6.15 - 80.11 and 0.8 - 16.38 respectively, whose median values differ slightly from the clinopyroxenite subtype I, as shown in Table 2.

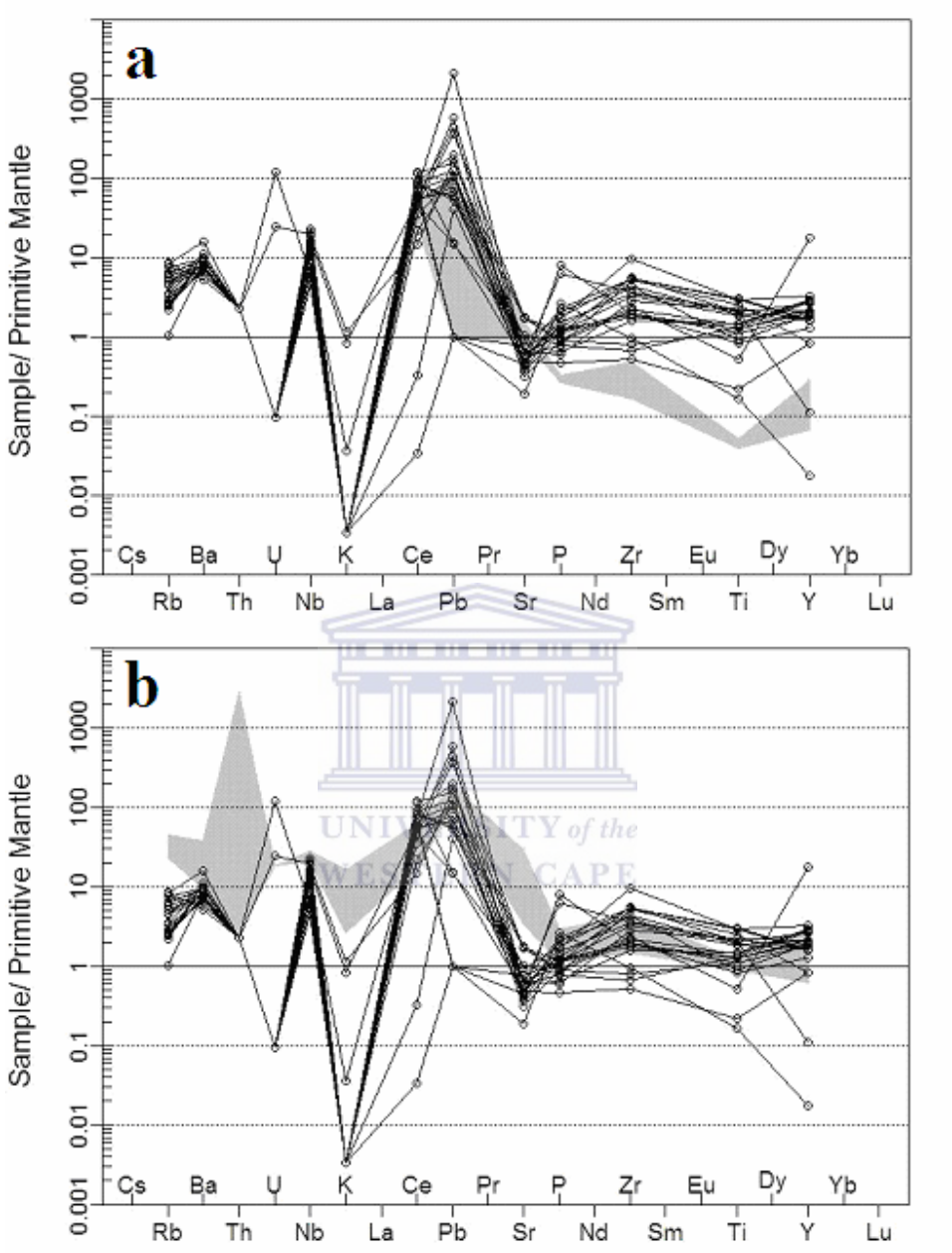

Fig. 15 Trace element compositions of clinopyroxenites from subtype I (CP I) for borehole SS 330. The grey field in (a) is the trace-element pattern of the metadolomites from SS 330 and in (b) the Lower Platreef from OY 482 is shown for comparison. Primitive mantle normalization values from Sun and McDonough (1989).

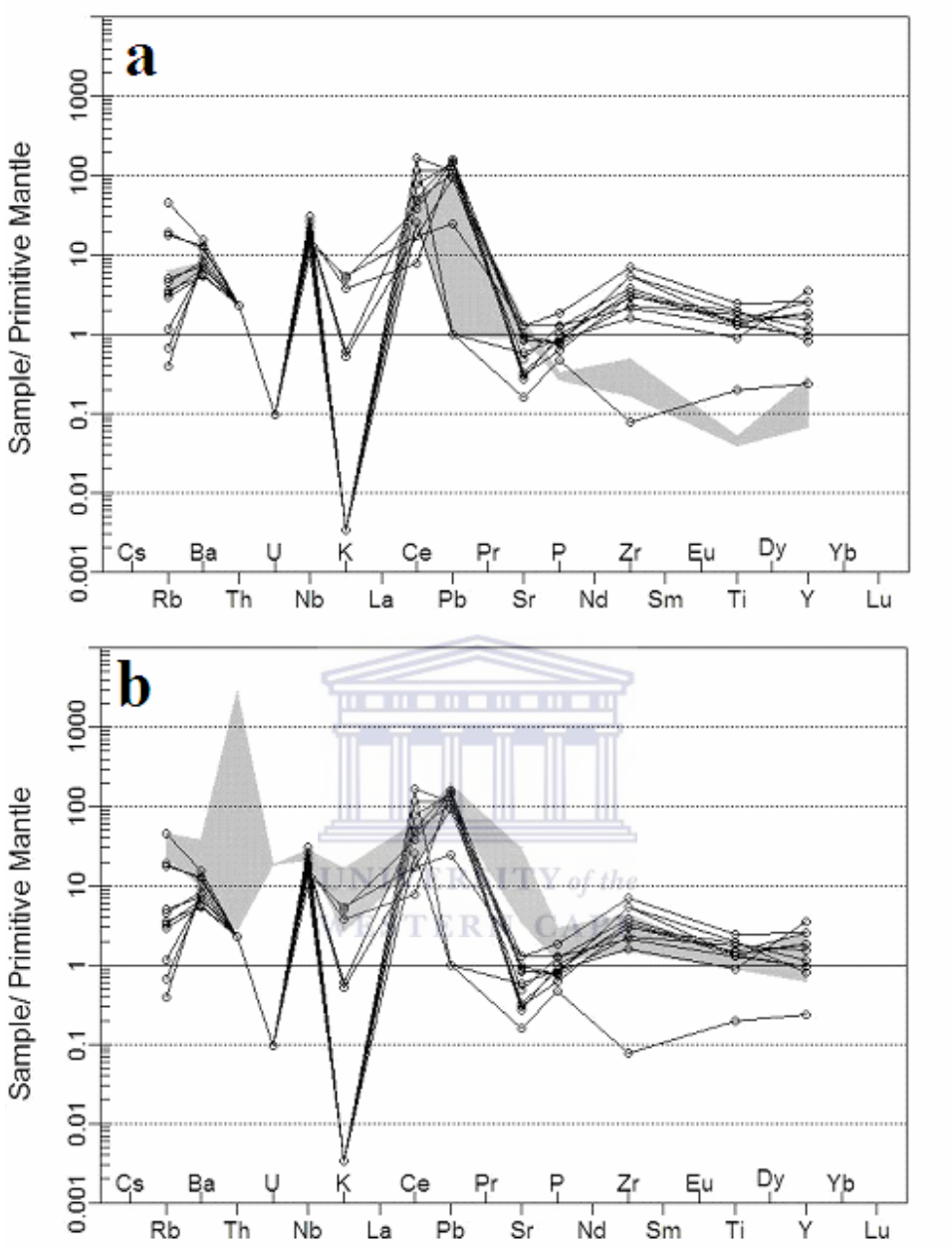

Fig. 16 Trace element compositions of clinopyroxenites from subtype II (CP II) for borehole SS 330. The grey field in (a) is the trace-element pattern of the metadolomites from SS 330 and in (b) the Lower Platreef from OY 482 is shown for comparison. Primitive mantle normalization values from Sun and McDonough (1989).

Spider diagrams in Figs. 16a & 16b show that clinopyroxenites II also display a nearly flat HFSE pattern with ratios which are also relatively higher than those in the

metadolomites (except sample 29 for Zr and Y) and also have a lower LILE pattern and ratios compared to those in the Lower Platreef.

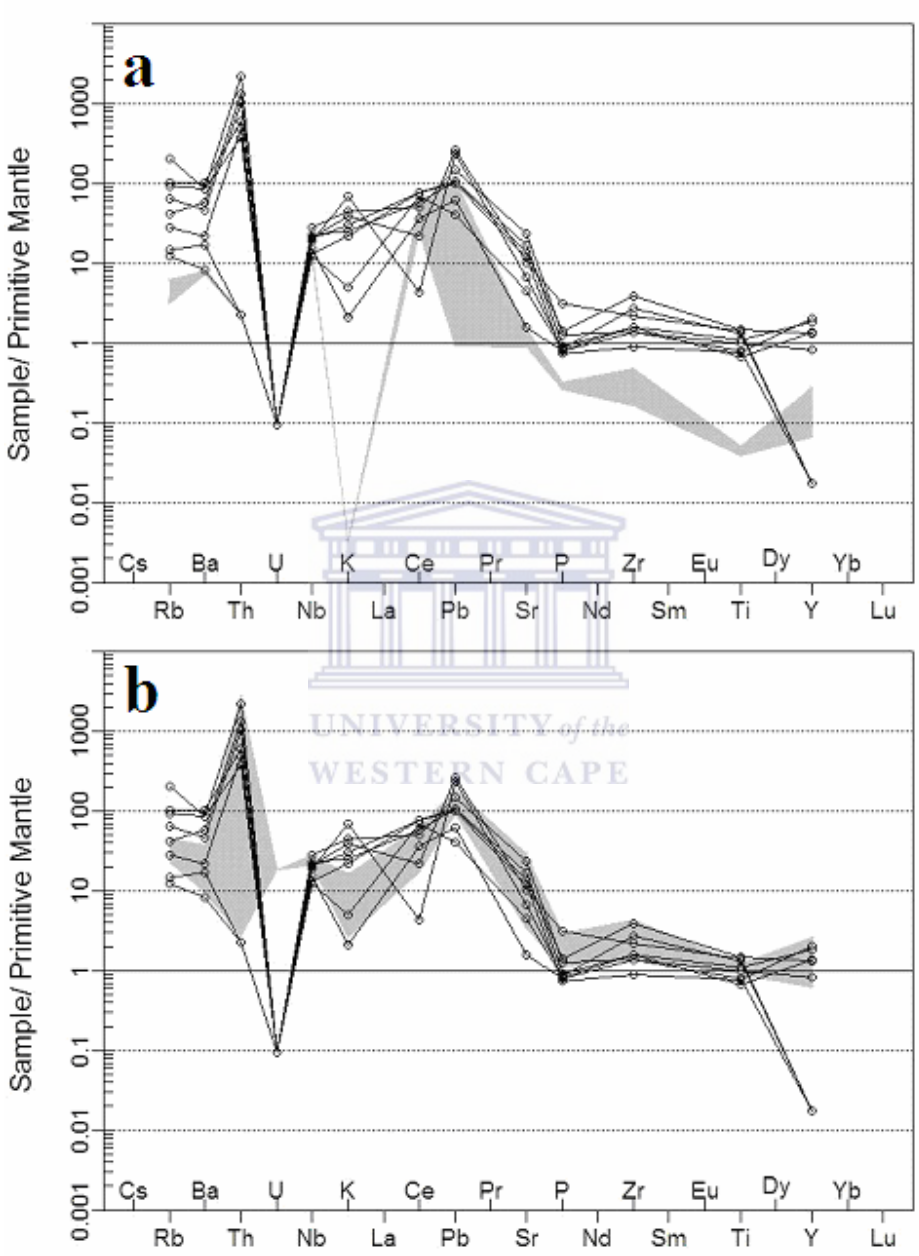

Fig. 17 Trace element compositions of clinopyroxenites from subtype III (CP III) for borehole SS 330. The grey field in (a) is the trace-element pattern of the metadolomites from SS 330 and in (b) the Lower Platreef from OY 482 is shown for comparison. Primitive mantle normalization values from Sun and McDonough (1989).

These rocks also possess negative K ($K^*_{(MN)}$ = <0.01 - 0.36), Sr ($Sr^*_{(MN)}$ = <0.01 - 0.63) and Rb ($Rb^*_{(MN)}$ = 0.04 - 3.00) anomalies relative to the Lower Platreef, while the Zr ($Zr^*_{(MN)}$ = 0.23 - 4.98) and Ti ($Ti^*_{(MN)}$ = 0.36 - 1.25) anomalies are positive relative to the metadolomites (Table 2; Figs. 16a & 16b). The median values of these trace element anomalies differ from the clinopyroxenite subtype I, as shown in table 2.

Table 2 shows that clinopyroxenite III displays varying CaO (8.10 - 19.68 wt. %), Al_2O_3 (8.12 - 14.85 wt. %), K_2O (0.06 - 2.07 wt. %), Nb (8.89 - 20.34 ppm) and Y (0.08 - 9.36 ppm) contents. This clinopyroxenite subtype, when compared to the clinopyroxenite subtypes I & II, shows a higher average content of SiO_2, Al_2O_3, Fe_2O_3, Na_2O and K_2O coupled with a lower content of CaO (Table 2). These rock samples are characterised by Al_2O_3/TiO_2 and Zr/Y ratios ranging between 32.09 - 79.46 and 1.07 - 382.50 respectively, with more elevated median values when compared to clinopyroxenite subtypes I & II (Table 2).

The spider diagrams in Figure 16b show HFSE and LILE patterns that are very similar to the Lower Platreef at Overysel. These patterns differ markedly from those of the other clinopyroxenite subtypes (CP I and CP II) and, in particular, the metadolomites of the Malmani Subgroup (Figs. 17a & 17b). The clinopyroxenite subtype III has more positive K ($K^*_{(MN)}$ = 0.08 - 5.87), Sr ($Sr^*_{(MN)}$ = 0.05 - 0.31) and Rb ($Rb^*_{(MN)}$ = 0.71 - 2.35) anomalies than both the clinopyroxenite subtypes I and II as seen in Table 2. The Ti ($Ti^*_{(MN)}$ = 0.45 - 1.25) and Zr ($Zr^*_{(MN)}$ = 0.97 - 2.77) anomalies have similar variation patterns (Table 2; Figs. 17a & 17b).

5.2.3.2 Olivine clinopyroxenites

The statistical summary of oxides, trace elements, element ratios and mantle normalized anomalies from the spider diagram for the metadolomites of the Malmani Subgroup, the Lower Platreef from borehole OY 482 and the olivine clinopyroxenites from borehole SS 330 are presented in Table 3.

Table 3: Statistical summary of oxides (wt. %), trace elements (ppm), element ratios, mantle normalized ($_{MN}$) trace anomalies and PGE (g/t) for olivine clinopyroxenites. Median for metadolomites (M-Dol., SS 330) and Lower Platreef (LP, OY 482) are used for comparison.

Rock type	Olivine clinopyroxenite I (N=11)			Olivine clinopyroxenite II (N=14)			Olivine clinopyroxenite III (N=11)			M-Dol. (N=3)	LP (N=4)
Variable	Min	Max	Median	Min	Max	Median	Min	Max	Median	Median	Median
SiO_2 (Wt %)	29.51	40.53	36.81	33.07	39.64	37.40	35.92	41.70	39.76	0.01	51.10
Al_2O_3	1.33	11.58	4.29	2.04	11.85	8.44	3.84	9.36	6.40	<0.01	10.84
Fe_2O_3	2.60	9.63	4.41	5.38	9.24	7.59	6.24	12.10	7.96	<0.01	10.70
MnO	0.16	1.07	0.59	0.32	0.79	0.60	0.28	0.59	0.39	0.26	0.16
MgO	30.25	37.28	33.42	25.26	30.14	29.09	25.67	31.23	27.70	28.71	14.03
CaO	4.07	13.04	8.82	6.15	14.46	11.19	7.46	12.40	10.28	35.15	6.59
Na_2O	0.07	0.40	0.19	0.23	0.47	0.28	0.25	0.54	0.35	0.62	2.05
K_2O	<0.01	<0.01	<0.01	<0.01	0.14	0.02	0.08	0.47	0.31	<0.01	0.34
P_2O_5	0.01	0.02	0.01	0.01	0.04	0.02	0.01	0.04	0.02	0.01	0.05
TiO_2	0.04	0.22	0.12	0.14	0.38	0.28	0.15	0.42	0.21	0.01	0.23
SO_3	<0.01	0.47	0.03	0.01	0.14	0.04	<0.01	0.27	0.04	<0.01	0.29
LOI	8.13	14.53	10.89	3.10	9.36	6.66	4.39	7.97	5.58	37.95	2.92
As (ppm)	<0.01	13.88	<0.01	<0.01	8.75	1.96	<0.01	18.12	1.94	101.15	4.53
Ba	41.50	59.49	47.98	36.72	81.77	63.13	59.87	150.19	83.19	54.69	144.67
Ce	3.09	59.11	30.46	0.06	112.73	80.02	35.00	124.75	66.79	85.61	78.85
Co	0.03	23.79	15.95	11.12	38.69	22.75	30.42	65.19	42.82	0.86	95.29
Cu	8.90	714.27	52.06	22.54	436.25	68.45	12.42	491.80	124.86	28.85	1034.30
Nb	5.22	14.13	11.45	9.21	17.17	11.74	10.13	14.97	12.24	9.47	18.54
Ni	17.84	1816.36	97.55	28.69	1471.19	342.52	74.92	1524.10	629.25	7.70	1653.05
Pb	0.07	5.17	0.19	0.07	10.20	1.89	0.07	9.77	2.40	1.07	8.21
Rb	0.05	7.62	1.54	0.20	22.55	4.71	5.20	56.83	17.97	2.19	19.77
Sr	0.03	17.97	2.48	1.94	98.65	24.31	11.51	145.08	66.90	28.69	208.31
V	4.38	46.73	10.89	25.97	99.56	61.40	26.70	124.53	57.21	0.57	88.31
Y	3.01	24.46	7.89	0.28	14.03	6.53	0.08	6.68	4.29	1.08	7.10
Zn	26.99	160.68	50.58	29.88	107.67	80.09	40.97	77.41	68.35	21.60	94.22
Zr	1.51	47.09	22.55	25.67	58.15	47.67	25.77	133.06	33.73	3.22	27.84
Mo	0.02	1.27	0.09	0.02	3.52	0.88	0.54	3.48	1.25	0.02	4.05
U	<0.01	25.24	<0.01	<0.01	<0.01	<0.01	<0.01	<0.01	<0.01	<0.01	0.39
Th	0.20	0.20	0.20	0.20	0.20	0.20	0.20	19.92	0.20	0.20	46.35
Al_2O_3/TiO_2	11.33	236.34	41.86	6.59	70.88	28.82	9.12	50.68	27.61	0.07	46.80
Ti/Zr	20.10	172.70	45.01	31.48	45.99	36.24	18.98	42.16	36.63	15.70	51.15
Zr/Y	0.28	7.93	1.80	3.06	91.68	7.16	4.64	446.25	8.91	5.00	5.65
$Rb^*_{(MN)}$	0.01	1.51	0.37	0.04	4.13	0.76	0.96	9.53	1.90	0.44	1.89
$K^*_{(MN)}$	<0.01	<0.01	<0.01	<0.01	0.15	0.02	0.08	0.80	0.30	<0.01	0.37
$Sr^*_{(MN)}$	<0.01	0.53	0.02	<0.01	3.60	0.12	0.01	4.40	0.20	0.18	0.15
$Zr^*_{(MN)}$	0.39	6.21	2.76	2.44	4.55	3.85	2.47	8.77	3.44	1.75	1.81
$Ti^*_{(MN)}$	0.08	0.50	0.34	0.30	0.68	0.49	0.31	0.59	0.51	0.20	0.50
		(N=2)			(N=3)			(N=3)			(N=2)
Au (g/t)	0.36	0.91	0.64	0.05	0.57	0.54	0.05	0.35	0.16	n.d	0.12
Pd	2.18	8.89	5.54	0.05	6.24	6.04	0.05	1.96	0.09	n.d	1.08
Pt	2.26	11.28	6.77	0.05	7.25	4.54	0.05	1.66	0.13	n.d	0.94

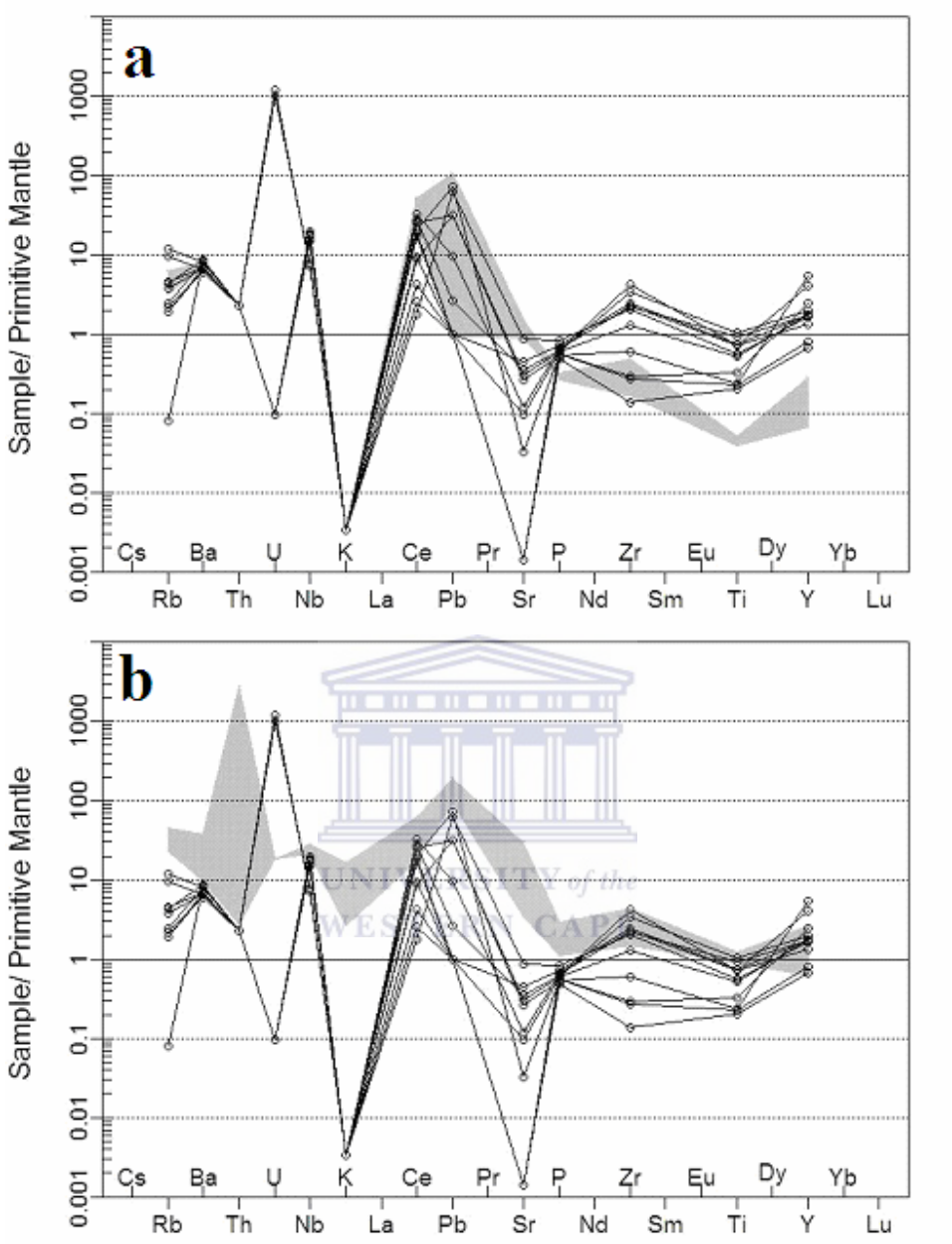

Fig. 18 Trace element compositions of olivine clinopyroxenites from subtype I (OCP I) for borehole SS 330. The grey field in (a) is the trace-element pattern of the metadolomites from SS 330 and in (b) the Lower Platreef from OY 482 is shown for comparison. Primitive mantle normalization values from Sun and McDonough (1989).

Relative to the metadolomites of the Malmani Subgroup, the olivine clinopyroxenites have higher median values of SiO_2, Al_2O_3, Fe_2O_3 and MnO coupled with a lower CaO, Na_2O and LOI median contents (Table 3). Most trace elements and the Al_2O_3/TiO_2, Ti/Zr ratios as well as $Zr^*_{(MN)}$, and $Ti^*_{(MN)}$ have lower contents in the metadolomites when

compared with the olivine clinopyroxenites (Table 3). The latter on the other hand, when compared with the Lower Platreef (OY 482), contain lower median contents of SiO_2, Al_2O_3, Fe_2O_3, Na_2O and K_2O as well as Al_2O_3/TiO_2 and Ti/Zr ratios and most trace elements which are coupled with more elevated median contents of MgO, CaO, MnO and LOI (Table 3). The $K^*_{(MN)}$ shows a lower median content while $Zr^*_{(MN)}$ has a more elevated median content when compared to the Lower Platreef (Table 3).

The three subtypes or subzones of the olivine clinopyroxenites also show highly variable geochemical characteristics as presented in Table 3 and Figs. 18, 19 & 20.
Olivine clinopyroxenite I shows the highest contents of MgO (30.25 - 37.28 wt. %) and LOI (8.13 - 14.53 wt. %) coupled with the lowest median contents of SiO_2 (36.81 wt. %), Fe_2O_3 (4.29 wt. %), CaO (8.82 wt. %), Na_2O (0.19 wt. %) and K_2O (<0.01 wt. %) when compared to olivine clinopyroxenite subtypes II and III (Table 3). With the exception of the base metals, the olivine clinopyroxenite I contains the lowest range/ content of trace elements compared to both olivine clinopyroxenite subtypes II and III (Table 3). Its high MgO coupled with subdued CaO contents distinguishes them from the clinopyroxenites.

The olivine clinopyroxenite I shows wide ranging values for Al_2O_3/TiO_2 and Ti/Zr ratios, and more subdued Zr/Y ratios compared to both olivine clinopyroxenite subtypes II and III (Table 3). In spider diagrams (Figs. 18a & 18b), these rocks display near flat but elevated HFSE patterns in contrast to the metadolomites. The relatively lower content of trace elements, mainly the LILE, in the olivine clinopyroxenite I when compared to the Lower Platreef is obvious in the spider diagrams (Fig. 18b). The olivine clinopyroxenite I is characterised by lower negative K ($K^*_{(MN)}$ = <0.01), Sr ($Sr^*_{(MN)}$ = 0.02), Rb ($Rb^*_{(MN)}$ = 0.37), Ti ($Ti^*_{(MN)}$ = 0.34) and Zr ($Zr^*_{(MN)}$ = 2.76) anomalies relative to olivine clinopyroxenite subtypes II and III (Table 3).

Olivine clinopyroxenite II has higher median contents of SiO_2 (37.40 wt. %), Fe_2O_3 (7.59 wt. %), Al_2O_3 (8.44 wt. %), CaO (11.19 wt. %), coupled with a more subdued MgO (29.09 wt. %) and LOI (6.6 wt. %) relative to olivine clinopyroxenite I (Table 3).

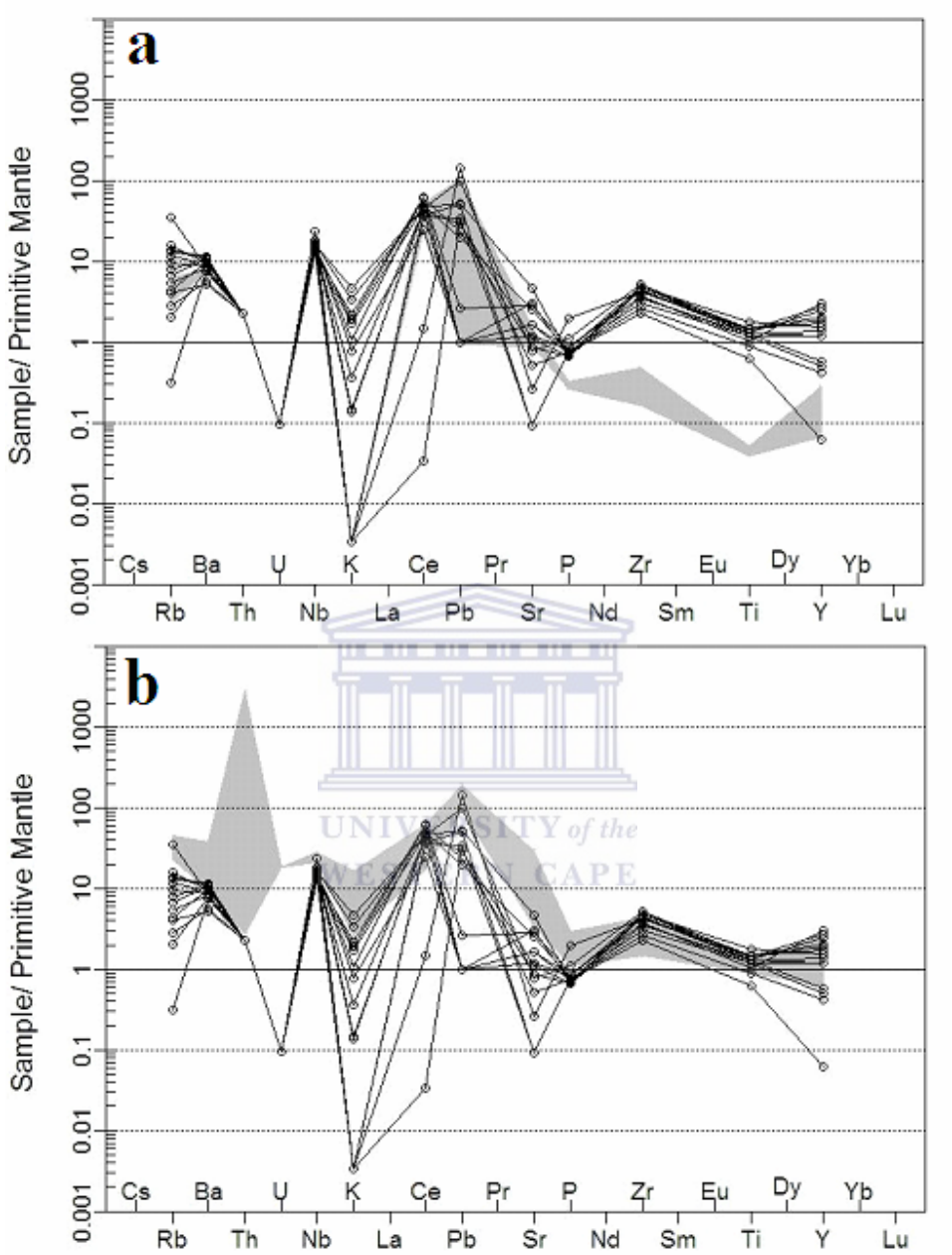

Fig. 19 Trace element compositions of olivine clinopyroxenites from subtype II (OCP II) for borehole SS 330. The grey field in (a) is the trace-element pattern of the metadolomites from SS 330 and in (b) the Lower Platreef from OY 482 is shown for comparison. Primitive mantle normalization values from Sun and McDonough (1989).

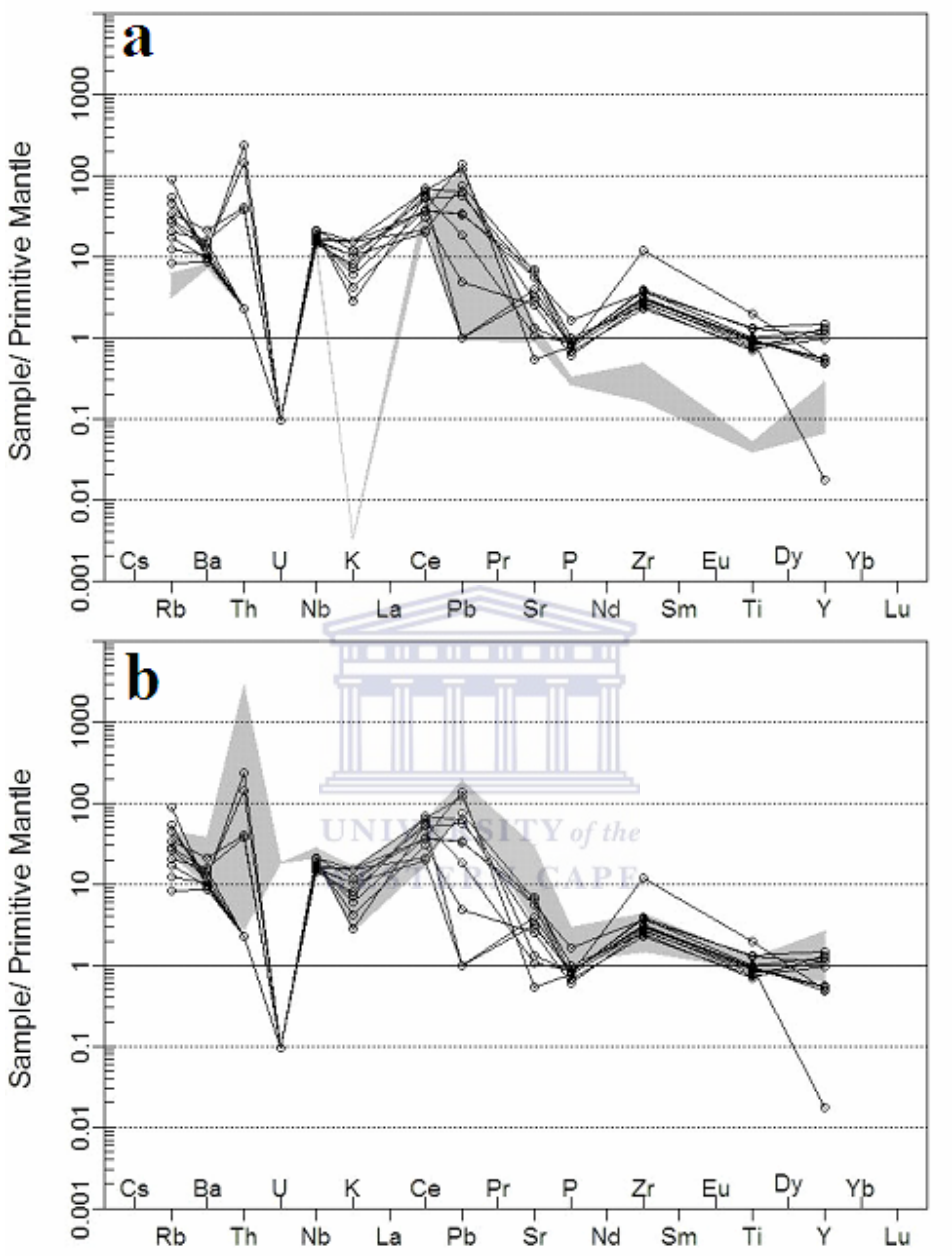

Fig. 20 Trace-element compositions of olivine clinopyroxenites from subtype III (OCP III) for borehole SS 330. The grey field in (a) is the trace-element pattern of the metadolomites from SS 330 and in (b) the Lower Platreef from OY 482 is shown for comparison. Primitive mantle normalization values from Sun and McDonough (1989).

These rocks also generally have higher trace element contents than the subtype I, which are coupled with a lower and higher median contents for Al_2O_3/TiO_2 and Ti/Zr, and Zr/Y respectively (Table 3). A more elevated and relatively near flat HFSE pattern when

compared to the metadolomites is evident on the spider diagrams of the olivine clinopyroxenite II, coupled with much more elevated LILE values compared to the olivine clinopyroxenite subtype I (Figs. 19a & 19b). In consonance, Table 3 shows more positive K ($K^*_{(MN)}$ = 0.02), Rb ($Rb^*_{(MN)}$ = 0.76), Sr ($Sr^*_{(MN)}$ = 0.12), Ti ($Ti^*_{(MN)}$ = 0.49) and Zr ($Zr^*_{(MN)}$ = 3.85) anomalies than the corresponding median values for olivine clinopyroxenite I (Table 3; Figs. 19a & 19b).

Olivine clinopyroxenite III, when compared to subtypes I and II, is characterised by slightly higher median contents for SiO_2 (39.76 wt. %), Fe_2O_3 (7.96 wt. %), Na_2O (0.35 wt. %) and K_2O (0.31 wt. %), coupled with intermediate contents of Al_2O_3 (6.4 wt. %) and CaO (10.28 wt. %), as seen in Table 3. In addition, this subtype also displays lower median contents of MnO (0.39 wt. %), MgO (27.70 wt. %) and LOI (5.58 wt. %) relative to subtypes I and II (Table 3). These rocks, similar to subtype II generally feature higher trace element contents than olivine clinopyroxenite subgroup I, which also are coupled with a lower median Al_2O_3/TiO_2 ratio and intermediate to higher median Ti/Zr and Zr/Y ratios respectively (Table 3).

The spider diagrams are very similar to the Lower Platreef at Overysel (Fig. 20b). A more elevated and relatively flat HFSE pattern compared to the metadolomites is also evident on the spider diagrams of the OCP III, but these are coupled with much more elevated LILE compared to the OCP I and II (Figs. 20a & 20b). In consonance, Table 3 shows more positive K ($K^*_{(MN)}$ = 0.3), Rb ($Rb^*_{(MN)}$ = 1.9) and Sr ($Sr^*_{(MN)}$ = 0.2) anomalies, and almost similar Ti ($Ti^*_{(MN)}$ = 0.51) and Zr ($Zr^*_{(MN)}$ = 3.44) anomalies than the corresponding values for the OCP II (Table 3; Figs. 20a & 20b).

5.2.3.3 Lower Platreef feldspathic pyroxenites

Relative to the Upper and Middle Platreef, the Lower Platreef pyroxenite is characterised by slightly higher median contents for SiO_2 (51.10 wt. %), Al_2O_3 (10.84 wt. %), Na_2O (2.05 wt. %), K_2O (0.34 wt. %) and TiO_2 (0.23 wt. %), coupled with slightly lower median contents for Fe_2O_3 (10.70 wt. %), MgO (14.03 wt. %) and CaO (6.59 wt. %), as seen in Table 4 below.

Table 4: Statistical summary of the major (wt. %), trace element (ppm), element ratios, mantle normalized ($_{MN}$) trace anomalies and PGE (g/t) for gabbronorites, Upper and Middle Platreef. Values for the Lower Platreef are used for comparison.

Rock type	Gabbronorite (N=23)			Upper & Middle Platreef (N=12)			Lower Platreef (N=4)		
Variable	Min	Max	Median	Min	Max	Median	Min	Max	Median
SiO_2 (Wt %)	46.56	56.02	49.44	38.59	52.44	49.18	49.14	53.94	51.10
Al_2O_3	9.97	18.24	13.77	4.30	11.45	9.39	3.94	15.02	10.84
Fe_2O_3	5.43	10.92	8.47	11.11	17.05	12.70	7.33	15.15	10.70
MnO	0.11	0.17	0.13	0.16	0.23	0.17	0.12	0.20	0.16
MgO	8.02	14.97	10.19	11.95	22.54	16.30	11.21	19.26	14.03
CaO	8.63	13.76	11.25	4.95	11.32	8.35	4.15	8.18	6.59
Na_2O	1.08	3.58	1.84	0.29	2.22	1.34	1.22	2.87	2.05
K_2O	0.05	1.00	0.44	0.02	0.38	0.14	0.08	0.50	0.34
P_2O_5	0.01	0.03	0.02	0.01	0.07	0.02	0.02	0.06	0.05
TiO_2	0.11	0.24	0.15	0.12	0.27	0.19	0.20	0.26	0.23
SO_3	<0.01	1.02	0.03	0.01	0.66	0.17	0.11	0.51	0.29
LOI	0.60	6.09	2.52	0.91	9.13	2.76	1.80	6.13	2.92
As (ppm)	0.56	16.49	4.68	0.56	36.67	8.71	0.56	16.70	4.53
Ba	74.83	272.73	133.15	57.01	139.95	87.71	66.21	263.05	144.67
Ce	6.69	86.18	62.25	52.26	179.43	125.13	30.90	112.51	78.85
Co	30.59	145.95	53.90	72.51	146.19	105.98	59.54	210.58	95.29
Cu	28.25	2348.10	120.47	45.47	2486.80	621.02	425.65	1937.71	1034.30
Nb	12.41	18.27	15.39	8.98	16.91	12.42	14.90	19.98	18.54
Ni	168.61	3024.22	314.16	442.41	4627.71	1411.55	1151.81	4492.36	1653.05
Pb	0.58	18.58	5.91	0.30	25.18	5.25	6.58	13.79	8.21
Rb	2.87	48.00	20.90	2.46	17.61	12.72	14.31	28.40	19.77
Sr	119.52	369.93	249.03	32.46	199.87	111.66	71.59	629.27	208.31
V	49.22	119.02	83.85	61.61	158.50	111.19	54.55	105.38	88.31
Y	0.81	15.03	6.10	0.34	12.20	8.15	2.87	11.91	7.10
Zn	47.39	91.87	66.63	76.34	173.07	95.59	80.60	128.05	94.22
Zr	9.94	23.36	14.49	4.40	29.10	15.86	16.35	48.61	27.84
Mo	0.36	6.05	2.76	0.36	5.69	2.07	1.16	4.56	4.05
U	0.39	0.39	0.39	0.39	3.98	0.39	0.39	0.39	0.39
Th	0.23	127.57	67.29	0.23	28.55	0.87	0.23	240.07	46.35
Al_2O_3/TiO_2	58.87	156.35	88.90	18.47	68.18	51.02	18.91	62.71	46.80
Ti/Zr	36.97	96.20	65.52	46.87	159.41	72.66	32.21	94.82	51.15
Zr/Y	1.17	19.21	2.37	1.42	40.88	2.31	1.37	7.42	5.65
$Rb^*_{(MN)}$	0.41	2.42	1.61	0.47	1.79	1.37	0.84	2.38	1.89
$K^*_{(MN)}$	0.08	2.53	0.53	0.01	0.33	0.13	0.06	0.65	0.37
$Sr^*_{(MN)}$	0.09	2.81	0.27	0.02	1.61	0.15	0.06	0.63	0.15
$Zr^*_{(MN)}$	0.89	2.39	1.47	0.64	2.55	1.48	0.77	2.64	1.81
$Ti^*_{(MN)}$	0.24	0.99	0.57	0.42	2.31	0.63	0.39	0.84	0.50
		(N=8)			(N=4)			(N=2)	
Au (g/t)	0.03	0.24	0.10	0.07	0.96	0.09	0.05	0.19	0.12
Pd	0.03	1.86	0.03	0.60	10.00	1.25	0.03	2.13	1.08
Pt	0.03	1.24	0.04	0.46	8.50	0.79	0.03	1.85	0.94

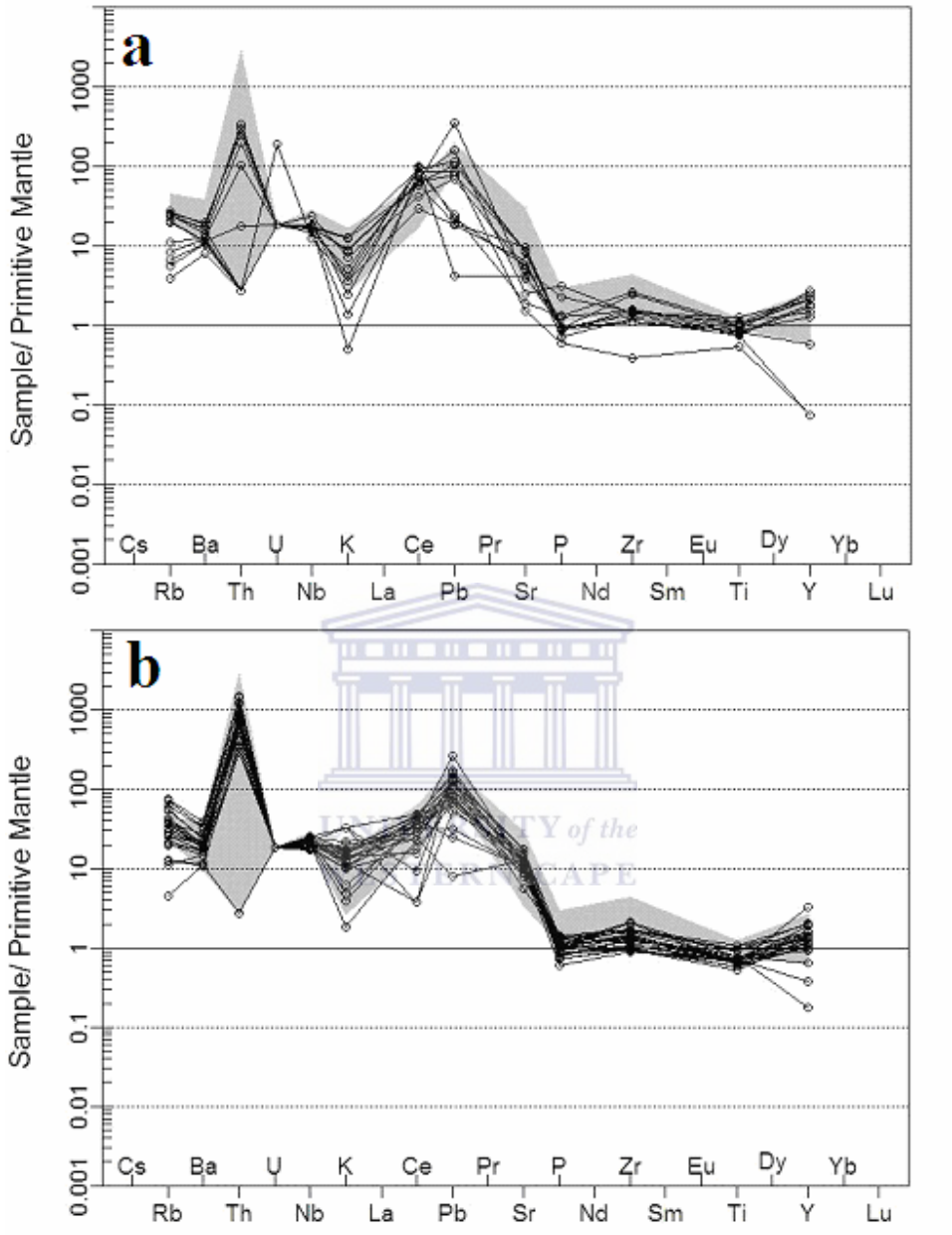

Fig. 21 Trace element compositions of the feldspathic pyroxenites from the Upper and Middle Platreef in (a) and the gabbronorites in (b) from OY 482. The grey field is the trace element pattern of the feldspathic pyroxenites from the Lower Platreef from core OY 482 shown for comparison. Primitive mantle normalization values from Sun and McDonough (1989).

In addition, the Lower Platreef pyroxenites also shows higher median contents for most trace elements, which are coupled with lower median ratios for Al_2O_3/TiO_2 and Ti/Zr,

and a higher median ratios for Zr/Y relative to the Upper and Middle Platreef pyroxenites (Table 4).

On a primitive mantle normalized trace element diagram (Fig. 21a) the Lower Platreef displays HFSE and LILE patterns that are similar to the Upper and Middle Platreef pyroxenites. The Lower Platreef has positive K ($K^*_{(MN)}$ = 0.37), Rb ($Rb^*_{(MN)}$ = 1.89) and Zr ($Zr^*_{(MN)}$ = 1.81) anomalies, similar Sr ($Sr^*_{(MN)}$ = 0.15) anomaly and a negative Ti ($Ti^*_{(MN)}$ = 0.50) anomaly relative to the Upper and Middle Platreef pyroxenites, as shown in Table 4. The trace element patterns in the spider diagrams for all Platreef pyroxenites; i.e. Lower, Middle and Upper, are similar to those displayed by CP III and OCP III.

5.2.3.4 Gabbronorites

Relative to the Platreef pyroxenites, the gabbronorite is characterised by a lower median content for Fe_2O_3 (8.47 wt. %), MgO (10.19 wt. %), TiO_2 (0.15 wt. %) and LOI (2.52 wt. %), coupled with higher median contents for Al_2O_3 (13.77 wt. %), CaO (11.25 wt. %) and K_2O (0.44 wt. %), as seen in Table 4. The gabbronorites show varying median contents for most trace elements when compared to the Platreef pyroxenites coupled with a higher median ratio for Al_2O_3/TiO_2 (Table 4). In addition, the gabbronorites also have lower and higher median ratios for Zr/Y and Ti/Zr respectively than the Lower Platreef (Table 4).

On a primitive mantle normalized trace element diagram (Fig. 21b) the gabbronorite shows HFSE and LILE patterns that are similar to the Lower Platreef. The gabbronorite has positive K ($K^*_{(MN)}$ = 0.53), Sr ($Sr^*_{(MN)}$ = 0.27) and Ti ($Ti^*_{(MN)}$ = 0.57) anomalies, and negative Rb ($Rb^*_{(MN)}$ = 1.61) and Zr ($Zr^*_{(MN)}$ = 1.47) anomalies when compared to the Lower Platreef pyroxenites (Table 4).

5.2.4 Geochemical trends in the studied rocks

The studied rocks in borehole SS 330; i.e. clinopyroxenites and olivine clinopyroxenites, resulted from the interaction between the Platreef magma and the carbonate floor rock with increasing or decreasing magmatic and metamorphic/ metasomatic processes.

To illustrate these processes, the oxide data for the studied rocks were used on a bivariate plot. On the basis of the geochemical characterisation of the studied rocks in sections above, CaO and MgO, which also reflects the predominant mineralogy (calcite/ dolomite, clinopyroxene, olivine, pyroxene and plagioclase), were selected to describe the observed trends in Figure 22.

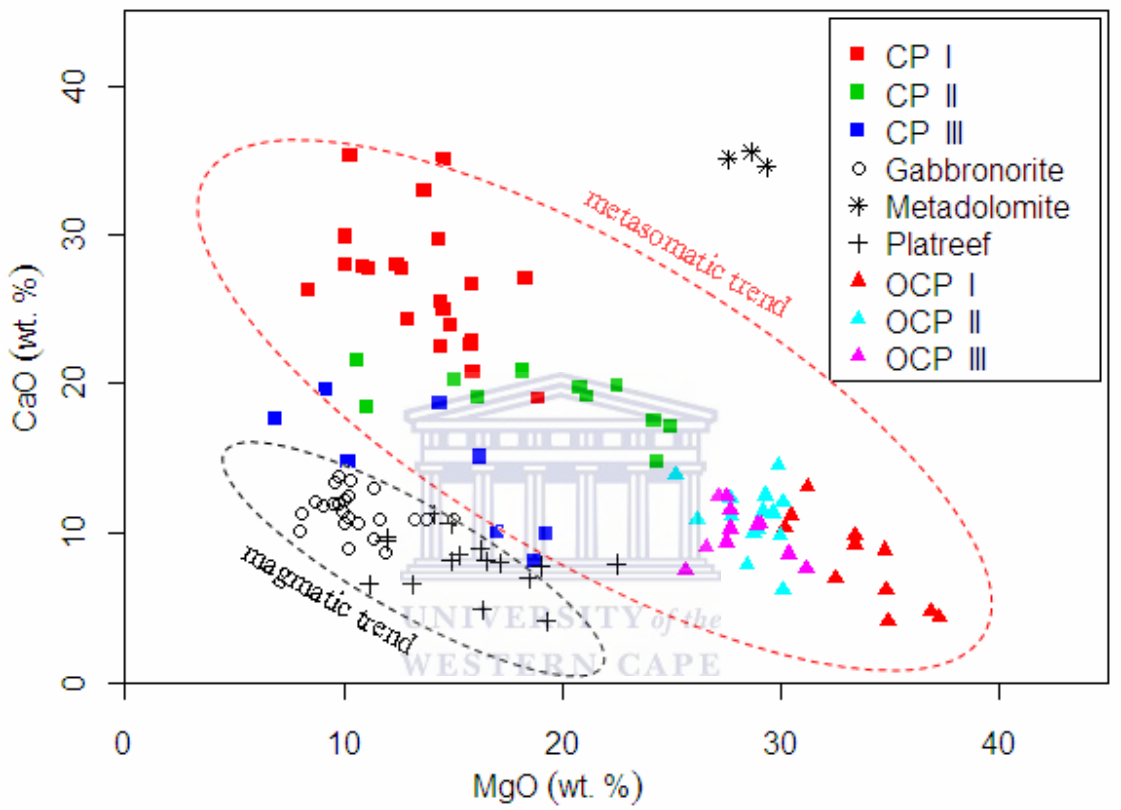

Fig. 22 Whole rock concentrations of CaO vs. MgO for samples from the studied boreholes. *CP: clinopyroxenite; OCP: olivine clinopyroxenite. I, II and III represent the various subtypes.*

Figure 22 shows the plot of CaO versus MgO for all the rock samples. In this figure, the sample points display two obvious parallel trends; i.e. magmatic and metasomatic, described by an inversely relationship between CaO and MgO (Fig. 22). The magmatic trend is defined by gabbronorite and Platreef feldspathic pyroxenite samples (Fig. 22). This trend is marked by the higher MgO and lower CaO contents in the Platreef samples when compared to the gabbronorites (Fig. 22). The metasomatic trend, which is defined by clinopyroxenite and olivine clinopyroxenite samples, is marked by the higher MgO and lower CaO contents in the olivine clinopyroxenites in contrast to the clinopyroxenites

(Fig. 22). By comparison with the olivine clinopyroxenites and the Platreef feldspathic pyroxenites, the clinopyroxenites have the highest CaO contents (Fig. 22). The olivine clinopyroxenites show the highest MgO contents, whereas the Platreef samples have the lowest CaO and MgO contents (Fig. 22).

Within the clinopyroxenites, the CaO contents show a progressive decrease from CP I to CP III (Fig. 22). Sample from the olivine clinopyroxenite subtype I (OCP I) have the highest MgO contents in this lithological unit followed by those in subtypes II and III, in that order (Fig. 22).

In addition, samples from the CP III plot closer to the magmatic trend (Fig. 22). Within the olivine clinopyroxenites, samples from the OCP III are mostly closer to the magmatic trend (Fig. 22). The serpentinised Platreef pyroxenite sample (OY 482-17) plots closer to metasomatic trend (Fig. 22).

5.2.5 Summary

In summary, the most important features to note from the rock characterisation are:

- Both the clinopyroxenite and olivine clinopyroxenite subtypes have higher and lower median contents of SiO_2, Al_2O_3, Fe_2O_3 and SO_3 when compared to the Malmani metadolomites and the Platreef feldspathic pyroxenites, respectively. Furthermore, these clinopyroxenites and olivine clinopyroxenites have higher median contents of CaO and MgO when compared to the Platreef feldspathic pyroxenites but lower median CaO and LOI contents relative to the metadolomites.

  The clinopyroxenite subtypes have a higher median content of CaO and lower median contents of MgO and LOI relative to the olivine clinopyroxenite subtypes.

  Within the clinopyroxenites, there is a progressive increase in the average contents of Al_2O_3 and K_2O coupled with a decrease in the average content of CaO from CP I to CP III. This varying content of CaO in the clinopyroxenites mimics the varying modal clinopyroxene content of these rocks, as seen in Table 1. Within the olivine clinopyroxenites, there is a progressive increase in the average contents of SiO_2,

Fe_2O_3, Na_2O and K_2O coupled with a decrease in the average MgO and LOI contents from OCP I to OCP III.

Relative to the Upper and Middle Platreef feldspathic pyroxenites, samples from the Lower Platreef have a slightly higher median content for SiO_2, Al_2O_3, Na_2O, K_2O and TiO_2, coupled with slightly lower median content for Fe_2O_3, MgO and CaO.

- The average Co, Cu, Ni and Zn contents in both clinopyroxenites and olivine clinopyroxenites are higher relative to the metadolomites and lower relative to the Platreef feldspathic pyroxenites. The trace elements (Nb and Y) show progressive increasing and decreasing patterns, respectively, in average content from CP I to CP III. Within the olivine clinopyroxenites, there is a progressive increase in the average contents of Ba, Rb, Sr, Pb and Nb, and a decrease in the average Y content from OCP I to OCP III.

  The feldspathic pyroxenite in the Lower Platreef when compared to those in the Upper and Middle Platreef shows a higher median content for Ba, Cu, Nb, Ni, Pb, Rb, Sr and Zr coupled with a lower median content for Y.

- Immobile element ratios Al_2O_3/TiO_2 and Zr/Y show progressive increases in average values from CP I to CP III. Within the olivine clinopyroxenites, the Al_2O_3/TiO_2 average value decreases while Zr/Y average value increases from OCP I to OCP III.

  In comparison to the Upper and Middle Platreef, the Lower Platreef shows a lower median value for Al_2O_3/TiO_2 and Ti/Zr, coupled with a higher median value for Zr/Y.

- The CP III and OCP III display both trace element patterns in spider diagrams that are similar to magmatic signature observed for the Platreef feldspathic pyroxenites.

- The trace element anomalies (i.e. Rb^*, K^* and Sr^*) in both the clinopyroxenites and olivine clinopyroxenites show progressive increase in average contents from subtype I to subtype III. The average contents of Ti^* and Zr* also increase progressively from OCP I to OCP III.

The average contents of the trace element anomalies (Rb^*, K^* and Zr^*) in the Lower Platreef feldspathic pyroxenite are higher relative to those in the Upper and Middle Platreef, whereas that of Ti^* is relatively lower. The average Sr^* contents in the Lower Platreef is similar to the Upper and Middle Platreef, both combined.

5.3 Metasomatism: elemental exchange between the Platreef magma and the floor rocks

5.3.1 Introduction

The petrographical examination shows that the rocks in SS 330 (clinopyroxenites and olivine-rich clinopyroxenites) and OY 482 (Platreef feldspathic pyroxenites) display variations in textural and mineralogical assemblage characteristics that are reminiscent of a progressively proximal to distally zoned contact metasomatism between the Platreef magma and surrounding Malmani metadolomites and Archaean granite.

Three metasomatic subzones occur in the clinopyroxenites and olivine clinopyroxenites in borehole SS 330 that exhibit variation in mineral assemblages in consonance with changes in major and trace element chemistry, in particular the HFSE and LILE. In borehole OY 482 the Lower Platreef feldspathic pyroxenites in proximity to the Archaean granite floor rock also display some differences in mineral assemblages and other geochemical attributes, as listed above, when compared to the Upper and Middle Platreef (Fig. 3).

In this section, mass balance calculations were applied to investigate the existence and patterns of an interconnected material exchange between the lithologies of interest and their respective floor rocks. The first step involved mass balance calculations applied to the median concentration data of clinopyroxenite and olivine clinopyroxenite subtypes relative to the metadolomites in borehole SS 330. Secondly, mass balance calculations were applied to the median concentrations data of the Middle Platreef relative to Upper and Lower Platreef from borehole OY 482. Due to the lack of Platreef magmatic rocks in borehole SS 330, data of the Middle Platreef feldspathic pyroxenites from borehole OY

482 were used to investigate the elemental exchange between olivine clinopyroxenites and the Platreef magma.

5.3.2 Metasomatism

The concept of metasomatism, which was firstly introduced by K. F. Naumman in 1826, is defined as a metamorphic process which alters the chemistry of a rock and involves the addition and/ or removal of chemical components (or mass transport) as a result of the interaction of the rock with aqueous fluids (Zharikov et al., 2009) or a tectonic event associated with a change in temperature and pressure conditions with the involvement of a fluid-driven event (Putnis and Austrheim, 2010).

Korzhinskii (1953) reports two metasomatic stages when metasomatism is associated with magmatism. Firstly, metasomatism of the magmatic stage which is connected with fluids that originated from a magmatic body and metasomatised the solid host rocks, and secondly, metasomatism of the post-magmatic stage which is connected with hydrothermal fluids originating both from the cooling magma and/ or other heated exogenic sources.

Depending on the geological environment, various types of metasomatism; such as auto-metasomatism, boundary metasomatism, contact metasomatism, near-vein metasomatism and regional metasomatism, can be recognized (Zharikov et al., 2009).

In geology, many authors have documented the usefulness of the exchange of material during metasomatism in rock discrimination, mapping alteration and vectoring towards ore zones, and the requirements to assess quantitatively material exchange entail knowledge of the protolith and its altered counterpart (Eilu et al., 2001; Deksissa and Koeberl, 2004; Derakhshani and Abdolzedah, 2009).

In this work, the petrographic studies identified various alteration profiles in the studied areas. In borehole SS 330, changes in the chemical composition occur between clinopyroxenites and olivine clinopyroxenites and metadolomites (protolith), while in OY 482 changes occur between the three Platreef lithostratigraphic units.

Straightforward assessment of the data is not a suitable technique to deduce processes in materials transfer. As an alternative, mass balance calculations can quantify the gain and loss of components that are added or removed.

5.3.3 Mass balance

The idea of geochemical mass balance was initiated by Gresens (1967) who quantified the inter-relationship of change in volume, composition and density of an altered rock to its protolith according to the following formula:

$$\Delta mi = fv\ (\rho_a / \rho_o)\ C_a - C_o,$$

where "o" and "a" represent the original and the altered rock, respectively, and ρ_a and ρ_o represent densities; Δmi is the mass change in component, C_o and C_a are the initial and final concentrations in the component, respectively, and fv is the volume factor or ratio of the final volume to the initial volume (López-Moro, 2012).

Mass balance defines quantitatively the amount of a constituent that is lost or gained during the alteration process or changes in the amount of an element moved per unit volume or mass of rock relative to its initial content (Utami et al., 2006). Therefore, mass balance calculations can be applied in all alteration processes providing the protolith and its altered product are known, and a reference frame about which mass balance calculations are made is defined (Mukherjee and Gupta, 2008).

5.3.4 Methods of mass balance

Several methods have been used to define a reference frame about which mass balance calculations are made: the volume factor method (Gresens, 1967), the isocon method (Grant, 1986) and the immobile element method (MacLean and Kranidiotis, 1987).

Gresens (1967) proposed to plot gains and losses as a function of arbitrary volume factors in composition-volume diagrams. In these diagrams, it is possible to choose a value for *fv* where the curves for several immobile elements together all cross the gain-loss zero line.

This *fv* is the reference frame used to estimate the gains and losses of the rest of the elements (López-Moro, 2012).

Grant (1986) rearranged Gresens's mass balance equation into a linear relationship which allows a straight comparison of mass transfer to composition of the protolith and its altered product through the isocon diagram. In this diagram the elemental abundances of the altered rock and its protolith are plotted on the X and Y-axis respectively. Grant (1986) proposed that all immobile elements would plot on a straight line through the origin (Line of no mass transfer or isocon line) in the isocon plot.
The isocon line gives a graphical solution to mass balance depicting the elements that are lost, gained or conserved depending upon its plot to the right, left or on the line respectively. The slope of the isocon is obtained and used to calculate the mass gains and losses of the rest of elements (Mukherjee and Gupta, 2008).

MacLean and Kranidiotis (1987) suggested that mass changes for each mobile element can be calculated based on the concentration of an immobile component. In this method, although the volume change can be calculated from mass change, it does not enter into mass change calculations. The mass of a sample after alteration (or termed reconstructed composition) is calculated from the initial chemical analysis on the basis of 100 mass units of the precursor rock, using Zr as the immobile monitor. The mass change for each element is then calculated by subtracting the precursor value of that element from the reconstructed composition of the sample (MacLean and Barrett, 1993).

In this study, mass gains and losses were calculated using the Grant's method not only because of its simplicity and adaptability as reported by Mukherjee and Gupta (2008) but also because mass gains and losses (1) are not plotted as a function of arbitrary volume factors and (2) this method does not consider only a single immobile element but instead considers all possible immobile elements. The evaluation of mass transfer was performed using the EASYGRESGRANT program since it provides an important advantage over other classic graphical methods (López-Moro, 2012).

5.3.5 EASYGRESGRANT program

López-Moro (2012) presents a friendly interactive Microsoft Excel spreadsheet program "EASYGRESGRANT" to quantify volume changes and perform mass-balance modelling in metasomatic systems. The program performs mass balance calculations considering all possible reference frames (e.g. immobile elements, constant volume and constant mass) between the protolith and its altered counterpart (López-Moro, 2012). Its advantages, as compared to other mass balance programs, are that the EASYGRESGRANT program does not encounter the same problems which are explained therein as follows:

1) Graphical plots, such as the Grant's isocon diagram or Gresens's composition-volume diagram, are not useful tools in order to find immobile elements when a large data set is being handled since the large number of lines or symbols represented obstructs the good visualization and distinction of the elements themselves.

2) The method of arbitrary scaling of compositional data proposed to mitigate this problem in the Grant's isocon diagram is inadequate, since scaling influences the best fit isocon, yielding errors in the mass balance calculations (Mukherjee and Gupta, 2008).

Instead, "EASYGRESGRANT" allows correct selection of immobile element(s) from the data using the clusters of slopes and volume factors (offering a reliable reference frame to perform mass balance calculations) and an improved isocon diagram, providing an error-free mass balance modelling (López-Moro, 2012).
The clusters of slopes and volume factors method consists of estimating the slopes and the volume factors for all the elements considered (Grant, 2005; Mukherjee and Gupta, 2008). The clusters of elements with close slope or volume factor values are selected as immobile elements and the average of these parameters would represent the reference frame for mass balance computation, which is the method suggested for selecting immobile elements (López-Moro, 2012). However, the computation of the average of

these parameters does not provide information about the uncertainties due to the selection of elements (López-Moro, 2012).

Other methods that have been proposed to establish the immobile elements can be also used in EASYGRESGRANT:

1) Composition-volume diagrams. These diagrams are not clear when a large data set is used. Since the excessive number of plotted lines obstructs the display of the point where lines representing elements with a similar geochemical behaviour intersect, the program solves this problem by plotting only the immobile elements selected previously by means of the clusters of volume factors. As a result, these diagrams are methods to verify the previous selection of immobile elements (López-Moro, 2012).
2) The isocon diagram. This diagram can also be used to check the selection of immobile elements previously performed from the clusters of slopes method.
3) However, since the isocon diagram obtained plots elements without scaling concentrations and the subsequent stacking of elements is eliminated (e.g. plotting diagrams at various scales, scaling axes and temporarily removing some elements), it can be also used to select immobile elements. A method to verify the selection of immobile elements is carried out by classical least squares regression or a regression index (López-Moro, 2012).
4) The component-ratio diagram. This diagram plots the ratio of elements of altered and unaltered rocks. Immobile elements appear immediately next to the 1:1 ratio line, whereas mobile elements are plotted away from the line (López-Moro, 2012).

5.3.6 Mass balance calculations using EASYGRESGRANT

As stated earlier in chapter 5.3.1, mass balance calculations were applied to investigate the exchange of materials between the lithologies of interest and the floor rocks.

The first step involved mass balance calculations applied to data of clinopyroxenites and olivine clinopyroxenites, as altered, relative to the metadolomites as unaltered (protolith) in borehole SS 330. Secondly, mass balance calculations were applied to data of Upper

and Lower Platreef feldspathic pyroxenites, as altered, relative to the Middle Platreef pyroxenites (unaltered) in borehole OY 482. The lack of Platreef magmatic rocks in borehole SS 330 hindered conclusive results of mass balance calculations based on the altered olivine clinopyroxenites. The coherent results were obtained by investigating the elemental exchange between olivine clinopyroxenites and the Platreef magma by using data of the Middle Platreef in borehole OY 482 as protolith.

The median concentration data, which include oxides and trace elements, used for mass balance calculations are shown in Tables 5 and 6. Table 5 shows median concentrations data of both clinopyroxenite and olivine clinopyroxenite subtypes as well as those of the metadolomites. Table 6 shows median concentrations data of the olivine clinopyroxenite subtypes, Upper Platreef, Lower Platreef and Middle Platreef.

Both, the metadolomites and Middle Platreef were used as protoliths since they display compositions relatively comparable to fresh dolomite and pristine feldspathic pyroxenite, respectively. Their compositions are medians of 3 metadolomite samples (SS 330-86, 93 and 94; Fig. 5) and 3 Middle Platreef samples (OY 482-27, 30 and 35; Fig. 3). As stated earlier in section 4.3.2.1, the metadolomites are chert-poor and belong to the Frisco Fm. Taking into consideration the mineralogy and textures in clinopyroxenites and olivine clinopyroxenites relatively to the metadolomites, the author suggests that the dolomite of the Frisco Fm involved in the formation of the rocks present in borehole SS 330 must have been relatively uniform. The Middle Platreef pyroxenite samples located near the contact boundaries with gabbronorite sills as well as the serpentinised pyroxenite sample (OY 482-17) were not incorporated for this study. The altered samples are consisting of clinopyroxenites, olivine clinopyroxenites, Lower Platreef and Upper Platreef.

For mass balance evaluation, median data of the abovementioned altered rocks were calculated using the EASYGRESGRANT program. Immobile elements were selected using the clusters of slopes method based on those showing similar automatically calculated slope values (Grant, 2005). The average slopes for the immobile elements

were automatically calculated and used as the slope of the isocon from which mass gains and losses were calculated.

Table 5: Median concentrations of oxides (wt. %) and trace elements (ppm) for metadolomites, clinopyroxenites (CP) and olivine clinopyroxenites (OCP).

Rock type	Metadolomites	Clinopyroxenites (CP)			Olivine clinopyroxenites (OCP)		
	-	CP I	CP II	CP III	OCP I	OCP II	OCP III
	(N=3)	(N=22)	(N=11)	(N=8)	(N=11)	(N=14)	(N=11)
Variable							
SiO_2 (wt %)	0.01	43.49	41.17	44.82	36.81	37.4	39.76
Al_2O_3	<0.01	4.14	5.06	10.6	4.29	8.44	6.4
Fe_2O_3	<0.01	8.9	8.53	10.06	4.41	7.59	7.96
MnO	0.26	0.24	0.34	0.23	0.59	0.6	0.39
MgO	28.71	14.39	20.8	15.29	33.42	29.09	27.7
CaO	35.15	26.91	19.13	14.88	8.82	11.19	10.28
Na_2O	0.62	0.73	0.53	1.09	0.19	0.28	0.35
K_2O	<0.01	<0.01	<0.01	0.84	<0.01	0.02	0.31
P_2O_5	0.01	0.03	0.02	0.02	0.01	0.02	0.02
TiO_2	0.01	0.31	0.31	0.23	0.12	0.28	0.21
SO_3	<0.01	0.11	0.14	0.11	0.03	0.04	0.04
LOI	37.95	1.84	2.99	2.13	10.89	6.66	5.58
As (ppm)	101.15	19.75	10.11	18.41	0	1.96	1.94
Ba	54.69	54.98	50.95	368.89	47.98	63.13	83.19
Ce	85.61	102.12	88.03	96.15	30.46	80.02	66.79
Co	0.86	40.94	33.8	76.34	15.95	22.75	42.82
Cu	28.85	320.34	183.86	395.78	52.06	68.45	124.86
Nb	9.47	8.26	12.74	14.05	11.45	11.74	12.24
Ni	7.7	438.17	1075.22	769.73	97.55	342.52	629.25
Pb	1.07	7.26	8.12	7.61	0.19	1.89	2.4
Rb	2.19	2.52	2.19	34	1.54	4.71	17.97
Sr	28.69	12.52	12.41	233.87	2.48	24.31	66.9
V	0.57	138.58	76.86	91.91	10.89	61.4	57.21
Y	1.08	8.55	6.99	4.89	7.89	6.53	4.29
Zn	21.6	60.35	60.36	74.12	50.58	80.09	68.35
Zr	3.22	28.92	34	17.65	22.55	47.67	33.73
Mo	0.02	5.05	2.91	3.32	0.09	0.88	1.25
U	<0.01	<0.01	<0.01	<0.01	<0.01	<0.01	<0.01
Th	0.2	0.2	0.2	46.9	0.2	0.2	0.2

Table 6: Median concentrations of oxides (wt. %) and trace elements (ppm) for the Middle Platreef, Upper Platreef, Lower Platreef and the olivine clinopyroxenites.

Rock type	Platreef			Olivine Clinopyroxenites		
	Middle	Upper	Lower	Subtype I	Subtype II	Subtype III
	(N=3)	(N=3)	(N=4)	(N=11)	(N=14)	(N=11)
Variable						
SiO_2 (wt %)	49.02	49.35	51.10	36.81	37.40	39.76
Al_2O_3	5.90	10.28	10.84	4.29	8.44	6.40
Fe_2O_3	15.24	12.47	10.70	4.41	7.59	7.96
MnO	0.18	0.17	0.16	0.59	0.60	0.39
MgO	16.35	16.53	14.03	33.42	29.09	27.70
CaO	7.97	8.11	6.59	8.82	11.19	10.28
Na_2O	1.36	1.08	2.05	0.19	0.28	0.35
K_2O	0.16	0.11	0.34	<0.01	0.02	0.31
P_2O_5	0.03	0.02	0.05	0.01	0.02	0.02
TiO_2	0.23	0.17	0.23	0.12	0.28	0.21
SO_3	0.38	0.12	0.29	0.03	0.04	0.04
LOI	3.02	1.38	2.92	10.89	6.66	5.58
As (ppm)	9.74	3.09	4.53	<0.01	1.96	1.94
Ba	88.67	86.74	144.67	47.98	63.13	83.19
Ce	133.95	115.88	78.85	30.46	80.02	66.79
Co	135.98	101.93	95.29	15.95	22.75	42.82
Cu	936.68	292.04	1034.30	52.06	68.45	124.86
Nb	10.54	13.04	18.54	11.45	11.74	12.24
Ni	1407.03	863.87	1653.05	97.55	342.52	629.25
Pb	7.36	1.30	8.21	0.19	1.89	2.40
Rb	12.50	5.29	19.77	1.54	4.71	17.97
Sr	54.46	136.38	208.31	2.48	24.31	66.90
V	119.43	105.00	88.31	10.89	61.40	57.21
Y	9.67	7.86	7.10	7.89	6.53	4.29
Zn	109.80	77.74	94.22	50.58	80.09	68.35
Zr	17.54	13.90	27.84	22.55	47.67	33.73
Mo	5.26	2.81	4.05	0.09	0.88	1.25
U	0.39	0.39	0.39	<0.01	<0.01	<0.01
Th	0.23	8.84	46.35	0.20	0.20	0.20

The results of the elemental exchange are presented below in the following order:

- Section 5.3.6.1 presents the results relative to the metadolomites.
- Section 5.3.6.2 presents the results relative to the Middle Platreef.

5.3.6.1 Mass changes relative to the metadolomites

Table 7: Mass balance calculations for median concentration of oxides (wt. %) and trace elements (ppm) for clinopyroxenite and olivine clinopyroxenite subtypes relative to the metadolomites.

Rock type	Clinopyroxenites			Olivine clinopyroxenites		
	Subtype I	Subtype II	Subtype III	Subtype I	Subtype II	Subtype III
	(N=22)	(N=11)	(N=8)	(N=11)	(N=14)	(N=11)
Slope	1.00	1.00	1.13	1.00	0.93	0.96
SiO_2 (wt %)	43.49	41.16	39.80	36.81	40.01	41.20
Al_2O_3	4.14	5.06	9.41	4.29	9.03	6.63
Fe_2O_3	8.90	8.53	8.94	4.41	8.11	8.25
MnO	-0.01	0.09	-0.06	0.33	0.38	0.15
MgO	-14.33	-7.92	-15.14	4.70	2.41	0.00
CaO	-8.24	-16.03	-21.93	-26.33	-23.18	-24.50
Na_2O	0.11	-0.09	0.34	-0.43	-0.32	-0.26
K_2O	0.00	0.00	0.74	0.00	0.02	0.32
P_2O_5	0.02	0.01	0.01	0.01	0.01	0.01
TiO_2	0.30	0.30	0.19	0.11	0.29	0.20
SO_3	0.10	0.13	0.09	0.03	0.04	0.04
LOI	-36.11	-34.96	-36.06	-27.06	-30.83	-32.16
As (ppm)	-81.40	-91.04	-84.80	0.00	-99.05	-99.14
Ba	0.29	-3.74	272.94	-6.71	12.86	31.54
Ce	16.51	2.43	-0.21	-55.15	0.00	-16.38
Co	40.09	32.95	66.95	15.10	23.48	43.53
Cu	291.49	155.01	322.67	23.21	44.38	100.57
Nb	-1.21	3.27	3.01	1.98	3.09	3.22
Ni	430.47	1067.52	675.94	89.85	358.75	644.53
Pb	6.19	7.05	5.69	-0.88	0.94	1.41
Rb	0.33	0.00	28.00	-0.65	2.84	16.43
Sr	-16.18	-16.28	179.02	-26.21	-2.69	40.65
V	138.02	76.30	81.06	10.33	65.12	58.73
Y	7.47	5.91	3.26	6.81	5.90	3.37
Zn	38.75	38.76	44.23	28.98	64.09	49.25
Zr	25.70	30.78	12.45	19.33	47.78	31.74
Mo	5.03	2.89	2.93	0.07	0.92	1.27
U	0.00	0.00	0.00	0.00	0.00	0.00
Th	0.00	0.00	41.46	0.00	0.01	0.01

The results of the mass balance calculations for the clinopyroxenites are presented in Tables 7 and 8.

The slope values and the relative proportion of mass loss and mass gained by each clinopyroxenite and olivine clinopyroxenite subtypes compared to the metadolomites are given in Table 7. A summary of the deduced pattern of elements gained and lost for the clinopyroxenite and olivine clinopyroxenite subtypes are presented in Table 8. The isocon diagrams showing the mobility of elements in selected clinopyroxenites and olivine clinopyroxenites are shown in Figs. 23 and 24 respectively. The enrichment-depletion diagrams that quantify the gains and losses of selected elements in the clinopyroxenites and olivine clinopyroxenites are graphically shown in Figs. 25 and 26, respectively.

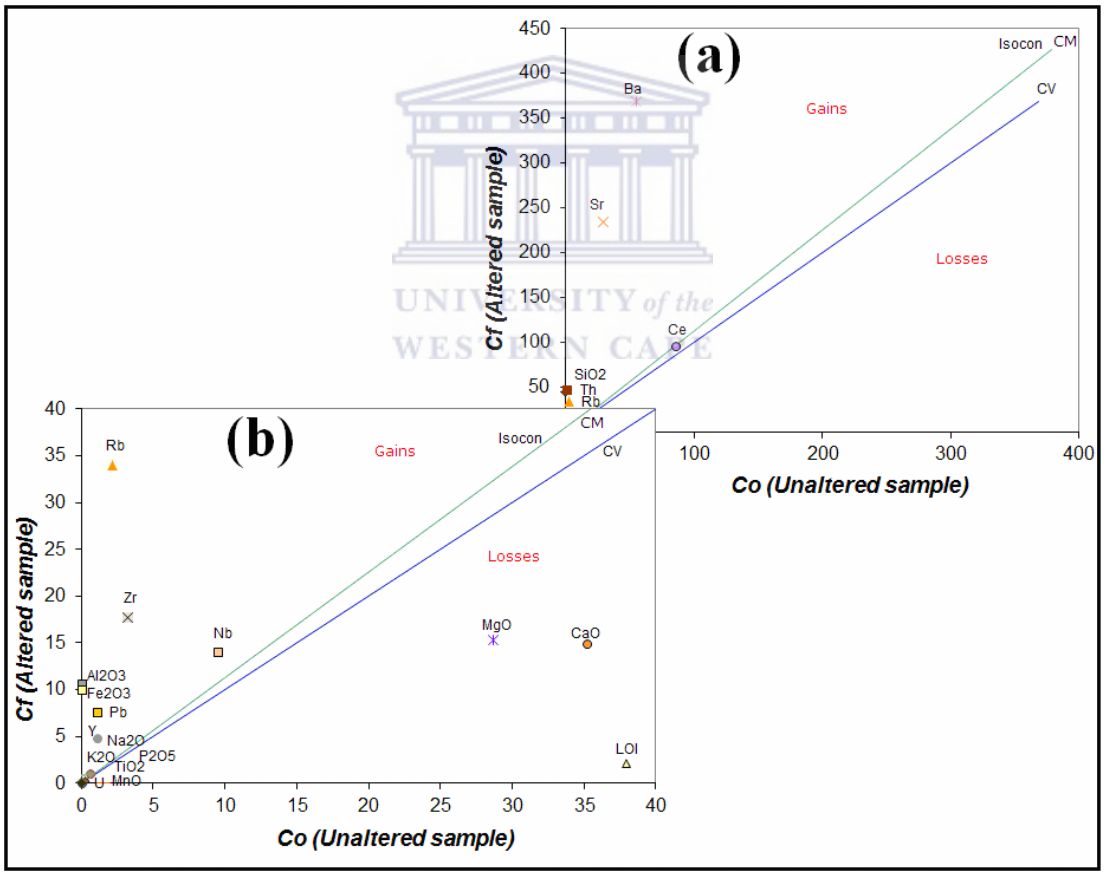

Fig. 23 Isocon diagrams of clinopyroxenite III relative to the metadolomites. *Data are median values from Table 7 (As, Cu, Co, Ni, V, Zn and SO_3 were not selected). Cf and Co are concentrations of clinopyroxenite III and the metadolomites, in that order. CM and CV are lines of constant mass and constant volume, respectively. Figure (b) is the expanded view of Figure (a) as indicated by the scale.*

Examples of isocon plots are presented in Figs. 23 and 24, and related data in Table 7 give a quantitative estimate of the percentage of mass loss and gain by the clinopyroxenite III and olivine clinopyroxenite III relative to the metadolomites. The lower portion of Fig. 23a is enlarged to produce the expanded view in Fig. 23b and thus presents the patterns of loss and gains in the major oxides and trace elements. The enlargement has been done for the subsequent isocon plots.

For example, the isocon plot for the clinopyroxenite III in Fig. 23 shows the highest gains for Ba and Sr in (a) followed by substantial gains in Rb and Zr, coupled with losses in MgO, CaO and LOI in (b). Weak gains and losses occur for Al_2O_3, Fe_2O_3, Na_2O, K_2O, P_2O_5 and TiO_2, and MnO and As, respectively (see also in Table 7).

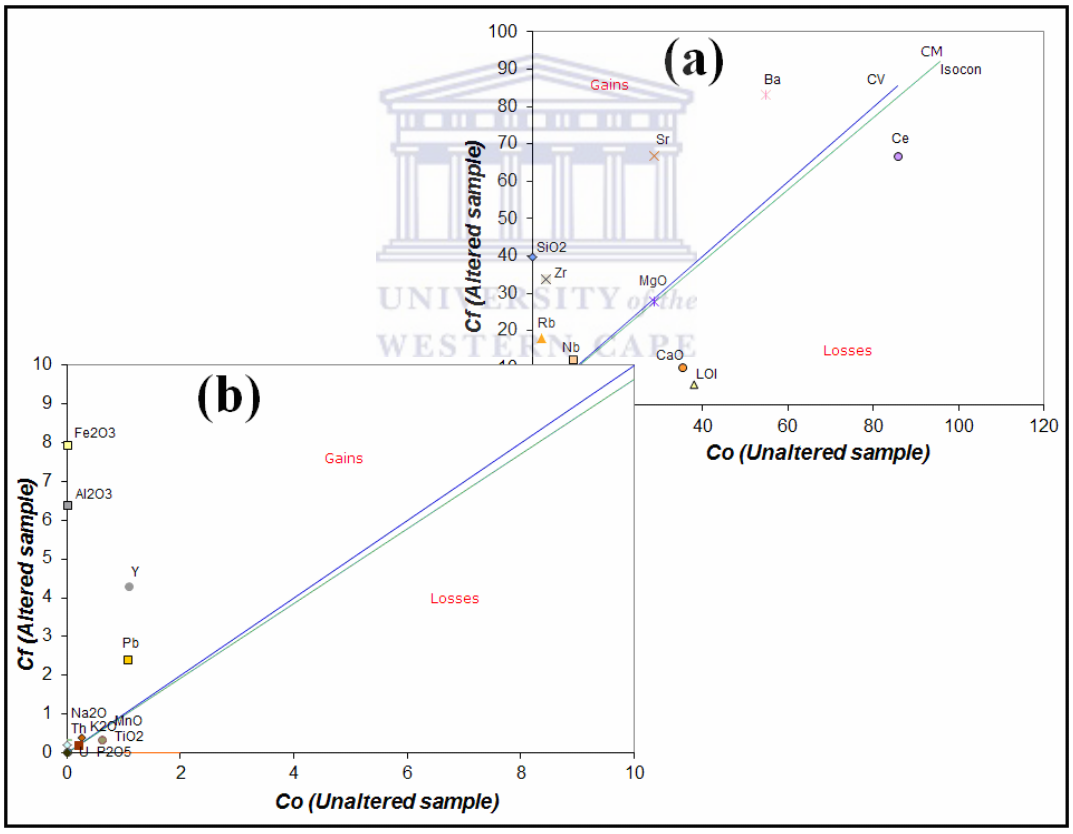

Fig. 24 Isocon diagrams of olivine clinopyroxenite III relative to the metadolomites. *Data are median values from Table 7 (As, Cu, Co, Ni, V, Zn and SO_3 were not selected). Cf and Co are concentrations of olivine clinopyroxenite III and the metadolomites, in that order. CM and CV are lines of constant mass and constant volume, respectively. Figure (b) is the expanded view of Figure (a) as indicated by the scale.*

Table 8: Summary of mobilized components through gain and loss for clinopyroxenites and olivine clinopyroxenites relative to the metadolomites

Rock type	Clinopyroxenites			Olivine clinopyroxenites		
	Subtype I	Subtype II	Subtype III	Subtype I	Subtype II	Subtype III
	(N=22)	(N=11)	(N=8)	(N=11)	(N=14)	(N=11)
Gains	SiO_2, Al_2O_3, Fe_2O_3, Na_2O, TiO_2, Ba, Ce, Pb, Rb, Y & Zr	SiO_2, Al_2O_3, Fe_2O_3, TiO_2, Ce, Nb, Pb, Y & Zr	SiO_2, Al_2O_3, Fe_2O_3, Na_2O, K_2O, TiO_2, Ba, Nb, Pb, Rb, Sr, Y & Zr	SiO_2, Al_2O_3, Fe_2O_3, MnO, MgO, TiO_2, Nb, Y & Zr	SiO_2, Al_2O_3, Fe_2O_3, MnO, MgO, TiO_2, Ba, Nb, Pb, Rb, Y & Zr	SiO_2, Al_2O_3, Fe_2O_3, MnO, K_2O, TiO_2, Ba, Nb, Pb, Rb, Sr, Y & Zr
Losses	MgO, CaO, LOI, As, Nb & Sr	MgO, CaO, Na_2O, LOI, As, Ba & Sr	MgO, CaO, LOI, As & Ce	CaO, Na_2O, LOI, Ba, Ce, Pb, Rb & Sr	CaO, Na_2O, LOI, As & Sr	CaO, Na_2O, LOI, As & Ce

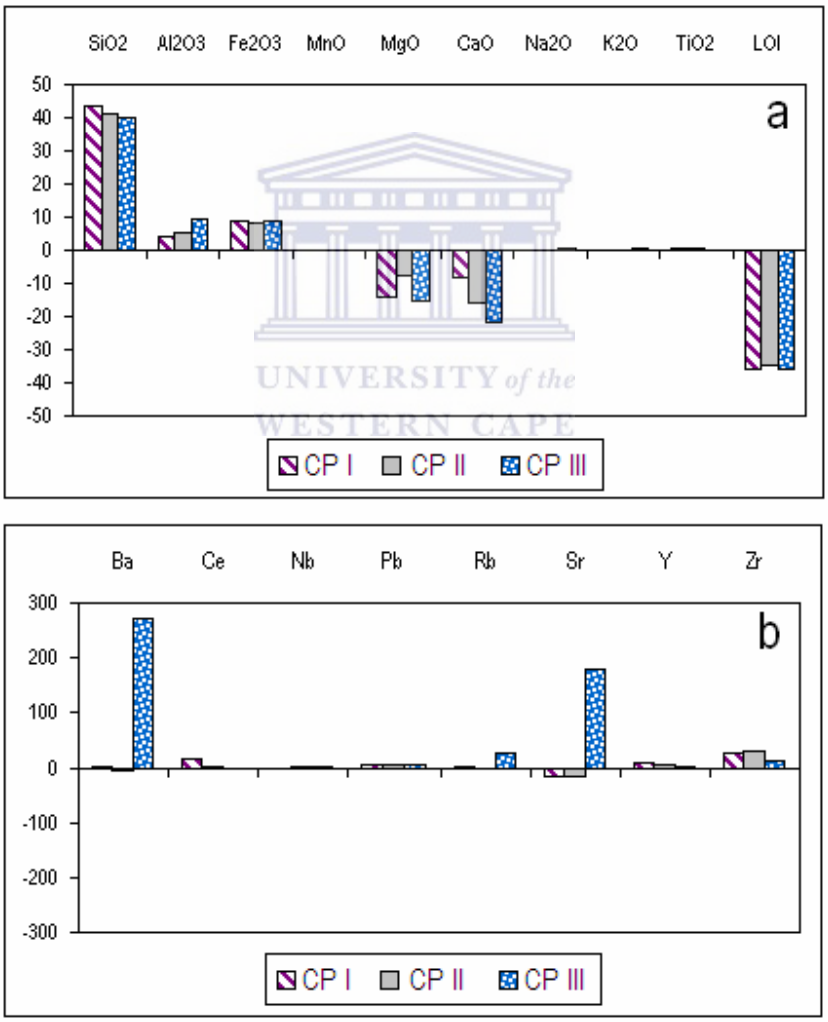

Fig. 25 Median gains and losses pattern for selected oxides in wt% (a) and selected trace elements in ppm (b) for the clinopyroxenites (CP I, CP II and CP III) relative to the metadolomites.

Figure 24 shows the isocon plot for the olivine clinopyroxenite III. In this Figure, substantial gains in SiO_2, Ba, Sr and Zr, coupled with losses in CaO and LOI are seen in (a) while weak gains occur for Fe_2O_3, Al_2O_3, Y and Pb in (b). These can also be seen in Table 7.

Relative to the metadolomites, the clinopyroxenite and olivine clinopyroxenite subtypes show consistent gains in SiO_2, Al_2O_3, Fe_2O_3, TiO_2, Zr and Y coupled with a relative loss in CaO and LOI (Table 8). Furthermore, the olivine clinopyroxenite subtypes, contrary to the clinopyroxenite subtypes, consistently show a mass gain in MgO that is coupled with a loss in Na_2O as seen in Table 8. The clinopyroxenites subtype III (CP III) and olivine clinopyroxenites subtype III (OCP III) are associated with mass gains in Rb, Sr and Ba as seen in Table 8. The latter group of elements displays changing patterns of mass loss and gain when compared to the other rock subtypes. The above is consistent with the trends observed in the spider diagrams.

5.3.6.1.1 Clinopyroxenites

Plots of the relative percentages of mass loss and gain in bar charts (Fig. 25a) shows that the clinopyroxenites in comparison to the metadolomites are particularly enriched in SiO_2 coupled with significant loss in LOI. The plot further shows a more subdued but consistent loss of MgO and CaO, and a gain of Al_2O_3 and Fe_2O_3. Pronounced mass gains in Ba, Sr and Rb are associated with the clinopyroxenite III (or CP III; Fig. 25b).

5.3.6.1.2 Olivine clinopyroxenites

The difference between the clinopyroxenites and the olivine clinopyroxenites lies in the positive mass balance for MgO in all the subtypes. Otherwise the olivine clinopyroxenite subtypes relative to the metadolomites consistently show a mass gain in SiO_2, Al_2O_3, Fe_2O_3, TiO_2, MnO, Nb, Y and Zr coupled with a loss of CaO, Na_2O and more elevated LOI (Fig. 26; Table 7). The olivine clinopyroxenite subtype III (OCP III) shows

appreciable mass gains in Ba, Sr, and Rb (Fig. 26b) though less pronounced than the clinopyroxenites subtype III (CP III).

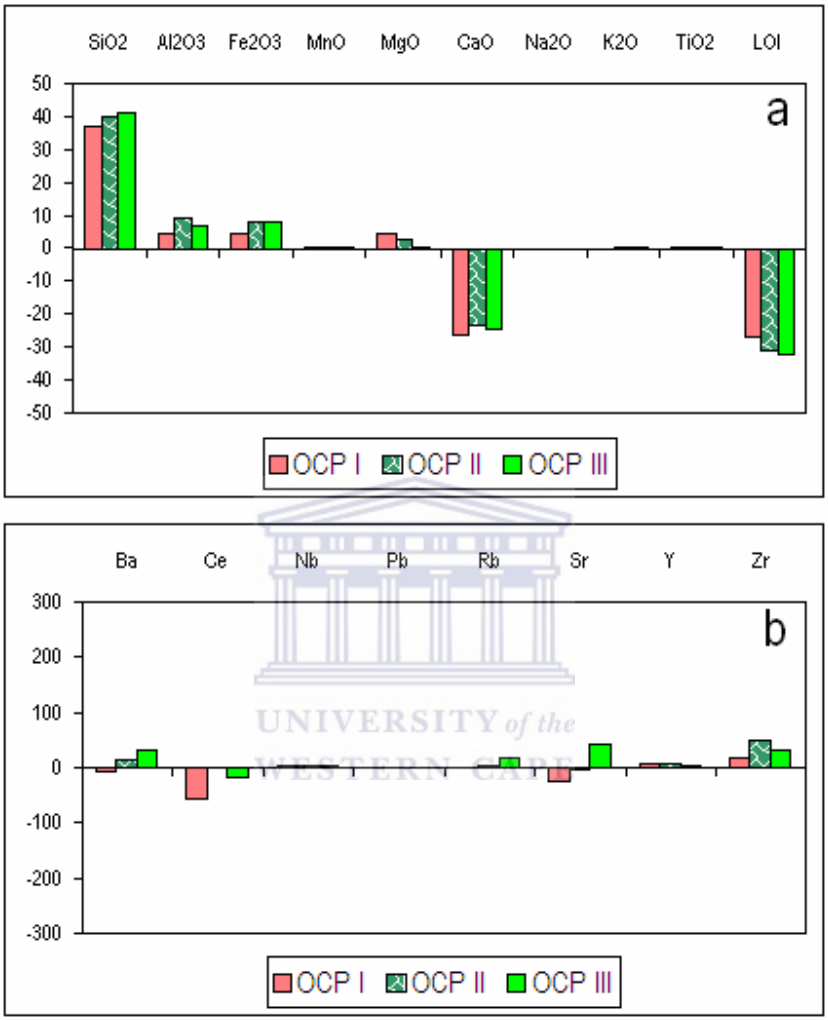

Fig. 26 Median gains and losses pattern for selected oxides in wt% (a) and selected trace elements in ppm (b) for the olivine clinopyroxenites (OCP I, OCP II and OCP III) relative to the metadolomites.

5.3.6.2 Mass changes relative to the Middle Platreef feldspathic pyroxenites

A mass balance estimate was undertaken to compare the Middle Platreef in borehole OY 482 with the Upper and Lower Platreef at Overysel and the olivine clinopyroxenite subgroups at Sandsloot.

The data used for the calculations and more examples of the isocon graphs are available in Appendix V. The results of the mass balance calculations are presented in Table 9. An example of an isocon graph and the general patterns of element mobilization are given in Figure 27 and Table 10, respectively.

Table 9: Mass balance calculations for median concentration of oxides (wt. %) and trace elements (ppm) for the Upper Platreef, Lower Platreef and olivine clinopyroxenites relative to the Middle Platreef.

Rock type	Platreef		Olivine clinopyroxenites		
	Upper	Lower	Subtype I	Subtype II	Subtype III
	(N=3)	(N=4)	(N=11)	(N=14)	(N=11)
Slope	1.01	1.00	1.09	1.11	0.94
SiO_2 (wt %)	-0.25	2.02	-15.13	-15.42	-6.65
Al_2O_3	4.26	4.93	-1.95	1.69	0.92
Fe_2O_3	-2.92	-4.54	-11.18	-8.42	-6.75
MnO	-0.02	-0.03	0.36	0.36	0.23
MgO	-0.02	-2.33	14.41	9.79	13.17
CaO	0.04	-1.39	0.14	2.08	2.98
Na_2O	-0.30	0.69	-1.19	-1.11	-0.99
K_2O	-0.05	0.18	-0.16	-0.14	0.17
P_2O_5	-0.01	0.02	-0.02	-0.01	-0.01
TiO_2	-0.07	0.00	-0.12	0.02	-0.01
SO_3	-0.26	-0.10	-0.35	-0.34	-0.33
LOI	-1.66	-0.10	7.00	2.96	2.93
As (ppm)	-6.69	-5.22	0.00	-7.98	-7.67
Ba	-2.97	55.84	-44.51	-31.97	-0.02
Ce	-19.46	-55.19	-105.91	-62.08	-62.78
Co	-35.27	-40.79	-121.30	-115.55	-90.35
Cu	-648.13	96.48	-888.76	-875.20	-803.63
Nb	2.34	7.97	0.00	0.00	2.50
Ni	-553.50	244.19	-1317.24	-1099.38	-736.50
Pb	-6.08	0.84	-7.19	-5.67	-4.80
Rb	-7.27	7.25	-11.08	-8.27	6.65
Sr	80.29	153.62	-52.18	-32.63	16.83
V	-15.69	-31.22	-109.41	-64.28	-58.47
Y	-1.90	-2.58	-2.41	-3.81	-5.10
Zn	-32.99	-15.68	-63.24	-37.86	-36.97
Zr	-3.81	10.26	3.22	25.28	18.40
Mo	-2.48	-1.21	-5.18	-4.47	-3.93
U	0.00	0.00	-0.39	-0.39	-0.38
Th	8.50	46.06	-0.05	-0.06	-0.03

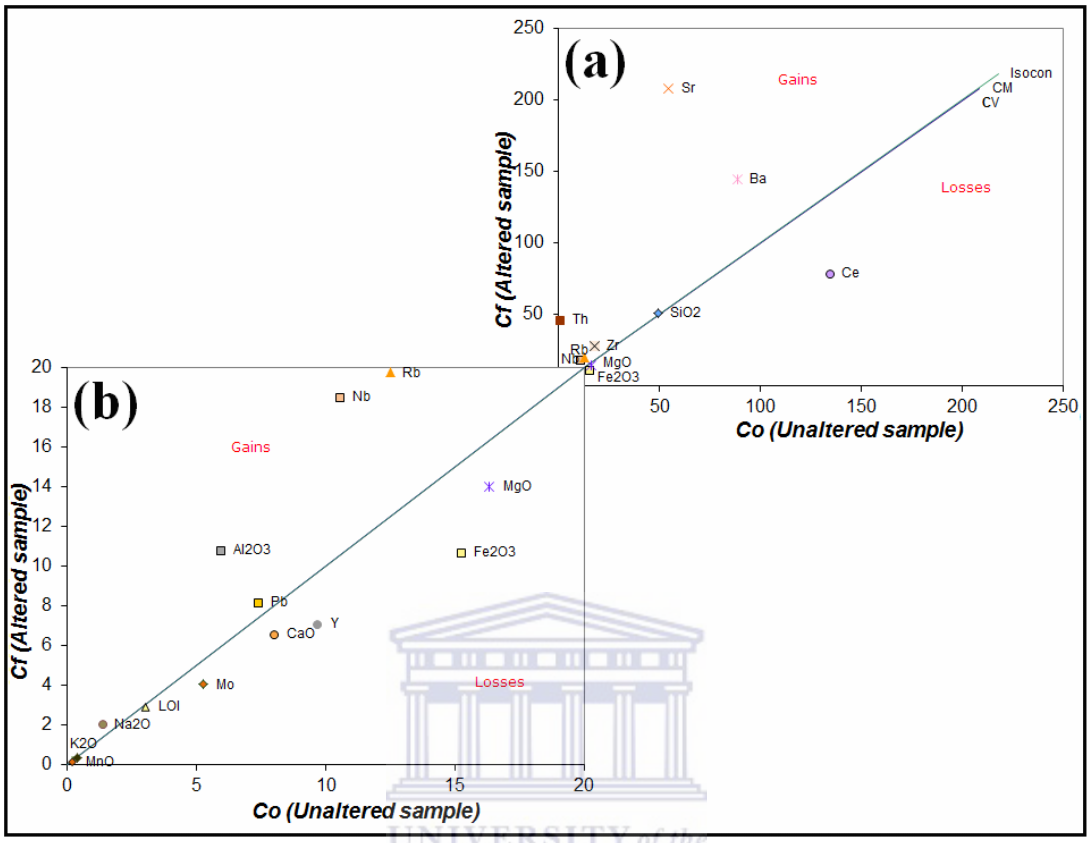

Fig. 27 Isocon diagrams for the Lower Platreef relative to the Middle Platreef. *Data are median values from Table 9 (As, Cu, Co, Ni, V, Zn and SO_3 were not selected). Cf and Co are concentrations of the Lower Platreef and the Middle Platreef, in that order. CM and CV are lines of constant mass and constant volume respectively. Figure (b) is the expanded view of Fig. (a) as indicated by the scale.*

The isocon plot in Fig. 27 clearly shows the significant gain in Sr, Ba and Rb in the Lower Platreef (in proximity to the Archaean granite/ gneisses) compared to the Middle Platreef. The Lower Platreef furthermore shows mass gains in Al_2O_3 that is coupled with a loss of MgO, Fe_2O_3 and CaO relative to the Middle Platreef (Fig. 27b).

The Upper and Lower Platreef, relative to the Middle Platreef, show a consistent gain in Al_2O_3, Nb, Sr and Th coupled with a loss in Fe_2O_3, MgO, MnO, LOI, As, Ce and Y, as seen in Tables 9 and 10. The Lower Platreef shows further gains in SiO_2, Na_2O, K_2O, Ba, Rb and Zr, which differentiates it from the Upper Platreef that show CaO enrichment (Tables 9 and 10).

All the olivine clinopyroxenite subtype, relative to the Middle Platreef pyroxenites, show a consistent mass gains in MgO, CaO, MnO, LOI and Zr coupled with a loss in SiO_2, Fe_2O_3, Na_2O, Ba, Ce, Pb, Y, U and Th (Tables 9 and 10). The olivine clinopyroxenite subtypes exhibit a changing pattern of mass loss in K_2O, Rb and Sr in OCP I and OCP II, and TiO_2 for OCP I and OCP III (Tables 9 and 10).

Table 10: Summary of mobilized components through gain and loss for the Upper Platreef, Lower Platreef and olivine clinopyroxenites relative to the Middle Platreef

Rock type	Platreef		Olivine Clinopyroxenites		
	Upper	Lower	Subtype I	Subtype I	Subtype III
	(N=3)	(N=4)	(N=11)	(N=14)	(N=11)
Gains	Al_2O_3, CaO, Nb, Sr & Th	SiO_2, Al_2O_3, Na_2O, K_2O, Ba, Nb, Pb, Rb, Sr, Zr & Th	MnO, MgO, CaO, LOI & Zr	Al_2O_3, MnO, MgO, CaO, TiO_2, LOI & Zr	Al_2O_3, MnO, MgO, CaO, K_2O, LOI, Nb, Rb, Sr & Zr
Losses	SiO_2, Fe_2O_3, MnO, MgO, Na_2O, K_2O, TiO_2, LOI, As, Ba, Ce, Pb, Rb, Y & Zr	Fe_2O_3, MnO, MgO, CaO, LOI, As, Ce & Y	SiO_2, Al_2O_3, Fe_2O_3, Na_2O, K_2O, TiO_2, Ba, Ce, Pb, Rb, Sr, Y, U & Th	SiO_2, Fe_2O_3, Na_2O, K_2O, As, Ba, Ce, Pb, Rb, Sr, Y, U & Th	SiO_2, Fe_2O_3, Na_2O, TiO_2, As, Ba, Ce, Pb, Y, U & Th

5.3.6.2.1 Upper and Lower Platreef feldspathic pyroxenites

Figure 28 shows that the relative percentages of mass lost and gained between the Lower Platreef relative to the Middle Platreef are relatively subdued compared to those in the preceding sections (See Figs. 25 and 26). The percentage of oxides loss and gain is consistently less than 5%.

Pronounced gains and losses occur in the Upper and Lower Platreef pyroxenites for Sr, Ba and Ce, and this is significantly most pronounced in Sr gain and Ce loss in the Lower and Upper Platreef (Fig. 28).

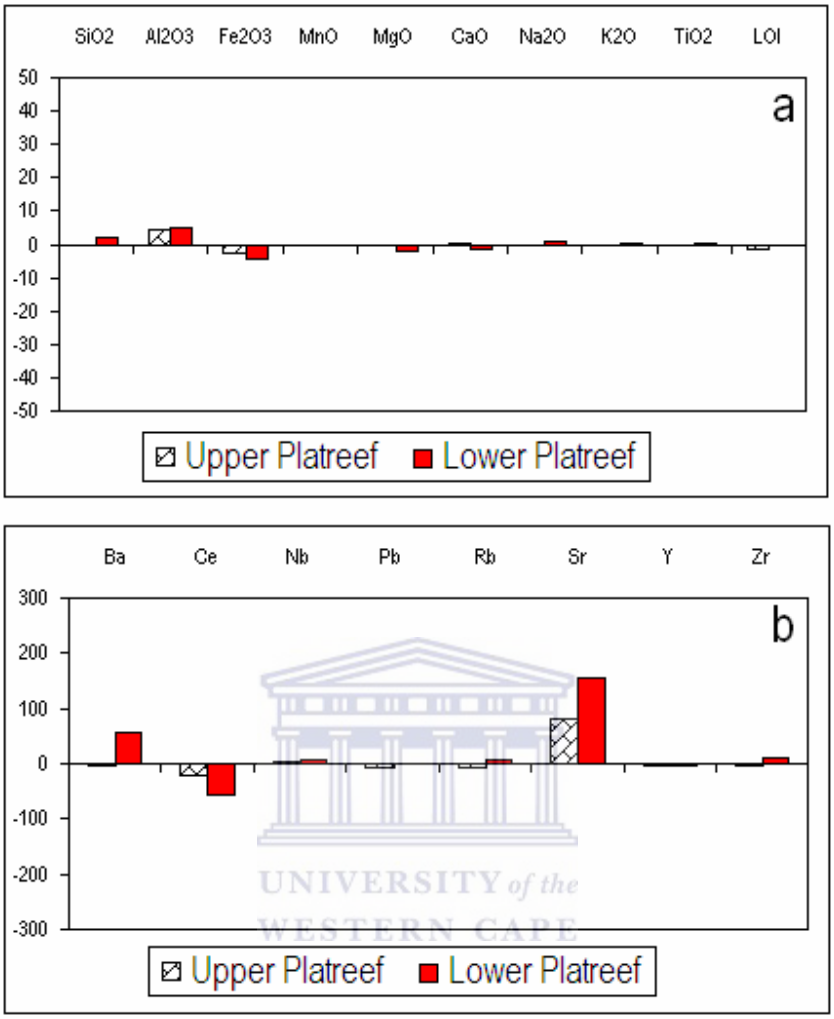

Fig. 28 Median gains and losses pattern for selected oxides in wt% (a) and selected trace elements in ppm (b) for the Upper Platreef and Lower Platreef relative to the Middle Platreef.

5.3.6.2.2 Olivine clinopyroxenites

The olivine clinopyroxenites, relative to the Middle Platreef pyroxenites, show the most significant gains in MgO, LOI and CaO that is coupled with a loss in SiO_2 and Fe_2O_3, and a more subdued degree of loss and gain of other oxides (Fig. 29).

Relative to the Middle Platreef, the olivine clinopyroxenites show a much subdued mass loss and gain intensity for the trace elements compared to the preceding section (See Fig. 26). Significant loss of Ce in all olivine clinopyroxenite subtypes is coupled with variable but subdued gain and loss of Ba, Sr and Zr (Fig. 29).

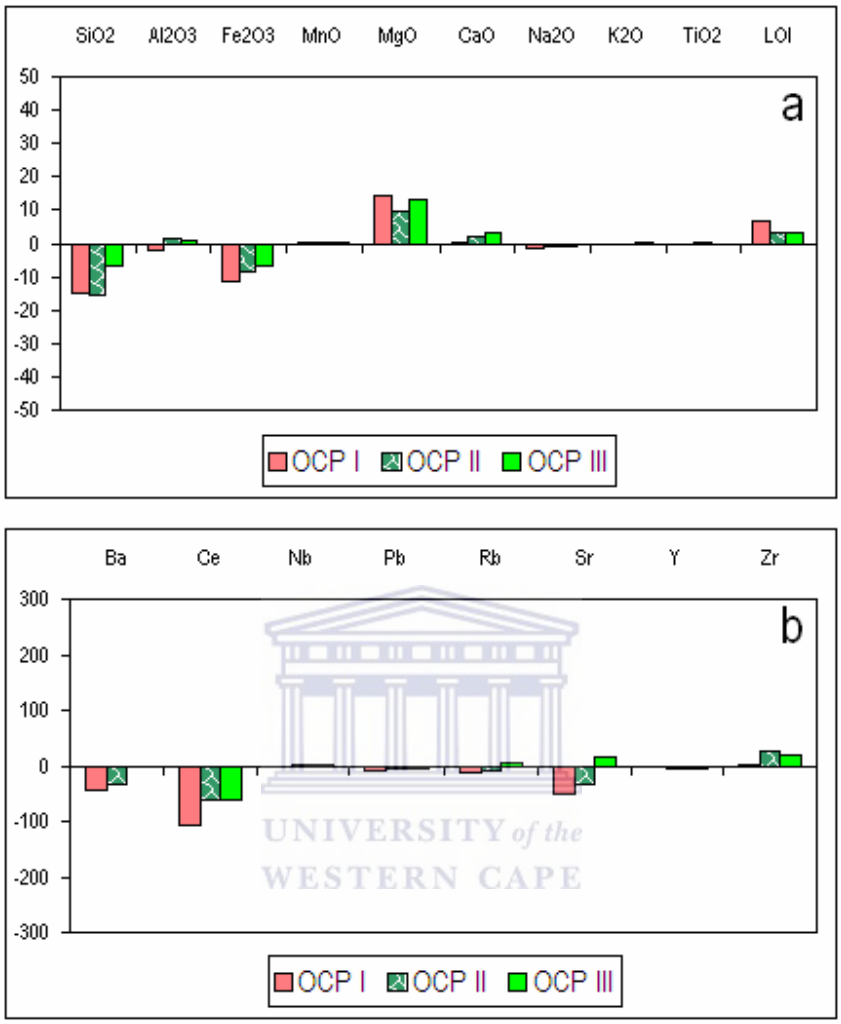

Fig. 29 Median gains and losses pattern for selected oxides in wt% (a) and selected trace elements in ppm (b) for the olivine clinopyroxenites (OCP I, II and III) relative to the Middle Platreef.

5.4 Geochemical indices and the PGE/ BMS mineralisation

5.4.1 Geochemical indices

The purpose of this section is to integrate the element patterns observed in the previous sections into defining chemostratigraphic indices and geochemical vectors that may act as indicators to the proximity of PGE/ BMS mineralisation within the rocks investigated.

For example, the mass balance calculations show that in comparison to MgO enrichment in the OCP, the CP is enriched in CaO, while the Platreef feldspathic pyroxenites are enriched in Fe_2O_3. These major elements also control the mineralogical composition in the OCP, CP and Platreef feldspathic pyroxenites, respectively, as observed from the geochemical classification (section 5.1). On these bases, MgO, CaO and Fe_2O_3 were used to develop the geochemical indices to separate these lithologies.

In order to differentiate between the CP, OCP and Platreef feldspathic pyroxenites, two indices were investigated. The CaO/(MgO+CaO) and MgO/(Fe_2O_3+MgO) ratios are used to distinguish CP from OCP and OCP from Platreef feldspathic pyroxenites, respectively. The first index expresses the enrichment of CaO relative to MgO while the second denotes the enrichment of MgO relative to Fe_2O_3.

Cann (1970) suggests an effective method to test the mobility of elements in which an immobile element is plotted on the X axis of bivariate variation plots and elements to be evaluated are plotted on the Y axis. In case both elements are highly incompatible and immobile (e.g. HFSE; TiO_2, Nb, Y and Zr), the data should give linear trends with slopes close to unity (Cann, 1970). This was investigated in this work and TiO_2 and Zr were selected as highly incompatible amongst the HFSE.

The plot of TiO_2 versus Zr (Fig. 30a) gives linear trends for the CP, OCP and Platreef feldspathic pyroxenites, demonstrating that both elements are immobile. The plot also shows higher contents of Zr and Ti in the CP. Low Zr and Ti values in the CP overlap with those of the OCP and Platreef feldspathic pyroxenites, which may be related to increasing assimilation of magmatic components.
The linear trend, in Fig. 30a, enabled the use of Zr as an immobile element on bivariate plots to illustrate the mobility of CaO and MgO in the CP and OCP samples; respectively, which occurred during contact metamorphism/ metasomatism and hydrothermal alteration between the Frisco dolomite and the Platreef-forming magma. This approach is comparable to that of Ordóñez-Calderón et al. (2008).

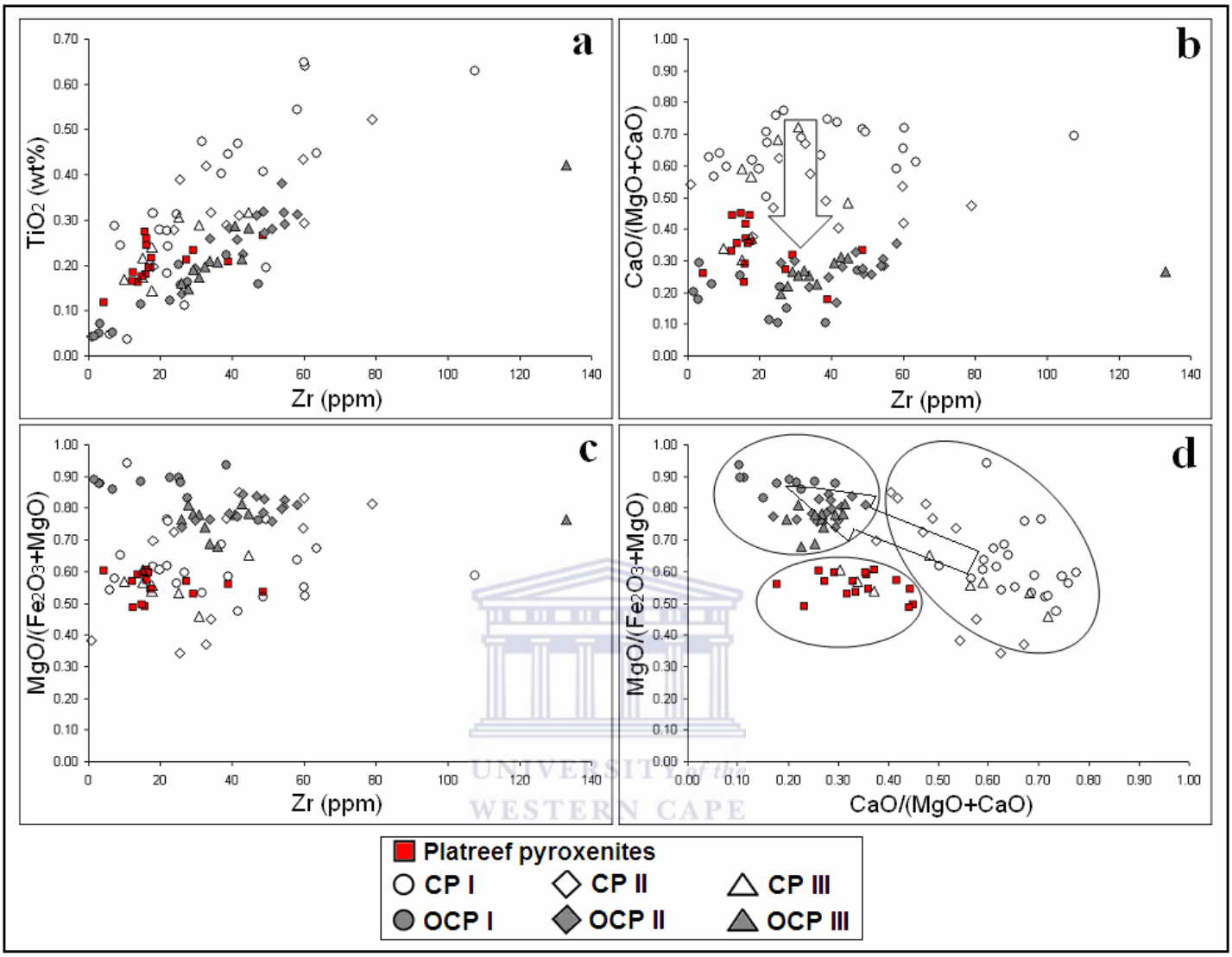

Fig. 30 Various scatter diagrams to describe the (a) components conserved during alteration, (b) contact metasomatic index, (c) assimilation-fractionation index and (d) lithogeochemical indices. *CP: Clinopyroxenite; OCP: Olivine clinopyroxenite. Arrow shows the direction of metasomatism.*

For example in Figure 30b, the plot of CaO/(MgO+CaO) and Zr, clearly separates the CP and the OCP as well as the Platreef feldspathic pyroxenites. Higher CaO/(MgO+CaO) contents separate the CP from the other rock types (Fig. 30b). Noticeable is the similar levels of CaO relative to MgO in the OCP and the Platreef feldspathic pyroxenites (Fig. 30b).

In Figure 30c, the plot of MgO/(Fe_2O_3+MgO) versus Zr, distinguishes the OCP from the Platreef and some CP samples. The plot shows that the OCP has a higher content of MgO

relative to Fe_2O_3 when compared with similar values in the Platreef and CP samples (Fig. 30c). Noticeable is also the similar levels of MgO relative to Fe_2O_3 in the CP and the Platreef feldspathic pyroxenites (Fig. 30c).

Fig. 30d therefore demonstrates that the three rock types can be separated by using the bivariate plot of CaO/(MgO+CaO) against MgO/(Fe_2O_3+MgO) and may be utilized to effectively discriminate the CP, OCP and Platreef feldspathic pyroxenites.

5.4.2 Major element indices and the BMS mineralisation

The relationship between the CaO/(MgO+CaO), MgO/(Fe_2O_3+MgO) ratios and the BMS mineralisation were further investigated using ternary diagram, as shown in Fig. 31.

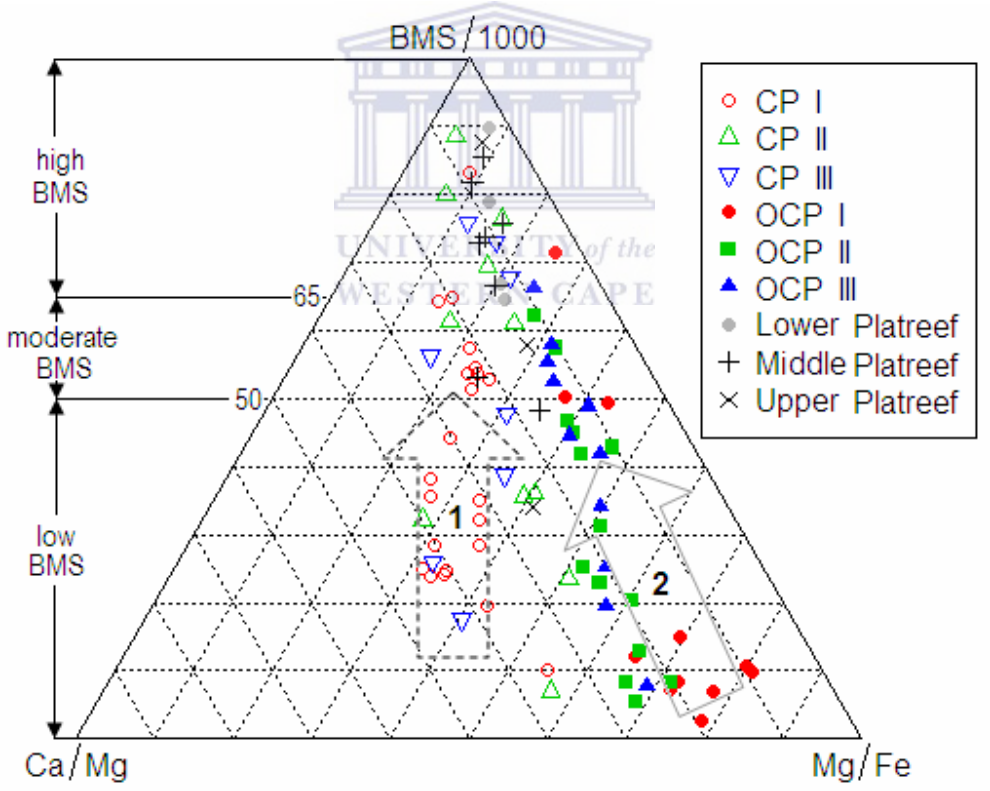

Fig. 31 Ternary diagram illustrating the relationship between the BMS mineralisation and the lithogeochemical indices. *Arrows indicate two base metal sulphide (BMS) distribution trends. Data for the BMS (Cu+Ni) were normalized (or divided by 1000) for visualization purposes. CP: Clinopyroxenites; OCP: Olivine clinopyroxenites. Ca/Mg = CaO/(MgO + CaO); Mg/Fe= MgO/(Fe_2O_3+MgO).*

As illustrated in Figure 31, the plot of CaO/(MgO+CaO), MgO/(Fe_2O_3+MgO) and BMS/1000 (i.e. BMS = Cu+Ni) shows two BMS distribution trends:

- The first trend, indicated by arrow "1", shows the relationship between BMS and CaO/(MgO+CaO) in the clinopyroxenites which are characterised by an increase in BMS contents associated with a decrease in the CaO/(MgO+CaO) ratio (Fig. 31).
- The second trend, indicated by arrow "2", shows the relationship between the BMS and MgO/(Fe_2O_3+MgO) in olivine clinopyroxenites which is characterised by an increase in BMS contents associated with a decrease in the MgO/(Fe_2O_3+MgO) ratio as shown in Figure 31.

Furthermore, on the basis of the median contents of Cu+Ni (BMS) in each rock subtypes shown in Tables 11 and 12, three BMS subgroups were defined. These are presented in Figure 31 above as:

- Low BMS (Cu+Ni < 1000 ppm);
- Moderate BMS (Cu+Ni in between 1000 – 2000 ppm);
- High BMS (Cu+Ni > 2000ppm).

In Figure 31, it can be further seen that the olivine clinopyroxenite subtype I (OCP I) is the least significant carrier of BMS (low) amongst the rock subtypes outlined while the Lower Platreef is the most intensely mineralised in BMS (high).

The CP I) is the least significant carrier of BMS amongst this rock subtype (Fig. 31). The CP II and III display two BMS distributions each (Fig. 31). Some samples have low BMS, while others have high BMS contents (Fig. 31), but in overall both subtypes, CP II and III, have a moderate BMS content (Table 11). This may be further investigated in the down-hole plot. Also evident is a gradational change from the CaO/(MgO+CaO)-rich CP I, with low BMS, to the CP II that is predominantly higher in MgO/(Fe_2O_3+MgO) ratio and BMS contents (Fig. 31).

A similar trend is also observable amongst the OCP subtypes. This trend is marked by an increase in MgO/(Fe_2O_3+MgO) ratio coupled with a decrease in BMS contents from OCP III to OCP I (Fig. 31). However, all the OCP subtypes have low BMS content (Fig. 31).

High BMS contents occur in both the Middle and Lower Platreef marked by relatively low MgO/(Fe_2O_3+MgO) ratio when compared to the Upper Platreef (Fig. 31). The Latter, which has three samples occurring each within different BMS subgroups, is considered to be of moderate Cu+Ni content (Fig. 31).

5.4.3 Trace element indices and the BMS/ PGE mineralisation

The primary focus of the geochemical vectoring is to relate the variation patterns of ore forming elements to locate area(s) of PGE mineralisation which, in the Platreef, is mainly associated with sulphides, tellurides, arsenides, antimonides, bismuthoantimonides and bismuthotellurides (Armitage et al., 2002; Kinnaird et al., 2005; Holwell and McDonald, 2006).

Based on the petrography conducted on the studied lithologies, the sulphides (pyrrhotite, pentlandite and chalcopyrite) were identified as the most dominant ore mineral (except the very low content of iron oxide). For this reason, the metal elements of the sulphides; that is, Ni, Cu, Co and Zn, were used to develop indices to vector towards PGE/ BMS mineralisation in the studied rocks. However, the author acknowledges the limitations of using few geochemical data and selected metal elements (Pt, Pd, Ni, Cu, Co and Zn) which are not the only trace metal elements partitioning in pyrrhotite, pentlandite and chalcopyrite (Paktunc et al., 1990).

There are two steps that were considered to develop the trace element indices (or vectors) useful to locate the PGE/ BMS mineralisation in the studied rocks:

1) An investigation of the relationship between both Ni and Cu with SO_3 (considered as sulphur) to establish whether the trace elements reflect the BMS in the studied rocks. These relationships were assessed using bivariate plots and are presented in Figure 32 below.
2) An investigation of the relationship between each trace element; i.e., Ni, Cu, Co and Zn with Pt and Pd separately in order to identify trends useful to develop indices of the PGE/ BMS in the studied rocks. These relationships were also evaluated using bivariate plots and are presented in Figures 33 and 34

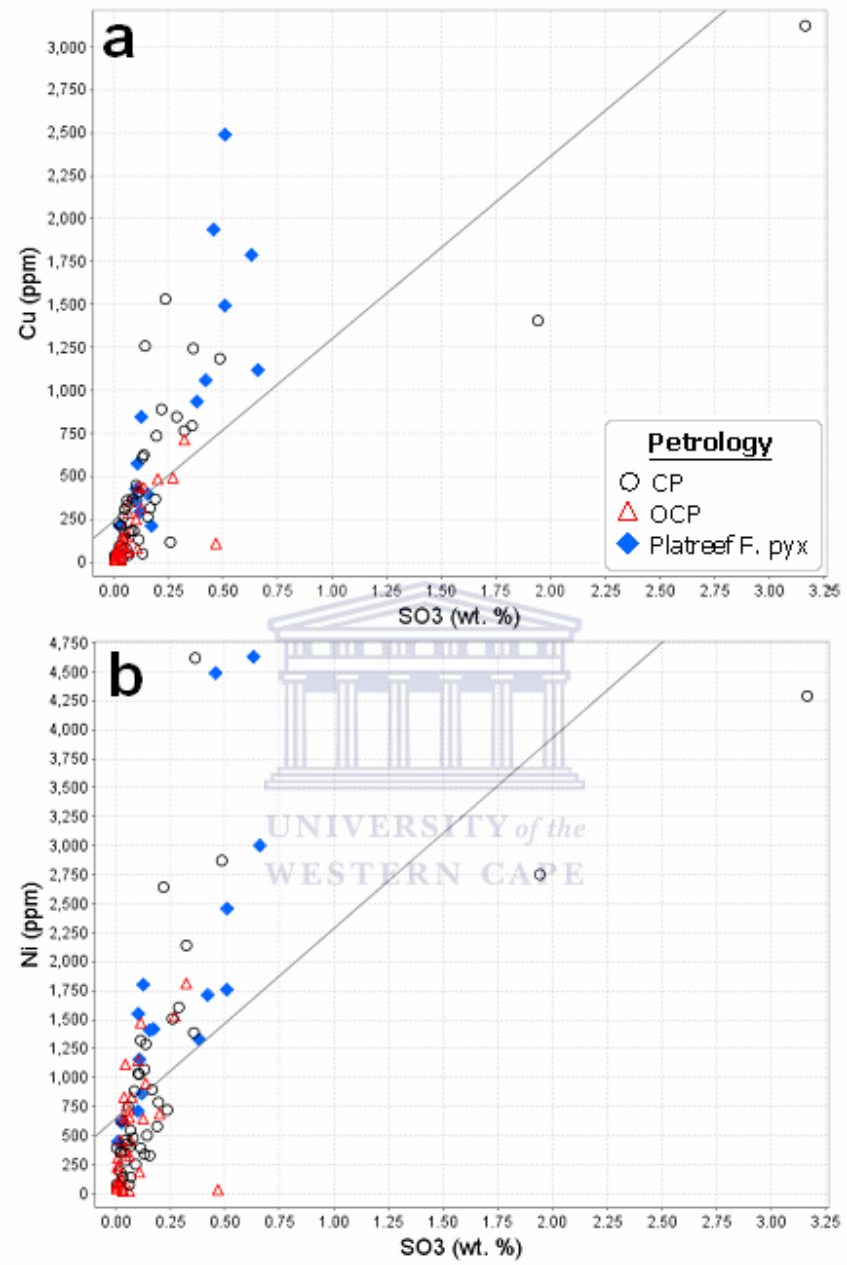

Fig. 32 Sulphur trioxide (SO_3) versus a) Cu and b) Ni concentrations in the rocks
CP: Clinopyroxenites; OCP: Olivine clinopyroxenites; F. pyx: Feldspathic pyroxenites

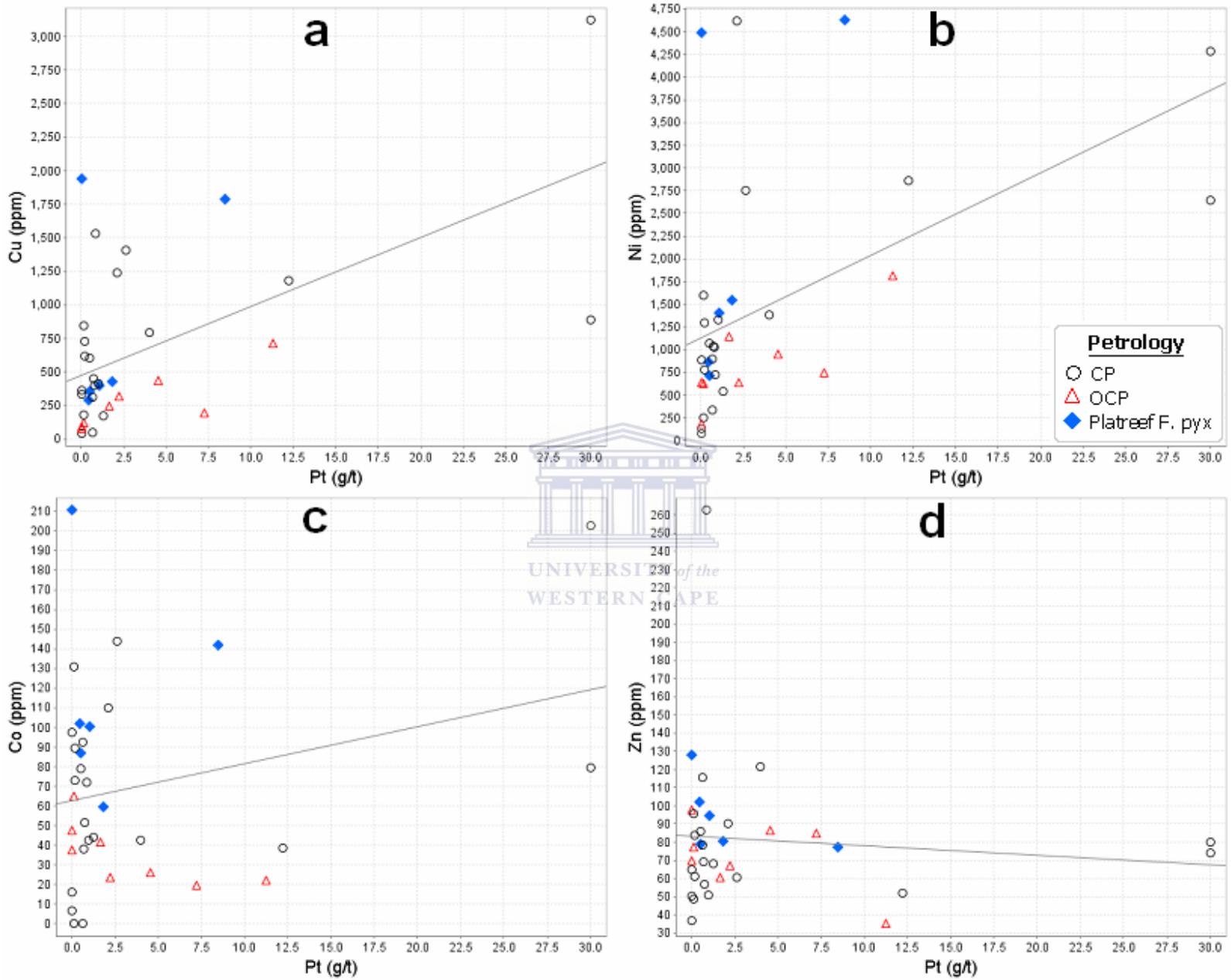

Fig. 33 Platinum (Pt) versus a) Cu, b) Ni, c) Co and d) Zn concentrations in the rocks.
CP: Clinopyroxenites; OCP: Olivine clinopyroxenites; F. pyx: Feldspathic pyroxenites

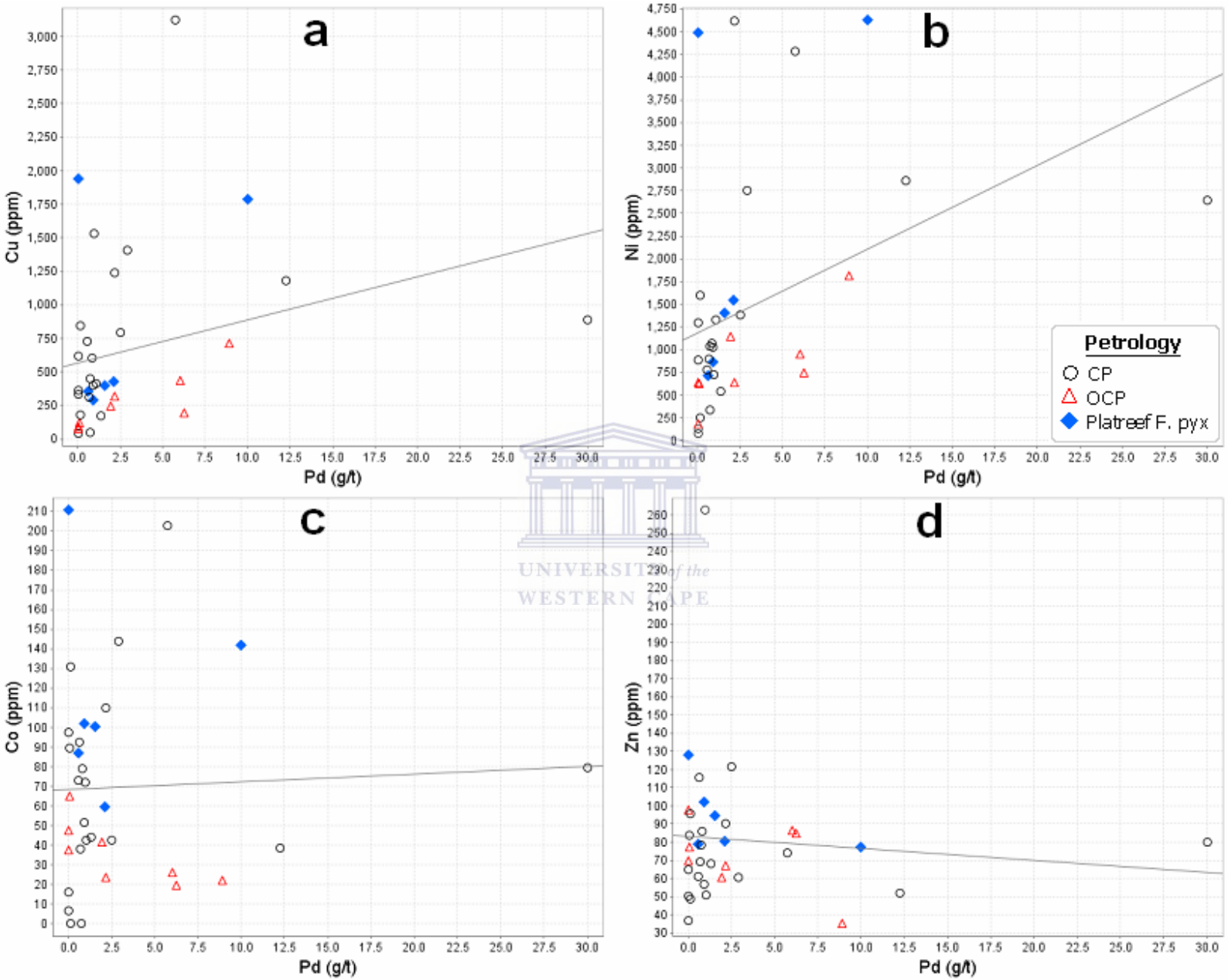

Fig. 34 Palladium (Pd) versus a) Cu, b) Ni, c) Co and d) Zn concentrations in the rocks.
CP: Clinopyroxenites; OCP: Olivine clinopyroxenites; F. pyx: Feldspathic pyroxenites

As shown in Figure 32, there are general positive correlations between both Cu and Ni with SO_3 in all the studied rocks. These rocks also have higher Ni content relative to Cu (Fig. 32). In this Figure, it can also be seen that the OCP, in general, has the lowest contents of Cu, Ni and SO_3, while the Platreef feldspathic pyroxenites have the highest contents in most cases. On the other hand the CP, as a whole, has Cu, Ni and SO_3 contents varying between the OCP and Platreef feldspathic pyroxenites (Fig. 32). Also remarkable, there are two CP samples having the highest SO_3 contents (Fig. 32).

The relationships between the trace elements (Ni, Cu, Co and Zn) with Pt and Pd are shown in Figures 33 and 34, respectively. In general, there are some positive correlations between Cu, Ni and Co with Pt and Pd, but a general negative correlation is seen between Zn with Pt and Pd (Figs. 33 & 34). However, for each of these rock types the overall elemental relationships show some differences (Figs. 33 & 34).

For the olivine clinopyroxenites, both Cu and Ni have positive correlations with the PGE (Pt and Pd) respectively, while Co and Zn appear to have some negative correlations with the PGE (Figs. 33 & 34). In average, the OCP samples have relatively lower Cu, Ni, Co and Zn, and higher Pt and Pd contents than the clinopyroxenites and Platreef feldspathic pyroxenite samples (Figs. 33 & 34). In the Platreef feldspathic pyroxenites Cu, Ni and Co also have positive correlations with the PGE (Pt and Pd) respectively, while a negative correlation is observed between Zn with Pt and Pd, respectively (Figs. 33 & 34). In average, the Platreef feldspathic pyroxenite samples have higher Cu, Ni, Co and Zn, and lower Pt and Pd contents than the CP and OCP samples (Figs. 33 & 34).
The relationships between the trace elements with the Pt and Pd in the clinopyroxenites are similar to those observed in the Platreef feldspathic pyroxenites (Figs. 33 & 34). However, these samples average trace elements contents varying between those in the OCP and the Platreef feldspathic pyroxenites (Figs. 33 & 34).

On the basis of the degree of dissimilarity between the element pairs, indices (e.g. Cu/Zn, Ni/Co, Ni/(Ni+Cu) and {Cu/Zn x Ni/Co}) were calculated and the ensuing values were used to locate Pt+Pd-bearing and barren lithologies.

5.5 Geochemical vectoring towards PGE/ BMS mineralisation

5.5.1 Introduction

This section aims at incorporating all geochemical trends obtained from the previous sections into chemostratigraphic indices and geochemical vectors that are indicators to the proximity of PGE/ BMS mineralisation within the rock studied.

The geochemical element patterns resulted from the classification of the rock types into subtypes/ units of clinopyroxenites, olivine clinopyroxenites and Platreef feldspathic pyroxenites. Other results derived from the geochemical characterisation of the rock subtypes, which indicates a single process of contact metasomatism coupled with elemental exchange that occurred during the interaction between the Platreef magma and the floor rocks.

A major objective is therefore to relate these metasomatic trends and associated element variation patterns to the location of BMS and PGE-enriched zones in the rocks studied. The chemostratigraphic correlation will be done using down-hole plots to illustrate the variation patterns of the geochemical indices and mineralised zones in the two boreholes. In borehole SS 330, drilled at Sandsloot, the PGE mineralisation occurs in both clinopyroxenites and olivine clinopyroxenites, while in borehole OY 482, drilled at Overysel, the PGE mineralisation is within the Platreef feldspathic pyroxenites.

Tables 11 and 12 summarize the lithogeochemical data in boreholes SS 330 and OY 482, in that order. These data are presented as follows:

- LILE and HFSE anomalies and related ratios in the clinopyroxenite and olivine clinopyroxenite subtypes, and Platreef feldspathic pyroxenites.
- The indices of CaO, MgO and Fe_2O_3, which defines the rocks types and/ or subtypes.
- The geochemical indices derived from the base metals; utilized here is also {Cu/Zn x Ni/Co} similar to the Kambalda vectors proposed by Brand (1999). This ratio and others (Ni/Co, Cu/Zn, etc) are rooted in the base metal trends observed in this study.
- The Cu+Ni and Pt+Pd contents, and the Pd/Pt in the various rocks types or subtypes.

Table 11: Lithogeochemical data summary of the studied rock types/ subtypes intersected in borehole SS 330 (Cu+Ni is in ppm and Pt+Pd in g/t).
CP: Clinopyroxenites; OCP: Olivine clinopyroxenites.

Rock type	CP I (N=22) Range (Median)	CP III (N=8) Range (Median)	CP II (N=11) Range (Median)	OCP I (N=11) Range (Median)	OCP II (N=14) Range (Median)	OCP III (N=11) Range (Median)
Sr/Rb	1.42 – 23.52 (5.44)	1.10 – 13.60 (7.70)	0.70 – 22.92 (5.67)	0.01 – 49.60 (2.30)	0.71 – 27.45 (6.16)	0.33 – 10.34 (4.76)
Sr/Ba	0.09 – 0.73 (0.21)	0.23 – 1.59 (0.80)	0.07 – 0.54 (0.19)	<0.01 – 0.32 (0.05)	0.04 – 1.28 (0.37)	0.17 – 1.74 (0.79)
Rb/Ba	0.01 – 0.15 (0.04)	0.06 – 0.21 (0.11)	<0.01 – 0.27 (0.05)	<0.01 – 0.14 (0.03)	<0.01 – 0.38 (0.07)	0.09 – 0.87 (0.17)
$Rb^*_{(MN)}$	0.13 – 1.62 (0.49)	0.71 – 2.34 (1.19)	0.04 – 3.00 (0.54)	0.01 – 1.51 (0.37)	0.04 – 4.13 (0.76)	0.96 – 9.53 (1.90)
$K^*_{(MN)}$	<0.01 – 0.07 (<0.01)	0.08 – 5.87 (0.63)	<0.01 – 0.36 (<0.01)	<0.01 – <0.01 (<0.01)	<0.01 – 0.15 (0.02)	0.08 – 0.80 (0.30)
$Sr^*_{(MN)}$	<0.01 – 0.74 (0.01)	0.05 – 0.31 (0.23)	<0.01 – 0.63 (0.01)	<0.01 – 0.53 (0.02)	<0.01 – 3.60 (0.12)	0.01 – 4.40 (0.20)
$Zr^*_{(MN)}$	0.43 – 4.14 (1.92)	0.97 – 2.77 (1.57)	0.23 – 4.98 (2.78)	0.39 – 6.21 (2.76)	2.44 – 4.55 (3.85)	2.47 – 8.77 (3.44)
$Ti^*_{(MN)}$	0.05 – 0.89 (0.66)	0.45 – 1.25 (0.78)	0.36 – 1.25 (0.61)	0.08 – 0.50 (0.34)	0.30 – 0.68 (0.49)	0.31 – 0.59 (0.51)
Ti/Zr	20.00 – 231.09 (65.34)	42.58 – 100.89 (70.64)	29.28 – 295.52 (55.98)	20.10 – 172.70 (45.01)	31.48 – 45.99 (36.24)	18.98 – 42.16 (36.63)
Zr/Y	0.32 – 134.50 (3.49)	1.07 – 382.50 (5.73)	0.80 – 16.38 (5.37)	0.28 – 7.93 (1.80)	3.06 – 91.68 (7.16)	4.64 – 446.25 (8.91)
Al_2O_3/TiO_2	3.64 – 33.20 (13.07)	32.09 – 79.46 (49.62)	6.15 – 80.11 (16.82)	11.33 – 236.34 (41.86)	6.59 – 70.88 (28.82)	9.12 – 50.68 (27.61)
Ca/Mg	0.50 – 0.77 (0.66)	0.30 – 0.72 (0.52)	0.38 – 0.67 (0.49)	0.10 – 0.29 (0.20)	0.17 – 0.35 (0.28)	0.20 – 0.31 (0.27)
Mg/ Fe	0.47 – 0.94 (0.60)	0.46 – 0.65 (0.56)	0.34 – 0.85 (0.73)	0.76 – 0.93 (0.88)	0.74 – 0.84 (0.79)	0.68 – 0.81 (0.78)
Ni/(Ni+Cu)	0.19 – 0.92 (0.67)	0.52 – 0.91 (0.71)	0.58 – 0.95 (0.72)	0.22 – 0.91 (0.67)	0.32 – 0.92 (0.78)	0.59 – 0.91 (0.83)
Cu/Zn	0.27 – 17.09 (5.77)	0.77 – 12.00 (4.95)	0.27 – 42.08 (3.19)	0.24 – 20.37 (0.86)	0.25 - 14.60 (1.00)	0.21 - 12.00 (1.61)
Ni/Co	4.58 – 42.02 (12.33)	5.77 – 33.28 (11.48)	2.69 – 74.31 (20.12)	1.97 – 82.04 (15.19)	1.40 – 46.03 (16.89)	2.15 – 32.36 (14.90)
(Cu/Zn)*(Ni/Co)	<0.001 – 576.99 (54.62)	6.15 – 369.25 (69.00)	<0.001 – 1699.64 (72.22)	<0.001 – 1671.38 (5.29)	0.36 – 672.07 (14.16)	0.45 – 388.43 (22.42)
Cu+Ni	175.96 – 5864.44 (748.30)	246.45 – 3537.19 (1172.90)	94.01 – 7409.88 (1625.28)	29.72 – 2530.63 (121.46)	62.11 – 1907.44 (447.21)	87.34 – 2015.90 (754.11)
Pt+Pd	0.10 – 6.53 (1.45)	0.27 – 60.00 (0.79)	0.30 – 35.72 (5.59)	4.44 – 20.17 (12.31)	0.10 – 13.49 (10.58)	0.10 – 3.62 (0.22)
Pd/Pt	0.63 - 1.21	0.35 - 2.59	0.19 - 1.55	0.79 - 0.96	0.86 - 1.33	0.69 - 1.18

Ca/Mg = CaO/(MgO+CaO); Mg/Fe= $MgO/(Fe_2O_3+MgO)$

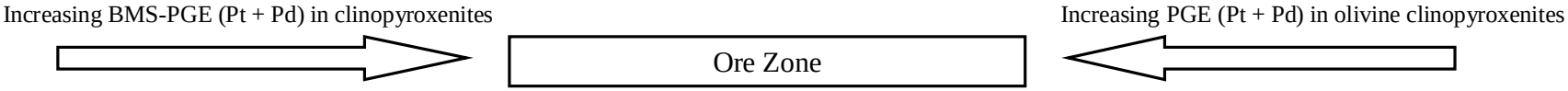

Table 12: Lithogeochemical data summary of the Platreef feldspathic pyroxenites intersected in borehole OY 482 (Cu+Ni is in ppm and Pt+Pd in g/t). *Data for the serpentinised pyroxenite are not included.*

Rock type	Upper Platreef (N=3)	Middle Platreef (N=8)	Lower Platreef (N=4)
	Range (Median)	Range (Median)	Range (Median)
Sr/Rb	11.48 - 25.78 (24.62)	4.35 - 19.65 (10.05)	5.00 - 31.35 (8.58)
Sr/Ba	1.15 - 1.84 (1.57)	0.45 - 1.54 (1.19)	1.08 - 2.39 (1.46)
Rb/Ba	0.05 - 0.16 (0.06)	0.06 - 0.16 (0.13)	0.08 - 0.22 (0.17)
$Rb^*_{(MN)}$	0.52 - 1.76 (0.67)	0.61- 1.79 (1.45)	0.84 - 2.38 (1.89)
$K^*_{(MN)}$	0.04 - 0.22 (0.15)	0.03 - 0.33 (0.16)	0.06 - 0.65 (0.37)
$Sr^*_{(MN)}$	0.22 - 1.61 (0.68)	0.02- 0.93 (0.15)	0.06 - 0.63 (0.15)
$Zr^*_{(MN)}$	1.32 - 2.55 (1.69)	0.64 - 2.16 (1.48)	0.77 - 2.64 (1.81)
$Ti^*_{(MN)}$	0.42 - 1.138 (0.54)	0.43 - 0.84 (0.63)	0.39 - 0.84 (0.50)
Ti/Zr	46.87 - 80.45 (70.09)	47.92 - 104.17 (72.66)	32.21 - 94.82 (51.15)
Zr/Y	1.57 - 40.88 (2.72)	1.42 - 6.15 (1.98)	1.37 - 7.42 (5.65)
Al_2O_3/TiO_2	38.25 - 68.18 (62.25)	18.47- 64.86 (47.40)	18.91 - 62.71 (46.80)
Ca/Mg	0.27- 0.36 (0.33)	0.23 - 0.45 (0.39)	0.18 - 0.37 (0.34)
Mg/ Fe (Mg#)	0.57 - 0.59 (0.57)	0.48 - 0.60 (0.54)	0.54 - 0.60 (0.58)
Ni/(Ni+Cu)	0.72 - 0.91 (0.75)	0.50 - 0.78 (0.67)	0.54 - 0.78 (0.68)
Cu/Zn	0.58 - 23.16 (2.86)	2.77 - 22.65 (6.76)	5.28 - 15.89 (10.61)
Ni/Co	5.775 - 32.59 (8.48)	8.23 - 20.50 (14.70)	13.94 - 25.98 (18.81)
(Cu/Zn)*(Ni/Co)	3.38 - 754.63 (24.22)	23.39 - 404.86 (93.32)	84.92 - 322.82 (198.05)
Cu+Ni	487.88 - 6416.24 (1155.91)	824.08 - 4948.63 (2454.12)	1727.21 - 6430.07 (2612.47)
Pt+Pd	1.39 - 18.5 (9.95)	1.12 - 2.63 (1.88)	0.06 - 3.98 (2.02)
Pd/Pt	1.18 - 2.02	1.15 - 1.48	1.00 - 1.15

Ca/Mg = CaO/(MgO+CaO); Mg/Fe= $MgO/(Fe_2O_3+MgO)$ or Mg#

Various styles of mineralisation are discernable on the basis of the Pt+Pd and Cu+Ni contents in the studied rocks as seen in Tables 11 and 12 as follows:

- A predominantly PGE-rich ore zone with low average BMS (Cu+Ni) of less than 500 ppm occurs in the OCP I and II, which are high in $MgO/(Fe_2O_3+MgO)$ ratios.
- A PGE-rich zone with an average BMS (Cu+Ni) of about 1500 ppm and Pt+Pd of ~5 g/t is exemplified by Upper Platreef and CP II.
- An overwhelmingly BMS-rich zone with Cu+Ni of more than 2000 ppm and Pt+Pd of ~2 g/t, as found in the Middle and Lower Platreef as examples.
- Finally, a low BMS and PGE zone with average Cu+Ni ~1000 ppm and PGE in the range of 1 g/t or less within CP I and III as well as OCP III as examples.

This implies that the OCP I and II are solely PGE reefs, while CP II and Upper Platreef are PGE-BMS reef zones. Predominantly BMS-PGE reefs are hosted within the Middle and Lower Platreef. The abovementioned are considered in the subsequent descriptions as the reefs while the CP I, CP III and the OCP III are regarded as weakly mineralised in BMS. All the vectors and indices towards PGE are described along these various styles of mineralisation.

5.5.2 Lithogeochemical variations

The down-hole plots of the various geochemical parameters for boreholes SS 330 and OY 482 are in Figs. 35 and 36, respectively. For borehole SS 330, the metasomatic subzones of the CP and OCP are presented, while for borehole OY 482 alteration and textural features of the Platreef feldspathic pyroxenites and gabbronorites are displayed on the plots. Summary descriptions of trends for each geochemical parameter in the two boreholes are presented in the following paragraphs.

5.5.2.1 Borehole SS 330

5.5.2.1.1 Lithological variation and mineralisation

Appropriate consideration is given to the occurrence of two main packages in borehole SS 330, which are designated as the upper and lower metasomatic packages occurring above and below the dolomite xenolith, respectively (Fig. 35). The upper metasomatic package comprises predominantly the CP I and III bordered at the top and below by a relatively thin zone of OCP I, II and III (Fig. 35). This section is weakly mineralised in BMS (Cu+Ni) and PGE (Pt+Pd) (Fig. 35).

In the lower metasomatic package, the CP I dominate the upper parts of the section (371-295 m depth) below which thick layers, up to 20 m, of this unit are attenuated with increasing depth and are coupled with a gradational change from largely intercalated layers of CP II to OCP III and then OCP I down to few meters above 450 m depth (Fig. 35).

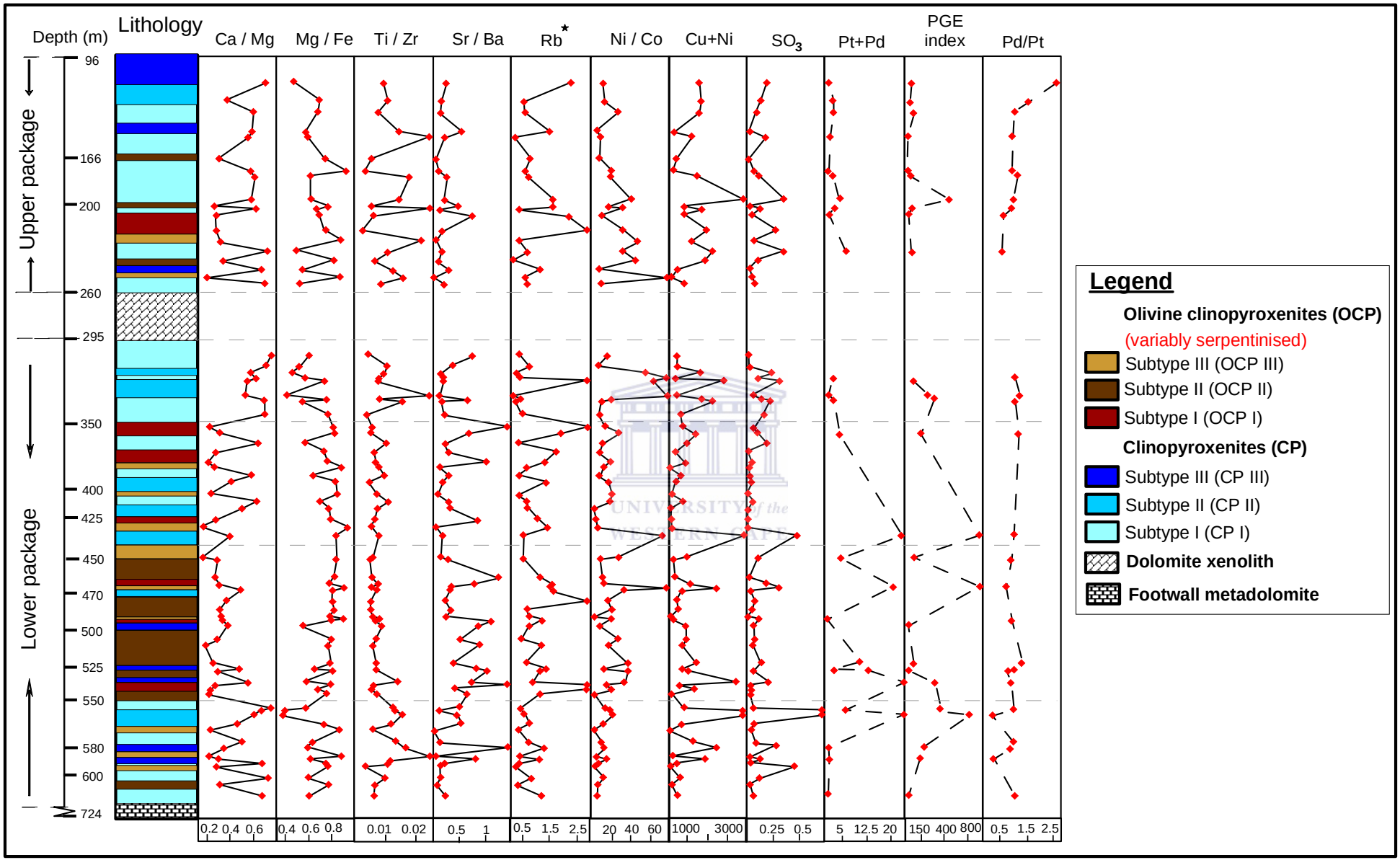

Fig. 35 Down-hole geochemical variations in borehole SS 330. Cu+Ni is expressed in ppm, SO_3 in wt. % and Pt+Pd in g/t. Ca/Mg= CaO/(MgO+CaO); Mg/Fe=MgO/(Fe2O3+MgO); Ti/Zr = TiO_2/Zr; Rb* is mantle normalized anomaly; PGE index= (Cu/Zn) x (Ni/Co).

From this depth, the zone of intercalated layers of CP II and OCP III and I transitions into a 100 m thick predominantly OCP II zone and then into layers of predominantly CP II and I toward the metadolomite floor rock (Fig. 35).

In terms of the styles of mineralisation, the weakly mineralised BMS zone occurs at the upper part of the lower metasomatic package, which changes gradually to a zone of largely intercalated layers of PGE/ BMS and PGE mineralised zones between 425 and 570 m depth (Fig. 35). These zones, in turn, grade into layers of predominantly weakly mineralised BMS zone near the floor rock (Fig. 35).

5.5.2.1.2 Geochemical variation

In the upper metasomatic package, slightly elevated Pt+Pd contents are coupled with predominantly BMS mineralisation with Cu+Ni contents averaging above 1000 ppm, which coincide with and/ or correspond with the occurrence of CP I (Fig. 35). The olivine clinopyroxenites have very low Pt+Pd contents (< 0.5 $g.t^{-1}$) coupled with Cu+Ni contents less than 1000 ppm as seen in Fig. 35. This section is therefore a low PGE and BMS zone.

The down-hole trends for the PGE index or [(Cu/Zn) x (Ni/Co)] and Pt+Pd as well as that of Cu+Ni and SO_3 are largely mirror images of one another (Fig. 35). The base metals (Cu+Ni) and SO_3 display the highest positive spikes noticeable in CP I samples SS 330-10 (5864.4 ppm for Cu+Ni; 0.36 wt % for SO_3) and SS 330-16 (2176.9 ppm for Cu+Ni; 0.36 wt % for SO_3) at 195 and 232 m depths respectively (Fig. 35). At these depths there are corresponding positive spikes in [(Cu/Zn) x (Ni/Co)] and Pt+Pd, while the base metal vector Ni/Co is relatively low when compared to higher values in OCP I samples SS 330-15 (35.35) and SS 330-19 (1041.02) at 224 and 250 m depth, in that order (Fig. 35).

In this profile, Ca/Mg varies widely from 0.18 to 0.74 (Fig. 35). Clinopyroxenites are marked by Ca/Mg values ≥ 0.38 distinguishing them from the olivine clinopyroxenites ($Ca/Mg \leq 0.33$) as shown in Fig. 35. In addition, the weakly mineralised clinopyroxenite (CP I) is characterised by lower Rb* values when compared to CP III (Fig. 35). In this package, the highest positive spikes for Rb* is also present in OCP III (Fig. 35).

In the lower metasomatic package, the Cu+Ni contents are slightly high in the CP I and II at depths between 295 and 350 m (Fig. 35). This is followed by decreasing base metal contents (also Ni/Co and SO_3) that is coupled with attenuation of the relative proportion of CP I in favour of CP II and that of the OCP III in favour of OCP I downward to a depth of 450 m (Fig. 35). This lithological variation mirrors a progression from low BMS contents in CP I to a BMS - PGE rich zone in CP II matched with a decrease in Ca/Mg and Ti/Zr along with an increase in Mg/Fe, which, in turn, corresponds to a decrease in the abundance of OCP III with increasing OCP I (Fig. 35).

From 450 - 550 m depth, a predominantly PGE-rich zone coincides with the occurrence of OCP I and II (Fig. 35). This zone features high Pt+Pd (>20 $g.t^{-1}$) values and low Cu+Ni contents when compared to the abovementioned sections although the down-hole trends of the Cu+Ni, SO_3 and the BMS vectors (i.e. Ni/Co and [(Cu/Zn) x (Ni/Co)]) mimic that of Pt+Pd (Figure 35). In addition, the OCP unit corresponds with lower Ca/Mg and Ti/Zr coupled with higher Mg/Fe relative to the CP (Fig. 35). The PGE zones (at 450 and 470 m depth) within the OCP I coincide with low Sr/Ba ratios when compared to those in the OCP II at 520 and 526 m depth respectively, which are marked by higher Sr/Ba (Fig. 35).

A reversal of the lithological sequences as described in the upper section of the lower metasomatic package occurs below 550 m depth. This sequence instead reflects a regression from a BMS - PGE rich zone in CP II to low BMS contents in CP I (Fig. 35). Initially, peak contents of Cu+Ni occur in CP II at 554 m (SS 330-71) and 557 m depth (SS 330-72), coinciding with peak Ca/Mg and low Mg/Fe ratio values (Fig. 35). These also match high Pt+Pd values and high [(Cu/Zn) x (Ni/Co)] while Ni/Co values are relatively low (Fig. 35). Further down towards the floor rock, BMS peaks no longer correspond with high Pt+Pd or any other ratios mentioned above (Fig. 35).

The Pd/Pt ratio is relatively constant throughout the section (Fig. 35). Exceptions are observed at 114 m depth in CP III where Pd is enriched relative to Pt (Fig. 35). Further

down at 557 and 588 m depth in CP II (Sample SS 330-72; Pd is 5.72 and Pt is 30 $g.t^{-1}$) and CP III (Sample SS 330-78; Pd is 0.07 and Pt is 0.20 $g.t^{-1}$), respectively, Pd is depleted relative to Pt (Fig. 35).

5.5.2.2 Borehole OY 482

5.5.2.2.1 Lithological variation and mineralisation

In borehole OY 482, three major lithostratigraphic units, designated as the Lower, Middle and Upper Platreef, occur proximal and distal to the Archaean granite/ gneisses footwall, respectively (Fig. 36). These units consist at least of 2 interrupted feldspathic pyroxenite sills intercalated with gabbronorites (Fig. 36).

The Upper Platreef comprises of two feldspathic pyroxenite sills separated by a ~80m thick gabbronorite (Fig. 36). The latter is weakly mineralised in BMS (Cu+Ni) and PGE (Pt+Pd) within the upper sill and highly mineralised in BMS and PGE within its lower sill around 390 m depth (Fig. 36). The Middle Platreef (between 440 - 410 m depth) comprises of 4 feldspathic pyroxenite sills separated by 3gabbronorite layers (Fig. 36). These pyroxenites, up to 7 m thick, increase in thickness with increasing depth and are BMS mineralised (Fig. 36). The Lower Platreef, occurring below 450 m depth, is also mainly BMS mineralised and comprises of two feldspathic pyroxenite sills (Fig. 36).

5.5.2.2.2 Geochemical variation

In this profile (Fig. 36), Ca/Mg varies between 0.18 and 0.58. The Platreef feldspathic pyroxenites have Ca/Mg values < 0.38 (except for 4 samples within the Middle Platreef) separating them firstly from the gabbronorites (Ca/Mg ≥ 0.42; Fig. 36) and secondly from the clinopyroxenites in SS 330 (Ca/Mg: 0.38 – 0.77; Fig. 35), which can also be seen in Figures 30b & 30d.

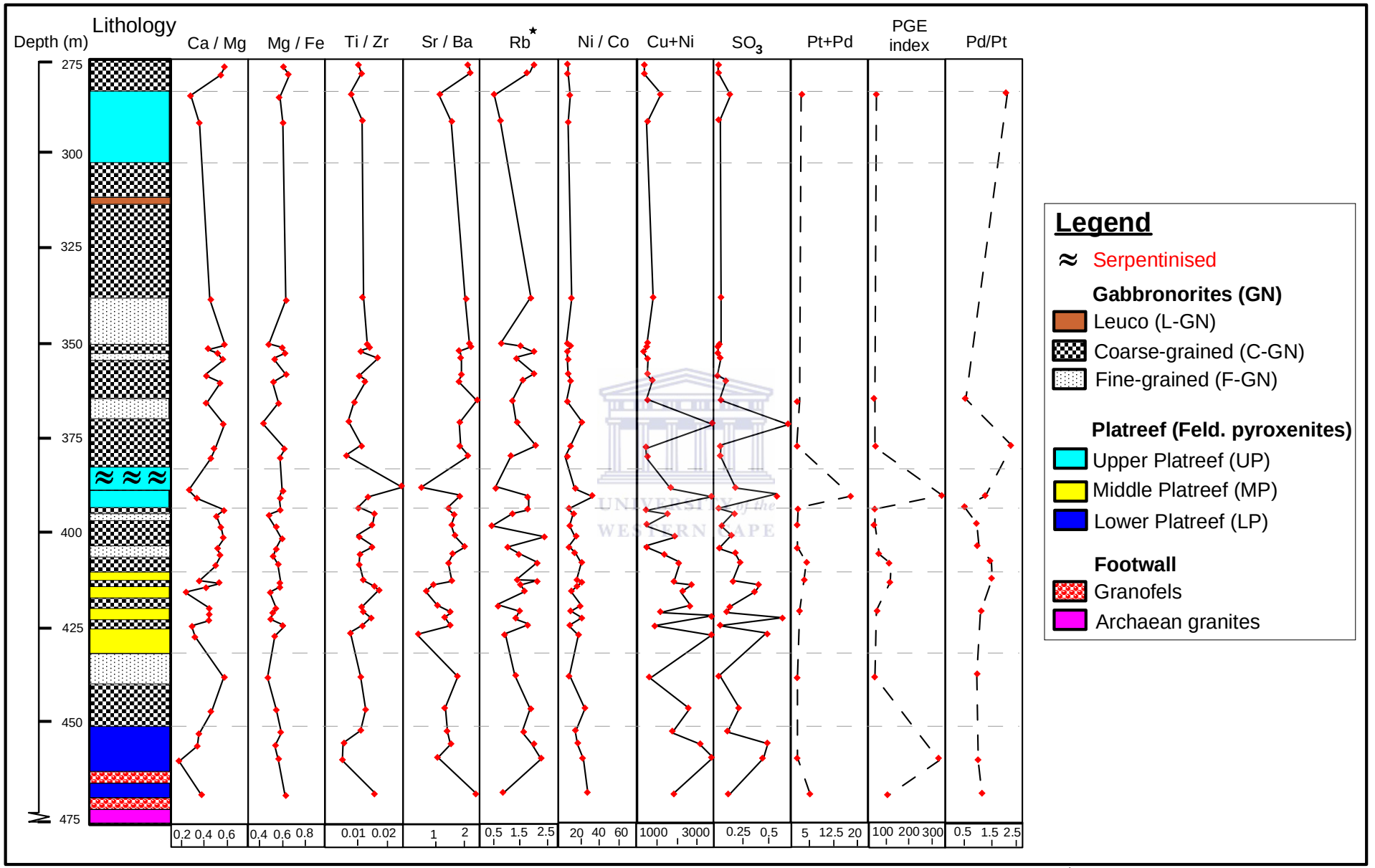

Fig. 36 Down-hole geochemical variations in borehole OY 482. Cu+Ni is expressed in ppm, SO_3 in wt. % and Pt+Pd in $g.t^{-1}$. Ca/Mg= CaO/(MgO+CaO); Mg/Fe=MgO/(Fe_2O_3+MgO) or Mg#; Ti/Zr = TiO_2/Zr; Rb* is mantle normalized anomaly; PGE index= (Cu/Zn) x (Ni/Co).

The Mg/Fe ratio profile ranges from 0.42 to 0.65 and does not exhibit considerable scattering of the data points to distinguish the Platreef feldspathic pyroxenites from the gabbronorites (Fig. 36). The Platreef feldspathic pyroxenites, however, have Mg/Fe values (ranging from 0.48 to 0.60; Fig. 36) distinguishable from the OCP in SS 330 (Mg/Fe: 0.68 – 0.93; Fig. 35), which can also be seen in Figs. 30c & 30d. The overall Mg/Fe profile, from the bottom to the top, shows a slight upwards decrease from the base of the Lower Platreef up to the Middle Platreef (Fig. 36). Further up, from the base of the Upper Platreef upwards, the Mg/Fe profile remains fairly constant, but slight higher than those of the Middle Platreef (Fig. 36).

As seen in core SS 330 at Sandsloot, the down-hole trends of Cu+Ni, base metal vectors and SO_3 are also mirror images in borehole OY 482 (Fig. 36). For samples with PGE data, the trend of [(Cu/Zn) x (Ni/Co)] mirrors that of Pt+Pd down-hole, but with differences in the Lower Platreef near the floor rock (Fig. 36).

The Upper Platreef is predominantly weakly mineralised in BMS (Cu+Ni) although its lower part, below the serpentinised area, is highly PGE/ BMS mineralised (Fig. 36).
The Middle and Lower Platreef are highly mineralised in BMS (Fig. 36). There is a progressively increasing trend in the Cu+Ni, Ni/Co and SO_3 contents from the Middle to the Lower Platreef (Fig. 36). This variation mirrors an increase in Mg/Fe, Sr/Ba and Rb*, which is coupled with a slight decrease in Ti/Zr (Fig. 36).
Pd/Pt displays a slight progressive decreasing trend in the Platreef feldspathic pyroxenites with increasing depth from the Upper through the Middle to the Lower Platreef above the floor rock (Fig. 36).

Chapter 6

6. Discussion, conclusions & recommendations

6.1 Introduction

This investigation was focused on two current issues related to the genesis of the Platreef and associated mineralisation. These issues centre on inadequate markers for stratigraphic correlations within and/ or between the Platreef and metamorphosed/ metasomatised footwall lithologies, and the relatively enigmatic styles of the PGE mineralisation. These issues affect the mineralogy and composition of these mineralised units both vertically and laterally, as alluded by various authors (Armitage et al., 2002; Harris and Chaumba, 2001; Hutchinson and Kinnaird, 2005; Holwell and McDonald, 2006; Pronost et al., 2008; Yudovskaya and Kinnaird, 2010). Inadequate solutions to these problems continue to pose serious challenges to exploration and mining companies in identifying possible exploration targets in the Platreef as a whole.

This study was set to identify and distinguish process-based mineralogical/ geochemical criteria which may be useful in stratigraphic correlations and characterizing the nature and style of PGE mineralisation within the Platreef and its metamorphosed floor rock. In addition, the work aimed at investigating the possible use of geochemical vectoring as a tool to locate the PGE mineralisation within the studied rocks.

The author however recognizes the shortcomings of using geochemical data from only two boreholes to demonstrate and generalize processes for the Platreef as a whole. The studied rocks are Platreef feldspathic pyroxenites in borehole OY 482 overlying Archaean granite/ gneisses, whereas in borehole SS 330 the rocks consist of footwall metamorphosed/ metasomatised clinopyroxenites and olivine-rich clinopyroxenites overlying the carbonate floor rock.
The discussions of the results are presented in the following paragraphs.

6.2 Discussion

Two boreholes were selected for this study. Borehole OY 482 transects mineralised Platreef pyroxenitic rocks that overlie the Archaean granite as floor rock. Borehole SS 330 crosscuts mineralised metamorphosed/ metasomatised footwall rocks that overlie dolomite of the Malmani Subgroup as floor rock. These mineralised rocks were chosen to study the mineralogical/ geochemical attributes that differentiates them and investigate the influence of the floor rocks on the nature and style of PGE mineralisation.

6.2.1 Borehole OY 482

The Platreef consists of three major interrupted feldspathic pyroxenite sills termed Lower, Middle and Upper Platreef separated from each other by various gabbronorite layers (Fig. 3). The Lower Platreef is predominantly comprised of a fine- to medium-grained orthopyroxene with interstitial plagioclase, low clinopyroxene, and abundant BMS and quartz. The Middle Platreef is comprised of medium-grained orthopyroxene, interstitial plagioclase and clinopyroxene with minor amount of BMS and quartz relative to the Lower Platreef. The Upper Platreef is composed of coarse-grained orthopyroxene, interstitial plagioclase and clinopyroxene with generally low BMS ores.

The abundance of quartz in the Lower Platreef (Plate 2a) points to assimilation of the footwall granite/ gneisses by the Platreef magma, as observed in the study by Holwell and McDonald (2006). In agreement with the above, the Lower Platreef has a slightly higher median content of SiO_2, Al_2O_3, Na_2O, K_2O and TiO_2, that is coupled with slightly lower median content for Fe_2O_3, MgO and CaO when compared to the Middle and Upper Platreef (Table 4). The high SiO_2 content suggests contamination of the Lower Platreef by granite/ gneisses, corroborating previous studies (Holwell and McDonald, 2006; Ihlenfeld and Keays, 2011). In addition, the Lower Platreef has also a higher median Zr/Y value relative to the other two units (Table 12) pointing to floor rock assimilation (Manyeruke et al., 2005). Furthermore, the patterns of the LILE (Rb^* and K^*) in the

Lower Platreef is slightly higher than those of the Middle and Upper Platreef which can also be interpreted as granite/ gneisses assimilation.

The results of mass balance calculations agree with the above. The Lower Platreef shows relative gains in certain oxides (SiO_2, Al_2O_3, Na_2O and K_2O) and trace elements (Ba, Nb, Rb, Sr and Zr) compared to the Middle and Upper Platreef (Table 9) which also suggest floor rock assimilation.

In terms of sequence of intrusion, there is an upward decrease in the $MgO/(Fe_2O_3+MgO)$ and Ni/(Cu+Ni) median values from the Lower to the Middle Platreef, which is later offset by a significant upward increase in both ratios median values from the Middle to the Upper Platreef (Table 12). Contrary to the latter trends, the CaO/(MgO+CaO) median values increase upward from the Lower to the Middle Platreef and decrease further upward within the Upper Platreef (Table 12). There is also an upward decrease in the Cu+Ni and Pt+Pd median contents from the Lower to the Middle Platreef (Table 12). From this unit, the median content in Cu+Ni decreases while that of Pt+Pd increases within the Upper Platreef (Table 12). The abovementioned trends may not be totally suggestive of two magmatic intrusive pulses (Ainsworth, 1998; Kinnaird, 2005).

There is a good correlation existing between the Cu+Ni and SO_3 contents, as shown in Figure 36, indicating the BMS mineralisation. In addition, an overall good correlation also exists between the Cu+Ni and Pt+Pd contents suggesting that the PGE are associated with the BMS mineralisation within the Upper and Middle Platreef. However within the Lower Platreef, the lowermost sample has high PGE and low BMS contents relative to the sample above which has low PGE and high BMS contents (Fig. 36). Although the PGE and BMS distribution can be said to have been controlled by gravity settling of the immiscible sulphide melt (Armitage et al., 2002; Kinnaird et al., 2005; Holwell and McDonald, 2006), this study has also shown that high BMS (Cu+Ni) contents do not always match with high PGE (Pt+Pd) contents and vice versa (Gain and Mostert, 1982; Kinnaird et al., 2005).

6.2.2 Borehole SS 330

The metamorphosed/ metasomatised lithologies consist of two major rock units termed clinopyroxenites and olivine clinopyroxenites. Clinopyroxenites are granoblastic and are predominantly made up of clinopyroxene, plagioclase with accessory calcite, prehnite, biotite and sulphides. The olivine clinopyroxenites contain olivine grains, which are variably serpentinised, occurring as inclusions mainly in granoblastic clinopyroxenes. This rock also contains plagioclase with accessory calcite, spinel, biotite, sulphides and oxide, and display igneous textures in places (i.e. interlocking grains of olivine and plagioclase; chapter 4.3.2.3.3, Plate 9c), that are crosscut by a network of fractures filled with Fe-oxides.

The two rock types were further subdivided each into three metamorphic/ metasomatic zones termed clinopyroxenite or olivine-rich clinopyroxenite subtypes I, II and III with increasing contact metamorphism/ metasomatism (Fig. 5). There is an asymmetrical contact metamorphic aureole in the hanging wall and footwall of a thick olivine clinopyroxenite unit (Fig. 5). This aureole is zoned and comprised essentially of a distal clinopyroxenites I and proximal clinopyroxenites II and III units. The zoned sequence or pattern of occurrence of these units is, however, interrupted by the occurrence of thin olivine clinopyroxenite layers. Of note are also the differing size/ symmetry of the hanging wall aureole above and below the dolomite xenolith (Fig. 5). These hanging wall aureoles are the most extensively developed in both zones (Fig. 5).

The mineral assemblages within the clinopyroxenites and olivine-rich clinopyroxenites, comprising of abundant clinopyroxenes, olivine inclusions and mineral phases such as spinel, calcite/ dolomite and dark brown biotite, are typically hallmarks of skarn deposits in magma-carbonate settings (Wenzel et al., 2002; Gaeta et al., 2009). These observations corroborate those of Armitage et al. (2002), which suggest that both the clinopyroxene and olivine in these footwall lithologies were derived from high-grade metamorphism/ metasomatism of the footwall dolomites considering their trace element characteristics.

The formation of the contact metasomatic zone/ skarn was accompanied by, or was subsequently followed by a hydro-magmatic phase evident in part as pervasive to oriented hydro-fracturing and possible hydrothermal alteration within the olivine-rich clinopyroxenites. A hydro-magmatic phase is also a common feature in carbonate-magma interaction environments (Gaeta et al., 2009). This is shown by the occurrence of poikiloblastic clinopyroxenes containing variably serpentinised olivine inclusions in the olivine-rich clinopyroxenites.

In line with the outlined mineralogy and metamorphic textures, the clinopyroxenites may have resulted from contact metamorphism of the footwall dolomites with limited influx of Platreef-forming magma (Harris and Chaumba, 2001; Armitage et al., 2002). The olivine clinopyroxenites however may conform to the footwall-reef hybrid described by McDonald et al. (2005) and the olivine-clinopyroxene cumulate (OCC) zone investigated by Gaeta et al. (2009). For this reason, it is inferred that the olivine clinopyroxenite is a product resulting from the mixture of the Platreef magma and the clinopyroxenites.

Along the same lines, the clinopyroxenites have high CaO and low MgO median contents when compared to the olivine clinopyroxenites, which is reflected by their modal compositions. This further supports the formation of the olivine clinopyroxenite in proximity to the Platreef-forming magma and that of a distal clinopyroxenite (Harris and Chaumba, 2001).

Three lines of geochemical evidence support a progressively proximal to distally zoned contact metasomatism between the Platreef magma and floor rock dolomite. These evidences emanate mainly from the trace element chemistry, in particular the HFSE and LILE. Their progressive patterns suggest the interconnectedness of three metasomatic sub-zones occurring within the clinopyroxenites and olivine clinopyroxenites in borehole SS 330. For example, transitional trends exist between the metasomatic subzones, from the weakly (CP I) to the feldspathic moderately metasomatised clinopyroxenite (CP III). These display a gradational decrease in the average contents of CaO equating to the presence of clinopyroxene and an increase in the average content of Al_2O_3 and K_2O

equating to the presence of sericitised plagioclase from sub-zone I to III. In consonance, the Al_2O_3/TiO_2 and Zr/Y ratios increase progressively from CP I to CP III.

For the olivine clinopyroxenites, the transition from the weakly (OCP I) to the highly metasomatised/ altered olivine clinopyroxenite (OCP III) is marked by a progressive decrease in the average content of MgO and LOI equating to the presence of olivine and serpentinisation. Accompanying the decrease in MgO and LOI is a concomitant increase in the contents of SiO_2, Fe_2O_3, Na_2O and K_2O. Similarly, the Zr/Y values increase progressively from OCP I to OCP III coupled with a progressive decrease in Al_2O_3/TiO_2 values. These characteristics, marked by a decrease in CaO and MgO contents, and increasing Al_2O_3 and SiO_2, Fe_2O_3, Na_2O and K_2O contents, in the clinopyroxenite and olivine clinopyroxenite, respectively, are hallmarks of a pervasive carbonate assimilation zone by the Platreef magma (Barnes et al., 2005).

The primitive mantle normalized HFSE (Zr, Ti and Y) patterns for both the clinopyroxenites and olivine clinopyroxenites are enriched relative to those of the dolomite and are relatively similar to those of the feldspathic pyroxenite at Overysel. The latter have a more pronounced magmatic signature (Holwell and McDonald, 2006). On the contrary, the LILE (Ba, Rb, K and Sr) patterns of both, the CP I and OCP I, are similar to those of the dolomite. The LILE are lower in the latter compared to the feldspathic pyroxenite at Overysel. There is a progressive increase in the LILE from CP I to CP III and OCP I to OCP III, with the overall patterns bearing increasing similarities to the feldspathic pyroxenite. The anomalies, Rb^*, K^* and Sr^* in both the clinopyroxenites and olivine clinopyroxenites also progressively increase in average content from CP I to CP III and OCP I to OCP III and further underpin these trends. These patterns suggest progressive enhancement in the LILE contents relative to the unchanged HFSE contents, from CP I to CP III and OCP I to OCP III. The LILE and HFSE patterns further support a transitional magma transfer zone or metasomatic zones between the Platreef and the floor rocks, as noted in previous studies in other complexes (Barnes et al., 2005; Polat et al. 2007; Ordóñez-Calderón et al., 2008).

Results of mass balance calculations are consistent with the aforesaid trends, suggesting that the clinopyroxenites and olivine clinopyroxenites are products resulting from the interaction between the Platreef-forming magma and the footwall dolomite. The mass balance results for both the clinopyroxenites and olivine clinopyroxenites are highlighted by gains in SiO_2, Fe_2O_3, SO_3, Co, Cu, Ni and Zn relative to the footwall dolomite, which denotes a magmatic signature (Mollaei et al., 2009). In this case, an influx from the Platreef magma into the floor rock dolomite is inferred. There are significant losses of MgO, CaO and LOI in the clinopyroxenites and of CaO and LOI in the olivine clinopyroxenites indicative of a carbonate signature (Mollaei et al., 2009), i.e. the floor rock dolomite. The gain in MgO in the olivine clinopyroxenites is interpreted as resulting from increased fractional assimilation of dolomite by the Platreef magma.

Furthermore, the enhancement of LILE (Rb and Sr) in both the clinopyroxenite III and olivine clinopyroxenite III, in consonance with the results from the spider diagram, can be attributed to varying degrees of fluid involvement in the metasomatic processes (Ordóñez-Calderón et al., 2008).

There is a good correlation existing between the Cu+Ni and SO_3 contents, as shown in Figure 35, indicating the presence of the BMS mineralisation. There is also a similarity in the down-hole pattern of Pt+Pd with that of Cu+Ni indicating some relationship existing between the PGE and the BMS (Fig. 35). However within the clinopyroxenites, high Pt+Pd contents do not always occur in zones with high Cu+Ni contents and vice versa (Fig. 35), as it has been reported elsewhere in the Platreef rocks (Gain and Mostert, 1982; Kinnaird et al., 2005). Therefore, the PGE mineralisation in metamorphosed footwall lithologies can be associated with sulphide-rich zones supporting previous study by Hutchinson and Kinnaird (2005). In contrast to the clinopyroxenites, the high Pt+Pd contents in the olivine-rich clinopyroxenites correspond generally with low BMS contents (Fig. 35). In this case, the PGE mineralisation therefore appears to have been strongly influenced by metamorphism and fluid activity validating previous observations (Armitage et al., 2002; Holwell et al., 2006; Barnes et al., 2008).

The BMS mineralisation shows a progressive increase in the average contents of Cu+Ni from CP I through CP III to CP II and is marked by an increase in the MgO and LOI average contents. The olivine-rich clinopyroxenites display a progressive increase in the average Cu+Ni, Fe_2O_3, Na_2O, K_2O and SiO_2 contents from OCP I through the OCP II to OCP III. Reverse trends are the case for MgO and LOI average contents in these rocks. The LILE contents progressively increase along with the BMS contents in the olivine-rich clinopyroxenites. These patterns suggest that the BMS mineralisation in the olivine-rich clinopyroxenites is controlled by metasomatism/ hydrothermal alteration (Armitage et al., 2002; Holwell et al., 2006).

The PGE mineralisation in clinopyroxenites is associated with zones of high Cu+Ni and MgO contents, and low Ca/Mg and Ti/Zr ratios. For the olivine clinopyroxenites, the PGE mineralisation is associated with zones of low Cu+Ni and LILE contents, and high Mg/Fe ratio. The latter observation is similar to that noted by Kinnaird (2005) within the Platreef pyroxenites.

6.2.3 Comparison of chemostratigraphic units in the studied boreholes

The clinopyroxenites and olivine clinopyroxenites, relative to the Platreef feldspathic pyroxenites, contain higher CaO and lower Fe_2O_3, Al_2O_3, Na_2O and SiO_2 median contents. In addition, they have lower Ba and Sr but higher Zr median contents relative to the Platreef feldspathic pyroxenites. These confirm earlier studies (Harris and Chaumba, 2001; McDonald et al., 2005; Pronost at al., 2008; Ihlenfeld and Keays, 2011) suggesting that these rocks are metamorphosed/ metasomatised resulting from the interaction between the Platreef magma and the footwall dolomite.

As opposed to the olivine clinopyroxenites, the clinopyroxenites have high CaO and low MgO median contents. This further supports the formation of the olivine clinopyroxenite in proximity to the Platreef magma and that of a distal clinopyroxenite (Harris and Chaumba, 2001). Along this line, two geochemical indices can be used to distinguish one lithological unit from the other. The CaO/(MgO+CaO) index separates clinopyroxenites

and olivine-rich clinopyroxenites, while the latter can be distinguished from the Platreef feldspathic pyroxenites using the $MgO/(Fe_2O_3+MgO)$ index.

In terms of mineralisation, the olivine-rich clinopyroxenites have the highest PGE and lowest BMS contents when compared to the clinopyroxenites and Platreef feldspathic pyroxenites. The clinopyroxenites, instead, show high PGE and BMS contents, while the Platreef feldspathic pyroxenites contain the highest BMS contents.

6.2.4 Nature and styles of PGE mineralisation

For this study, the following nature and style of the PGE/ BMS mineralisation were identified in the rocks studied:

- PGE-rich zone with low BMS in the olivine clinopyroxenites I and II.
- PGE-rich zone with moderate BMS in the Upper Platreef and clinopyroxenites II.
- BMS-rich zone with moderate PGE in the Middle and Lower Platreef.
- Low BMS with low PGE zone in clinopyroxenite subtypes I and III as well as olivine clinopyroxenites III.

These styles of mineralisation are in agreement with previous investigations validating, firstly, the occurrence of the PGE mineralisation in the Platreef and metamorphosed/ metasomatised rocks and, secondly, its variability across strike and with depth (Armitage et al., 2002; Kinnaird et al., 2005; Hutchinson and Kinnaird, 2005; Holwell and McDonald, 2006; Maier et al., 2008; Hutchinson and McDonald, 2008).

In borehole OY 482, where the floor rock is Archaean granite, the Pt+Pd content in the Upper and Middle Platreef feldspathic pyroxenites is mainly associated with the BMS and SO_3 abundances, except within the Lower Platreef as noted earlier. In borehole SS 330, where the floor rock is dolomite, the PGE mineralisation is generally associated with the BMS with some exceptions where high BMS content do correspond with low Pt+Pd contents. Previous investigations (Kinnaird et al., 2005; Kinnaird, 2005; Holwell et al.,

2006) noted this lack of correlation between the Pt+Pd content and that of Cu+Ni as a decoupling behaviour of the PGE from the BMS.

Furthermore, the Platreef feldspathic pyroxenite samples of the three units from borehole OY 482 have Pd/Pt ratios ≥1 (1 - 2.02) whereas the metamorphosed footwall samples from borehole SS 330 have Pd/Pt ratios ranging between 0.19 - 2.59. These are indicative of some fractionation of Pd over Pt in OY 482 and of Pd over Pt and vice versa in SS 330 (Armitage et al., 2002; Manyeruke et al., 2005).

These observations, which can be attributed to the effect of the various floor rocks on the PGE mineralisation, corroborate previous studies which suggests a magmatic style of mineralisation due to the anhydrous nature of the floor rock, in this case the Archaean granite in borehole OY 482, and a contact-style of mineralisation likely due to the volatile-rich nature of the floor rock, in this case the dolomite in borehole SS 330 (Armitage et al., 2002; Kinnaird et al., 2005; Hutchinson and Kinnaird, 2005; Holwell and McDonald, 2006; Maier et al., 2008; Hutchinson and McDonald, 2008).

6.2.5 Application of the base metal indices as vector towards PGE mineralisation

One of the aims of this study was to develop geochemical vectors which could be used to locate the PGE mineralisation in the studied rock. These vectors or element ratios, derived in this work, are based on patterns of the metal elements in the BMS (pyrrhotite, pentlandite and chalcopyrite) which was identified as the most dominant ore mineral in the rocks. For this reason, the metal elements of the sulphides (Ni, Cu, Co and Zn) were used to develop indices to vector towards PGE mineralisation in the studied rocks.
In other words, are the base metal indices able to discriminate PGE-bearing zones from barren ones?

A similar approach to that of Brand (1999) was undertaken in this work to develop the element ratios that can vector towards ores. From the study of the degree of dissimilarity between the element pairs as described earlier in section 5.4.3, it was suggested that base

metal ratios (Cu/Zn, Ni/Co and Ni/(Ni+Cu)) may be useful to vector towards the PGE mineralisation. Furthermore, multiplying any two of the above elemental pairs of ratios (e.g. {Cu/Zn x Ni/Co}) would increase the contrast of the vector.

In borehole OY 482 drilled at Overysel, the [(Cu/Zn) x (Ni/Co)] pattern appears to mirror that of Pt+Pd within the Upper and Middle Platreef (Fig. 36). However, further down in the Lower Platreef, the higher [(Cu/Zn) x (Ni/Co)] value does not correspond with higher Pt+Pd value and vice versa (Fig. 36).
In borehole SS 330 (Sandsloot), the [(Cu/Zn) x (Ni/Co)] patterns mirrors that of Pt+Pd within the clinopyroxenites and olivine clinopyroxenites in places (Fig. 35). However, not all higher [(Cu/Zn) x (Ni/Co)] values correspond with higher Pt+Pd values and vice versa (Fig. 35).

Various factors can be put forward to explain the lack of ability for the proposed base metal index; i.e. (Cu/Zn) x (Ni/Co), to define consistent trend with the Pt+Pd content:
(1) The various styles of PGE mineralisation identified in this study (PGE-rich with moderate BMS, PGE-rich with low BMS, BMS-rich with moderate PGE and low BMS with low PGE) indicate a lack of good correlation between the BMS and the PGEs; (2) The concentrations of the base metal elements and PGEs have shown to vary within the sulphide phases (Paktunc et al., 1990; Barnes et al., 2008); (3) Besides being mainly hosted within the BMS, the PGMs also occur in primary and secondary silicates assemblages after processes, such as metamorphism and fluid activity, affect their initial distribution among sulphide phases (Armitage et al., 2002; Hutchinson and Kinnaird, 2005; Holwell et al., 2006; Barnes et al., 2008); and (4) The availability of semi-metals (such as As, Bi and Te), which can also derive from volatile-rich floor rock assimilation, in the system would have a control on the behaviour and the amount of PGEs in the sulphides (Paktunc et al., 1990; Hutchinson and Kinnaird, 2005; Hutchinson and McDonald, 2008; Holwell and McDonald, 2010).

6.3 Conclusions

The major conclusions of the work are as follows:

- The geochemical data evaluation has positively revealed consistent elemental patterns through hierarchical clustering, rock characterisation and mass balance calculations that are related to magmatic, metamorphic/ metasomatic and floor rock assimilation processes in the studied rocks (feldspathic pyroxenites, olivine clinopyroxenites and clinopyroxenites).

- In borehole OY 482, drilled at Overysel farm, the Platreef consists of three major feldspathic pyroxenite sills, intercalated with gabbronorites, referred to as Lower, Middle and Upper Platreef units, from the bottom to the top, respectively. The Lower Platreef (overlaying the Archaean granite floor rock) and the Middle Platreef are fine to medium-grained and are comprised of two and four feldspathic pyroxenite sills, respectively. The Upper Platreef is coarse-grained and comprises two feldspathic pyroxenite sills. From the base of the Platreef upwards, there is an upward decrease in the Mg# and Ni/Cu median values from the Lower (0.58; 0.68) to the Middle Platreef (0.54; 0.67). In contrast, the Ca/Mg median value increases upward from the Lower (0.34) to the Middle Platreef (0.39). The Upper Platreef, however, is characterised by Mg# and Ni/Cu median values of 0.57 and 0.75, respectively. In addition, the Upper Platreef has a Ca/Mg median value of 0.33.

  This observation may not fully agree with the multiple magmatic intrusive pulses proposed by previous authors (Kinnaird, 2005; Yudovskaya and Kinnaird, 2010; Mitchell and Scoon, 2012). The intrusion of the Lower Platreef was accompanied with assimilation of the Archaean granite floor rock (Holwell and McDonald, 2006).

- Borehole SS 330, drilled at Sandsloot, consists of intercalated clinopyroxenites and variably serpentinised olivine clinopyroxenites; both are products resulted from the injection of Platreef magma sills within the dolomite floor rock. The clinopyroxenites are characterised by enrichment of CaO relative to MgO as a result of contact

metamorphism of the floor rock with limited influx of Platreef magma. However the olivine clinopyroxenites are characterised by enrichment of MgO relative to CaO as a resulted of mixture between the Platreef magma and clinopyroxenites (Harris and Chaumba, 2001). In addition, both units are made up of three metasomatic subzones each marked by an enrichment of LILE relative to the HFSE.

- The Platreef feldspathic pyroxenites, olivine clinopyroxenites and clinopyroxenites can be easily distinguished from each other. The Platreef feldspathic pyroxenites are characterised by CaO/(MgO+CaO) and MgO/(Fe_2O_3+MgO) ratio values of <0.5 and <0.6, respectively. Olivine clinopyroxenites are marked by CaO/(MgO+CaO) ratio values <0.4 and MgO/(Fe_2O_3+MgO) ratio values >0.6. Clinopyroxenites are marked by CaO/(MgO+CaO) ratio values >0.4.

- The PGE mineralisation in clinopyroxenites is associated with zones of low Ca/Mg median values. In the Platreef feldspathic pyroxenites and olivine clinopyroxenites, it is marked by zones of high Mg/Fe median values. The latter reflects magmatic variability for the Platreef pyroxenites in OY 482 and fluid activity or the occurrence of altered olivine-rich clinopyroxenites (Ainsworth, 1998; Armitage et al., 2002; Kinnaird, 2005).

- The PGE mineralisation in borehole OY 482, where the floor rock is Archaean granite, is controlled by magmatic process (Holwell and McDonald, 2006), whereas in borehole SS 330, where the Malmani dolomite floor rock is volatile-rich, it is controlled by metamorphism and hydrothermal activity (Armitage et al., 2002).

- The proposed base metal index [(Cu/Zn) x (Ni/Co)] used to vector towards PGE-rich zones does not provide consistent trend in identifying mineralised zones from barren ones. In BMS-rich zones, mainly those within the Platreef feldspathic pyroxenites and clinopyroxenites, the base metal index appears to correlate with the Pt+Pd. However in the low BMS zones, especially of the olivine clinopyroxenites, the vector index

does not appear to correlate with the Pt+Pd. Amongst other factors, this is interpreted as changes in the mineralogy of the BMS.

- This study has positively identified criteria useful for stratigraphic correlations within and/ or between the Platreef and the metamorphosed/ metasomatised floor rock. However, the two boreholes studies show different petrographic and geochemical characteristics such that borehole OY 482, drilled at Overysel, comprises Platreef magmatic rocks as opposed to borehole SS 330, drilled at Sandsloot, which has intersected metamorphic/ metasomatic rocks.

6.4 Recommendations

The genesis of the Platreef and the effect of the floor rock assimilation and metasomatism on the styles of mineralisation are still unresolved. Further investigations along these issues should continue in order to have a better understanding of the various processes involved in its formation. These unanswered questions amongst other make the Platreef undoubtedly a complex PGE deposit.

References

Abdel-Halim, R. & Abdel-Aal, R. 1999, "Classification of urinary stones by cluster analysis of ionic composition data", *Computer methods and programs in biomedicine*, vol. 58, no. 1, pp. 69-81.

Ainsworth, C. 1998, "How many magma injections did it take to bring PGE enrichment to the Platreef in the Sandsloot area", *8th International platinum symposium*, pp. 3.

Ames, D., McClenaghan, M. & Averill, S. 2007, "Footwall-hosted Cu-PGE (Au, Ag), Sudbury Canada: towards a new exploration vector", *Exploration 07, Exploration in the New Millennium*, , pp. 1013-1017.

Armitage, P.E.B., McDonald, I., Edwards, S. & Manby, G. 2002, "Platinum-group element mineralization in the Platreef and calc-silicate footwall at Sandsloot, Potgietersrus District, South Africa", *Applied Earth Science: Transactions of the Institutions of Mining and Metallurgy: Section B*, vol. 111, no. 1, pp. 36-45.

Ashwal, L.D., Webb, S.J. & Knoper, M.W. 2005, "Magmatic stratigraphy in the Bushveld Northern Lobe: continuous geophysical and mineralogical data from the 2950 m Bellevue drillcore", *South African Journal of Geology*, vol. 108, no. 2, pp. 199-232.

Banacos, P.C. 2011, *Box and whisker plots for local climate datasets: Interpretation and creation using Excel 2007/2010*, US Department of Commerce, National Oceanic and Atmospheric Administration, National Weather Service.

Barnes, C.G., Prestvik, T., Sundvoll, B. & Surratt, D. 2005, "Pervasive assimilation of carbonate and silicate rocks in the Hortavaer igneous complex, north-central Norway", *Lithos*, vol. 80, no. 1, pp. 179-199.

Barnes, S. & Maier, W.D. 2002, "Platinum-group element distributions in the Rustenburg layered suite of the Bushveld Complex, South Africa", *The geology, geochemistry, mineralogy and mineral beneficiation of platinum-group elements*, vol. 54, pp. 431-458.

Barnes, S., Prichard, H.M., Cox, R.A., Fisher, P.C. & Godel, B. 2008, "The location of the chalcophile and siderophile elements in platinum-group element ore deposits (a textural, microbeam and whole rock geochemical study): implications for the formation of the deposits", *Chemical Geology*, vol. 248, no. 3, pp. 295-317.

Barton, J., Cawthorn, R.G. & White, J. 1986, "The role of contamination in the evolution of the Platreef of the Bushveld Complex", *Economic Geology*, vol. 81, no. 5, pp. 1096-1104.

Brady, J.B. 1977, "Metasomatic zones in metamorphic rocks", *Geochimica et Cosmochimica Acta*, vol. 41, no. 1, pp. 113-125.

Brand, N.W. 1999, "Element ratios in nickel sulphide exploration: vectoring towards ore environments", *Journal of Geochemical Exploration*, vol. 67, no. 1, pp. 145-165.

Bye, A. & Bell, F. 2001, "Stability assessment and slope design at Sandsloot open pit, South Africa", *International Journal of Rock Mechanics and Mining Sciences*, vol. 38, no. 3, pp. 449-466.

Cann, J. 1970, "Rb, Sr, Y, Zr and Nb in some ocean floor basaltic rocks", *Earth and Planetary Science Letters*, vol. 10, no. 1, pp. 7-11.

Cawthorn, R.G., Barton, J. & Viljoen, M.J. 1985, "Interaction of floor rocks with the Platreef on Overysel, Potgietersrus, northern Transvaal", *Economic Geology,* vol. 80, no. 4, pp. 988-1006.

Cawthorn, R.G. & Walraven, F. 1998, "Emplacement and crystallization time for the Bushveld Complex", *Journal of Petrology,* vol. 39, no. 9, pp. 1669-1687.

Cawthorn, R. 1999a, "The discovery of the platiniferous Merensky Reef in 1924", *South African Journal of Geology,* vol. 102, no. 3, pp. 178-183.

Cawthorn, R. 1999b, "The platinum and palladium resources of the Bushveld Complex.", *South African Journal of Science,* vol. 95.

De Klerk, L. 2005, "Bushveld stratigraphy on Rooipoort, Potgietersrus limb", *Workshop on Platinum exploration and exploitation in Africa.*

De Villiers, J. 1970, "The structure and petrology of the mafic rocks of the Bushveld Complex south of Potgietersrus", *Geol Soc S Afr,* pp. 23.

Deksissa, D.J. & Koeberl, C. 2004, "Geochemistry, alteration, and genesis of gold mineralization in the Okote area, southern Ethiopia", Geochemical Journal-*Japan,* vol. 38, no. 4, pp. 307-332.

Derakhshani, R. & Abdolzadeh, M. 2009, "Mass Change Calculations During Hydrothermal Alteration/Mineralization in the Porphyry Copper Deposit of Darrehzar, Iran.", *Research Journal of Environmental Sciences,* vol. 3, no. 1.

Eales, H., Botha, W., Hattingh, P., De Klerk, W., Maier, W. & Odgers, A. 1993, "The mafic rocks of the Bushveld Complex: a review of emplacement and crystallization history, and mineralization, in the light of recent data", *Journal of African Earth Sciences (and the Middle East),* vol. 16, no. 1, pp. 121-142.

Eales, H. & Cawthorn, R. 1996, "The Bushveld Complex", *Developments in Petrology,* vol. 15, pp. 181-229.

Eilu, P., Mikucki, E.J. & Dugdale, A.L. 2001, "Alteration zoning and primary geochemical dispersion at the Bronzewing lode-gold deposit, Western Australia", *Mineralium Deposita,* vol. 36, no. 1, pp. 13-31.

Ferry, J.M., Wing, B.A., Penniston-Dorland, S.C. & Rumble, D. 2002, "The direction of fluid flow during contact metamorphism of siliceous carbonate rocks: new data for the Monzoni and Predazzo aureoles, northern Italy, and a global review", *Contributions to Mineralogy and Petrology,* vol. 142, no. 6, pp. 679-699.

Finch, H. 2005, "Comparison of distance measures in cluster analysis with dichotomous data", *Journal of Data Science,* vol. 3, no. 1, pp. 85-100.

Gaeta, M., Di Rocco, T. & Freda, C. 2009, "Carbonate assimilation in open magmatic systems: the role of melt-bearing skarns and cumulate-forming processes", *Journal of Petrology,* vol. 50, no. 2, pp. 361-385.

Gain, S.B. & Mostert, A. 1982, "The geological setting of the platinoid and base metal sulfide mineralization in the Platreef of the Bushveld Complex in Drenthe, north of Potgietersrus", *Economic Geology,* vol. 77, no. 6, pp. 1395-1404.

Good, N. & De Wit, M.J. 1997, "The Thabazimbi-Murchison lineament of the Kaapvaal craton, South Africa: 2700 Ma of episodic deformation", *Journal of the Geological Society,* vol. 154, no. 1, pp. 93-97.

Grant, J.A. 2005, "Isocon analysis: a brief review of the method and applications", *Physics and Chemistry of the Earth, Parts A/B/C,* vol. 30, no. 17, pp. 997-1004.

Grant, J.A. 1986, "The isocon diagram; a simple solution to Gresens' equation for metasomatic alteration", *Economic Geology*, vol. 81, no. 8, pp. 1976-1982.
Gresens, R.L. 1967, "Composition-volume relationships of metasomatism", *Chemical Geology*, vol. 2, pp. 47-65.
Hall, A.L. 1932, *The Bushveld Igneous Complex of the central Transvaal,* The Government printer.
Hall, G., Pelchat, J. & Dunn, C. 1990, "The determination of Au, Pd and Pt in ashed vegetation by ICP-mass spectrometry and graphite furnace atomic absorption spectrometry", *Journal of Geochemical Exploration*, vol. 37, no. 1, pp. 1-23.
Harmer, R., Pillay, N. & Davies, P. 2004, "The Aurora Project–Main Zone hosted PGE-base metal mineralization at the northern outcrop limit of the Bushveld northern limb, north of Mokopane", *Abstract volume Geoscience Africa, University of the Witwatersrand, South Africa, .*
Harris, C. & Chaumba, J.B. 2001, "Crustal contamination and fluid–rock interaction during the formation of the Platreef, northern limb of the Bushveld Complex, South Africa", *Journal of Petrology*, vol. 42, no. 7, pp. 1321-1347.
Holwell, D.A., Armitage, P.E.B. & McDonald, I. 2005, "Observations on the relationship between the Platreef and its hangingwall", *Applied Earth Science: Transactions of the Institution of Mining & Metallurgy, Section B,* vol. 114, no. 4, pp. 199-207.
Holwell, D.A., Boyce, A. & McDonald, I. 2007, "Sulfur isotope variations within the Platreef Ni-Cu-PGE deposit: Genetic implications for the origin of sulfide mineralization", *Economic Geology*, vol. 102, no. 6, pp. 1091-1110.
Holwell, D.A., Jones, A., Smith, J. & Boyce, A. 2013, "New mineralogical and isotopic constraints on Main Zone-hosted PGE mineralisation at Moorddrift, northern Bushveld Complex", *Mineralium Deposita*, vol. 48, no. 6, pp. 675-686.
Holwell, D.A. & Jordaan, A. 2006, "Three-dimensional mapping of the Platreef at the Zwartfontein South mine: implications for the timing of magmatic events in the northern limb of the Bushveld Complex, South Africa", *Applied Earth Science: Transactions of the Institutions of Mining and Metallurgy: Section B*, vol. 115, no. 2, pp. 41-48.
Holwell, D.A. & McDonald, I. 2010, "A review of the behaviour of platinum group elements within natural magmatic sulfide ore systems", *Platinum Metals Review,* vol. 54, no. 1, pp. 26-36.
Holwell, D.A. & McDonald, I. 2006, "Petrology, geochemistry and the mechanisms determining the distribution of platinum-group element and base metal sulphide mineralisation in the Platreef at Overysel, northern Bushveld Complex, South Africa", *Mineralium Deposita,* vol. 41, no. 6, pp. 575-598.
Holwell, D.A., McDonald, I. & Armitage, P.E.B. 2006, "Platinum-group mineral assemblages in the Platreef at the Sandsloot Mine, northern Bushveld Complex, South Africa", *Mineralogical Magazine,* vol. 70, no. 1, pp. 83-101.
Hulbert, L.J. 1983, "A petrographical investigation of the Rustenburg Layered Suite and associated mineralisation south of Potgietersrus", Unpublished DSc dissertation, University of Pretoria, pp. 511.
Hulbert, L.J. & Von Gruenewaldt, G. 1986, "The structure and petrology of the upper and lower chromitite layers on the farms Grasvally and Zoetveld, south of

Potgietersrus", *Mineral Deposits of Southern Africa. Geol Soc South Africa, Johannesburg*, vol. 2, pp. 1237-1249.

Hulbert, L.J. & Von Gruenewaldt, G. 1982, "Nickel, copper, and platinum mineralization in the lower zone of the Bushveld Complex, south of Potgietersrus", *Economic Geology*, vol. 77, no. 6, pp. 1296-1306.

Hutchinson, D. & Kinnaird, J.A. 2005, "Complex multistage genesis for the Ni–Cu–PGE mineralisation in the southern region of the Platreef, Bushveld Complex, South Africa", *Applied Earth Science: Transactions of the Institutions of Mining and Metallurgy: Section B*, vol. 114, no. 4, pp. 208-224.

Hutchinson, D. & McDonald, I. 2008, "Laser ablation ICP-MS study of platinum-group elements in sulphides from the Platreef at Turfspruit, northern limb of the Bushveld Complex, South Africa", *Mineralium Deposita*, vol. 43, no. 6, pp. 695-711.

Ihlenfeld, C. & Keays, R.R. 2011, "Crustal contamination and PGE mineralization in the Platreef, Bushveld Complex, South Africa: evidence for multiple contamination events and transport of magmatic sulfides", *Mineralium Deposita*, vol. 46, no. 7, pp. 813-832.

Johnson, T.E., Brown, M. & White, R.W. 2010, "Petrogenetic modelling of strongly residual metapelitic xenoliths within the southern Platreef, Bushveld Complex, South Africa", *Journal of Metamorphic Geology*, vol. 28, no. 3, pp. 269-291.

Keays, R.R., Lightfoot, P.C. & Hamlyn, P.R. 2012, "Sulfide saturation history of the Stillwater Complex, Montana: chemostratigraphic variation in platinum group elements", *Mineralium Deposita*, vol. 47, no. 1-2, pp. 151-173.

King, P., White, A., Chappell, B. & Allen, C. 1997, "Characterization and origin of aluminous A-type granites from the Lachlan Fold Belt, southeastern Australia", *Journal of Petrology*, vol. 38, no. 3, pp. 371-391.

Kinnaird, J.A. 2005, "Geochemical evidence for multiphase emplacement in the southern Platreef", *Applied Earth Science: Transactions of the Institution of Mining & Metallurgy, Section B*, vol. 114, no. 4, pp. 225-242.

Kinnaird, J.A., Hutchinson, D., Schurmann, L., Nex, P. & de Lange, R. 2005, "Petrology and mineralisation of the southern Platreef: northern limb of the Bushveld Complex, South Africa", *Mineralium Deposita*, vol. 40, no. 5, pp. 576-597.

Kinnaird, J.A. & McDonald, I. 2005, "An introduction to mineralisation in the northern limb of the Bushveld Complex", *Applied Earth Science: Transactions of the Institutions of Mining and Metallurgy: Section B*, vol. 114, no. 4, pp. 194-198.

Kinnaird, J.A., Yudovskaya, M., Naldrett, A., Botha, M. & Chunnett, G. 2012, "PGE mineralisation in the Main Zone of the northern limb of the Bushveld Complex", *12th Int Ni–Cu–(PGE) Symp, Guiyang, China. Abstracts*, pp. 73.

Korzhinskii, D.S. 1953, "Outline of metasomatic processes" In: Main problems on the science of magmatogenic ore deposits, Acad. Sci. Publishing, Moscow, pp. 334-456, (In Russian). German edition, 1965. Abriss der metasomatischen Prozesse, Akad. Verl., Berlin.

Kruger, F.J. 2005, "Filling the Bushveld Complex magma chamber: lateral expansion, roof and floor interaction, magmatic unconformities, and the formation of giant chromitite, PGE and Ti-V-magnetitite deposits", *Mineralium Deposita*, vol. 40, no. 5, pp. 451-472.

Large, R.R. & McGoldrick, P.J. 1998, "Lithogeochemical halos and geochemical vectors to stratiform sediment hosted Zn–Pb–Ag deposits, 1. Lady Loretta Deposit, Queensland", *Journal of Geochemical Exploration*, vol. 63, no. 1, pp. 37-56.

Lee, C. 1996, "A review of mineralization in the Bushveld Complex and some other layered intrusions", *Developments in Petrology*, vol. 15, pp. 103-145.

López-Moro, F.J. 2012, "EASYGRESGRANT—A Microsoft Excel spreadsheet to quantify volume changes and to perform mass-balance modeling in metasomatic systems", *Computers & Geosciences*, vol. 39, pp. 191-196.

MacLean, W. & Barrett, T. 1993, "Lithogeochemical techniques using immobile elements", *Journal of Geochemical Exploration*, vol. 48, no. 2, pp. 109-133.

MacLean, W. & Kranidiotis, P. 1987, "Immobile elements as monitors of mass transfer in hydrothermal alteration; Phelps Dodge massive sulfide deposit, Matagami, Quebec", *Economic Geology*, vol. 82, no. 4, pp. 951-962.

Maier, W. 2005, "Platinum-group element (PGE) deposits and occurrences: mineralization styles, genetic concepts, and exploration criteria", *Journal of African Earth Sciences*, vol. 41, no. 3, pp. 165-191.

Maier, W., Barnes, S. & Groves, D. 2013, "The Bushveld Complex, South Africa: formation of platinum–palladium, chrome-and vanadium-rich layers via hydrodynamic sorting of a mobilized cumulate slurry in a large, relatively slowly cooling, subsiding magma chamber", *Mineralium Deposita*, vol. 48, no. 1, pp. 1-56.

Maier, W., De Klerk, L., Blaine, J., Manyeruke, T., Barnes, S., Stevens, M. & Mavrogenes, J. 2008, "Petrogenesis of contact-style PGE mineralization in the northern lobe of the Bushveld Complex: comparison of data from the farms Rooipoort, Townlands, Drenthe and Nonnenwerth", *Mineralium Deposita*, vol. 43, no. 3, pp. 255-280.

Manyeruke, T.D., Maier, W.D. & Barnes, S. 2005, "Major and trace element geochemistry of the Platreef on the farm Townlands, northern Bushveld Complex.", *South African Journal of Geology*, vol. 108, no. 3.

Martins, R., Mateus, A., Figueiras, J., Barroso, M. & Oliveira, V. 2003, "Post-metamorphic evolution of the Lower Cambrian section at Enfermarias (Moura, Portugal); its record and metallogenic implications", .

McClenaghan, S., Lentz, D. & Fyffe, L. 2006, "Chemostratigraphy of volcanic rocks hosting massive sulfide clasts within the Meductic Group, west-central New Brunswick", *Exploration and Mining Geology*, vol. 15, no. 3-4, pp. 241-261.

McDonald, I., Harmer, R.E. 2010, "The nature of PGE mineralization in the aurora project area, northern Bushveld Complex, South Africa", In: Jugo P.J., Lesher C.M., Mungall, J.E. (Eds.), 11th International Platinum Symposium, 21-24 June 2010, Sudbury, Ontario, Canada. Ontario Geological Survey, Miscellaneous Release-Data 269, extended abstracts.

McDonald, I. & Holwell, D.A. 2007, "Did lower zone magma conduits store PGE-rich sulphides that were later supplied to the Platreef?", *South African Journal of Geology*, vol. 110, no. 4, pp. 611-616.

McDonald, I., Holwell, D.A. & Armitage, P.E.B. 2005, "Geochemistry and mineralogy of the Platreef and “Critical Zone” of the northern lobe of the Bushveld Complex, South Africa: implications for Bushveld stratigraphy and the development of PGE mineralisation", *Mineralium Deposita*, vol. 40, no. 5, pp. 526-549.

McDonald, I., Holwell, D.A. & Wesley, B. 2009, "Assessing the potential involvement of an early magma staging chamber in the generation of the Platreef Ni–Cu–PGE deposit in the northern limb of the Bushveld Complex: a pilot study of the Lower Zone Complex at Zwartfontein", *Applied Earth Science: Transactions of the Institution of Mining & Metallurgy, Section B,* vol. 118, no. 1, pp. 5-20.

McDonough, W., Sun, S., Ringwood, A., Jagoutz, E. & Hofmann, A. 1992, "Potassium, rubidium, and cesium in the Earth and Moon and the evolution of the mantle of the Earth", *Geochimica et Cosmochimica Acta,* vol. 56, no. 3, pp. 1001-1012.

Mellor, E. & Hall, A. 1910, "Explanation of sheet no. 7 (Potgietersrust)", *Geol.Surv.Union of South Africa, South Africa,* .

Merensky, H. 1925, "The platinum occurrence on the properties of Potgietersrus Platinums Limited Report to the Directors", *London and Rhodesia Mining and Land Company Limited, Johannesburg,* .

Miller, J.D., Green, J.C., Severson, M.J., Chandler, V.W., Hauck, S.A., Peterson, D.M. & Wahl, T.E. 2002, *Geology and mineral potential of the Duluth Complex and related rocks of northeastern Minnesota,* University of Minnesota, Minnesota Geological Survey.

Mitchell, A.A. & Scoon, R.N. 2012, "The Platreef of the Bushveld Complex, South Africa: a New Hypothesis of Multiple, Non-Sequential Magma Replenishment Based on Observations at the Akanani Project, North-West of Mokopane", *South African Journal of Geology,* vol. 115, no. 4, pp. 535-550.

Mollaei, H., Yaghubpur, A. & Attar, R.S. 2009, "Geology and geochemistry of skarn deposits in the northern part of Ahar batholith, East Azarbaijan, NW Iran", *Iranian Journal of Earth Sciences,* vol. 1, pp. 15-34.

Montero-Serrano, J.C., Palarea-Albaladejo, J., Martín-Fernández, J.A., Martínez-Santana, M. & Gutiérrez-Martín, J.V. 2010, "Sedimentary chemofacies characterization by means of multivariate analysis", *Sedimentary Geology,* vol. 228, no. 3, pp. 218-228.

Mukherjee, P. & Gupta, P. 2008, "Arbitrary scaling in ISOCON method of geochemical mass balance: An evaluation of the graphical approach", *Geochemical Journal,* vol. 42, no. 3, pp. 247.

Naldrett, A., Wilson, A., Kinnaird, J. & Chunnett, G. 2009, "PGE tenor and metal ratios within and below the Merensky Reef, Bushveld Complex: implications for its genesis", *Journal of Petrology,* vol. 50, no. 4, pp. 625-659.

Naldrett, A., Wilson, A., Kinnaird, J., Yudovskaya, M. & Chunnett, G. 2012, "The origin of chromitites and related PGE mineralization in the Bushveld Complex: new mineralogical and petrological constraints", *Mineralium Deposita,* vol. 47, no. 3, pp. 209-232.

Naldrett, T., Kinnaird, J., Wilson, A. & Chunnett, G. 2008, "Concentration of PGE in the Earth's Crust with Special Reference to the Bushveld Complex", *Earth Science Frontiers,* vol. 15, no. 5, pp. 264-297.

Naumann, K.F. 1826, "Lehrbuch der Mineralogie", Leipzig, Engelman, pp. 209.

Nex, P.A.M. 2005, "The structural setting of mineralisation on Tweefontein Hill, northern limb of the Bushveld Complex, South Africa", *Applied Earth Science: Transactions of the Institution of Mining & Metallurgy, Section B,* vol. 114, no. 4, pp. 243-251.

Norrish, K. & Hutton, J.T. 1969, "An accurate X-ray spectrographic method for the analysis of a wide range of geological samples", *Geochimica et Cosmochimica Acta*, vol. 33, no. 4, pp. 431-453.

Ordóñez-Calderón, J.C., Polat, A., Fryer, B.J., Gagnona, J.E., Raith, J.G., Appel, P.W.U. 2008, "Evidence for HFSE and REE mobility during calc-silicate metasomatism, Mesoarchean (~3075 Ma) Ivisaartoq greenstone belt, southern west Greenland", Precambrian Research, vol. 161, no. 3, pp. 317-340.

Paktunc, A.D., Hulbert, L.J. & Harris, D.C. 1990, "Partitioning of the platinum-group and other trace elements in sulfides from the Bushveld Complex and Canadian occurrences of nickel–copper sulfides", *Canadian Mineralogist*, vol. 28, pp. 475-488.

Pearce, J.A. 1983, "Role of the sub-continental lithosphere in magma genesis at active continental margins", .

Pearce, T.J., Besly, B.M., Wray, D.S. & Wright, D.K. 1999, "Chemostratigraphy: a method to improve interwell correlation in barren sequences — A case study using onshore Duckmantian/Stephanian sequences (West Midlands, U.K.)", *Sedimentary Geology*, vol. 124, no. 1-4, pp. 197-220.

Penniston-Dorland, S.C., Wing, B.A., Nex, P.A., Kinnaird, J.A., Farquhar, J., Brown, M. & Sharman, E.R. 2008, "Multiple sulfur isotopes reveal a magmatic origin for the Platreef platinum group element deposit, Bushveld Complex, South Africa", *Geology*, vol. 36, no. 12, pp. 979-982.

Phinney, W. 1972, "Duluth Complex, history and nomenclature", *Geology of Minnesota: A Continental Volume. Minneapolis: Minnesota Geological Survey,* , pp. 333-334.

Polat, A., Appel, P.W.U., Frei, R., Pan, Y., Dilek, Y., Ordóñez-Calderón, J.C., Fryer, B., Hollis, J.A., Raith, J.G. 2007, "Field and geochemical characteristics of the Mesoarchean (~3075 Ma) Ivisaartoq greenstone belt, southern West Greenland: Evidence for seafloor hydrothermal alteration in supra-subduction oceanic crust", *Gondwana Research*, vol. 11, no. 1, pp. 69-91.

Potts, P.J. 1987, *A handbook of silicate rock analysis*, Blackie Glasgow; London.

Pronost, J., Harris, C. & Pin, C. 2008, "Relationship between footwall composition, crustal contamination, and fluid–rock interaction in the Platreef, Bushveld Complex, South Africa", *Mineralium Deposita*, vol. 43, no. 8, pp. 825-848.

Putnis, A. & Austrheim, H. 2010, "Fluid-induced processes: metasomatism and metamorphism", *Geofluids*, vol. 10, no. 1-2, pp. 254-269.

Ragno, G., Luca, M.D. & Ioele, G. 2007, "An application of cluster analysis and multivariate classification methods to spring water monitoring data", *Microchemical Journal*, vol. 87, no. 2, pp. 119-127.

Ramkumar, M. & Sathish, G. 2006, "Integrated sequence and chemostratigraphic modelling: A sure-fire technique for stratigraphic correlation, petroleum exploration and reservoir characterization", *Mineral Exploration: Recent Strategies. New India Publishers,* , pp. 21-40.

Ramkumar, M., Stüben, D. & Berner, Z. 2011, "Barremian–Danian chemostratigraphic sequences of the Cauvery Basin, India: Implications on scales of stratigraphic correlation", *Gondwana Research*, vol. 19, no. 1, pp. 291-309.

Reátegui, K., Martínez, M., Esteves, I., Gutiérrez, J.V., Martínez, A., Meléndez, W. & Urbani, F. 2005, "Geochemistry of the Mirador Formation (Late Eocene-Early

Oligocene), southwestern Venezuela: Chemostratigraphic constraints on provenance and the influence of the sea level", *Geochem J*, vol. 39, no. 3, pp. 213-226.

Reisberg, L., Tredoux, M., Harris, C., Coftier, A. & Chaumba, J. 2011, "Re and Os distribution and Os isotope composition of the Platreef at the Sandsloot–Mogolakwena mine, Bushveld complex, South Africa", *Chemical Geology*, vol. 281, no. 3, pp. 352-363.

Roelofse, F. & Ashwal, L.D. 2012, "The Lower Main Zone in the Northern Limb of the Bushveld Complex—a> 1· 3 km thick sequence of intruded and variably contaminated crystal mushes", *Journal of Petrology*, vol. 53, no. 7, pp. 1449-1476.

Roelofse, F. & Ashwal, L.D. 2008, "Symplectitic augite from the Platreef–textural evidence for fluid/rock interaction in the Northern Sector of the Northern Limb of the Bushveld Complex?", *South African Journal of Geology*, vol. 111, no. 1, pp. 21-26.

Roelofse, F., Ashwal, L.D., Pineda-Vargas, C. & Przybylowicz, W. 2009, "Enigmatic textures developed along plagioclase-augite grain boundaries at the base of the Main Zone, Northern Limb, Bushveld Complex–evidence for late stage melt infiltration into a nearly solidified crystal mush", *South African Journal of Geology*, vol. 112, no. 1, pp. 39-46.

Ridley, W.I. 2012, "Petrology of associated igneous rocks in volcanogenic massive sulfide occurrence model", U.S. Geological Survey Scientific Investigations Report 2010 - 5070 - C, chap. 15, pp. 32. [Online] Available at: <http://pubs.usgs.gov/sir/2010/5070/c/Chapter15SIR10-5070-C-3.pdf> [Accessed 13 April 2013].

Rollinson, H.R. 1993, "Using geochemical data: Evaluation, presentation and interpretation", John Wiley and Sons, New York, pp. 352.

Saunders, A.D. & Tarney, J. 1984, "Geochemical characteristics of basaltic volcanism within back-arc basins", *Geological Society, London, Special Publications*, vol. 16, no. 1, pp. 59-76.

Scoates, J.S., Wall, C.J., Friedman, R.M. & Chamberlain, K.R. 2011, "Revisiting the age of the Merensky Reef, Bushveld Complex", *Abstract, Goldschmidt Conference 2011*.

Scoates, J.S. & Friedman, R.M. 2008, "Precise age of the platiniferous Merensky Reef, Bushveld Complex, South Africa, by the U-Pb zircon chemical abrasion ID-TIMS technique", *Economic Geology*, vol. 103, no. 3, pp. 465-471.

Sharman-Harris, E., Kinnaird, J., Harris, C. & Horstmann, U. 2005, "A new look at sulphide mineralisation of the northern limb, Bushveld Complex: a stable isotope study", *Applied Earth Science: Transactions of the Institutions of Mining and Metallurgy: Section B*, vol. 114, no. 4, pp. 252-263.

South African Committee for Stratigraphy (SACS), (1980). Stratigraphy of South Africa. Part 1 (Comp. L. E. Kent). Lithostratigraphy of the Republics of South Africa, South West Africa / Namibia, and the Republics of Bophuthatswana, Transkei and Venda. *Geological Survey of South Africa*, Handbook 8, pp. 690.

Stahl, K. & Demuth, S. 1999, "Methods for regional classification of streamflow drought series: Cluster analysis", *Univ. of Freiburg, Freiburg, Germany*, .

Sun, S. & McDonough, W. 1989, "Chemical and isotopic systematics of oceanic basalts: implications for mantle composition and processes", *Geological Society, London, Special Publications*, vol. 42, no. 1, pp. 313-345.

Taylor, S.R. & McLennan, S.M. 1985, "The continental crust: its composition and evolution", .

Templ, M., Filzmoser, P. & Reimann, C. 2008, "Cluster analysis applied to regional geochemical data: problems and possibilities", *Applied Geochemistry*, vol. 23, no. 8, pp. 2198-2213.

Thompson, R. 1982, "Magmatism of the British Tertiary volcanic province", *Scottish Journal of Geology*, vol. 18, no. 1, pp. 49-107.

Thompson, R., Morrison, M., Dickin, A. & Hendry, G. 1983, "Continental flood basalts... arachnids rule OK", *Continental Basalts and Mantle Xenoliths CJ Hawkesworth, MJ Norry*, , pp. 158-185.

Truter, F. 1947, "A remarkable transcurrent fault near Potgietersrust, Transvaal", *Trans Geol Soc S Afr*, vol. 50, pp. 1-15.

Tukey, J.W. 1977, "Exploratory data analysis", .

Uken, R. & Watkeys, M.K. 1997, "Diapirism initiated by the Bushveld complex, South Africa", *Geology*, vol. 25, no. 8, pp. 723-726.

Urqueta, E., Kyser, T.K., Clark, A.H., Stanley, C.R. & Oates, C.J. 2009, "Lithogeochemistry of the Collahuasi porphyry Cu–Mo and epithermal Cu–Ag (–Au) cluster, northern Chile: Pearce element ratio vectors to ore", *Geochemistry: Exploration, Environment, Analysis*, vol. 9, no. 1, pp. 9-17.

Utami, P., Browne, P.R.L., Simmons, S.F., Suroto. 2006, "Mass transfer during hydrothermal alteration at the Lahendong geothermal system, North Sulawesi", *Proceedings 28th, New Zealand, geothermal workshop*.

Van der Merwe, F., Viljoen, F. & Knoper, M. 2012, "The mineralogy and mineral associations of platinum group elements and gold in the Platreef at Zwartfontein, Akanani Project, Northern Bushveld Complex, South Africa", *Mineralogy & Petrology*, vol. 106, no. 1, pp. 25-38.

Van der Merwe, M. 2008, "The geology and structure of the Rustenburg Layered Suite in the Potgietersrus/Mokopane area of the Bushveld Complex, South Africa", *Mineralium Deposita*, vol. 43, no. 4, pp. 405-419.

Van der Merwe, M. 1998, "Platiniferous horizons of the Potgietersrus lobe of the Bushveld Complex", *8th internaional platinum symposium. S Afr Inst Min Metall Symposium Series S*, pp. 407.

Van der Merwe, M. 1978, *The geology of the basic and ultramafic rocks of the Potgietersrus limb of the Bushveld Complex*, .

Van der Merwe, M. 1976, "The layered sequence of the Potgietersrus limb of the Bushveld Complex", *Economic Geology*, vol. 71, no. 7, pp. 1337-1351.

Van Rooyen, D. 1954, "Die geologie van ‘n gedeelte van gebied 7 (Potgietersrus)", *Report. Geological Survey of South Africa, Pretoria*, .

Von Gruenewaldt, G., Hulbert, L.J. & Naldrett, A.J. 1989, "Contrasting platinum-group element concentration patterns in cumulates of the Bushveld Complex", *Mineralium Deposita*, vol. 24, no. 3, pp. 219-229.

Wagner, P.A. 1929, The platinum deposits and mines of South Africa, Oliver and Boyd, Edinburgh, pp. 326.

Walraven, F., Armstrong, R. & Kruger, F. 1990, "A chronostratigraphic framework for the north-central Kaapvaal craton, the Bushveld Complex and the Vredefort structure", *Tectonophysics*, vol. 171, no. 1, pp. 23-48.

Ward Jr, J.H. 1963, "Hierarchical grouping to optimize an objective function", *Journal of the American statistical association*, vol. 58, no. 301, pp. 236-244.

Wenzel, T., Baumgartner, L.P., Brügmann, G.E., Konnikov, E.G. & Kislov, E.V. 2002, "Partial melting and assimilation of dolomitic xenoliths by mafic magma: the Ioko-Dovyren intrusion (North Baikal Region, Russia)", *Journal of Petrology*, vol. 43, no. 11, pp. 2049-2074.

White, J. 1994, "The Potgietersrus Prospect, geology and exploration history", *Proceedings XVth CMMI Congress*, pp. 173.

Wikipedia contributors, "Metasomatism," *Wikipedia, The Free Encyclopedia*, http://en.wikipedia.org/w/index.php?title=Metasomatism&oldid=613859865 (accessed April 14, 2014).

Wilhelm, H., Zhang, H., Chen, F., Elsenbroek, J., Lombard, M. & De Bruin, D. 1997, "Geochemical exploration for platinum-group elements in the Bushveld Complex, South Africa", *Mineralium Deposita*, vol. 32, no. 4, pp. 349-361.

Wills, A., Lentz, D. & Roy, G. 2006, "Chemostratigraphy at the Brunswick No. 6 volcanic-sediment-hosted massive sulfide deposit, New Brunswick: Resolving geometry from drill core in deformed felsic volcanic rocks", *Exploration and Mining Geology*, vol. 15, no. 3-4, pp. 35-51.

Wood, D.A., Joron, J. & Treuil, M. 1979, "A re-appraisal of the use of trace elements to classify and discriminate between magma series erupted in different tectonic settings", *Earth and Planetary Science Letters*, vol. 45, no. 2, pp. 326-336.

Xu, Y. 2002, "Evidence for crustal components in the mantle and constraints on crustal recycling mechanisms: pyroxenite xenoliths from Hannuoba, North China", *Chemical Geology*, vol. 182, no. 2, pp. 301-322.

Yudovskaya, M.A. & Kinnaird, J.A. 2010, "Chromite in the Platreef (Bushveld Complex, South Africa): occurrence and evolution of its chemical composition", *Mineralium Deposita*, vol. 45, no. 4, pp. 369-391.

Zharikov, V.A., Pertsev, N.N., Rusinov, V.L., Callegari, E., Fettes, D.J. 2009, "Metasomatism and metasomatic rocks", British Geological Survey, Natural Environment Research Council. [Online] Available at: <http://www.bgs.ac.uk /scmr/docs/papers/paper_9.pdf>[Accessed 20 October 2012].

APPENDIX I

Modal composition for selected rock samples in the studied boreholes (i.e. estimated volume percentage; vol. %)

Sample ID	Rock subtypes	Opx	Cpx	Plag
OY482-3	Upper Platreef	75	10	15
OY482-4	Upper Platreef	75	15	10
OY482-17	Serp. Pyx	55	30	15
OY482-18	Upper Platreef	80	15	5
OY482-27	Middle Platreef	90	5	5
OY482-29	Middle Platreef	70	25	5
OY482-30	Middle Platreef	75	20	5
OY482-31	Middle Platreef	80	15	5
OY482-32	Middle Platreef	75	15	10
OY482-33	Middle Platreef	85	10	5
OY482-34	Middle Platreef	70	20	10
OY482-35	Middle Platreef	80	15	5
OY482-38	Lower Platreef	90	5	5
OY482-39	Lower Platreef	95	2	3
OY482-40	Lower Platreef	95	2	3
OY482-42	Lower Platreef	95	3	2

Cpx: clinopyroxene; Opx: orthopyroxene; Plag: plagioclase. Accessory minerals were not considered.

Sample ID	Rock subtypes	Ol	Plag	Cpx	Acc
SS330-1	CP III	0	39	54	7
SS330-2	CP II	0	6	60	34
SS330-3	CP I	0	2	87	11
SS330-4	CP III	0	37	59	4
SS330-8	CP I	0	0	50	50
SS330-9	CP I	0	3	93	4
SS330-13	OCP III	54	10	30	6
SS330-14	OCP III	30	15	50	5
SS330-16	CP I	0	2	93	5
SS330-18	CP III	0	38	55	7
SS330-24	CP I	0	0	75	25
SS330-26	CP II	0	4	92	4
SS330-31	CP I	0	0	92	8
SS330-34	OCP III	49	15	30	6
SS330-35	CP I	0	0	93	7
SS330-37	OCP III	40	49	10	1
SS330-42	CP I	0	0	91	9
SS330-46	CP II	0	7	82	11
SS330-47	OCP I	45	0	53	2
SS330-51	OCP III	29	10	55	6
SS330-52	OCP I	88	0	5	7
SS330-57	OCP I	80	0	10	10
SS330-58	OCP III	20	5	69	6
SS330-59	CP III	0	29	59	12
SS330-61	OCP II	29	0	64	7
SS330-62	OCP II	16	0	79	5
SS330-63	OCP II	19	0	76	5
SS330-64	CP III	0	29	64	7
SS330-65	OCP II	10	5	79	6
SS330-66	CP III	0	24	69	7
SS330-68	OCP III	20	15	59	6
SS330-69	OCP II	25	5	55	15
SS330-70	CP I	0	0	30	70
SS330-71	CP II	0	5	58	37
SS330-72	CP II	0	8	75	17
SS330-76	CP III	0	20	54	26
SS330-78	CP III	0	25	50	25
SS330-83	OCP II	10	0	43	47

CP I, CP II and CP III denote weakly, moderately and feldspathic rich moderately metasomatised clinopyroxenites.
OCP I, OCP II and OCP III denote weakly, moderately and highly metasomatised/ altered olivine clinopyroxenites.
Acc: accessory; Cpx: clinopyroxene; Ol: olivine; Plag: plagioclase (sericitised).
The accessory minerals consist of biotite, spinel, sulphide, calcite, oxides, etc…

APPENDIX II

Whole rock geochemical data for the studied boreholes

Borehole Sample #	SS330-1	SS330-2	SS330-3	SS330-4	SS330-5	SS330-7	SS330-8	SS330-9	SS330-10	SS330-11	SS330-12	SS330-13	SS330-14
Lithology	CP III	CP II	CP I	CP III	CP I	OCP II	CP I	CP I	CP I	OCP II	CP I	OCP III	OCP III
SiO_2	45.21	42.71	45.17	52.59	45.44	37.81	51.98	45.03	41.96	34.43	44.61	39.14	39.94
Al_2O_3	14.85	6.34	6.57	11.09	3.23	9.68	0.13	4.15	6.01	8.85	5.32	7.54	3.84
Fe_2O_3	8.04	10.56	6.96	7.86	11.60	9.18	1.11	9.33	10.31	9.24	7.71	12.08	8.89
MnO	0.14	0.35	0.23	0.14	0.27	0.49	0.49	0.31	0.27	0.45	0.23	0.28	0.38
MgO	6.84	24.39	14.41	10.21	15.90	26.22	18.30	14.87	15.81	28.79	14.41	26.62	29.11
CaO	17.63	14.72	22.58	14.70	20.81	10.86	27.13	23.98	22.72	9.94	25.60	9.00	10.57
Na_2O	1.42	0.60	0.67	3.05	0.63	0.23	0.53	0.73	1.07	0.24	0.77	0.45	0.43
K_2O	2.07	<0.01	0.03	0.06	<0.01	<0.01	<0.01	<0.01	<0.01	0.03	<0.01	0.21	0.18
P_2O_5	0.02	0.02	0.02	0.02	0.02	0.02	0.06	0.01	0.03	0.02	0.02	0.02	0.02
TiO_2	0.29	0.20	0.45	0.22	0.29	0.14	0.04	0.32	0.28	0.28	0.24	0.21	0.42
SO_3	0.20	0.14	0.11	0.02	0.17	0.01	0.07	0.11	0.36	0.04	0.12	0.04	0.27
LOI	3.27	0.02	2.79	0.04	1.69	5.37	0.20	1.20	1.19	7.66	0.99	4.39	5.94
As	21.25	15.21	11.08	17.26	16.17	3.00	11.51	13.08	27.79	2.83	22.82	9.22	<0.01
Ba	609.57	47.11	112.68	57.48	55.17	36.72	45.11	55.52	36.96	68.25	62.27	83.89	66.88
Ce	7.74	94.20	26.06	64.89	88.79	63.91	0.06	90.03	105.15	109.66	39.05	124.75	66.23
Co	73.14	79.17	37.97	32.66	92.25	33.48	6.93	51.65	110.02	37.52	42.53	65.19	47.10
Cu	731.12	606.81	448.59	57.92	310.63	71.93	38.39	396.83	1241.10	93.56	413.04	124.86	491.80
Nb	13.59	7.40	13.57	11.06	9.19	9.74	14.06	7.33	5.29	11.75	7.56	10.88	12.36
Ni	783.42	1075.22	1040.47	188.53	894.98	234.51	137.57	1029.42	4623.34	635.04	1325.91	629.25	1524.10
Pb	17.14	11.42	12.32	4.39	41.37	2.43	0.07	7.28	31.41	0.07	7.75	4.49	9.77
Rb	130.09	2.04	5.31	7.96	0.66	2.53	2.14	3.67	5.45	10.26	1.65	17.03	34.36
Sr	142.99	6.84	12.56	33.88	12.51	1.94	4.06	12.52	7.75	34.76	6.52	62.51	11.51
V	187.16	196.37	114.90	170.47	245.85	25.97	11.35	226.95	152.12	44.15	177.41	70.61	53.03
Y	0.08	15.78	0.51	3.83	12.44	0.28	0.08	13.49	9.11	2.67	8.37	2.18	2.29
Zn	60.92	85.73	69.32	46.83	115.43	60.14	36.77	57.03	90.39	97.71	50.70	77.41	40.97
Zr	30.60	18.01	63.51	15.29	7.43	25.67	10.76	17.92	19.80	50.92	9.04	33.73	133.06
Mo	4.29	3.35	7.51	1.98	1.91	1.18	2.47	3.91	8.38	1.56	9.41	0.81	1.25
U	<0.01	<0.01	<0.01	<0.01	<0.01	<0.01	0.52	<0.01	<0.01	<0.01	<0.01	<0.01	0.00
Th	32.08	0.20	0.20	0.20	0.20	0.20	0.20	0.20	0.20	0.20	0.20	0.20	0.20
Au	0.12	0.07	0.12	n.d	0.09	n.d	0.05	0.09	0.30	0.05	0.15	0.05	n.d
Pd	0.57	0.82	0.73	n.d	0.65	n.d	0.05	0.93	2.17	0.05	1.05	0.09	n.d
Pt	0.22	0.53	0.72	n.d	0.65	n.d	0.05	0.77	2.12	0.05	1.01	0.13	n.d

CP I, CP II and CP III denote weakly, moderately and feldspathic rich moderately metasomatised clinopyroxenites.
OCP I, OCP II and OCP III denote weakly, moderately and highly metasomatised/ altered olivine clinopyroxenites.
*n.d: not determined; sample # annotated with A & B are original and duplicate.

Borehole Sample #	SS330-15	SS330-16	SS330-17	SS330-18	SS330-19	SS330-20	SS330-24	SS330-25	SS330-26	SS330-27	SS330-28	SS330-29	SS330-30A
Lithology	OCP I	CP I	OCP II	CP III	OCP I	CP I	CP I	CP I	CP II	CP I	CP II	CP II	CP I
SiO_2	40.53	40.69	39.64	47.78	32.44	40.82	34.25	43.33	38.98	39.01	42.32	33.04	36.92
Al_2O_3	1.33	5.96	2.04	9.81	11.58	5.90	3.20	4.13	3.87	0.48	6.29	3.36	3.46
Fe_2O_3	4.41	11.16	5.74	8.03	4.53	10.27	6.99	9.93	18.43	13.46	6.53	26.22	4.23
MnO	0.80	0.19	0.53	0.19	1.07	0.21	0.26	0.46	0.25	0.27	0.34	0.22	0.23
MgO	31.25	10.05	29.91	9.17	32.51	11.12	10.29	10.91	15.04	15.86	18.19	16.14	13.68
CaO	13.04	28.04	14.46	19.68	6.95	27.82	35.27	27.92	20.34	26.69	20.93	19.09	32.93
Na_2O	0.38	0.97	0.47	1.08	0.14	0.69	0.68	0.66	0.43	0.51	0.87	0.43	1.17
K_2O	<0.01	<0.01	<0.01	1.16	<0.01	<0.01	<0.01	<0.01	<0.01	<0.01	0.15	<0.01	<0.01
P_2O_5	0.01	0.14	0.04	0.07	0.01	0.05	0.02	0.04	0.01	0.01	0.02	0.01	0.03
TiO_2	0.07	0.47	0.31	0.31	0.05	0.41	0.11	0.64	0.32	0.05	0.44	0.04	0.18
SO_3	0.07	0.36	0.11	0.05	0.06	0.06	0.01	0.03	0.26	0.13	0.33	0.09	0.15
LOI	8.13	1.99	6.75	2.67	10.57	2.69	8.94	2.00	2.09	3.57	3.59	1.39	7.07
As	0.00	29.93	<0.01	19.55	<0.01	25.34	353.42	16.04	116.21	52.41	15.41	7.79	45.27
Ba	45.88	68.25	51.38	717.96	47.30	49.23	50.34	52.10	50.92	49.00	106.54	50.95	54.43
Ce	37.02	131.12	2.62	39.33	33.50	130.82	209.58	128.77	299.65	203.86	67.38	290.25	80.73
Co	17.70	42.75	31.96	46.99	0.03	43.31	27.78	45.94	26.68	0.03	33.80	0.03	26.62
Cu	353.88	795.82	436.25	139.26	52.06	358.93	35.65	58.91	117.70	47.03	760.13	183.20	1258.69
Nb	14.13	10.87	17.17	15.43	13.22	3.86	8.72	4.97	10.39	16.38	11.36	15.73	10.75
Ni	834.31	1381.03	1471.19	287.05	26.55	408.45	396.84	353.92	1507.58	334.66	2137.50	255.85	504.74
Pb	5.17	152.61	10.20	18.83	0.07	0.07	10.99	7.24	8.12	1.11	10.38	0.07	26.15
Rb	1.19	3.94	0.20	66.07	2.36	2.83	1.56	3.34	0.72	1.65	29.07	0.42	1.62
Sr	0.68	12.40	5.49	220.04	0.03	9.46	36.69	19.38	6.35	10.38	20.48	3.39	35.77
V	10.01	190.79	28.79	206.66	8.14	80.03	31.33	144.57	52.71	15.10	47.28	4.74	32.07
Y	11.08	7.55	12.46	0.08	3.67	9.39	82.00	7.30	11.40	3.78	3.64	1.06	5.90
Zn	160.68	121.39	29.88	56.43	60.84	49.00	93.47	222.22	182.07	78.39	478.98	48.99	73.65
Zr	3.23	41.49	46.76	25.00	3.07	48.63	26.49	60.12	34.00	5.84	59.61	0.85	21.79
Mo	0.09	13.14	2.42	7.58	0.02	5.32	2.39	5.92	2.34	1.32	8.07	0.02	2.80
U	<0.01	<0.01	<0.01	<0.01	<0.01	<0.01	<0.01	<0.01	<0.01	<0.01	<0.01	<0.01	<0.01
Th	0.20	0.20	0.20	52.47	0.20	0.20	0.20	0.20	0.20	0.20	0.20	0.20	0.20
Au	n.d	0.18	n.d	n.d	n.d	n.d	n.d	n.d	n.d	0.14	n.d	0.05	n.d
Pd	n.d	2.53	n.d	n.d	n.d	n.d	n.d	n.d	n.d	0.75	n.d	0.16	n.d
Pt	n.d	4.00	n.d	n.d	n.d	n.d	n.d	n.d	n.d	0.67	n.d	0.14	n.d

CP I, CP II and CP III denote weakly, moderately and feldspathic rich moderately metasomatised clinopyroxenites.
OCP I, OCP II and OCP III denote weakly, moderately and highly metasomatised/ altered olivine clinopyroxenites.
*n.d: not determined; sample # annotated with A & B are original and duplicate.

Borehole Sample #	SS330-30B	SS330-31	SS330-32	SS330-33	SS330-34	SS330-35	SS330-36	SS330-37	SS330-38	SS330-39	SS330-40A	SS330-40B	SS330-41
Lithology	CP I	CP I	CP I	OCP III	OCP III	CP I	OCP III	OCP III	OCP I	CP I	CP II	CP II	OCP I
SiO_2	36.84	41.91	39.16	39.76	40.38	45.10	41.70	38.48	39.81	45.29	41.99	41.98	36.81
Al_2O_3	3.43	2.80	3.59	6.93	6.79	3.37	4.27	4.46	4.24	3.99	4.93	4.91	3.01
Fe_2O_3	4.19	11.10	4.50	7.13	6.24	10.58	9.76	9.60	4.00	9.03	4.88	4.87	5.42
MnO	0.23	0.33	0.24	0.31	0.35	0.21	0.39	0.29	0.43	0.25	0.34	0.34	0.42
MgO	13.63	12.62	14.57	30.42	27.22	12.91	27.70	31.23	30.25	15.89	24.26	24.26	33.41
CaO	32.82	27.73	35.05	8.58	12.38	24.39	10.28	7.61	10.29	22.97	17.48	17.42	9.77
Na_2O	1.17	1.33	1.25	0.40	0.43	0.78	0.35	0.25	0.21	0.74	0.38	0.37	0.19
K_2O	<0.01	<0.01	<0.01	0.47	0.31	<0.01	0.25	0.31	<0.01	<0.01	0.11	0.11	<0.01
P_2O_5	0.03	0.01	0.03	0.02	0.02	0.05	0.02	0.01	0.01	0.02	0.02	0.02	0.01
TiO_2	0.18	0.47	0.19	0.15	0.21	0.65	0.20	0.16	0.11	0.54	0.29	0.29	0.05
SO_3	0.15	0.24	0.16	0.07	0.10	0.19	0.01	0.04	0.01	0.02	0.04	0.04	<0.01
LOI	7.07	1.50	1.30	5.75	5.58	1.79	5.08	7.57	10.66	1.29	5.28	5.28	10.89
As	41.91	26.25	18.74	1.94	11.07	5.98	4.57	<0.01	13.88	4.58	9.70	11.90	<0.01
Ba	51.21	77.04	50.42	90.56	104.31	63.39	66.53	111.88	47.98	69.01	91.35	76.50	48.18
Ce	88.56	163.44	146.05	38.19	35.00	147.10	101.75	93.71	15.51	83.15	13.86	0.11	45.11
Co	27.74	71.97	39.35	30.42	41.60	50.14	36.58	42.82	4.91	51.19	20.31	30.33	4.53
Cu	1258.15	1531.61	260.31	287.97	245.49	368.07	31.30	81.59	31.84	225.99	20.78	19.55	8.90
Nb	8.51	7.27	3.22	12.24	11.50	7.79	10.13	11.02	12.67	9.50	12.30	13.66	12.33
Ni	510.49	720.49	327.34	453.19	1148.54	581.85	309.73	833.26	56.45	360.11	361.62	361.69	91.00
Pb	26.86	14.30	4.07	5.30	0.07	3.85	1.33	4.00	2.23	1.04	11.52	12.59	2.27
Rb	1.74	1.38	1.88	28.33	17.97	1.87	10.87	12.99	2.82	2.21	11.19	10.58	1.20
Sr	35.85	13.48	12.52	134.96	66.90	13.72	22.53	120.09	6.48	21.72	17.45	20.63	5.60
V	12.40	135.52	164.17	26.70	35.75	114.32	57.21	34.05	9.95	99.35	64.82	48.59	4.38
Y	2.88	9.52	8.68	5.94	5.64	7.43	2.55	4.29	8.11	3.75	8.24	8.42	24.46
Zn	77.94	262.76	58.63	51.89	60.48	60.59	75.37	70.82	50.58	60.10	63.25	62.23	33.82
Zr	18.17	31.35	49.31	27.59	42.68	59.84	32.39	25.77	14.59	57.94	59.96	57.16	6.74
Mo	2.98	3.62	8.04	0.54	0.60	7.05	1.89	2.32	0.88	4.34	3.81	1.78	0.02
U	<0.01	<0.01	<0.01	<0.01	<0.01	<0.01	<0.01	<0.01	<0.01	<0.01	<0.01	<0.01	<0.01
Th	0.20	0.20	0.20	12.03	0.20	0.20	0.20	3.22	0.20	0.20	0.20	0.20	0.20
Au	n.d	0.09	n.d	n.d	0.16	n.d	n.d	n.d	n.d	n.d	n.d	n.d	n.d
Pd	n.d	0.96	n.d	n.d	1.96	n.d	n.d	n.d	n.d	n.d	n.d	n.d	n.d
Pt	n.d	0.86	n.d	n.d	1.66	n.d	n.d	n.d	n.d	n.d	n.d	n.d	n.d

CP I, CP II and CP III denote weakly, moderately and feldspathic rich moderately metasomatised clinopyroxenites.
OCP I, OCP II and OCP III denote weakly, moderately and highly metasomatised/ altered olivine clinopyroxenites.
*n.d: not determined; sample # annotated with A & B are original and duplicate.

Borehole Sample #	SS330-42	SS330-43	SS330-44	SS330-45	SS330-46	SS330-47	SS330-48	SS330-50A	SS330-50B	SS330-51	SS330-52	SS330-53	SS330-54
Lithology	CP I	CP II	OCP III	OCP I	CP II	OCP I	OCP II	OCP II	OCP II	OCP III	OCP I	CP II	OCP II
SiO_2	45.19	41.17	41.34	37.36	42.11	38.66	38.02	39.39	39.35	40.80	34.18	39.16	39.13
Al_2O_3	5.23	7.75	5.20	4.79	5.82	3.25	7.55	6.65	6.58	4.55	5.61	9.13	8.38
Fe_2O_3	6.66	6.26	7.96	2.60	4.44	6.98	5.38	5.95	5.94	7.87	4.26	4.82	5.96
MnO	0.26	0.36	0.41	0.77	0.79	0.59	0.69	0.79	0.79	0.56	0.52	0.62	0.48
MgO	14.58	20.80	28.94	37.28	25.04	34.84	29.20	28.99	29.03	27.75	36.90	21.11	25.26
CaO	25.04	19.84	10.52	4.29	17.03	6.18	11.41	10.23	10.21	11.50	4.72	19.13	13.85
Na_2O	0.71	0.46	0.31	0.08	0.96	0.26	0.25	0.27	0.26	0.54	0.40	0.47	0.33
K_2O	<0.01	<0.01	0.13	<0.01	0.02	<0.01	<0.01	0.05	0.05	0.46	<0.01	0.17	0.14
P_2O5	0.02	0.02	0.01	0.01	0.03	0.02	0.02	0.02	0.02	0.04	0.02	0.04	0.02
TiO_2	0.40	0.29	0.19	0.22	0.31	0.16	0.23	0.27	0.27	0.29	0.12	0.52	0.31
SO_3	0.04	<0.01	<0.01	0.02	0.49	0.13	0.02	0.01	0.02	0.20	0.33	0.03	0.07
LOI	1.89	3.07	4.98	12.59	2.99	8.95	7.27	7.37	7.37	5.44	12.95	4.78	6.08
As	14.15	4.62	<0.01	<0.01	0.75	<0.01	<0.01	<0.01	0.01	1.50	<0.01	2.82	4.10
Ba	54.78	39.27	59.87	45.07	59.07	59.49	39.10	76.91	69.60	150.19	55.51	84.32	60.04
Ce	116.41	45.66	53.87	16.29	30.78	30.46	0.06	83.61	42.84	64.80	3.09	30.00	81.69
Co	23.96	29.95	34.84	16.86	38.57	23.79	17.38	17.26	21.77	50.25	22.14	18.63	18.32
Cu	260.75	13.39	12.42	14.56	1182.49	315.63	26.83	60.10	57.84	487.02	714.27	94.38	64.97
Nb	11.33	13.35	13.63	5.51	12.74	11.45	12.08	9.21	11.62	14.93	5.22	9.85	11.72
Ni	453.84	80.62	74.92	97.55	2866.16	643.56	139.86	216.02	215.14	691.43	1816.36	632.98	326.43
Pb	0.07	0.07	0.34	0.07	6.63	0.07	2.23	3.77	1.33	2.40	4.39	1.73	7.11
Rb	2.94	2.19	5.20	6.02	2.90	2.75	1.78	8.38	8.59	21.59	7.62	12.02	22.55
Sr	16.58	12.41	52.68	2.04	10.12	9.61	10.89	98.65	95.40	118.18	17.97	27.13	16.04
V	144.39	53.05	75.99	38.26	76.86	45.63	35.64	50.20	60.35	107.47	4.61	97.46	69.55
Y	7.60	4.33	2.48	8.83	8.33	7.71	14.03	5.39	12.36	6.68	7.58	11.59	8.65
Zn	38.33	48.97	59.71	53.93	51.70	66.98	107.67	62.06	62.31	54.40	35.06	44.40	62.74
Zr	36.77	38.35	29.13	38.28	41.82	27.35	43.00	48.89	48.28	40.68	22.55	78.91	58.15
Mo	7.45	2.30	3.48	0.10	2.91	1.27	0.92	3.52	2.89	2.23	0.36	1.72	2.15
U	<0.01	<0.01	<0.01	21.43	<0.01	<0.01	<0.01	<0.01	<0.01	<0.01	25.24	<0.01	<0.01
Th	0.20	0.20	0.20	0.20	0.20	0.20	0.20	0.20	0.20	3.48	0.20	0.20	0.20
Au	n.d	n.d	n.d	n.d	1.02	0.36	n.d	n.d	n.d	n.d	0.91	n.d	n.d
Pd	n.d	n.d	n.d	n.d	12.24	2.18	n.d	n.d	n.d	n.d	8.89	n.d	n.d
Pt	n.d	n.d	n.d	n.d	12.24	2.26	n.d	n.d	n.d	n.d	11.28	n.d	n.d

CP I, CP II and CP III denote weakly, moderately and feldspathic rich moderately metasomatised clinopyroxenites.
OCP I, OCP II and OCP III denote weakly, moderately and highly metasomatised/ altered olivine clinopyroxenites.
*n.d: not determined; sample # annotated with A & B are original and duplicate.

Borehole Sample #	SS330-55	SS330-56	SS330-57	SS330-58	SS330-59	SS330-61	SS330-62	SS330-63	SS330-64	SS330-65	SS330-66	SS330-67	SS330-68
Lithology	OCP II	OCP II	OCP I	OCP III	CP III	OCP II	OCP II	OCP II	CP III	OCP II	CP III	OCP III	OCP III
SiO_2	39.08	38.34	30.88	39.14	42.51	36.58	33.07	35.90	43.55	37.00	38.85	38.14	35.92
$Al2O_3$	4.66	7.68	10.29	6.40	11.46	9.83	11.08	7.31	10.61	8.50	10.58	8.83	9.36
Fe_2O_3	6.29	6.71	4.03	7.67	14.70	8.10	8.84	8.26	8.70	7.07	11.43	7.83	12.10
MnO	0.62	0.54	0.72	0.52	0.35	0.67	0.69	0.65	0.25	0.58	0.34	0.59	0.53
MgO	30.11	27.72	34.96	27.57	17.04	29.70	30.14	30.01	16.18	27.79	14.39	27.56	25.67
CaO	11.98	12.25	4.07	12.40	10.06	11.28	6.15	9.83	15.07	11.11	18.66	9.33	7.46
Na_2O	0.33	0.29	0.07	0.32	1.16	0.30	0.25	0.41	0.77	0.32	0.94	0.27	0.26
K_2O	0.02	0.06	<0.01	0.08	0.90	0.01	0.07	<0.01	0.77	<0.01	0.15	0.36	0.46
P_2O_5	0.02	0.01	0.01	0.02	0.02	0.02	0.02	0.01	0.03	0.01	0.02	0.02	0.02
TiO_2	0.29	0.32	0.20	0.28	0.14	0.32	0.26	0.28	0.32	0.38	0.24	0.17	0.21
SO_3	0.05	0.01	0.01	0.11	0.06	0.07	0.07	0.14	0.07	0.05	0.22	0.02	0.04
LOI	6.53	6.08	14.53	5.48	1.59	3.10	9.36	7.15	3.69	7.15	4.18	6.85	7.97
As	<0.01	2.44	0.00	6.37	10.38	5.51	7.92	8.75	20.56	<0.01	25.31	<0.01	18.12
Ba	73.64	74.97	57.41	71.74	409.21	70.91	66.22	57.80	328.56	59.46	121.73	83.19	65.63
Ce	44.26	106.89	59.11	95.35	136.57	78.37	112.73	74.00	101.78	81.66	124.00	66.79	114.81
Co	17.42	28.24	5.83	47.35	94.99	25.87	38.69	26.06	44.09	19.62	79.54	30.75	59.70
Cu	144.40	22.54	11.37	76.56	75.22	141.34	53.16	435.05	170.04	195.74	889.87	74.07	127.33
Nb	12.00	10.91	10.46	14.43	14.51	10.84	9.62	13.32	16.30	12.14	8.89	14.97	11.25
Ni	358.61	39.57	110.09	188.94	756.04	722.63	651.94	954.75	544.93	748.24	2647.32	458.92	1117.18
Pb	0.07	1.71	0.68	0.07	7.58	0.07	0.19	2.06	7.64	0.07	2.85	2.34	8.63
Rb	4.25	5.16	0.05	7.98	26.53	2.78	7.30	3.46	41.46	6.01	9.28	28.81	56.83
Sr	25.05	17.90	2.48	82.50	355.60	35.30	60.36	23.56	290.85	63.10	94.09	145.08	27.58
V	42.47	79.69	16.34	124.53	50.24	63.17	63.70	59.63	94.63	99.56	89.18	55.70	90.00
Y	11.04	9.25	7.89	4.98	6.34	7.78	5.44	6.16	5.95	6.89	8.30	5.04	0.08
Zn	54.16	88.55	46.49	69.77	97.30	75.30	103.95	86.32	68.03	84.88	80.21	68.35	75.83
Zr	54.49	54.14	24.83	44.37	17.77	48.58	41.35	39.19	44.46	53.61	17.53	30.59	35.70
Mo	0.44	0.84	0.02	3.34	3.38	1.42	0.02	0.67	2.86	0.28	2.65	0.97	0.92
U	<0.01	<0.01	<0.01	<0.01	<0.01	<0.01	<0.01	<0.01	<0.01	<0.01	<0.01	<0.01	<0.01
Th	0.20	0.20	0.20	0.20	115.25	0.20	0.20	0.20	87.46	0.20	0.20	19.92	0.20
Au	n.d	n.d	n.d	0.35	n.d	n.d	n.d	0.57	0.20	0.54	2.05	n.d	n.d
Pd	n.d	n.d	n.d	0.05	n.d	n.d	n.d	6.04	1.35	6.24	30.00	n.d	n.d
Pt	n.d	n.d	n.d	0.05	n.d	n.d	n.d	4.54	1.29	7.25	30.00	n.d	n.d

CP I, CP II and CP III denote weakly, moderately and feldspathic rich moderately metasomatised clinopyroxenites.
OCP I, OCP II and OCP III denote weakly, moderately and highly metasomatised/ altered olivine clinopyroxenites.
*n.d: not determined; sample # annotated with A & B are original and duplicate.

Borehole Sample #	SS330-69	SS330-70	SS330-71	SS330-72	SS330-73	SS330-74	SS330-75	SS330-76	SS330-77	SS330-78A	SS330-78B	SS330-79	SS330-80
Lithology	OCP II	CP I	CP II	CP II	CP II	OCP I	CP I	CP III	OCP I	CP III	CP III	CP I	OCP I
SiO_2	35.25	44.65	39.51	38.78	41.58	39.78	42.30	44.43	36.20	47.62	47.66	46.41	29.51
Al_2O_3	11.85	10.35	5.06	2.39	3.11	1.78	4.81	8.12	4.29	9.21	9.15	2.95	6.61
Fe_2O_3	8.74	6.53	17.97	21.15	8.53	4.54	11.65	14.55	4.27	12.20	12.19	4.54	9.63
MnO	0.62	0.20	0.25	0.40	0.29	0.61	0.24	0.23	0.16	0.22	0.22	0.24	0.27
MgO	28.49	8.35	10.59	11.08	22.55	33.42	18.87	19.27	34.80	18.67	18.68	14.37	30.52
CaO	7.84	26.31	21.60	18.40	19.92	9.21	19.02	9.88	8.82	8.10	8.08	29.70	11.17
Na_2O	0.23	0.74	1.08	1.87	0.53	0.17	0.60	1.09	0.18	0.87	0.86	0.67	0.24
K_2O	0.10	<0.01	<0.01	<0.01	0.02	<0.01	0.03	0.67	<0.01	1.37	1.37	<0.01	<0.01
P_2O_5	0.02	0.02	0.02	0.02	0.03	0.01	0.03	0.02	0.01	0.03	0.03	0.17	0.01
TiO_2	0.26	0.31	0.42	0.39	0.28	0.16	0.28	0.17	0.04	0.17	0.17	0.24	0.16
SO_3	0.03	0.05	1.94	3.17	0.08	0.03	0.09	0.29	0.03	0.14	0.14	0.04	0.47
LOI	6.53	2.49	1.59	2.39	3.09	10.42	2.09	1.29	11.17	1.39	1.39	0.69	11.45
As	0.20	20.75	12.52	17.70	10.11	<0.01	29.24	4.57	<0.01	15.82	11.03	14.69	4.96
Ba	81.77	69.63	66.67	37.77	49.58	56.11	62.44	155.34	41.50	602.36	601.29	52.35	47.86
Ce	86.18	62.03	139.87	201.99	88.03	7.42	97.12	139.93	4.52	90.52	98.90	0.58	48.20
Co	12.47	29.25	144.06	202.69	44.27	7.97	97.61	130.97	23.77	89.24	85.45	23.47	15.95
Cu	60.84	306.71	1409.03	3123.06	183.86	11.88	363.92	843.75	68.29	621.52	622.78	211.53	108.77
Nb	11.91	15.35	18.59	21.45	13.62	12.19	11.92	9.61	11.35	20.34	19.38	6.01	10.48
Ni	28.69	422.50	2749.07	4286.82	476.58	17.84	888.73	1603.36	125.19	1292.22	1276.73	140.42	31.48
Pb	1.39	7.38	10.35	8.16	7.70	0.07	5.55	7.10	0.07	10.61	9.80	2.91	0.19
Rb	8.67	2.98	0.25	1.84	3.23	1.54	4.05	18.21	1.38	59.13	61.96	1.72	1.21
Sr	53.82	35.59	5.73	17.93	27.01	0.03	9.70	247.69	0.03	496.33	496.59	9.01	7.44
V	76.97	162.75	214.19	295.10	130.00	26.15	141.64	87.64	10.89	73.22	86.70	85.21	46.73
Y	2.30	12.98	5.22	6.99	4.37	18.61	9.79	9.36	3.01	0.08	1.90	8.42	5.94
Zn	105.07	53.75	60.36	74.21	57.55	26.99	65.12	95.86	36.44	84.02	83.27	39.68	78.35
Zr	33.75	24.38	32.68	25.19	23.48	25.52	21.68	10.06	1.51	15.30	17.26	21.97	47.09
Mo	0.82	6.42	5.77	1.17	3.07	0.02	2.14	3.70	0.28	3.26	3.19	4.45	0.04
U	<0.01	<0.01	<0.01	<0.01	<0.01	<0.01	<0.01	<0.01	<0.01	<0.01	<0.01	<0.01	<0.01
Th	0.20	0.20	0.20	0.20	0.20	0.20	0.20	41.33	0.20	188.41	190.52	0.20	0.20
Au	n.d	n.d	0.81	0.33	n.d	n.d	0.08	0.19	n.d	0.23	n.d	n.d	n.d
Pd	n.d	n.d	2.94	5.72	n.d	n.d	0.05	0.14	n.d	0.07	n.d	n.d	n.d
Pt	n.d	n.d	2.65	30.00	n.d	n.d	0.05	0.16	n.d	0.20	n.d	n.d	n.d

CP I, CP II and CP III denote weakly, moderately and feldspathic rich moderately metasomatised clinopyroxenites.
OCP I, OCP II and OCP III denote weakly, moderately and highly metasomatised/ altered olivine clinopyroxenites.
*n.d: not determined; sample # annotated with A & B are original and duplicate.

Borehole Sample #	SS330-82	SS330-83	SS330-84A	SS330-84B	SS330-86	SS330-93	SS330-94
Lithology	CP I	OCP II	CP I	CP I	M-Dol	M-Dol	M-Dol
SiO_2	43.66	33.17	40.53	40.56	0.01	0.01	0.01
Al_2O_3	6.72	8.52	6.12	6.11	<0.01	<0.01	<0.01
Fe_2O_3	7.20	9.16	8.77	8.71	0.91	<0.01	<0.01
MnO	0.21	0.32	0.26	0.25	0.06	0.26	0.37
MgO	10.10	29.30	12.43	12.42	27.68	29.40	28.71
CaO	29.91	12.48	28.03	27.92	35.15	34.65	35.62
Na_2O	0.73	0.26	0.74	0.74	0.62	0.62	0.64
K_2O	<0.01	<0.01	<0.01	<0.01	<0.01	<0.01	<0.01
P_2O_5	0.03	0.02	0.04	0.04	0.01	0.01	0.01
TiO_2	0.45	0.19	0.63	0.63	0.01	0.01	0.01
SO_3	0.12	0.04	0.07	0.07	0.10	<0.01	<0.01
LOI	0.90	6.57	2.39	2.39	36.48	38.50	37.95
As	12.73	1.48	24.34	30.71	104.20	94.49	101.15
Ba	66.65	53.92	42.87	69.95	50.71	56.19	54.69
Ce	99.08	68.18	161.34	151.23	85.61	92.79	43.03
Co	32.04	11.12	16.38	10.38	0.86	0.03	2.26
Cu	132.31	25.28	330.05	331.82	35.84	27.23	28.85
Nb	4.23	10.29	7.63	13.37	10.28	8.53	9.47
Ni	395.19	68.82	75.02	79.14	45.32	7.70	2.93
Pb	4.74	3.60	8.73	9.18	0.07	7.71	1.07
Rb	4.79	1.32	4.74	5.21	1.98	3.93	2.19
Sr	8.30	1.94	10.24	10.40	19.04	31.88	28.69
V	145.17	65.78	49.61	69.88	0.57	0.57	0.57
Y	12.04	1.91	15.04	13.77	1.30	0.30	1.08
Zn	38.15	48.86	50.56	47.94	34.66	20.70	21.60
Zr	38.88	29.46	107.45	106.50	1.87	3.22	5.40
Mo	8.36	0.31	4.78	3.11	0.02	0.02	0.02
U	2.51	<0.01	<0.01	<0.01	<0.01	<0.01	<0.01
Th	0.20	0.20	0.20	0.20	0.20	0.20	0.20
Au	n.d	n.d	0.05	n.d	n.d	n.d	n.d
Pd	n.d	n.d	0.05	n.d	n.d	n.d	n.d
Pt	n.d	n.d	0.05	n.d	n.d	n.d	n.d

CP I, CP II and CP III denote weakly, moderately and feldspathic rich moderately metasomatised clinopyroxenites.
OCP I, OCP II and OCP III denote weakly, moderately and highly metasomatised/ altered olivine clinopyroxenites.
M-Dol: metadolomites.
*n.d: not determined; sample # annotated with A & B are original and duplicate.

Borehole Sample #	OY482-1	OY482-2	OY482-3	OY482-4	OY482-6A	OY482-6B	OY482-7	OY482-8	OY482-9	OY482-10	OY482-11A	OY482-11B	OY482-12
Lithology	GN	GN	UP	UP	GN	GN	GN	GN	GN	GN	GN	GN	GN
SiO_2	48.44	48.98	49.35	49.68	49.31	49.32	50.77	47.87	48.95	50.05	49.22	49.13	50.22
Al_2O_3	15.96	18.24	8.13	11.08	13.56	13.58	13.87	13.07	15.30	15.51	12.13	12.16	13.63
Fe_2O_3	6.12	5.43	14.07	11.31	7.70	7.71	10.00	8.88	6.68	8.46	8.60	8.58	9.04
MnO	0.11	0.11	0.20	0.17	0.12	0.13	0.15	0.13	0.11	0.14	0.14	0.14	0.15
MgO	9.77	10.22	18.52	16.25	13.19	13.18	9.04	13.73	11.38	9.56	14.97	15.09	10.02
CaO	13.76	12.42	6.93	8.95	10.87	10.87	11.77	10.84	12.94	13.34	10.83	10.76	12.18
Na_2O	1.63	1.89	1.01	1.08	1.42	1.39	2.21	1.35	1.46	1.84	1.08	1.09	1.88
K_2O	0.44	0.36	0.07	0.11	0.45	0.45	0.19	0.31	0.51	0.31	0.48	0.47	0.46
P_2O_5	0.02	0.02	0.02	0.02	0.02	0.02	0.03	0.02	0.02	0.01	0.02	0.02	0.03
TiO_2	0.15	0.12	0.21	0.16	0.14	0.14	0.24	0.15	0.13	0.16	0.15	0.15	0.23
SO_3	0.00	0.01	0.12	0.01	0.04	0.04	0.03	0.01	0.01	0.02	<0.01	<0.01	0.09
LOI	3.58	2.20	1.38	1.20	3.19	3.19	1.70	3.62	2.51	0.60	2.40	2.40	2.09
As	6.20	4.94	6.10	2.48	0.56	7.28	5.03	16.49	3.24	5.61	10.95	3.48	4.32
Ba	133.15	128.33	75.94	86.74	127.27	125.41	104.63	115.17	139.38	114.55	126.10	130.68	139.44
Ce	41.62	6.69	169.20	52.26	27.48	57.15	56.12	51.61	62.25	31.60	73.42	89.18	65.03
Co	38.49	30.59	101.93	76.60	54.23	52.03	57.31	43.14	44.31	53.90	57.86	52.79	48.64
Cu	28.25	44.85	292.04	45.47	182.11	181.60	100.57	50.77	38.12	113.43	28.40	26.52	363.48
Nb	14.62	14.87	13.12	13.04	15.72	17.33	14.84	12.41	15.19	13.70	16.87	15.84	15.04
Ni	188.65	168.61	863.87	442.41	506.25	503.41	242.90	310.01	286.91	292.95	366.94	371.79	385.46
Pb	0.58	12.17	0.30	1.30	5.14	4.96	2.27	5.14	4.84	4.74	1.73	3.76	18.58
Rb	24.46	20.90	3.55	5.29	23.06	22.73	6.95	16.66	26.30	13.78	23.94	25.12	20.36
Sr	271.63	273.30	87.39	136.38	252.68	248.00	220.70	255.00	249.03	205.58	226.55	226.34	238.84
V	83.85	49.22	125.23	105.00	63.35	78.65	114.72	68.07	64.60	102.17	85.61	88.22	119.02
Y	7.22	5.84	10.00	0.34	5.29	5.44	8.88	6.23	4.77	4.19	6.55	3.54	6.45
Zn	47.39	58.41	102.18	77.74	59.55	58.32	85.37	66.63	62.98	91.87	64.27	61.51	84.62
Zr	16.01	10.90	27.18	13.90	11.81	11.05	18.99	12.00	11.30	9.94	14.24	11.60	19.04
Mo	0.41	3.59	2.81	1.29	0.49	1.69	4.53	0.36	4.03	2.64	1.04	0.96	3.68
U	0.39	0.39	0.39	0.39	0.39	0.39	0.39	0.39	0.39	0.39	0.39	0.39	0.39
Th	75.37	80.23	0.23	8.84	72.01	67.12	49.53	67.78	67.29	42.90	60.12	55.60	60.54
Au	n.d	n.d	0.08	n.d	n.d	n.d	n.d	n.d	n.d	n.d	n.d	n.d	n.d
Pd	n.d	n.d	0.93	n.d	n.d	n.d	n.d	n.d	n.d	n.d	n.d	n.d	n.d
Pt	n.d	n.d	0.46	n.d	n.d	n.d	n.d	n.d	n.d	n.d	n.d	n.d	n.d

GN: Gabbronorites; UP: Upper Platreef; MP: Middle Platreef; LP: Lower Platreef; Serp-Pyx: Serpentinised pyroxenite.
*n.d: not determined; sample # annotated with A & B are original and duplicate.

Borehole Sample #	OY482-13	OY482-14	OY482-15A	OY482-15B	OY482-16	OY482-17	OY482-18	OY482-19	OY482-20	OY482-21	OY482-22	OY482-23	OY482-24
Lithology	GN	GN	GN	GN	GN	Serp-Pyx	UP	GN	GN	GN	GN	GN	GN
SiO_2	54.13	51.70	49.51	49.52	56.02	38.59	47.05	49.29	49.07	54.50	49.20	53.86	49.79
Al_2O_3	9.97	12.57	13.77	13.80	12.48	6.13	10.28	17.36	13.43	11.62	14.47	11.11	13.82
Fe_2O_3	9.69	10.92	7.64	7.59	7.43	14.87	12.47	6.37	10.85	7.80	6.77	8.47	9.62
MnO	0.17	0.13	0.11	0.12	0.16	0.21	0.16	0.11	0.16	0.12	0.11	0.13	0.15
MgO	11.88	8.02	11.65	11.67	10.19	22.54	16.53	8.72	10.23	9.45	10.29	9.99	9.77
CaO	8.63	10.06	10.88	10.84	8.97	7.95	8.11	12.06	11.06	11.97	13.52	11.40	12.00
Na_2O	2.26	3.58	1.59	1.60	2.55	0.29	1.87	1.79	2.32	1.75	1.99	1.63	2.15
K_2O	0.15	0.30	0.53	0.53	0.32	0.02	0.27	1.00	0.37	0.05	0.62	0.12	0.39
P_2O_5	0.03	0.02	0.02	0.02	0.02	0.01	0.02	0.02	0.02	0.03	0.02	0.02	0.02
TiO_2	0.17	0.17	0.15	0.15	0.14	0.12	0.17	0.11	0.20	0.15	0.16	0.15	0.21
SO_3	0.04	1.02	0.02	0.02	0.03	0.18	0.63	0.01	0.19	0.03	0.15	0.02	0.19
LOI	2.90	1.50	4.12	4.12	1.70	9.13	2.51	3.15	2.11	2.52	2.69	3.10	1.89
As	11.34	2.45	2.50	12.37	0.56	36.67	3.09	4.68	2.25	3.71	11.08	0.56	3.94
Ba	74.83	103.23	145.00	146.42	126.03	57.01	99.33	232.89	140.89	76.68	164.48	82.97	140.19
Ce	72.88	80.86	82.24	32.86	63.98	151.75	115.88	6.69	63.50	41.06	41.58	70.47	72.88
Co	61.44	145.95	38.57	45.05	43.00	110.03	142.00	39.13	75.54	42.30	81.91	38.11	68.37
Cu	94.42	2348.10	72.58	75.53	131.92	208.93	1788.53	74.23	565.73	91.75	605.11	120.47	507.68
Nb	17.65	12.54	18.24	15.76	16.27	12.43	12.09	15.98	15.80	15.39	13.16	15.38	15.46
Ni	305.51	3024.22	314.16	312.26	269.92	1416.07	4627.71	264.28	988.08	279.68	1223.58	280.76	920.47
Pb	4.37	11.51	8.19	5.36	9.38	6.19	5.47	3.71	5.43	8.79	6.99	7.18	5.82
Rb	8.10	13.13	27.95	29.14	12.41	2.46	15.88	39.28	16.10	2.87	36.15	7.91	18.27
Sr	183.92	186.55	265.06	269.48	262.25	32.46	182.34	326.78	229.20	119.52	272.82	162.98	224.88
V	78.68	109.46	76.73	74.14	71.59	61.61	78.06	55.57	114.34	85.30	79.07	96.59	97.36
Y	6.50	2.99	6.10	6.70	15.03	0.34	7.86	6.13	9.24	8.69	4.99	5.18	4.31
Zn	91.44	66.19	49.00	48.34	72.88	173.07	77.24	51.78	83.13	82.90	63.97	70.44	78.35
Zr	18.12	23.36	14.49	16.63	22.70	4.40	12.31	10.94	13.28	10.13	15.09	10.49	19.09
Mo	2.71	4.65	3.13	1.77	6.05	0.36	3.04	1.74	3.39	5.77	1.80	4.22	3.44
U	0.39	0.39	0.39	0.39	0.39	0.39	0.39	0.39	0.39	0.39	0.39	0.39	0.39
Th	34.80	29.40	74.90	79.27	70.23	0.23	17.04	103.92	54.99	0.23	78.13	25.18	54.02
Au	0.03	n.d	0.03	n.d	n.d	n.d	0.96	0.06	n.d	0.24	n.d	0.03	n.d
Pd	0.03	n.d	0.05	n.d	n.d	n.d	10.00	0.03	n.d	0.03	n.d	0.03	n.d
Pt	0.05	n.d	0.03	n.d	n.d	n.d	8.50	0.05	n.d	0.03	n.d	0.03	n.d

GN: Gabbronorites; UP: Upper Platreef; MP: Middle Platreef; LP: Lower Platreef; Serp-Pyx: Serpentinised pyroxenite.
*n.d: not determined; sample # annotated with A & B are original and duplicate.

Borehole Sample #	OY482-25	OY482-27	OY482-28A	OY482-28B	OY482-29A	OY482-29B	OY482-30	OY482-31	OY482-32	OY482-33	OY482-34	OY482-35	OY482-36
Lithology	GN	MP	GN	GN	MP	MP	MP	MP	MP	MP	MP	MP	GN
SiO_2	48.76	48.56	46.56	46.55	50.32	50.33	52.44	43.44	50.67	49.60	44.97	49.02	51.51
Al_2O_3	15.20	9.79	16.00	16.01	7.06	7.08	5.90	10.24	11.45	10.72	8.98	4.30	13.76
Fe_2O_3	8.84	12.72	7.41	7.36	11.11	11.11	17.05	11.78	12.12	12.69	12.83	15.24	9.05
MnO	0.12	0.17	0.12	0.12	0.16	0.16	0.23	0.17	0.18	0.16	0.16	0.18	0.16
MgO	10.68	15.26	10.05	10.11	14.88	14.88	16.35	14.15	11.95	11.95	19.03	17.17	8.09
CaO	10.65	8.59	10.69	10.67	10.61	10.58	4.95	11.32	9.76	9.46	7.82	7.97	11.25
Na_2O	1.89	1.32	1.75	1.77	1.51	1.52	1.36	1.27	1.82	2.22	0.85	1.81	2.77
K_2O	0.67	0.26	0.97	0.98	0.22	0.22	0.11	0.04	0.37	0.38	0.13	0.16	0.53
P_2O_5	0.02	0.02	0.02	0.02	0.05	0.05	0.07	0.03	0.02	0.02	0.02	0.03	0.02
TiO_2	0.17	0.22	0.14	0.14	0.24	0.24	0.27	0.20	0.18	0.19	0.18	0.23	0.20
SO_3	0.24	0.16	0.17	0.17	0.42	0.42	0.38	0.13	0.10	0.66	0.03	0.51	0.03
LOI	2.76	3.02	6.09	6.09	3.41	3.41	0.91	7.22	1.40	2.00	5.00	3.39	2.62
As	3.86	9.74	4.76	11.02	0.56	4.20	8.46	20.23	8.95	3.68	18.61	15.69	11.20
Ba	170.47	116.13	240.33	232.36	116.26	105.74	81.25	75.24	130.02	139.95	79.41	88.67	194.33
Ce	49.73	110.68	16.67	41.93	73.91	87.37	133.95	116.31	101.82	164.99	179.43	153.33	79.08
Co	72.01	100.29	59.77	58.01	111.12	109.31	135.98	101.88	86.78	146.19	72.51	137.72	53.23
Cu	623.84	398.26	597.08	595.32	1055.97	1057.17	936.68	843.78	355.27	1117.67	211.30	2486.80	195.38
Nb	16.78	12.41	18.27	17.59	16.91	13.13	8.98	11.26	12.04	12.68	12.53	10.54	14.37
Ni	1507.71	1407.03	1324.30	1313.36	1709.00	1713.30	1327.89	1799.88	714.80	2997.35	612.78	2461.83	323.62
Pb	8.95	7.36	9.09	8.36	5.02	4.42	11.16	25.18	1.38	8.07	1.58	1.72	5.91
Rb	34.07	15.21	46.50	46.62	15.51	16.93	12.50	4.19	17.61	16.43	12.94	7.09	24.00
Sr	246.78	175.42	369.93	369.88	105.23	106.54	54.46	82.33	199.87	180.18	118.08	39.58	333.12
V	88.19	98.30	60.15	55.78	139.49	120.41	119.43	111.36	111.02	103.07	111.41	158.50	115.89
Y	0.81	9.67	4.66	3.77	6.62	8.67	9.66	12.20	8.44	5.84	2.59	11.03	7.23
Zn	75.44	94.70	76.22	76.30	78.03	79.32	142.14	121.90	78.89	96.47	76.34	109.80	66.18
Zr	15.56	17.54	16.78	17.09	16.34	16.11	15.78	17.34	14.87	12.55	15.93	29.10	18.52
Mo	2.76	0.36	2.55	2.63	5.09	4.62	5.69	2.84	1.33	0.68	0.95	5.26	1.38
U	0.39	0.39	0.39	0.39	0.39	0.39	3.98	0.39	0.39	0.39	0.39	0.39	0.39
Th	67.20	28.55	127.57	129.20	0.23	0.23	0.23	0.23	26.16	22.27	1.51	0.23	107.80
Au	0.17	0.09	0.20	0.20	n.d	n.d	n.d	n.d	0.07	n.d	n.d	n.d	0.14
Pd	1.86	1.57	0.94	0.94	n.d	n.d	n.d	n.d	0.60	n.d	n.d	n.d	0.03
Pt	1.24	1.06	0.53	0.53	n.d	n.d	n.d	n.d	0.52	n.d	n.d	n.d	0.03

GN: Gabbronorites; UP: Upper Platreef; MP: Middle Platreef; LP: Lower Platreef; Serp-Pyx: Serpentinised pyroxenite.
*n.d: not determined; sample # annotated with A & B are original and duplicate.

Borehole Sample #	OY482-37	OY482-38	OY482-39	OY482-40	OY482-42
Lithology	GN	LP	LP	LP	LP
SiO_2	49.44	49.14	53.94	49.17	53.02
Al_2O_3	14.31	12.27	9.41	3.94	15.02
Fe_2O_3	9.75	10.06	11.34	15.15	7.33
MnO	0.14	0.15	0.16	0.20	0.12
MgO	11.36	14.93	13.13	19.26	11.21
CaO	9.57	8.18	6.58	4.15	6.60
Na_2O	1.84	1.55	2.55	1.22	2.87
K_2O	0.99	0.50	0.24	0.08	0.44
P_2O_5	0.03	0.02	0.06	0.04	0.06
TiO_2	0.16	0.20	0.26	0.21	0.26
SO_3	0.20	0.11	0.51	0.46	0.11
LOI	2.21	2.87	1.80	6.13	2.97
As	6.37	4.62	0.56	16.70	4.43
Ba	272.73	188.73	100.61	66.21	263.05
Ce	86.18	69.00	88.69	112.51	30.90
Co	83.53	82.62	107.96	210.58	59.54
Cu	747.75	575.40	1493.19	1937.71	425.65
Nb	15.89	18.18	18.89	14.90	19.98
Ni	1894.90	1151.81	1759.12	4492.36	1546.97
Pb	10.06	7.78	13.79	8.64	6.58
Rb	48.00	28.40	19.47	14.31	20.07
Sr	357.67	262.62	153.99	71.59	629.27
V	70.08	80.67	95.94	105.38	54.55
Y	1.69	2.87	8.96	5.23	11.91
Zn	65.44	94.46	93.98	128.05	80.60
Zr	12.74	16.85	48.61	38.82	16.35
Mo	2.12	1.16	3.81	4.29	4.56
U	0.39	0.39	0.39	0.39	0.39
Th	121.75	74.72	17.97	0.23	240.07
Au	n.d	n.d	n.d	0.05	0.19
Pd	n.d	n.d	n.d	0.03	2.13
Pt	n.d	n.d	n.d	0.03	1.85

GN: Gabbronorites; UP: Upper Platreef; MP: Middle Platreef; LP: Lower Platreef; Serp-Pyx: Serpentinised pyroxenite.
*n.d: not determined; sample # annotated with A & B are original and duplicate.

APPENDIX III

Normalized trace element concentration data for the studied boreholes

Borehole Sample #	SS330-1	SS330-2	SS330-3	SS330-4	SS330-5	SS330-7	SS330-8	SS330-9	SS330-10	SS330-11	SS330-12	SS330-13	SS330-14
Lithology	CP III	CP II	CP I	CP III	CP I	OCP II	CP I	CP I	CP I	OCP II	CP I	OCP III	OCP III
Rb_N	204.87	3.21	8.36	12.54	1.04	3.98	3.37	5.78	8.58	16.16	2.60	26.82	54.11
Ba_N	87.22	6.74	16.12	8.22	7.89	5.25	6.45	7.94	5.29	9.77	8.91	12.00	9.57
Th_N	377.45	2.29	2.29	2.29	2.29	2.29	2.29	2.29	2.29	2.29	2.29	2.29	2.29
U_N	0.10	0.10	0.10	0.10	0.10	0.10	24.57	0.10	0.10	0.10	0.10	0.10	0.10
Nb_N	19.06	10.38	19.03	15.51	12.89	13.66	19.72	10.28	7.42	16.48	10.60	15.26	17.34
K_N	68.70	<0.01	1.16	2.15	<0.01	<0.01	<0.01	<0.01	0.04	1.06	<0.01	7.12	6.10
Ce_N	4.36	53.07	14.68	36.56	50.02	36.01	0.03	50.72	59.24	61.78	22.00	70.28	37.31
Pb_N	241.41	160.85	173.52	61.83	582.68	34.23	0.99	102.54	442.39	0.99	109.16	63.24	137.61
Sr_N	6.78	0.32	0.60	1.61	0.59	0.09	0.19	0.59	0.37	1.65	0.31	2.96	0.55
P_N	0.86	0.85	1.12	0.80	0.77	0.75	2.60	0.64	1.16	0.73	0.90	0.86	0.77
Zr_N	2.73	1.61	5.67	1.37	0.66	2.29	0.96	1.60	1.77	4.55	0.81	3.01	11.88
Ti_N	1.34	0.91	2.06	1.00	1.32	0.63	0.17	1.46	1.29	1.29	1.13	0.97	1.94
Y_N	0.02	3.47	0.11	0.84	2.73	0.06	0.02	2.97	2.00	0.59	1.84	0.48	0.50

Borehole Sample #	SS330-15	SS330-16	SS330-17	SS330-18	SS330-19	SS330-20	SS330-24	SS330-25	SS330-26	SS330-27	SS330-28	SS330-29	SS330-30
Lithology	OCP I	CP I	OCP II	CP III	OCP I	CP I	CP I	CP I	CP II	CP I	CP II	CP II	CP I
Rb_N	1.87	6.21	0.32	104.05	3.72	4.46	2.46	5.26	1.13	2.60	45.78	0.66	2.55
Ba_N	6.57	9.77	7.35	102.73	6.77	7.04	7.20	7.46	7.29	7.01	15.24	7.29	7.79
Th_N	2.29	2.29	2.29	617.32	2.29	2.29	2.29	2.29	2.29	2.29	2.29	2.29	2.29
U_N	0.10	0.10	0.10	0.10	0.10	0.10	0.10	0.10	0.10	0.10	0.10	0.10	0.10
Nb_N	19.82	15.25	24.08	21.64	18.54	5.41	12.23	6.97	14.57	22.97	15.93	22.06	15.08
K_N	<0.01	<0.01	<0.01	38.62	<0.01	<0.01	<0.01	<0.01	<0.01	<0.01	4.97	<0.01	<0.01
Ce_N	20.86	73.87	1.48	22.16	18.87	73.70	118.07	72.55	168.82	114.85	37.96	163.52	45.48
Pb_N	72.82	2149.44	143.66	265.21	0.99	0.99	154.79	101.97	114.37	15.63	146.20	0.99	368.31
Sr_N	0.03	0.59	0.26	10.43	<0.01	0.45	1.74	0.92	0.30	0.49	0.97	0.16	1.70
P_N	0.57	6.20	1.99	3.21	0.56	2.15	0.94	1.75	0.63	0.47	0.78	0.47	1.20
Zr_N	0.29	3.70	4.18	2.23	0.27	4.34	2.37	5.37	3.04	0.52	5.32	0.08	1.95
Ti_N	0.33	2.16	1.43	1.41	0.23	1.87	0.51	2.95	1.46	0.22	2.01	0.19	0.84
Y_N	2.44	1.66	2.74	0.02	0.81	2.06	18.02	1.60	2.51	0.83	0.80	0.23	1.30

CP I, CP II and CP III denote weakly, moderately and feldspathic rich moderately metasomatised clinopyroxenites.
OCP I, OCP II and OCP III denote weakly, moderately and highly metasomatised/ altered olivine clinopyroxenites.

Borehole Sample #	SS330-31	SS330-32	SS330-33	SS330-34	SS330-35	SS330-36	SS330-37	SS330-38	SS330-39	SS330-40	SS330-41	SS330-42	SS330-43
Lithology	CP I	CP I	OCP III	OCP III	CP I	OCP III	OCP III	OCP I	CP I	CP II	OCP I	CP I	CP II
Rb_N	2.17	2.96	44.61	28.30	2.95	17.12	20.46	4.44	3.48	17.62	1.89	4.63	3.45
Ba_N	11.02	7.21	12.96	14.93	9.07	9.52	16.01	6.87	9.87	13.07	6.89	7.84	5.62
Th_N	2.29	2.29	141.53	2.29	2.29	2.29	37.84	2.29	2.29	2.29	2.29	2.29	2.29
U_N	0.10	0.10	0.10	0.10	0.10	0.10	0.10	0.10	0.10	0.10	0.10	0.10	0.10
Nb_N	10.20	4.52	17.17	16.13	10.93	14.21	15.46	17.77	13.32	17.25	17.29	15.89	18.72
K_N	<0.01	<0.01	15.46	10.17	<0.01	8.16	10.37	<0.01	<0.01	3.74	<0.01	<0.01	<0.01
Ce_N	92.08	82.28	21.52	19.72	82.87	57.32	52.79	8.74	46.85	7.81	25.41	65.58	25.72
Pb_N	201.41	57.32	74.65	0.99	54.23	18.73	56.34	31.41	14.65	162.25	31.97	0.99	0.99
Sr_N	0.64	0.59	6.40	3.17	0.65	1.07	5.69	0.31	1.03	0.83	0.27	0.79	0.59
P_N	0.60	1.33	0.98	0.80	2.31	0.87	0.68	0.60	0.80	0.80	0.53	1.14	0.87
Zr_N	2.80	4.40	2.46	3.81	5.34	2.89	2.30	1.30	5.17	5.35	0.60	3.28	3.42
Ti_N	2.19	0.90	0.68	0.99	2.99	0.91	0.75	0.53	2.51	1.35	0.23	1.86	1.34
Y_N	2.09	1.91	1.31	1.24	1.63	0.56	0.94	1.78	0.82	1.81	5.38	1.67	0.95

Borehole Sample #	SS330-44	SS330-45	SS330-46	SS330-47	SS330-48	SS330-50	SS330-51	SS330-52	SS330-53	SS330-54	SS330-55	SS330-56	SS330-57
Lithology	OCP III	OCP I	CP II	OCP I	OCP II	OCP II	OCP III	OCP I	CP II	OCP II	OCP II	OCP II	OCP I
Rb_N	8.19	9.48	4.57	4.33	2.80	13.20	34.00	12.00	18.93	35.51	6.69	8.13	0.08
Ba_N	8.57	6.45	8.45	8.51	5.60	11.00	21.49	7.94	12.07	8.59	10.54	10.73	8.21
Th_N	2.29	2.29	2.29	2.29	2.29	2.29	40.94	2.29	2.29	2.29	2.29	2.29	2.29
U_N	0.10	1020.24	0.10	0.10	0.10	0.10	0.10	1201.81	0.10	0.10	0.10	0.10	0.10
Nb_N	19.12	7.73	17.87	16.06	16.94	12.92	20.94	7.32	13.82	16.44	16.83	15.30	14.67
K_N	4.16	<0.01	0.52	<0.01	<0.01	1.72	15.12	<0.01	5.48	4.67	0.79	1.88	<0.01
Ce_N	30.35	9.18	17.34	17.16	0.03	47.10	36.51	1.74	16.90	46.02	24.94	60.22	33.30
Pb_N	4.79	0.99	93.38	0.99	31.41	53.10	33.80	61.83	24.37	100.14	0.99	24.09	9.58
Sr_N	2.50	0.10	0.48	0.46	0.52	4.68	5.60	0.85	1.29	0.76	1.19	0.85	0.12
P_N	0.60	0.60	1.25	0.73	0.74	0.70	1.62	0.85	1.82	1.13	0.84	0.66	0.68
Zr_N	2.60	3.42	3.73	2.44	3.84	4.37	3.63	2.01	7.05	5.19	4.87	4.83	2.22
Ti_N	0.88	1.02	1.43	0.76	1.04	1.26	1.32	0.56	2.41	1.44	1.34	1.46	0.93
Y_N	0.55	1.94	1.83	1.70	3.08	1.19	1.47	1.67	2.55	1.90	2.43	2.03	1.73

CP I, CP II and CP III denote weakly, moderately and feldspathic rich moderately metasomatised clinopyroxenites.
OCP I, OCP II and OCP III denote weakly, moderately and highly metasomatised/ altered olivine clinopyroxenites.

Borehole Sample #	SS330-58	SS330-59	SS330-61	SS330-62	SS330-63	SS330-64	SS330-65	SS330-66	SS330-67	SS330-68	SS330-69	SS330-70	SS330-71
Lithology	OCP III	CP III	OCP II	OCP II	OCP II	CP III	OCP II	CP III	OCP III	OCP III	OCP II	CP I	CP II
Rb_N	12.57	41.78	4.38	11.50	5.45	65.29	9.47	14.61	45.37	89.50	13.65	4.69	0.39
Ba_N	10.27	58.55	10.15	9.48	8.27	47.01	8.51	17.42	11.90	9.39	11.70	9.96	9.54
Th_N	2.29	1355.86	2.29	2.29	2.29	1028.98	2.29	2.29	234.38	2.29	2.29	2.29	2.29
U_N	0.10	0.10	0.10	0.10	0.10	0.10	0.10	0.10	0.10	0.10	0.10	0.10	0.10
Nb_N	20.24	20.35	15.20	13.49	18.68	22.86	17.03	12.47	21.00	15.78	16.70	21.53	26.07
K_N	2.79	30.01	0.36	2.17	0.15	25.59	0.14	5.09	11.93	15.28	3.38	<0.01	<0.01
Ce_N	53.72	76.94	44.15	63.51	41.69	57.34	46.01	69.86	37.63	64.68	48.55	34.95	78.80
Pb_N	0.99	106.76	0.99	2.68	29.01	107.61	0.99	40.14	32.96	121.55	19.58	103.94	145.78
Sr_N	3.91	16.85	1.67	2.86	1.12	13.78	2.99	4.46	6.88	1.31	2.55	1.69	0.27
P_N	0.79	0.94	0.83	0.88	0.67	1.41	0.68	0.84	0.79	0.85	0.78	0.87	0.98
Zr_N	3.96	1.59	4.34	3.69	3.50	3.97	4.79	1.57	2.73	3.19	3.01	2.18	2.92
Ti_N	1.30	0.67	1.47	1.19	1.30	1.46	1.75	1.10	0.80	0.95	1.19	1.44	1.93
Y_N	1.10	1.39	1.71	1.20	1.35	1.31	1.51	1.82	1.11	0.02	0.51	2.85	1.15

Borehole Sample #	SS330-72	SS330-73	SS330-74	SS330-75	SS330-76	SS330-77	SS330-78	SS330-79	SS330-80	SS330-82	SS330-83	SS330-84
Lithology	CP II	CP II	OCP I	CP I	CP III	OCP I	CP III	CP I	OCP I	CP I	OCP II	CP I
Rb_N	2.90	5.09	2.43	6.38	28.68	2.17	93.12	2.71	1.91	7.54	2.08	7.47
Ba_N	5.40	7.09	8.03	8.93	22.23	5.94	86.19	7.49	6.85	9.54	7.72	6.13
Th_N	2.29	2.29	2.29	2.29	486.27	2.29	2216.62	2.29	2.29	2.29	2.29	2.29
U_N	0.10	0.10	0.10	0.10	0.10	0.10	0.10	0.10	0.10	119.57	0.10	0.10
Nb_N	30.08	19.10	17.10	16.72	13.48	15.92	28.53	8.43	14.70	5.93	14.43	10.70
K_N	<0.01	0.60	<0.01	0.83	22.36	<0.01	45.39	<0.01	<0.01	<0.01	<0.01	<0.01
Ce_N	113.80	49.59	4.18	54.72	78.83	2.55	51.00	0.33	27.16	55.82	38.41	90.90
Pb_N	114.93	108.45	0.99	78.17	100.00	0.99	149.44	40.99	2.68	66.76	50.70	122.96
Sr_N	0.85	1.28	<0.01	0.46	11.74	<0.01	23.52	0.43	0.35	0.39	0.09	0.49
P_N	0.74	1.28	0.64	1.25	0.76	0.49	1.28	7.92	0.63	1.54	0.74	1.72
Zr_N	2.25	2.10	2.28	1.94	0.90	0.14	1.37	1.96	4.20	3.47	2.63	9.59
Ti_N	1.79	1.28	0.73	1.28	0.78	0.20	0.80	1.12	0.73	2.06	0.89	2.91
Y_N	1.54	0.96	4.09	2.15	2.06	0.66	0.02	1.85	1.31	2.65	0.42	3.31

CP I, CP II and CP III denote weakly, moderately and feldspathic rich moderately metasomatised clinopyroxenites.
OCP I, OCP II and OCP III denote weakly, moderately and highly metasomatised/ altered olivine clinopyroxenites.

Borehole Sample #	SS330-86	SS330-93	SS330-94
Lithology	M-Dol	M-Dol	M-Dol
Rb_N	3.12	6.19	3.45
Ba_N	7.26	8.04	7.82
Th_N	2.29	2.29	2.29
U_N	0.10	0.10	0.10
Nb_N	14.41	11.96	13.28
K_N	<0.01	<0.01	<0.01
Ce_N	48.23	52.28	24.24
Pb_N	0.92	108.52	15.11
Sr_N	0.90	1.51	1.36
P_N	0.33	0.29	0.26
Zr_N	0.17	0.29	0.48
Ti_N	0.05	0.04	0.05
Y_N	0.29	0.07	0.24

Borehole Sample #	OY482-1	OY482-2	OY482-3	OY482-4	OY482-6	OY482-7	OY482-8	OY482-9	OY482-10	OY482-11	OY482-12	OY482-13	OY482-14
Lithology	GN	GN	UP	UP	GN	GN	GN	GN	GN	GN	GN	GN	GN
Rb_N	38.52	32.91	5.59	8.33	36.32	10.95	26.24	41.42	21.70	37.70	32.06	12.76	20.68
Ba_N	19.05	18.36	10.87	12.41	18.21	14.97	16.48	19.94	16.39	18.04	19.95	10.71	14.77
Th_N	886.68	943.89	2.75	103.94	847.21	582.71	797.38	791.68	504.72	707.25	712.21	409.35	345.85
U_N	18.43	18.43	18.43	18.43	18.43	18.43	18.43	18.43	18.43	18.43	18.43	18.43	18.43
Nb_N	20.51	20.86	18.40	18.29	22.05	20.81	17.41	21.30	19.22	23.66	21.09	24.76	17.59
K_N	14.54	12.11	2.44	3.59	15.01	6.30	10.43	17.07	10.16	15.85	15.19	4.85	9.99
Ce_N	23.45	3.77	95.32	29.44	15.48	31.62	29.08	35.07	17.80	41.36	36.64	41.06	45.56
Pb_N	8.17	171.41	4.23	18.31	72.39	31.97	72.39	68.17	66.76	24.37	261.69	61.55	162.11
Sr_N	12.87	12.95	4.14	6.46	11.98	10.46	12.09	11.80	9.74	10.74	11.32	8.72	8.84
P_N	1.00	0.73	0.92	0.72	0.81	1.45	0.87	0.73	0.59	0.78	1.34	1.26	1.12
Zr_N	1.43	0.97	2.43	1.24	1.05	1.70	1.07	1.01	0.89	1.27	1.70	1.62	2.09
Ti_N	0.71	0.57	0.98	0.75	0.64	1.09	0.70	0.58	0.74	0.68	1.06	0.76	0.77
Y_N	1.59	1.28	2.20	0.08	1.16	1.95	1.37	1.05	0.92	1.44	1.42	1.43	0.66

M-Dol: Metadolomites; GN: Gabbronorites; UP: Upper Platreef; MP: Middle Platreef; LP: Lower Platreef;
Serp-Pyx: Serpentinised pyroxenite.

Borehole Sample #	OY482-15	OY482-16	OY482-17	OY482-18	OY482-19	OY482-20	OY482-21	OY482-22	OY482-23	OY482-24	OY482-25	OY482-27	OY482-28
Lithology	GN	GN	Serp-Pyx	UP	GN	GN	GN	GN	GN	GN	GN	MP	GN
Rb_N	44.02	19.54	3.87	25.01	61.86	25.35	4.52	56.93	12.46	28.77	53.65	23.95	73.23
Ba_N	20.75	18.03	8.16	14.21	33.32	20.16	10.97	23.53	11.87	20.06	24.39	16.62	34.39
Th_N	881.21	826.18	2.75	200.46	1222.58	646.98	2.75	919.18	296.22	635.54	790.64	335.89	1500.87
U_N	18.43	18.43	18.43	18.43	18.43	18.43	18.43	18.43	18.43	18.43	18.43	18.43	18.43
Nb_N	25.58	22.82	17.43	16.96	22.41	22.16	21.59	18.46	21.57	21.68	23.53	17.41	25.62
K_N	17.71	10.71	0.50	9.05	33.11	12.20	1.82	20.71	3.89	12.93	22.10	8.72	32.36
Ce_N	46.33	36.05	85.49	65.29	3.77	35.78	23.13	23.43	39.70	41.06	28.02	62.36	9.39
Pb_N	115.35	132.11	87.18	77.04	52.25	76.48	123.80	98.45	101.13	81.97	126.06	103.66	128.03
Sr_N	12.56	12.43	1.54	8.64	15.49	10.86	5.66	12.93	7.72	10.66	11.70	8.31	17.53
P_N	1.11	1.05	0.60	0.90	0.86	0.92	1.35	1.11	1.08	1.07	0.91	0.86	1.02
Zr_N	1.29	2.03	0.39	1.10	0.98	1.19	0.90	1.35	0.94	1.70	1.39	1.57	1.50
Ti_N	0.71	0.65	0.54	0.76	0.51	0.93	0.68	0.72	0.70	0.96	0.77	1.00	0.62
Y_N	1.34	3.30	0.08	1.73	1.35	2.03	1.91	1.10	1.14	0.95	0.18	2.13	1.02

Borehole Sample #	OY482-29	OY482-30	OY482-31	OY482-32	OY482-33	OY482-34	OY482-35	OY482-36	OY482-37	OY482-38	OY482-39	OY482-40	OY482-42
Lithology	MP	MP	MP	MP	MP	MP	MP	GN	GN	LP	LP	LP	LP
Rb_N	24.43	19.69	6.60	27.73	25.87	20.38	11.17	37.80	75.59	44.72	30.66	22.54	31.61
Ba_N	16.64	11.63	10.77	18.60	20.02	11.36	12.69	27.81	39.02	27.00	14.40	9.47	37.64
Th_N	2.75	2.75	2.75	307.77	262.04	17.81	2.75	1268.24	1432.40	879.07	211.40	2.75	2824.38
U_N	18.43	189.52	18.43	18.43	18.43	18.43	18.43	18.43	18.43	18.43	18.43	18.43	18.43
Nb_N	23.72	12.60	15.79	16.89	17.78	17.57	14.78	20.15	22.29	25.50	26.49	20.90	28.02
K_N	7.31	3.58	1.36	12.25	12.66	4.20	5.29	17.76	32.81	16.74	8.07	2.68	14.68
Ce_N	41.64	75.47	65.53	57.36	92.95	101.09	86.38	44.55	48.55	38.87	49.97	63.39	17.41
Pb_N	70.70	157.18	354.65	19.44	113.66	22.25	24.23	83.24	141.69	109.58	194.23	121.69	92.68
Sr_N	4.99	2.58	3.90	9.47	8.54	5.60	1.88	15.79	16.95	12.45	7.30	3.39	29.82
P_N	2.29	3.11	1.27	0.92	0.97	0.93	1.34	1.14	1.38	1.09	2.89	1.67	2.58
Zr_N	1.46	1.41	1.55	1.33	1.12	1.42	2.60	1.65	1.14	1.50	4.34	3.47	1.46
Ti_N	1.12	1.26	0.90	0.81	0.85	0.83	1.07	0.93	0.72	0.90	1.22	0.96	1.19
Y_N	1.46	2.12	2.68	1.86	1.28	0.57	2.42	1.59	0.37	0.63	1.97	1.15	2.62

GN: Gabbronorites; UP: Upper Platreef; MP: Middle Platreef; LP: Lower Platreef; Serp-Pyx: Serpentinised pyroxenite.

APPENDIX IV

Normalized trace element anomalies data for the studied boreholes

Borehole Sample #	SS330-1	SS330-2	SS330-3	SS330-4	SS330-5	SS330-7	SS330-8	SS330-9	SS330-10	SS330-11	SS330-12	SS330-13	SS330-14
Lithology	CP III	CP II	CP I	CP III	CP I	OCP II	CP I	CP I	CP I	OCP II	CP I	OCP III	OCP III
Rb*	2.35	0.48	0.52	1.52	0.13	0.76	0.52	0.73	1.62	1.65	0.29	2.23	5.65
K*	5.87	<0.01	0.07	0.08	<0.01	<0.01	<0.01	<0.01	<0.01	0.03	<0.01	0.17	0.22
Sr*	0.06	<0.01	0.01	0.05	<0.01	0.01	0.11	0.01	<0.01	1.92	0.01	0.09	0.01
Zr*	2.49	1.83	3.57	1.52	0.64	3.32	0.69	1.53	1.45	4.50	0.80	3.30	8.77
Ti*	0.97	0.36	0.71	0.90	0.78	0.53	0.34	0.64	0.68	0.50	0.85	0.56	0.31

Borehole Sample #	SS330-15	SS330-16	SS330-17	SS330-18	SS330-19	SS330-20	SS330-24	SS330-25	SS330-26	SS330-27	SS330-28	SS330-29	SS330-30
Lithology	OCP I	CP I	OCP II	CP III	OCP I	CP I	CP I	CP I	CP II	CP I	CP II	CP II	CP I
Rb*	0.29	0.64	0.04	1.01	0.55	0.63	0.34	0.71	0.16	0.37	3.00	0.09	0.33
K*	<0.01	<0.01	<0.01	1.76	<0.01	<0.01	<0.01	<0.01	<0.01	<0.01	0.18	<0.01	<0.01
Sr*	<0.01	<0.01	<0.01	0.08	<0.01	0.29	0.02	0.02	0.01	0.06	0.01	0.22	0.01
Zr*	0.64	0.89	2.44	0.97	0.70	2.16	3.26	2.28	2.91	1.52	3.82	0.23	1.91
Ti*	0.24	0.81	0.41	1.25	0.42	0.58	0.05	0.85	0.53	0.32	0.66	1.25	0.52

Borehole Sample #	SS330-31	SS330-32	SS330-33	SS330-34	SS330-35	SS330-36	SS330-37	SS330-38	SS330-39	SS330-40	SS330-41	SS330-42	SS330-43
Lithology	CP I	CP I	OCP III	OCP III	CP I	OCP III	OCP III	OCP I	CP I	CP II	OCP I	CP I	CP II
Rb*	0.20	0.41	3.44	1.90	0.32	1.80	1.28	0.65	0.35	1.35	0.27	0.59	0.61
K*	<0.01	<0.01	0.80	0.57	<0.01	0.23	0.30	<0.01	<0.01	0.30	<0.01	<0.01	<0.01
Sr*	0.01	0.02	0.17	3.55	0.02	0.11	0.20	0.02	0.13	0.01	0.02	0.74	0.63
Zr*	2.01	3.96	2.96	4.27	2.01	3.25	3.24	2.31	3.13	4.98	1.57	2.19	3.11
Ti*	0.89	0.28	0.36	0.39	0.86	0.53	0.46	0.34	0.84	0.38	0.08	0.75	0.61

Borehole Sample #	SS330-44	SS330-45	SS330-46	SS330-47	SS330-48	SS330-50	SS330-51	SS330-52	SS330-53	SS330-54	SS330-55	SS330-56	SS330-57
Lithology	OCP III	OCP I	CP II	OCP I	OCP II	OCP II	OCP III	OCP I	CP II	OCP II	OCP II	OCP II	OCP I
Rb*	0.96	1.47	0.54	0.51	0.50	1.20	1.58	1.51	1.57	4.13	0.64	0.76	0.01
K*	0.17	<0.01	0.03	<0.01	<0.01	0.06	0.53	<0.01	0.36	0.15	0.04	0.05	<0.01
Sr*	0.93	0.12	0.01	0.53	0.03	0.17	0.32	0.03	0.10	0.02	1.30	0.07	0.02
Zr*	3.52	4.22	2.78	3.29	4.32	4.45	2.47	2.86	3.33	4.05	4.46	4.55	2.76
Ti*	0.56	0.38	0.51	0.36	0.30	0.45	0.52	0.30	0.50	0.41	0.37	0.43	0.47

CP I, CP II and CP III denote weakly, moderately and feldspathic rich moderately metasomatised clinopyroxenites.
OCP I, OCP II and OCP III denotes weakly, moderately and highly metasomatised/ altered olivine clinopyroxenites.

Borehole Sample #	SS330-58	SS330-59	SS330-61	SS330-62	SS330-63	SS330-64	SS330-65	SS330-66	SS330-67	SS330-68	SS330-69	SS330-70	SS330-71
Lithology	OCP III	CP III	OCP II	OCP II	OCP II	CP III	OCP II	CP III	OCP III	OCP III	OCP II	CP I	CP II
Rb*	1.22	0.71	0.43	1.21	0.66	1.39	1.11	0.84	3.81	9.53	1.17	0.47	0.04
K*	0.08	0.62	0.01	0.06	<0.01	0.64	<0.01	0.12	0.41	0.38	0.10	<0.01	<0.01
Sr*	4.40	0.31	1.84	1.61	0.08	0.25	3.60	0.22	0.41	0.02	0.25	0.03	<0.01
Zr*	3.79	1.98	3.76	3.57	3.56	2.77	3.94	1.62	3.44	3.55	3.05	1.88	2.00
Ti*	0.51	0.45	0.49	0.49	0.54	0.55	0.56	0.65	0.42	0.59	0.68	0.57	0.95

Borehole Sample #	SS330-72	SS330-73	SS330-74	SS330-75	SS330-76	SS330-77	SS330-78	SS330-79	SS330-80	SS330-82	SS330-83	SS330-84
Lithology	CP II	CP II	OCP I	CP I	CP III	OCP I	CP III	CP I	OCP I	CP I	OCP II	CP I
Rb*	0.54	0.72	0.30	0.71	1.29	0.37	1.08	0.36	0.28	0.79	0.27	1.22
K*	<0.01	0.02	<0.01	0.02	0.48	<0.01	1.14	<0.01	<0.01	<0.01	<0.01	<0.01
Sr*	0.01	0.02	<0.01	0.01	0.23	<0.01	0.31	0.02	0.21	0.01	<0.01	0.01
Zr*	1.78	1.64	3.34	1.53	1.17	0.39	1.31	0.43	6.21	1.93	3.24	4.14
Ti*	0.95	0.84	0.23	0.62	0.53	0.50	1.16	0.59	0.26	0.67	0.58	0.45

Borehole Sample #	SS330-86	SS330-93	SS330-94
Lithology	M-Dol	M-Dol	M-Dol
Rb*	0.43	0.77	0.44
K*	<0.01	<0.01	<0.01
Sr*	1.45	0.03	0.18
Zr*	0.89	1.75	3.05
Ti*	0.20	0.22	0.15

CP I, CP II and CP III denote weakly, moderately and feldspathic rich moderately metasomatised clinopyroxenites.
OCP I, OCP II and OCP III denotes weakly, moderately and highly metasomatised/ altered olivine clinopyroxenites; M-Dol: Metadolomites.

Borehole Sample #	OY482-1	OY482-2	OY482-3	OY482-4	OY482-6	OY482-7	OY482-8	OY482-9	OY482-10	OY482-11	OY482-12	OY482-13	OY482-14
Lithology	GN	GN	UP	UP	GN	GN	GN	GN	GN	GN	GN	GN	GN
Rb*	2.02	1.79	0.51	0.67	1.99	0.73	1.59	2.08	1.32	2.09	1.61	1.19	1.40
K*	0.66	0.98	0.04	0.15	0.80	0.24	0.45	0.61	0.55	0.49	0.53	0.15	0.32
Sr*	2.81	0.15	1.61	0.68	0.33	0.63	0.33	0.34	0.29	0.85	0.09	0.28	0.11
Zr*	1.67	1.49	2.55	1.69	1.45	1.34	1.37	1.54	1.34	1.74	1.42	1.60	2.20
Ti*	0.47	0.51	0.42	1.14	0.58	0.60	0.57	0.56	0.81	0.50	0.68	0.50	0.56

Borehole Sample #	OY482-15	OY482-16	OY482-17	OY482-18	OY482-19	OY482-20	OY482-21	OY482-22	OY482-23	OY482-24	OY482-25	OY482-27	OY482-28
Lithology	GN	GN	Serp-Pyx	UP	GN	GN	GN	GN	GN	GN	GN	MP	GN
Rb*	2.12	1.08	0.47	1.76	1.86	1.26	0.41	2.42	1.05	1.43	2.20	1.44	2.13
K*	0.49	0.36	0.01	0.22	2.53	0.42	0.08	0.99	0.13	0.41	0.86	0.22	1.85
Sr*	0.22	0.19	0.04	0.22	0.58	0.28	0.09	0.26	0.15	0.26	0.18	0.16	0.27
Zr*	1.42	2.39	0.69	1.32	1.43	1.28	0.89	1.47	1.05	1.68	1.65	1.69	1.82
Ti*	0.54	0.24	2.31	0.54	0.44	0.58	0.48	0.59	0.67	0.73	0.99	0.54	0.49

Borehole Sample #	OY482-29	OY482-30	OY482-31	OY482-32	OY482-33	OY482-34	OY482-35	OY482-36	OY482-37	OY482-38	OY482-39	OY482-40	OY482-42
Lithology	MP	MP	MP	MP	MP	MP	MP	GN	GN	LP	LP	LP	LP
Rb*	1.47	1.69	0.61	1.49	1.29	1.79	0.88	1.36	1.94	1.66	2.13	2.38	0.84
K*	0.22	0.08	0.03	0.33	0.23	0.07	0.10	0.55	0.93	0.52	0.21	0.06	0.65
Sr*	0.14	0.03	0.02	0.93	0.15	0.48	0.15	0.37	0.24	0.22	0.07	0.06	0.63
Zr*	0.85	0.64	1.43	1.53	1.23	1.61	2.16	1.59	1.08	1.51	2.11	2.64	0.77
Ti*	0.77	0.72	0.43	0.51	0.71	0.84	0.43	0.58	0.96	0.84	0.39	0.42	0.59

GN: Gabbronorites; UP: Upper Platreef; MP: Middle Platreef; LP: Lower Platreef; Serp-Pyx: Serpentinised pyroxenite.

APPENDIX V

Examples of the isocon graphs

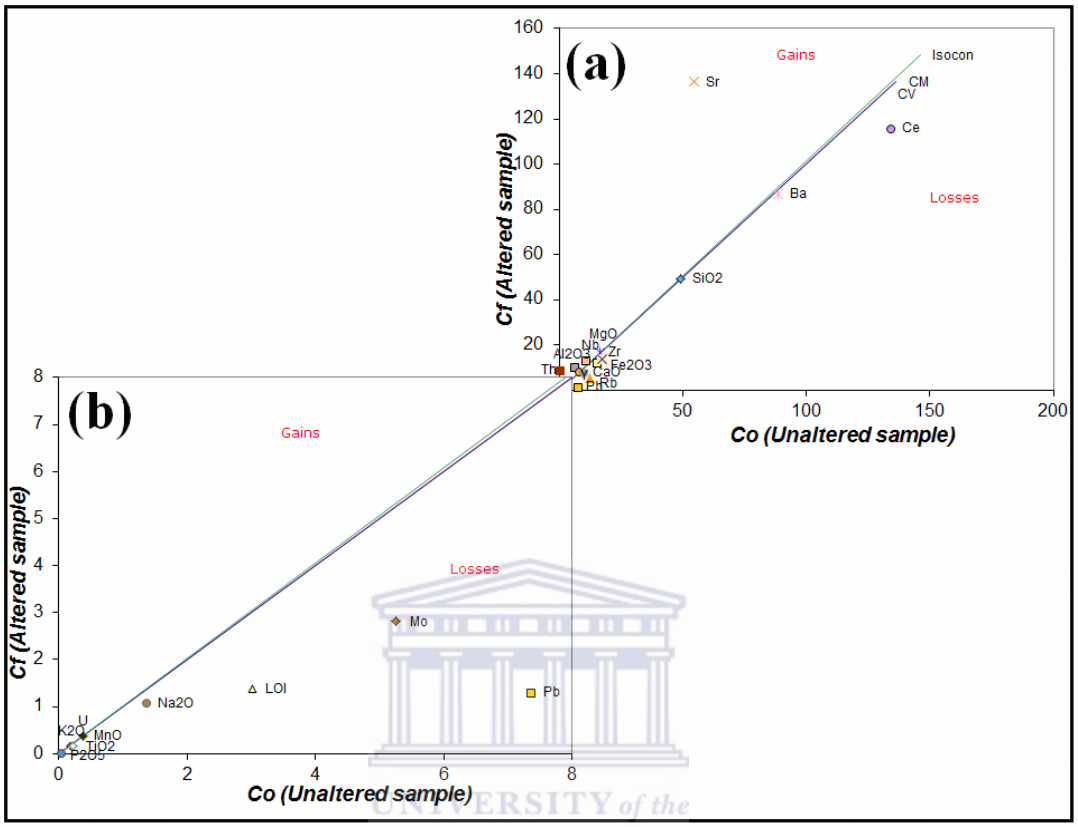

Isocon diagrams for the upper Platreef relative to the least altered middle Platreef. *Data are median values from Table 9 (As, Cu, Co, Ni, V, Zn and SO_3 were not selected). Cf and Co are concentrations of the hanging wall pyroxenite and the least altered pyroxenite, in that order. CM and CV are lines of constant mass and constant volume, respectively. Figure (b) is the expanded view of Fig. (a) as indicated by scale.*

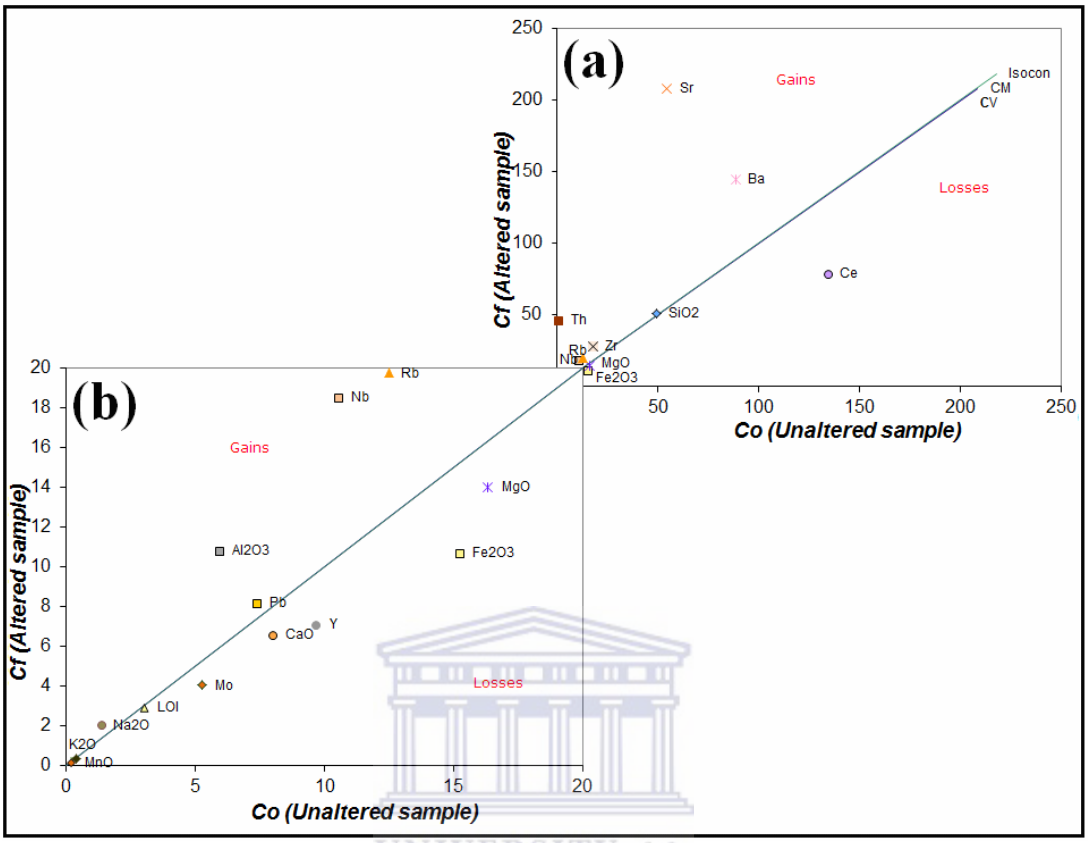

Isocon diagrams for the lower Platreef relative to the least altered middle Platreef. *Data are median values from Table 9 (As, Cu, Co, Ni, V, Zn and SO_3 were not selected). Cf and Co are concentrations of the footwall pyroxenite and the least altered pyroxenite, in that order. CM and CV are lines of constant mass and constant volume, respectively. Figure (b) is the expanded view of Fig. (a) as indicated by scale.*

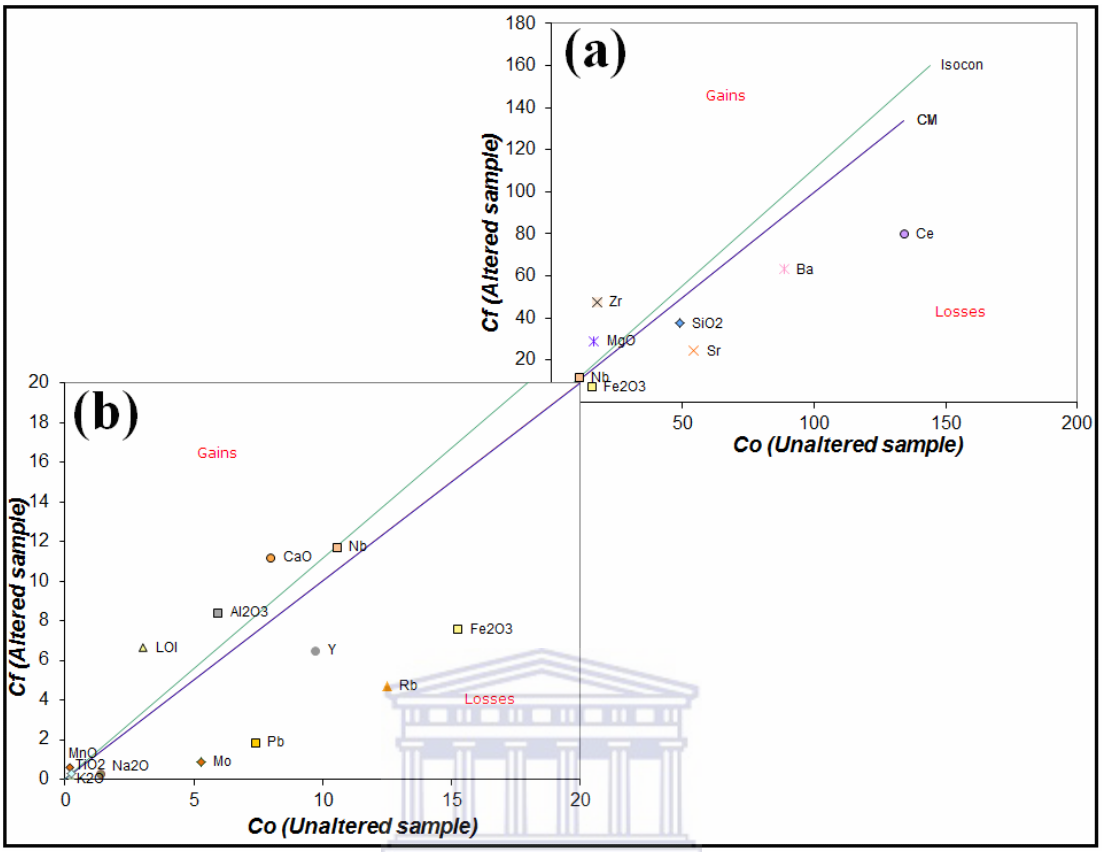

Isocon diagrams for the olivine clinopyroxenites II relative to the least altered Middle Platreef. *Data are median values from Table 9 (As, Cu, Co, Ni, V, Zn and SO_3 were not selected). Cf and Co are concentrations of the olivine clinopyroxenite II and the least altered pyroxenite, in that order. CM and CV are lines of constant mass and constant volume, respectively. Figure (b) is the expanded view of Fig. (a) as indicated by the scale.*